

**Photodynamically-Active Electrospun Fibres with Selective
On-Demand Antibacterial Capability**

Amy Louise Contreras

Submitted in accordance with the requirements for the degree of
Doctor of Philosophy

The University of Leeds
School of Mechanical Engineering

December 2019

The candidate confirms that the work submitted is her own, except where work which has formed part of jointly authored publications has been included. The contribution of the candidate and the other authors to this work has been explicitly indicated below. The candidate confirms that appropriate credit has been given within the thesis where reference has been made to the work of others.

Chapters 3, 4 and 5 of this thesis contain work which has been in the jointly authored publication: A. Contreras, M.J. Raxworthy, S. Wood, J.D. Schiffman, G. Tronci. *ACS Appl. Bio Mater* **2019**, 2, 4258. The entirety of the work contained within this publication is directly attributed to myself with support from the co-authors.

This copy has been supplied on the understanding that it is copyright material and that no quotation from the thesis may be published without proper acknowledgement.

© 2019 The University of Leeds and Amy Louise Contreras

Acknowledgements

I would like to thank everyone who has supported me during this research project. Thank you to my supervisors Giuseppe Tronci, Mike Raxworthy and Simon Wood. Thank you to Claire Brockett, Joanne Tipper, Cheryl Harris and Claire Perry for the opportunity to undertake this PhD research and for their help with everything 'CDT-related'. Thank you to the many laboratory managers, technicians and academics who have assisted me over the past 4 years - particularly Sarah Myers, Jackie Hudson, Matty Percival and Tim Smith.

I also gratefully acknowledge both the EPSRC and Neotherix Ltd. for funding this research.

Thank you to Jessica Schiffman and Helen Colley, who hosted me during my external placements at the University of Massachusetts Amherst and the University of Sheffield respectively. Those two placements were amongst the highlights of my PhD experience. I really appreciate the time and effort spent supporting me during my work and for welcoming me into each of your research groups.

Thank you to my friends, and the many students across the University of Leeds and beyond who have helped to make this experience so much more enjoyable.

I owe everything I have achieved to my parents. You support and encourage me in all aspects of my life, and I am eternally grateful.

And finally, Loz. Thank you for everything, every day, but mostly thank you for believing in me unconditionally.

This is for you.

Abstract

The design of advanced biomaterials is a promising strategy to aid the regeneration of oral soft tissue which can be lost during surgery or disease. Bacterial infection is a common surgery-associated complication which could prevent successful tissue integration. Misuse of antibiotics has led to the concerning spread of antimicrobial resistance (AMR) so alternative antibiotic-free treatments need to be explored. PhotoTherix™ is a product concept based on a bioresorbable electrospun polymer scaffold equipped with antimicrobial photodynamic therapy (aPDT) technology aimed for use in maxillofacial applications. Typically, in aPDT, a photosensitiser (PS) is loaded in its inert form and then activated on-demand through a light source to enable its antibacterial function and this principle is central to the PhotoTherix™ concept. To enable translation to clinical use, this thesis aims to investigate how the scaffold architecture, antimicrobial functionality and selectivity can be controlled via variation of chemical and physical properties of the polymer as well as process electrospinning parameters. Fibrous scaffolds based on Food and Drug Administration (FDA)-approved biodegradable polyesters (poly(ϵ -caprolactone) (PCL) and poly(lactic-co-glycolic acid) (PLGA)) were obtained via electrospinning. Electrospinning parameters were investigated to establish defined structure-function relationships. The incorporation and controlled release of two PS (methylene blue and erythrosin B) from the material was studied with regards to scaffold bactericidal effectiveness against two model bacterial strains (*Streptococcus mutans* and *Escherichia coli*). Evaluation of the viability of cells populating the scaffold was performed using L929 fibroblasts to determine cell-scaffold relationships. Finally, the selectivity achievable between the bacterial and mammalian cells was determined through *in vitro* models. The resulting prototype, PhotoTherix™, could be further developed into a commercial medical device aimed to improve patient outcomes, reduce the health economic burden and control the spread of AMR.

Table of Contents

Chapter 1 Literature Review	1
1.1 Clinical Needs.....	1
1.1.1 Oral Soft Tissue Loss	2
1.1.2 Antimicrobial Resistance	5
1.2 Regenerative Biomaterials for Oral Soft Tissue Loss	7
1.2.1 Current Biomaterials for Oral Mucosa Regeneration	7
1.2.1.1 Tissue Grafts	7
1.2.1.1.1 Autograft.....	8
1.2.1.1.2 Allograft/Xenograft.....	9
1.2.1.2 Polymer Scaffolds.....	10
1.2.1.2.1 Natural Polymers.....	12
1.2.1.2.2 Synthetic Polymers.....	13
1.2.1.2.3 Hybrid Polymer Systems	14
1.2.2 Desirable Properties of Polymeric Biomaterials for Oral Mucosa Regeneration	15
1.2.2.1 Biocompatibility	15
1.2.2.2 Biodegradability	16
1.2.2.3 Mechanical Properties	20
1.2.2.4 Manufacture of Fibrous Scaffolds	20
1.2.2.4.1 Wet Spinning.....	21
1.2.2.4.2 Melt Electrospinning.....	21
1.2.2.4.3 Electrospinning.....	22
1.3 Antimicrobial Strategy.....	25
1.3.1 Types of Antimicrobials	26
1.3.1.1 Antimicrobial Photodynamic Therapy.....	27
1.3.1.1.1 Photochemical Mode of Action.....	27
1.3.1.1.2 Photodynamic Therapy in Antimicrobial or Anticancer Strategies	29
1.3.1.1.3 Choice of Photosensitiser.....	30
1.3.1.2 Existing Antimicrobial Photodynamic Therapy Biomaterials.....	31
1.3.1.2.1 Antimicrobial Photodynamic Therapy in Dentistry	33

Chapter 2 PhD Research Aim.....	36
2.1.1 Research Strategies.....	37
2.1.2 Research Objectives	40
Chapter 3 Manufacture and Characterisation of Photosensitiser-Loaded Electrospun Scaffolds	41
3.1 Introduction.....	41
3.2 Materials and Methods	41
3.2.1 Materials.....	41
3.2.2 Electrospinning Solution Preparation.....	42
3.2.3 Viscosity Measurements.....	43
3.2.4 Surface Tension	43
3.2.5 Electrospinning.....	43
3.2.6 Scanning Electron Microscopy	44
3.2.7 Loading Efficiency	44
3.2.8 Brunauer–Emmett–Teller Analysis	44
3.2.9 Porometry.....	45
3.2.10 Scaffold Colour Measurements	45
3.2.11 Differential Scanning Calorimetry	46
3.2.12 Tensile Testing	46
3.2.13 Statistical Analysis.....	46
3.3 Results and Discussion	47
3.3.1 Characterisation of Electrospinning Solutions	47
3.3.1.1 Initial Concentration Determination	47
3.3.1.2 Viscosity and Surface Tension with Photosensitiser Inclusion.....	49
3.3.2 Characterisation of Electrospun Scaffolds.....	52
3.3.2.1 Scaffold Formation.....	52
3.3.2.2 Polymer Scaffold Colour	56
3.3.2.3 Crystallinity	58
3.3.2.4 Mechanical Properties of Scaffolds.....	60
3.4 Conclusion.....	64
Chapter 4 Interactions of Photosensitiser-Loaded Electrospun Scaffolds with Aqueous Medium.....	66
4.1 Introduction.....	66
4.2 Materials and Methods	66
4.2.1 Contact Angle.....	66

4.2.2	Release Kinetics.....	67
4.2.3	Water Uptake Analysis	67
4.2.4	Hydrolytic Degradation	67
4.2.5	Scanning Electron Microscopy	68
4.2.6	Statistical Analysis.....	68
4.3	Results and Discussion	68
4.3.1	Wettability.....	68
4.3.1.1	Contact Angle	68
4.3.1.2	Photosensitiser Release	70
4.3.1.3	Water Uptake.....	72
4.3.2	Degradation.....	74
4.4	Conclusion.....	78
Chapter 5 Selection of Photosensitiser for Antimicrobial Photodynamic Therapy		79
5.1	Introduction.....	79
5.2	Materials and Methods	80
5.2.1	Quantification of Light Intensity	80
5.2.2	General Cell Culture.....	80
5.2.2.1	Cell Culture Materials.....	80
5.2.2.2	Cell Culture Passage	81
5.2.2.3	Cell Culture Counting.....	81
5.2.2.4	Cell Culture Freezing and Thawing.....	82
5.2.3	General Bacterial Culture	82
5.2.3.1	Bacterial Culture Materials.....	82
5.2.3.2	Broth and Agar Plate Preparation	82
5.2.3.3	Bacterial Strain Characterisation.....	83
5.2.3.4	Growth Curve Characterisation.....	84
5.2.4	Photosensitiser Uptake Study	86
5.2.4.1	Mammalian Cells - Photosensitiser Uptake	86
5.2.4.2	Bacteria - Photosensitiser Uptake.....	87
5.2.5	Photosensitiser-Loaded Solution Toxicity.....	88
5.2.5.1	Mammalian Cells - Photosensitiser-Loaded Solution Toxicity.....	88
5.2.5.2	Bacteria - Photosensitiser-Loaded Solutions Antimicrobial Photodynamic Therapy Activity	90
5.2.6	Photosensitiser-Encapsulated PCL Scaffold Toxicity	90

5.2.6.1	Mammalian Cells - Photosensitiser-Encapsulated PCL Scaffold Extract Toxicity.....	90
5.2.6.2	Bacteria - Photosensitiser-Encapsulated PCL Scaffolds Antibacterial Photodynamic Therapy Activity	91
5.2.7	Statistical Analysis.....	93
5.3	Results and Discussion	93
5.3.1	Quantification of Light Intensity	93
5.3.2	Photosensitiser Uptake.....	95
5.3.3	<i>In vitro</i> testing with Photosensitiser-Loaded Solutions....	97
5.3.3.1	Mammalian Cell Photosensitiser-Loaded Solution Testing.....	97
5.3.3.2	Antimicrobial Photodynamic Therapy Capability of Photosensitiser-Loaded Solutions	103
5.3.4	<i>In vitro</i> testing with Photosensitiser-Encapsulated PCL Scaffolds.....	107
5.3.4.1	<i>In vitro</i> Testing of Photosensitiser-Encapsulated PCL Scaffolds on Mammalian Cells.....	108
5.3.4.2	<i>In vitro</i> Testing of Photosensitiser-encapsulated PCL Scaffolds with Bacteria.....	111
5.4	Conclusion	115
Chapter 6 Optimisation of Polymer Carrier with Methylene Blue for Use as a Regenerative Electrospun Scaffold in Oral Environments.....		117
6.1	Introduction	117
6.2	Materials and Methods	118
6.2.1	Materials.....	118
6.2.2	Electrospinning Solution Preparation.....	118
6.2.3	Viscosity Measurements.....	118
6.2.4	Electrospinning.....	119
6.2.5	Scanning Electron Microscopy	119
6.2.6	Loading Efficiency	119
6.2.7	Scaffold Colour Measurements	119
6.2.8	Differential Scanning Calorimetry	119
6.2.9	Tensile Testing	119
6.2.10	Water Uptake Analysis	119
6.2.11	pH Testing.....	119
6.2.12	Hydrolytic Degradation	119

6.2.12.1	Hydrolytic Degradation Trial with Controlled pH in Tris Buffer	119
6.2.12.2	Modified Hydrolytic Degradation	120
6.2.13	Modified Release Kinetics	120
6.2.14	Statistical Analysis.....	120
6.3	Results and Discussion	120
6.3.1	PLGA1090 Characterisation.....	120
6.3.1.1	PLGA1090 Polymer Solution Characteristics.....	120
6.3.1.2	PLGA1090 Electrospun Scaffold Characteristics..	122
6.3.1.3	PLGA1090 Electrospun Scaffold Interactions in Aqueous Medium.....	128
6.3.2	Blended PCL and PLGA1090 Scaffold Characterisation 134	
6.3.2.1	Polymer Blend Solution Characteristics	135
6.3.2.2	Polymer Blend Scaffold Characteristics	136
6.3.2.3	Polymer Blend Scaffold Interactions in Aqueous Medium.....	144
6.3.2.4	5050 Polymer Blend Scaffold with Reduced Methylene Blue Concentrations	148
6.4	Conclusion.....	151
Chapter 7 <i>In vitro</i> Testing of Prototype Scaffolds.....		153
7.1	Introduction.....	153
7.2	Materials and Methods	155
7.2.1	Mammalian Cell Toxicity Testing.....	155
7.2.1.1	Mammalian Cell Extract Testing – Luminosity Assay	155
7.2.1.2	Mammalian Cell Contact Testing – Scanning Electron Microscopy Morphology	155
7.2.2	Antibacterial Photodynamic Therapy Activity Testing...	156
7.2.2.1	Bacteria Extract Testing – Luminosity Assay	156
7.2.2.2	Bacteria Extract Testing – Colony Counting	157
7.2.2.3	Bacteria Contact Testing - Zone of Inhibition	157
7.2.3	Statistical Analysis.....	158
7.3	Results and Discussion	158
7.3.1	Mammalian Cell Cytotoxicity Testing.....	158
7.3.1.1	Mammalian Cell Extract Testing	158
7.3.1.2	Mammalian Cell Contact Testing	163

7.3.2	Antibacterial Photodynamic Therapy Activity of Lead Prototype	168
7.3.2.1	Bacteria Extract Testing	168
7.3.2.2	Bacteria Contact Testing.....	176
7.4	Conclusion	181
	Chapter 8 Discussion.....	184
8.1	General Discussion.....	184
8.1.1	Project Rationale	184
8.1.2	Key Findings.....	184
8.1.2.1	Initial Choice of Polymers for Scaffolds.....	185
8.1.2.2	Selection of Photosensitiser for Antimicrobial Photodynamic Therapy	186
8.1.2.3	Optimisation of Polymers of Polymer Building Blocks for Electrospun Scaffolds	187
8.1.2.4	<i>In vitro</i> Testing of Optimised Prototype Scaffold ...	188
8.2	Commercialisation Discussion	188
8.2.1	Technology Readiness Levels.....	188
8.2.2	Regulation and Classification	191
8.2.3	Use in Dental Surgery	193
8.2.3.1	Gingival Recession treatment	194
8.2.3.2	Split Thickness Tissue Grafting	194
8.2.3.3	Closure of Extraction Socket.....	195
8.2.3.4	Surgical Technique	195
8.2.4	Competitor Analysis.....	196
8.2.5	Patentability.....	197
	Chapter 9 Future Work.....	198
9.1	Choice of Light Source and Exposure Time	198
9.2	Photosensitiser Release Profile Accuracy	198
9.3	Mammalian Cell Cytotoxicity.....	199
9.4	Antimicrobial Photodynamic Therapy Capability Against Oral Bacteria	199
9.5	Sterilisation Methods	200
9.5.1	Additional Use in Chronic Wound Applications.....	201
	Chapter 10 Conclusions	202
	Bibliography	203
	Appendix A	237

List of Tables

Table 1.1 - The physiological components of saliva^[29,30]	3
Table 1.2 – Four main classes of antibiotic agents^[76,77]	6
Table 1.3 –Antimicrobial Resistance (AMR) mechanisms of bacteria against the main classes of antibiotics^[78]	6
Table 1.4 - Advantages and disadvantages of different soft tissue graft sources used in tissue engineering and example commercial products^[86–88].....	8
Table 1.5 – Advantages and disadvantages of the different polymer types used in tissue engineering^[86–88]	11
Table 1.6 - The relative reactivity of different polymer types increases from the top to the bottom of the table^[219]	18
Table 1.7 – Summary of the main classes of photosensitisers for antimicrobial photodynamic therapy	31
Table 1.8 – Examples of photosensitiser and scaffold combinations aimed to treat infections via antimicrobial photodynamic therapy	32
Table 2.1 – Summary of scaffold requirements for oral applications	39
Table 3.1 – Electrospinning Solution Surface Tension. Results reported as Mean±SD (n=3).....	51
Table 3.2 - Loading efficiency (LE) and percent release measured in PCL and PLGA7525 scaffolds electrospun in the presence of either MB or ER. Results reported as Mean±SD (n=3).	53
Table 3.3 – LAB colour space results for PS-loaded scaffolds. Colours of associated rows represent the colour of the scaffold as per the LAB result.	57
Table 3.4 – DSC Thermal Analysis Values for PCL or PLGA7525 samples of either ‘Raw’ polymer pellets, PS-free (ND) control scaffolds, MB-incorporated scaffolds or ER-incorporated scaffolds	59
Table 5.1 – Summary of average light intensity tested in various experimental conditions. No water refers to readings taken without the presence of the water bath. The energy density values are calculated from light intensity values with water bath. Results reported as Mean±SD (n=3)	94
Table 5.2 – Conversion of concentration of photosensitiser in solution into molarity.....	100
Table 5.3 – A set of live/dead images showing an example set of the data from testing <i>E. coli</i> bacteria on PCL-PS scaffolds following 60 minute light exposure	112

Table 6.1 – DSC Thermal Analysis Values for PLGA1090 samples of either ‘Raw’ polymer pellets, PS-free (ND) control scaffold samples or MB-incorporated scaffold samples.....	125
Table 6.2 – pH Values of the PBS supernatant containing the Pol-MB scaffold following 4-weeks incubation at 37°C. Results reported as Mean±SD (n=3).....	131
Table 6.3 – LAB colour space results for PS-loaded scaffolds. Colours of associated rows of the table represent the colour of the scaffold as per the LAB result.....	137
Table 6.4 – DSC Thermal Analysis Values for pure and blended scaffolds for PS-free (ND) control samples	140
Table 6.5 – DSC Thermal Analysis Values for pure and blended scaffolds with MB inclusion	140
Table 6.6 – Comparison of DSC Thermal Analysis Values for 5050 polymer blended scaffolds with MB inclusion at a higher and lower concentration	150
Table 7.1 – ISO 10993 morphological grading of cells ^[192]	154
Table 7.2 – Series of Solutions and Incubation Times for Dehydrating Cells on Scaffold Samples prior to Scanning Electron Microscopy.....	156
Table 7.3 – Expected concentrations of MB in extract solutions collected following 0, 2 or 24 hour incubations times	159
Table 8.1 – Technology Readiness Level (TRL) description^[538]....	189
Table 8.2 – Medical device classifications^[542]	192
Table 10.1 – Summary of scaffold requirements for oral applications	202

List of Figures

Figure 1.1 - The structural components of the human oral mucosa^[26]	2
Figure 1.2 - The states of polymer arrangement: crystalline, amorphous and semi-crystalline	19
Figure 1.3 - The basic electrospinning apparatus^[125,248]	22
Figure 1.4 - The process of applied voltage resulting in a Taylor cone being generated at the needle tip of electrospinning apparatus^[269]	23
Figure 1.5 – General membrane structure of (A) Gram-negative and (B) Gram-positive bacteria^[284]	25
Figure 1.6 - Jablonski diagram showing the movement of electrons upon light stimulation within a photosensitiser (PS). ⁰PS: PS Ground State; ¹PS*: PS Excited Singlet State; ³PS*: PS Excited Triplet State; hv: Light Energy; ISC: Inter-System Crossing; ROS: Reactive Oxygen Species^[313]	28
Figure 2.1 - The light activation of the incorporated PS (photosensitiser) within the biodegradable polymer scaffold initiating antimicrobial activity.....	36
Figure 2.2 – Design and clinical applicability of photodynamically-active electrospun fibrous scaffolds for antibiotic-free infection control	37
Figure 3.1 - (A-D): Chemical structure of selected polymers and PS. (A): Poly(ϵ-caprolactone) (PCL); (B): Poly[(rac-lactide)-co-glycolide] (PLGA7525) with 75:25 monomer ratio; (C): Methylene Blue (MB); (D): Erythrosin B (ER).....	42
Figure 3.2 - Viscosity of electrospinning polymer solutions at different concentrations in HFIP. (■): PCL-ND-6 wt.%; (■): PCL-ND-9 wt.%; (●): PLGA7525-ND-6 wt.%; (●): PLGA7525-ND-9 wt.%; (●): PLGA7525-ND-12 wt.%. Lines are guidelines to the eye	48
Figure 3.3 - Scanning Electron Micrographs to determine fibre morphology from electrospinning different concentrations of PLGA7525 and PCL solutions. Electrospinning was not possible for the PCL-ND 12 wt.% formulation due to high viscosity.....	49
Figure 3.4 - Viscosity of native and PS-loaded electrospinning polymer solutions. (■): PCL-ND; (■): PCL-MB; (■): PCL-ER; (●): PLGA7525-ND; (●): PLGA7525-MB; (●): PLGA7525-ER. Lines are guidelines to the eye.	50

Figure 3.5 - Microstructural analysis of PS-encapsulated scaffolds and electrospun controls. SEM images taken at 1000x magnification and Specific Surface Area (SSA) measurements obtained via BET analysis.....	52
Figure 3.6 - (A) Average Fibre Diameter determined from SEM images for each electrospun scaffold. (B) Average Mean Flow Pore Size determined from porometry analysis for each electrospun scaffold. Grey bars: Control scaffolds; Blue bars: MB-included scaffolds; Red bars: ER-included scaffolds. Results reported as Mean±SD (n=3). ‘*’ denotes significantly different means ($p < 0.05$, t-test).....	54
Figure 3.7 - Pore size distribution of scaffold types. (A) PCL scaffolds; (B) PLGA7525 scaffolds. Black lines: Polymer-ND scaffolds; Blue lines: Polymer-MB scaffolds; Red lines: Polymer-ER scaffolds. Values of mean flow pore size (μm) are given for each scaffold type. Results reported as Mean±SD (n=3).....	55
Figure 3.8 - Macroscopic images of PS-free and PS-encapsulated scaffolds.....	56
Figure 3.9 – (A) Encapsulation of MB in the monomeric state results in a blue colour of respective fibres. (B) Aggregation of MB molecules results in a purple colour of PS-encapsulated fibres^[420].....	58
Figure 3.10 – Differential Scanning Calorimetry heat flow plots of (A) PCL scaffolds and (B) PLGA7525 scaffolds. (—): Unprocessed polymer; (—): Pol-ND scaffolds; (—): Pol-MB scaffolds; (—): Pol-ER scaffolds.....	59
Figure 3.11 - (A): Stress-strain curve of PS-encapsulated scaffolds and electrospun controls. (—): PCL-ND; (—): PCL-MB; (—): PCL-ER; (...): PLGA7525-ND; (...): PLGA7525-MB; (...): PLGA7525-ER. (B): Experimental setup employed during tensile testing.....	61
Figure 3.12 (A) Elastic Modulus (E) and (B) Strain at Break (ϵ) measured in PCL or PLGA7525 samples (C) Ultimate Toughness (U_T). Grey bars: control polymer scaffolds; Blue bars: MB-loaded scaffolds; Red bars: ER-loaded scaffolds. Results reported as Mean±SD (n=3). ‘*’ denotes significantly different means ($p < 0.05$, t-test).....	62
Figure 4.1 - Water contact angle (WCA) images and measurements on dry PS-encapsulated and PS-free (ND) samples in the form of electrospun scaffold (top) and film (bottom). Results reported as Mean±SD (n=3). (a)-(c): significantly different means ($p < 0.05$, t-test).....	69

Figure 4.2 - Typical PS release profiles measured via UV-Vis spectroscopy of the supernatant collected during incubation (PBS, 37 °C) of MB- and ER-encapsulated scaffolds at selected time points over (A): 6 hours or (B): 672 hours (4 weeks). (-■-): PCL-MB; (-■-): PCL-ER; (·▲·): PLGA7525-MB; (·▲·): PLGA7525-ER. Lines are guidelines to the eye. Results reported as Mean±SD (n=3).....	71
Figure 4.3 – Water uptake measured gravimetrically following incubation (H ₂ O, 37 °C) of either PS-loaded or electrospun control (ND) samples. Grey bars: Polymer-ND scaffolds; Blue bars: Polymer-MB scaffolds; Red bars: Polymer-ER scaffolds. Results reported as Mean±SD (n=3). ‘*’ denotes significantly different means ($p < 0.05$, t -test).....	73
Figure 4.4 - Scanning Electron Microscopy (SEM) of electrospun PCL scaffolds following 8-week incubation in PBS at 37 °C ...	75
Figure 4.5 - Scanning Electron Microscopy (SEM) of electrospun PLGA7525 scaffolds following 8-week incubation in PBS at 37 °C	75
Figure 4.6 – Mass loss measured on PS-encapsulated or PS-free control (ND) samples following hydrolytic degradation (PBS, 37 °C). (-■-): PCL-ND; (-■-): PCL-MB; (-■-): PCL-ER; (·◀·): PLGA7525-ND; (·◀·): PLGA7525-MB; (·◀·): PLGA7525-ER. Lines are guidelines to the eye. Results reported as Mean±SD (n=3)	76
Figure 4.7 – Macroscopic volume change of (A) PCL scaffolds and (B) PLGA7525 scaffolds following 1 week incubation in PBS. The yellow grid has 1 cm ² dimensions.....	77
Figure 5.1 – Examples of Gram-Staining of two bacterial strains used in this study. (A) <i>Escherichia coli</i> (<i>E. coli</i>) 11954 (gram-negative); (B) <i>Streptococcus mutans</i> (<i>S. mutans</i>) Ingbritt (gram-positive)	84
Figure 5.2 – OD ₆₀₀ with respect to time of bacterial suspensions. Orange: <i>E. coli</i> 11954; Purple: <i>S. mutans</i> Ingbritt; (←→): Mid-log phase. Results reported as Mean±SD (n=3)	85
Figure 5.3 – Experimental setup for light activation step. Water bath was used to dissipate any heat which may arise from the light source during exposure time. (A): Light off; (B): Light on. ■: Location of well plate during experiment; ■: Arrow represents 15 cm.....	89

- Figure 5.4 – PS Uptake by either cells or bacteria during a 2 hour incubation in PS-loaded solutions. ■: MB-loaded PBS solutions; ■: ER-loaded PBS solutions. (A) L929 mammalian cells, (B) *S. mutans* Ingbritt gram-positive bacteria, (C) *E. coli* 11954 gram-negative bacteria. Results reported as Mean±SD (n=3). ‘*’ denotes significantly different means ($p < 0.05$, *t*-test) 96**
- Figure 5.5 - L929 Solution Toxicity. (A) 30 min ‘dark’ control; (B) 30 min light exposure. (C) 60 min ‘dark’ control; (D) 60 min light exposure. ■: MB-loaded PBS solutions; ■: ER-loaded PBS solutions; □: fresh PBS negative control; ■: PBS-Triton™ X-100 solution positive control. Results reported as Mean±SD (n=3). ‘*’ denotes significantly different means ($p < 0.05$, *t*-test) 98**
- Figure 5.6 - L929 Solution Toxicity Comparison with three photosensitisers. (A) 30 min ‘dark’ control; (B) 30 min light exposure. (C) 60 min ‘dark’ control; (D) 60 min light exposure. ■: MB-loaded PBS solutions; ■: TB-loaded PBS solutions; ■: NMB-loaded PBS solutions. Results reported as Mean±SD (n=3). ‘*’ denotes significantly different means ($p < 0.05$, *t*-test) 102**
- Figure 5.7 – Bactericidal toxicity of *S. mutans* following incubation in PBS solutions containing PS. (A) 30 min ‘dark’ control; (B) 30 min light exposure. (C) 60 min ‘dark’ control; (D) 60 min light exposure. ■: MB-loaded PBS solutions; ■: ER-loaded PBS solutions; □: fresh PBS negative control; ■: PBS-Triton™ X-100 solution positive control. Results reported as Mean±SD (n=3). ‘*’ denotes significantly different means ($p < 0.05$, *t*-test) 104**
- Figure 5.8 – Bactericidal toxicity of *E. coli* following incubation in PBS solutions containing PS. (A) 30 min ‘dark’ control; (B) 30 min light exposure. (C) 60 min ‘dark’ control; (D) 60 min light exposure. ■: MB-loaded PBS solutions; ■: ER-loaded PBS solutions; □: fresh PBS negative control; ■: PBS-Triton™ X-100 solution positive control. Results reported as Mean±SD (n=3). ‘*’ denotes significantly different means ($p < 0.05$, *t*-test) 105**
- Figure 5.9 – L929 monolayer cytotoxicity following application of PCL scaffold PBS extract solution. (A) 30 min ‘dark’ control; (B) 30 min light exposure. (C) 60 min ‘dark’ control; (D) 60 min light exposure. ■: PCL-ND control scaffold extract solutions; ■: PCL-MB scaffold extract solutions; ■: PCL-ER scaffold extract solutions; □: fresh PBS negative control; ■: PBS-Triton™ X-100 solution positive control. Results reported as Mean±SD (n=3). ‘*’ denotes significantly different means ($p < 0.05$, *t*-test) 109**

- Figure 5.10 – Log reductions of *E. coli* bacteria on PCL scaffolds. (A) 30 min ‘dark’ control; (B) 30 min light exposure. (C) 60 min ‘dark’ control; (D) 60 min light exposure. ■: PCL-ND control scaffolds; ■: PCL-MB scaffolds; ■: PCL-ER scaffolds; □: Fresh M9 medium negative control; ■: Ethanol positive control. Results reported as Mean±SD (n=3)..... 113
- Figure 6.1 – Viscosity of PS-free (ND) electrospinning polymer solutions at different concentrations in HFIP. (▲): PLGA1090-ND-6 wt.%; (▲): PLGA1090-ND-9 wt.%; (■): PCL-ND-6 wt.%; (●): PLGA7525-ND-12 wt.%. Lines are guidelines to the eye 121
- Figure 6.2 – Viscosity of electrospinning polymer solutions at different concentrations in HFIP at 6 wt.% polymer concentration with or without 2.2mM MB. (▲): PLGA1090-ND; (▲): PLGA1090-MB. Lines are guidelines to the eye 122
- Figure 6.3 – Microstructural analysis of MB-encapsulated scaffolds and electrospun ‘ND’ controls. SEM images taken at 1000x magnification and Specific Surface Area (SSA) measurements obtained via BET analysis 123
- Figure 6.4 – Average Fibre Diameter determined from SEM images for each PLGA1090 electrospun scaffold. Grey bars: Control scaffolds; Blue bars: MB-included scaffolds. Results reported as Mean±SD (n=3). ‘*’ denotes significantly different means ($p < 0.05$, t -test) 124
- Figure 6.5 – Differential Scanning Calorimetry heat flow plots. (—): Unprocessed PLGA1090 polymer; (—): PLGA1090-ND scaffolds; (—): PLGA1090-MB scaffolds..... 125
- Figure 6.6 – Stress-strain curve of PS-encapsulated PLGA1090 polymer scaffolds. (—): PLGA1090-ND; (—): PLGA1090-MB 126
- Figure 6.7 – Mechanical properties measured in PLGA1090 samples. (A) Elastic Modulus (E); (B) Strain at Break (ϵ) and (C) Ultimate Toughness (U_T). Grey bars: control polymer scaffolds; Blue bars: MB-loaded scaffolds. Results reported as Mean±SD (n=3). ‘*’ denotes significantly different means ($p < 0.05$, t -test) 127
- Figure 6.8 – Water uptake measured gravimetrically following incubation (H_2O , $37\ ^\circ C$) of either PS-loaded or electrospun control PLGA1090 samples. Grey bars: Pol-ND scaffolds; Blue bars: Pol-MB scaffolds. Results reported as Mean±SD (n=3)128
- Figure 6.9 – Mass loss measured on samples following hydrolytic degradation in PBS (PBS, $37\ ^\circ C$). (-●-): PLGA1090-ND; (-●-): PLGA1090-MB. Lines are guidelines to the eye. Results reported as Mean±SD (n=3)..... 129
- Figure 6.10 – Scanning Electron Microscopy (SEM) of electrospun PLGA1090 scaffolds. W1 and W2 refer to 1 week and 2 weeks incubation time points 130

Figure 6.11 - Mass loss measured on samples following hydrolytic degradation in PBS with controlled pH (PBS, 37 °C, pH ~7.4). (●): PLGA1090-ND; (●): PLGA1090-MB. Lines are guidelines to the eye. Results reported as Mean±SD (n=3).....	132
Figure 6.12 - Scanning Electron Microscopy (SEM) of electrospun PLGA1090 scaffolds. W1 and W2 refer to 1 week and 2 weeks incubation time points.....	132
Figure 6.13 – Typical PS release profile measured via UV-Vis spectroscopy of the supernatant collected during incubation with controlled pH (PBS, 37 °C, pH ~7.4) from PLGA1090-MB scaffolds at selected time points over 672 hours (4 weeks). Line is guideline to the eye. Results reported as Mean±SD (n=3)	133
Figure 6.14 – Viscosity of electrospinning PCL and PLGA1090 polymer blend solutions at different concentrations in HFIP. (◆):8020-ND; (◆):8020-MB; (★):5050-ND; (★):5050-MB; (▶):2080-ND; (▶): 2080-MB. Lines are guidelines to the eye	135
Figure 6.15 – Microstructural analysis of PS-encapsulated PCL and PLGA1090 electrospun polymer blend scaffolds and controls. SEM images taken at 1000x magnification	136
Figure 6.16 – Average Fibre Diameter determined from SEM images for each PCL and PLGA1090 polymer blend electrospun scaffold. Grey bars: Control scaffolds; Blue bars: MB-included scaffolds. Results reported as Mean±SD (n=3). ‘*’ denotes significantly different means ($p < 0.05$, t -test)	138
Figure 6.17 - Differential Scanning Calorimetry heat flow plots of PCL:PLGA1090 blended polymer scaffolds. (A) 80:20, (B) 50:50, (C) 20:80 polymer blends. (—): Polymer-ND scaffolds; (—): Polymer-MB scaffolds	139
Figure 6.18 - Differential Scanning Calorimetry heat flow plots of the first cycle from PCL:PLGA1090 blended polymer scaffolds at 80:20 ratio and MB (—)	141
Figure 6.19 - Stress-strain curve of PS-encapsulated PCL and PLGA1090 polymer blend scaffolds. (—): 8020-ND; (—): 8020-MB; (---): 5050-ND; (---): 5050-MB; (...): 2080-ND; (...): 2080-MB	142
Figure 6.20 – Mechanical properties measured in PCL and PLGA1090 polymer blend samples. (A) Elastic Modulus (E); (B) Strain at Break (ϵ) and (C) Ultimate Toughness (U_T). Grey bars: control polymer scaffolds; Blue bars: MB-loaded scaffolds. Results reported as Mean±SD (n=3). ‘*’ denotes significantly different means ($p < 0.05$, t -test)	143

- Figure 6.21 – Water uptake measured gravimetrically following incubation (H₂O, 37 °C) of either PS-loaded or electrospun control PCL and PLGA1090 polymer blend samples. Grey bars: ND scaffolds; Blue bars: MB scaffolds. Results reported as Mean±SD (n=3). ‘*’ denotes significantly different means ($p < 0.05$, t -test) 144
- Figure 6.22 – Mass loss measured on PCL and PLGA1090 polymer blend samples following hydrolytic degradation in PBS with controlled pH (PBS, 37 °C, pH ~7.4). (■):8020-ND; (■):8020-MB; (●):5050-ND; (●):5050-MB; (▲):2080-ND; (▲):2080-MB. Lines are guidelines to the eye. Results reported as Mean±SD (n=3) 145
- Figure 6.23 – Scanning Electron Microscopy (SEM) of electrospun PLGA1090 scaffolds. W1, W2, W6 and W8 refers to 1, 2, 6 and 8 week incubation time points respectively. N/A samples had degraded so were unable to be analysed 146
- Figure 6.24 – Typical PS release profiles measured via UV-Vis spectroscopy of the supernatant collected during incubation with controlled pH (PBS, 37 °C, pH ~7.4) from MB-incorporated scaffolds at selected time points over (A) 6 hours or (B) 672 hours (4 weeks). (■):8020-MB; (●):5050-MB; (▲):2080-MB. Lines are guidelines to the eye. Results reported as Mean±SD (n=3) 147
- Figure 6.25 – Microstructural analysis of MB-encapsulated electrospun polymer blend (5050) scaffolds from electrospinning solutions with various concentrations of MB. 0.2mM: 10% MB; 1.1mM: 50% MB; 2.2mM: 100% MB. SEM images taken at 1000x magnification 148
- Figure 6.26 - Average Fibre Diameter determined from SEM images for each MB concentration of 5050 polymer blend electrospun scaffold. Results reported as Mean±SD (n=3). ‘*’ denotes significantly different means ($p < 0.05$, t -test) 149
- Figure 6.27 - Differential Scanning Calorimetry heat flow plots of 5050 PCL:PLGA1090 blended polymer scaffolds with a reduced MB concentration. (—): 10%-MB 5050 scaffolds 150
- Figure 7.1 – Experimental setup schematic for ‘Zone of Inhibition’ microbiological testing 155
- Figure 7.2 - L929 extract solution toxicity. (A) 30 min ‘dark’ control; (B) 30 min light exposure. (C) 60 min ‘dark’ control; (D) 60 min light exposure. Solutions extracted from various 5050 polymeric electrospun scaffolds. ■: MB-free (ND) controls; ■: 100%-MB; ■: 50%-MB; ■: 10%-MB; □: fresh PBS negative control; ■: PBS-Triton™ X-100 solution positive control; (–): 30% reduction in cell viability. Results below this line are accepted as ‘non-cytotoxic’ in line with ISO 10993. Results reported as Mean±SD (n=3) 160

Figure 7.3 - L929 Extract Solution Toxicity with no pre-incubation prior to light activation. L929 Extract Solution Toxicity. (A) 30 min 'dark' control; (B) 30 min light exposure. (C) 60 min 'dark' control; (D) 60 min light exposure. Solutions extracted from various 5050 polymeric electrospun scaffolds. ■: MB-free (ND) controls; ■: 100%-MB; ■: 50%-MB; ■: 10%-MB; □: fresh PBS negative control; ■: PBS-Triton™ X-100 solution positive control; (--) : 30% reduction in cell viability. Results below this line are accepted as 'non-cytotoxic' in line with ISO 10993. Results reported as Mean±SD (n=3)..... 162

Figure 7.4 - L929 Cell Morphology following 30 or 60 minutes light activation (or kept in the dark as a control) and then 24 hours incubation on electrospun scaffolds. Scanning electron micrographs taken at 1000x or 4000x magnification 165

Figure 7.5 - L929 Cell Morphology following 30 or 60 minutes light activation (or kept in the dark as a control) and then 7 days incubation on electrospun scaffolds. Scanning electron micrographs taken at 1000x or 4000x magnification 166

Figure 7.6 – *S. mutans* Extract Solution Toxicity with no pre-incubation time prior to light activation. (A) 30 min 'dark' control; (B) 30 min light exposure. (C) 60 min 'dark' control; (D) 60 min light exposure. Solutions extracted from various 5050 polymeric electrospun scaffolds. ■: MB-free (ND) controls; ■: 10%-MB; □: fresh PBS negative control; ■: PBS-Triton™ X-100 solution positive control. Results reported as Mean±SD (n=3). '' denotes significantly different means ($p < 0.05$, *t*-test)..... 169**

Figure 7.7 – *E. coli* Extract Solution Toxicity with no pre-incubation time prior to light activation. (A) 30 min 'dark' control; (B) 30 min light exposure. (C) 60 min 'dark' control; (D) 60 min light exposure. Solutions extracted from various 5050 polymeric electrospun scaffolds. ■: MB-free (ND) controls; ■: 10%-MB; □: fresh PBS negative control; ■: PBS-Triton™ X-100 solution positive control. Results reported as Mean±SD (n=3). '' denotes significantly different means ($p < 0.05$, *t*-test)..... 170**

Figure 7.8 – Example set of plates grown overnight of *E. coli* suspended in extract solutions from 10% MB scaffolds. D: Dark controls; L: Light controls; PBS: Positive control; 0hr, 2hr, 24hr: Time of incubation prior to extract solution collection. All plates presented are 10^{-6} dilution from the original inoculation to allow for direct visual comparison.... 172

Figure 7.9 – *S. mutans* Extract Solution Toxicity with Agar Plate Testing for 10%-MB Scaffolds. (A) 30 min 'dark' control; (B) 30 min light exposure. (C) 60 min 'dark' control; (D) 60 min light exposure. Solutions extracted from various 5050 polymeric electrospun scaffolds. Results reported as Mean±SD (n=3). '' denotes significantly different means ($p < 0.05$, *t*-test)..... 173**

- Figure 7.10 – *E. coli* Extract Solution Toxicity with Agar Plate Testing for 10%-MB Scaffolds. (A) 30 min ‘dark’ control; (B) 30 min light exposure. (C) 60 min ‘dark’ control; (D) 60 min light exposure. Solutions extracted from various 5050 polymeric electrospun scaffolds. Results reported as Mean±SD (n=3). ‘**’ denotes significantly different means ($p < 0.05$, *t*-test)..... 174**
- Figure 7.11 – Zone of Inhibition Plates for (A) *S. mutans* or (B) *E. coli*. (···): Example zone of inhibition measured; (1): ND (MB-free) control scaffold; (2): 10%-MB; (3): 50%-MB; (4): 100%-MB; (30D) 30 min ‘dark’ control; (30L): 30 min light exposure; (60D): 60 min ‘dark’ control; (60L): 60 min light exposure 177**
- Figure 7.12 – *S. mutans* Zone of Inhibition Testing. (A) 30 min ‘dark’ control; (B) 30 min light exposure. (C) 60 min ‘dark’ control; (D) 60 min light exposure. Results reported as Mean±SD (n=3). ‘**’ denotes significantly different means ($p < 0.05$, *t*-test) 178**
- Figure 7.13 – *E. coli* Zone of Inhibition Testing. (A) 30 min ‘dark’ control; (B) 30 min light exposure. (C) 60 min ‘dark’ control; (D) 60 min light exposure. Results reported as Mean±SD (n=3). ‘**’ denotes significantly different means ($p < 0.05$, *t*-test) 179**
- Figure 8.1 – A collection of the formulations discussed in each chapter of this thesis. □: successful formulations following that stage of development; ■: final formulation (lead prototype). Abbreviations were explained in the relevant chapter. 185**

List of Equations

Equation 3.1 – Loading Efficiency	44
Equation 3.2 – Young-Laplace	45
Equation 4.1 – Percentage Water Uptake	67
Equation 4.2 – Percentage Mass Loss	68
Equation 5.1 – Cell Concentration	81
Equation 5.2 – Colony Forming Units.....	85
Equation 5.3 - CFU <i>E. coli</i>	86
Equation 5.4 – CFU <i>S. mutans</i>	86
Equation 5.5 – Percentage Cell PS Uptake	87
Equation 5.6 – Percentage Bacterial PS Uptake	88
Equation 5.7 – Percentage Killing.....	89
Equation 5.8 – Log Reduction of Live Bacteria	93

Presentations, Publications and Collaborations

Conference posters	<p>A.L. Smith. 2018. Light Activated Antimicrobial Biomaterials. BioMedEng18, 06-09.09.2018, Imperial College London.</p> <p>A.L. Smith. 2017. Tissue Repair Capacity of a Prototype Antimicrobial-Releasing Scaffold. CDT/DTC Industry Day. 26.01.17. The Village - Urban Resort Leeds North, Leeds.</p> <p>A.L. Smith. Tissue Repair Capacity of a Prototype Antimicrobial-Releasing Scaffold. L IMM Symposium. 21.04.17. Wellcome Trust Brenner Building, Leeds.</p> <p>A.L. Smith. 2017. Tissue Repair Capacity of a Prototype Antimicrobial-Releasing Scaffold. CDT Annual Joint Conference. 09.10.17. Royal Armouries Museum, Leeds.</p> <p>A.L. Smith. 2016. Tissue Repair Capacity of Prototype Antimicrobial-Releasing Scaffold. EPSRC & MRC Centre of Doctoral Training (CDT) in Regenerative Medicine. 08.07.16. University of Manchester.</p> <p>A.L. Smith. 2016. Tissue Repair Capacity of Prototype Antimicrobial-Releasing Scaffold. CDT Poster Evening. 05.05.16. University of Leeds.</p>
Conference oral presentations	<p>A.L. Contreras. 2019. Optimisation of Photodynamically Active Electrospun Scaffolds for Antibiotic-Free Infection Control. School of Dentistry Research Day, 11.07.2019, University of Leeds.</p> <p>A.L. Contreras. 2019. Photodynamically Active Electrospun Scaffolds for Antibiotic-Free Infection Control. Royal Society of Chemistry Biomaterials</p>

	<p>Conference,09-11.01.2019, University of Liverpool (First Place Prize).</p> <p>A.L. Contreras. 2018. On-Demand Activation of an Antimicrobial Biomaterial for Oral Soft Tissue Regeneration. BiTEG, 17.12.2018, University of Sheffield.</p> <p>A.L. Smith. 2017. University of Massachusetts Amherst Laboratory Placement. CDT TERM External Placement Presentations. 19.09.17. University of Leeds.</p>
Journal publications	<p>A. Contreras, M.J. Raxworthy, S. Wood, J.D. Schiffman, G. Tronci. <i>ACS Appl. Bio Mater</i> 2019, 2, 4258.</p>
Collaboration/ visits	<p>Dr H. Colley. Department of Clinical Dentistry - University of Sheffield, June-August 2018.</p> <p>Prof. J. Schiffman. Department of Chemical Engineering – University of Massachusetts Amherst. June-August 2017.</p>

Abbreviations

1,1,1,3,3,3-hexafluoro-2-propanol	HFIP
Active Implantable Medical Devices	AIMD
Adenosine Triphosphate	ATP
Antimicrobial photodynamic therapy	aPDT
Antimicrobial resistance	AMR
Arg-Gly-Asp Peptide	RGD
Brain Heart Infusion	BHI
British Standards Institute	BSI
Brunauer–Emmett–Teller	BET
Carbenicillin	Carb
Centers for Disease Control and Prevention	CDC
Colony Forming Units	CFU
Columbia Blood Agar Base	CB
Differential Scanning Calorimetry	DSC
Dilution Factor	DF
Dimethyl sulfoxide	DMSO
Distilled water	dH ₂ O
Elastic Modulus	<i>E</i>
Erythrosin B	ER
Escherichia coli	<i>E. coli</i>
European Union	EU
Excited singlet state	¹ PS*
Extracellular Matrix	ECM
Fetal Bovine Serum	FBS
Glass Transition Temperature	T _g
Green fluorescent protein	GFP
Ground state	⁰ PS
Highest occupied molecular orbital	HOMO
Human amniotic membranes	HAM
Hydrochloric Acid	HCl

International Organization for Standardization	ISO
Inter-system crossing	ISC
Loading Efficiency	LE
Lowest unoccupied molecular orbital	LUMO
Luria-Bertani media	LB
Medical Device Directive	MDD
Medical Device Regulation	MDR
Medicines and Healthcare Products Regulatory Agency	MHRA
Melting Point Temperature	T_m
Methylene blue	MB
Minimum Essential Media Eagle – alpha modification	α -MEM
Mouse Fibroblast Cells	L929
National Health Service	NHS
New Methylene Blue	NMB
No Dye	ND
Optical Density (Absorbance) at 600 nm	OD ₆₀₀
Percentage Elongation at Break	ϵ
Phosphate Buffered Saline	PBS
Photosensitiser	PS
Poly(ethylene glycol)	PEG
Poly(glycolic acid)	PGA
Poly(lactic acid)	PLA
Poly(<i>rac</i> -lactic-co-glycolic acid)	PLGA
PLGA with 10:90 ratio of lactide:glycolide monomers	PLGA1090
PLGA with 75:25 ratio of lactide:glycolide monomers	PLGA7525
Poly(ϵ -caprolactone)	PCL
Propidium iodide	PI
Reactive oxygen species	ROS
Replace, Reduce, Refine	3Rs
Scanning Electron Microscopy	SEM
Small and Medium Enterprises	SMEs
Small intestinal mucosa	SIS
Specific Surface Area	SSA

<i>Streptococcus mutans</i>	<i>S. mutans</i>
Surface Tension	σ
Technology Readiness Level	TRL
Thermogravimetric Analysis	TGA
Toluidine Blue O	TB
Triplet excited state	³ PS*
Tyr-Ile-Gly-Ser-Arg Peptide	YIGSR
Ultimate Toughness	U_T
Ultraviolet-visible	UV-vis
Unique Device Identification	UDI
US Food and Drug Administration	FDA
Water Uptake	WU
World Health Organisation	WHO
Zone of inhibition	ZOI

Chapter 1 Literature Review

1.1 Clinical Needs

The field of regenerative medical devices began to gain momentum in the 1980s^[1]. This rise in popularity was due to the shortage of donors for organ/tissue transplantation causing an increasing demand from surgeons to regenerate a range of damaged tissue within the human body^[2]. The combined efforts of scientists and engineers towards this common goal has led to the development of a range of biomaterial scaffolds which can be used alone^[3,4] or in combination with cells^[5,6] and bioactive agents^[7,8].

The field of dentistry requires medical device products to aid regeneration of hard and soft tissue in the oral cavity^[9]. Difficulties arise here as the mouth is a moist environment made up of lytic enzymes and over 700 bacterial species as well as having a complex structure with distinct regions owing different patterns of keratinisation^[10,11]. Biomaterials used in this context would need to tolerate the harsh, high moisture environment without degrading before repair and neotissue formation has occurred^[12].

A commonly occurring issue with oral surgeries is bacterial infection^[9]. One study found that up to 10% of dental implant surgeries result in postoperative bacterial infection^[13]. These infections could lead to graft loss or the need for further surgical interventions^[14]. Current infection treatments rely on oral antibiotics but, due to the alarming rise in antimicrobial resistance (AMR), antibiotic-free infection control techniques are being explored^[15-17].

Antimicrobial photodynamic therapy (aPDT) is an alternative treatment which uses photosensitisers (PS) to kill bacterial cells locally following application of convenient light sources without the need to administer antibiotics^[18]. There now arises an opportunity to develop a new regenerative medical device in the form of a biomaterial scaffold with controlled degradability and the ability to support the formation of new soft tissue whilst displaying on-demand bactericidal activity through incorporated PS.

1.1.1 Oral Soft Tissue Loss

The oral cavity consists of a range of soft and hard tissues^[19]. The oral mucosa is the mucous membrane of soft tissue lining the oral cavity and can be divided into three main sections^[20]:

- Sensory mucosa e.g. taste buds on the tongue^[20]
- Lining mucosa e.g. cheeks and soft palate^[20]
- Masticatory mucosa e.g. gingiva^[20]

The oral mucosa is a very specialised tissue covering under 5% of the total human body and has a structure more similar to skin than any other mucous membrane^[21,22]. The main differences between the oral mucosa and skin are that the oral mucosa is moist, it does not contain hair follicles or sweat glands, it is more permeable than skin, it has different keratinization patterns and it appears more pink in colour due to a greater degree of vascularisation^[19,23–25]. There are two main structural components which make up the oral mucosa; the epithelium and the lamina propria (**Figure 1.1**)^[26].

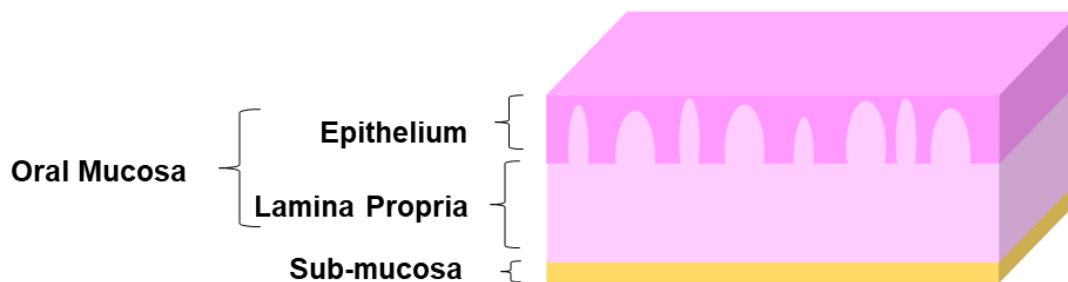


Figure 1.1 - The structural components of the human oral mucosa^[26]

The upper, stratified epithelial layer is predominantly made up of epithelial cells^[10,22]. The lower lamina propria comprises of a combination of connective tissues, fibroblasts, capillaries and extracellular matrix (ECM)^[10,22]. Below this lies the sub-mucosa.

The function of the oral mucosa is to provide protection to the periodontal tissues from harmful environmental (e.g. chemical or mechanical)

stimuli and bacterial infections^[27,28]. The physiological conditions within the oral cavity are unlike those on the skin^[29,30]. This is largely due to the presence of saliva^[29,30] (**Table 1.1**).

Parameter	Value
pH	5.5-7.0
Continuous available volume (µl)	696±312
Viscosity (mPa.s)	1.1±0.1
Protein Present (mg/ml)	0.7±0.3

Table 1.1 - The physiological components of saliva^[29,30]

Wounds within the oral mucosa heal more quickly and result in less scarring than those within the skin^[31]. In a study directly comparing oral mucosal healing to skin healing in pigs, small gingiva wounds showed no scab formation at day 7 and were clinically closed by day 14^[31]. At day 28, the oral wound was hard to distinguish from the rest of the oral mucosa^[31]. Comparatively, even after 49 days the same sized skin wounds were clearly visible^[31].

However, complications arise when large amounts of oral mucosa tissue are lost through disease, accidents and congenital defects^[32-37]. Large tissue defects cannot be healed naturally which results in a loss of barrier function, resulting in a potentially negative physiological and psychological impact on the patient due to the aesthetic and functional importance of the maxillofacial tissues^[38].

Common causes of oral mucosa damage or loss include oral cancer, congenital defects, periodontal disease and peri-implantitis^[39,40]. In the UK, oral cancer incidence rates are continually increasing^[41]. 7591 new oral cancer cases were reported in the UK in 2013 and cases have increased by 68% over the last 20 years^[42,43]. Oral surgery is required to remove cancerous tissue within the oral cavity, which causes the release of tissue fluid^[44]. Due to

this, bacteremia (a condition in which bacteria are found present in the blood) is a common occurrence^[45,46].

Cleft lip and palate is a congenital condition which affects approximately 7 in every 100 live births^[35,47]. If left untreated, it can have a great impact on speech, appearance and psychology of the affected individual^[35,48]. Dental surgeons are required to close the opening in the palate or lip, but this procedure is limited by the amount of oral mucosa available for transplantation^[49]. It is hoped that tissue engineering will produce a material that can provide the correct amount of graft material of sufficiently high quality for these surgeries to allow fully functional and aesthetic healing post-surgery^[50].

Periodontal diseases such as gingivitis or periodontitis are worldwide public health problems^[32]. These diseases are classified as infections of the periodontium which consists of the tissues supporting the teeth, namely the gingiva, cementum, periodontal ligament and alveolar bone^[38,51]. The bacterial destruction of these tissues ultimately results in tooth loss^[32,52]. In the US, prevalence of periodontitis ranges from 38-53% of the total population^[53]. As this condition is more common in older age, ageing populations in the Western world are likely to demonstrate a continuing increase in prevalence^[32,54]. Bacteria such as *Porphyromonas gingivalis* and *Streptococcus mutans* have been associated with the occurrence of tooth decay and periodontitis^[55,56]. Consequently, clinical treatments able to eradicate bacterial contamination or limit bacterial growth are greatly needed to reduce the spread of periodontal disease^[55,57].

Peri-implantitis is a disease which is caused by an infection of the hard and soft tissue supporting dental implants^[51,58]. A report by National Health Service (NHS) England found that half a million adults now have at least one dental implant^[59]. This is thought to occur in 10% of all dental implants between 5-10 years following application *in vivo*^[60]. If implants become infected, they need to be removed completely before the site can be cleared out and new implants can be fitted^[61,62]. This can be time-consuming, costly and painful for the patient^[63]. Although antibacterial coatings designed for implants are currently being studied and progress is being made towards a

solution to prevent this disease from occurring, there is still no effective treatment in clinical practice^[64,65].

1.1.2 Antimicrobial Resistance

A serious complication with dental surgery to repair oral soft tissue loss is bacterial infection^[66,67]. Should a post-operative oral infection occur, graft survival rates are low, with reported values of 65% of grafts needing to be removed^[68]. The current management of bacterial infections in oral surgery is the administration of antibiotics, in some cases as a precaution prior to detection of an infection arising^[69,70]. A major issue with this treatment route is the onset of antibiotic resistance, which is encompassed within the more general term of antimicrobial resistance (AMR)^[15]. AMR covers resistance to current treatments for bacterial, fungal, virulent and parasitic infections^[71]. In the past 10 years, several large organisations including the World Health Organisation (WHO) and the Centers for Disease Control and Prevention (CDC) have filed reports on the importance of minimising AMR^[16,72]. In April 2014, WHO declared the issue as a “threat to modern medicine”^[16]. CDC have stated that in excess of 2 million people become infected with antibiotic resistant bacteria each year^[73]. O’Neill reported in 2014 that at least 50,000 people die in Europe and the US each year due to the acquisition of antimicrobial-resistant infections^[74]. As well as being a serious clinical condition AMR poses a great economic burden as well, with yearly costs of up to \$30 billion being reported in the US alone^[75].

The most frequently used antimicrobials for use against bacterial infections (i.e. antibiotics) can be classified into four main classes based upon their chemical structure (**Table 1.2**)^[76].

Class	Example	Function
β-lactams	Penicillins	Inhibit protein synthesis
	Cephalosporins	Interfere with cell wall synthesis
Tetracyclines	Tigecyclines	Inhibit protein synthesis
Macrolides	Erythromycin	Inhibit protein synthesis
Aminoglycosides	Gentamicin	Inhibit protein synthesis

Table 1.2 – Four main classes of antibiotic agents^[76,77]

Bacteria typically develop resistance against these antibiotics through three main mechanisms (**Table 1.3**)^[78].

Resistance Mechanism	Class of Antibiotics
Modification or degradation of the antimicrobial agent	β-lactams and aminoglycosides
Mutation of the bacterial target site resulting in a lower affinity for the antimicrobial agent	β-lactams, tetracyclines, macrolides, and aminoglycosides
Decreased uptake or increased efflux of the antimicrobial agent resulting in a decreased accumulation within the bacteria	Tetracyclines and macrolides

Table 1.3 –Antimicrobial Resistance (AMR) mechanisms of bacteria against the main classes of antibiotics^[78]

The causes of AMR are known to be complex, with several interlinking factors^[79]. Despite ongoing research, the precise relationship between

humans and microbes is still unknown^[72]. The main drivers are thought to be the inappropriate use of antibiotics, both in medicine and agriculture^[15,79]. The term ‘inappropriate use’ is related to the overuse of antibiotics through unnecessary, preventative or incorrect prescriptions, unregulated use within agriculture, and through not following prescription guidelines^[15,79,80]. This has led to the urgent and ongoing need to treat infections via means which do not involve administering antibiotics, in the hope that the scaling-back in widespread use will reduce this dangerous spread of AMR^[75,81].

1.2 Regenerative Biomaterials for Oral Soft Tissue Loss

Regenerative biomaterial scaffolds provide one option to encourage repair of oral mucosa. They are required to support neotissue formation by being physically, biologically and chemically suitable for the application^[82,83].

1.2.1 Current Biomaterials for Oral Mucosa Regeneration

Biomaterial scaffolds are supporting structures which aim to aid tissue regeneration by providing support for *in vivo* cell proliferation and tissue growth within large defect sites^[84]. Current scaffolds to aid regeneration of oral mucosa can be categorised into two main groups; tissue grafts and polymeric scaffolds.

1.2.1.1 Tissue Grafts

Tissue grafts can be in the form of autogeneic (same individual human), allogeneic (other humans) or xenogeneic (other species) tissue^[85]. Each of these tissue graft sources has associated advantages and disadvantages and, where commercially available, have been associated with various degrees of clinical success^[86–88] (**Table 1.4**).

Tissue Graft	Advantages	Disadvantages	Examples of Commercial Products for Soft Tissue Repair
Autograft	<ul style="list-style-type: none"> • No adverse immune response 	<ul style="list-style-type: none"> • Lack of tissue availability • Donor site morbidity 	N/A
Allograft	<ul style="list-style-type: none"> • Greater availability than autograft 	<ul style="list-style-type: none"> • Possible adverse immune response • Disease transmission risk • Relies on donated tissue • Ethical/religious issues 	<ul style="list-style-type: none"> • Alloderm® (BioHorizons) • SureDerm® (Hans Biomed)
Xenograft	<ul style="list-style-type: none"> • Greater availability than autograft/allograft 	<ul style="list-style-type: none"> • Possible adverse immune response • Disease transmission risk • Ethical/religious issues 	<ul style="list-style-type: none"> • OASIS® Wound Matrix (Smith and Nephew)

Table 1.4 - Advantages and disadvantages of different soft tissue graft sources used in tissue engineering and example commercial products^[86–88]

1.2.1.1.1 Autograft

Autologous connective tissue graft transplants commonly taken from the gingiva or the hard or soft palate are the current ‘gold standard’ for the treatment of oral soft tissue loss^[89–93]. The main issue with this method is the lack of available oral mucosa for transplantation to the wound site^[94]. Due to this, sources of autologous skin tissue have been attempted from the thigh^[93], the forearm^[95] or the pectoralis^[95]. Further disadvantages of the use of autologous tissue including unwanted hair growth within the oral cavity^[96],

wound contraction^[97,98] and donor site morbidity^[99] have led to the search for alternative sources of tissue.

1.2.1.1.2 Allograft/Xenograft

A well-researched and documented skin or oral mucosa graft is the commercially available product, 'Alloderm®' (BioHorizons)^[26,36,92,98,100–112]. This product consists of a donated and processed human cadaveric dermis which can be preoperatively processed *ex vivo* into an oral mucosa equivalent to improve clinical success^[98]. This process involves obtaining and culturing oral mucosa keratinocytes from the dental patient which are then seeded onto the Alloderm® scaffold prior to implantation^[98]. The use of this technique compared to using the acellular scaffold showed a reduction in re-epithelization time from 46 ± 2.8 days to 27.4 ± 1.2 days^[98]. The obvious drawback to this technique is the cost of treatment and the time taken to produce the oral mucosa equivalent prior to surgery and the need for immune suppression drugs to prevent rejection^[113,114].

A similar approach has been used by a competitor, SureDerm® (Hans Biomed)^[115,116]. This also consists of a human cadaveric dermis^[115]. Good healing rates and vascularisation were observed in several *in vivo* studies in athymic mice when compared to an autogenic graft treatment group and clinical safety and efficacy have been demonstrated^[26,36,92,98,100,101,103,107–112].

Freeze-dried human amniotic membranes (HAM) donated by women undergoing elective caesareans have also been used in oral mucosal surgery^[5,117–119]. This has the advantage of being a good use for a common biomedical waste substance^[117]. HAM processing typically involves cryopreserving or dehydrating the tissue. A full tissue engineered oral mucosa construct can be produced by removing the epithelial layer, decellularising and sterilising the remaining membrane, and then using this in combination with oral mucosa epithelial cells^[118]. The resulting graft has been shown to have favourable mechanical properties and has been shown through histological analysis to be successfully integrated in mouse and rabbit animal models^[5,117,118]. However, the use of HAM still has the same complications related to those with the cadaveric dermis products in terms of ethical

considerations and the need to administer immune suppression drugs to prevent rejection^[114].

Studies have been reported on the use of porcine small intestinal mucosa (SIS) seeded with human oral mucosa fibroblasts and epithelial cells in an *in vitro* study that resulted in successful cell infiltration and revascularisation upon histological analysis^[120]. Another more recent *in vitro* xenograft study demonstrated the ability of acellular urinary bladder matrix from porcine sources to successfully treat oral soft tissue loss in rat models^[121].

However, ethical or religious complications with the use of cadaveric or animal tissue and the time taken to obtain a biopsy and to culture the cells are the main problems with the use of allograft and xenograft tissue sources^[122]. Another risk factor is that no matter how trustworthy the source of donor tissue, there is always a risk of viral transmission or host rejection^[123]. Therefore, it can be concluded that there is no 'perfect' graft material available currently for use as an oral mucosa regenerating scaffold^[122].

1.2.1.2 Polymer Scaffolds

Polymeric scaffolds can be made of naturally-derived polymers, synthetic polymers, or a combination of the two^[124]. Again, each of these has associated advantages and disadvantages^[86-88] (**Table 1.5**).

Polymer	Advantages	Disadvantages	Commercial Products
Natural	<ul style="list-style-type: none"> • Readily available • Inherent cell adhesion motifs • No ethical/ religious concerns 	<ul style="list-style-type: none"> • Possible adverse immune response • Disease transmission risk • Limited control of degradation • Batch to batch variation 	<ul style="list-style-type: none"> • Bio-Gide® and Bio-GidePro® (Geistlich) • CollaTape® (Zimmer Dental) • MucoGraft® (Geistlich) • Collagene AT® (Sistema AT) • INTEGRA® Dermal (Integra)
Synthetic	<ul style="list-style-type: none"> • Readily available • Relatively cheap • No disease transmission risk • Scaffold properties can be finely tuned to suit application • No ethical/ religious concerns 	<ul style="list-style-type: none"> • Possible adverse immune response • No adhesion cell adhesion motifs • Possible toxicity 	<ul style="list-style-type: none"> • BioMesh® (Samyang) • Vicryl (Ethicon, Johnson and Johnson Medical) • Costar® (Corning)
Hybrid	<ul style="list-style-type: none"> • Scaffold properties can be finely tuned to suit application • Readily available • Inherent cell adhesion motifs 	<ul style="list-style-type: none"> • Possible adverse immune response • Possible toxicity • Potentially non-uniform degradation 	<ul style="list-style-type: none"> • BIOBRANE™ (Smith and Nephew)

Table 1.5 – Advantages and disadvantages of the different polymer types used in tissue engineering^[86–88]

1.2.1.2.1 Natural Polymers

Naturally-derived polymers (e.g. proteins such as collagen or elastin, or polysaccharides such as chitosan) are commonly used as building blocks of regenerative devices in light of their higher biocompatibility and lower toxicity compared to synthetically produced polymers^[125,126].

One of the most commonly studied natural polymers for oral mucosa regenerating scaffolds is collagen^[2,88,89,127–133]. Several processes have been used to form collagen scaffolds, such as electrospinning, freeze drying and chemically crosslinked hydrogel formation^[6,134]. Many of these collagen-based matrices are available commercially, including Bio-Gide® and Bio-GidePro® (Geistlich)^[120], CollaTape® (Zimmer Dental)^[37,90,91,135,136], MucoGraft® (Geistlich)^[91], Collagene AT® (Sistema AT)^[115], INTEGRA® Dermal Regeneration Template Single Layer (Integra)^[137], TissuFoil E (Baxter)^[137] and CelTx® (Organogenesis)^[138]. However, concerns with the use of bovine collagen remain as despite being approved for use by the US Food and Drug Administration (FDA), there have been outbreaks of bovine spongiform encephalitis after implantation of these scaffolds^[123]. Blending collagen with other natural polymers has been attempted to improve parameters such as cell viability (e.g. with chitosan)^[23,139,140], and mechanical stability in physiological conditions (e.g. with elastin)^[141].

Histological analysis confirmed successful integration following the use of pure chitosan scaffolds implanted in the hard palate of dog animal models^[142]. However, despite new methods for crosslinking^[143], chitosan has been found to have low mechanical stability^[144].

Nanofibrous gelatin can be generated by thermal-induced phase separation followed by porogen leaching^[145]. These scaffolds were analysed using confocal microscopy to demonstrate favourable cell-cell and cell-matrix interactions with human gingival fibroblasts^[145].

Another natural biomaterial which has been explored for oral mucosa regenerative devices is based on a blend of fibrin and agarose^[145–151]. Fibrin has been found to have many favourable properties such as biocompatibility and controllable degradation, but the key disadvantage was the limited

mechanical properties of the protein^[152]. When combined with agarose and autologous cells, the properties of the resulting biomaterial product become more favourable which has led these prototypes to be moved into clinical trials^[66,153]. The concerns found in these case studies were the time taken to produce the scaffolds seeded with autologous cells (limiting suitability of this technique to non-oncological cases due to the time pressure to treat these patients) and observed wound contracture^[66,153].

1.2.1.2.2 Synthetic Polymers

Synthetic polymers such as poly(ethylene glycol) (PEG), poly(lactic acid) (PLA), poly(glycolic acid) (PGA), poly(caprolactone) (PCL) and poly(lactic-co-glycolic acid) (PLGA) are all commonly used in oral medical devices^[82,154–157]. PLA is used due to many desirable properties such as it being biocompatible, having good mechanical strength and it being able to be shaped easily^[82,154]. PGA has good biocompatibility and is readily biodegraded so it is used frequently in applications such as resorbable sutures^[154]. PEG is used as a biomaterial as it is non-toxic, hydrophilic, biocompatible and only causes a minimal immune response^[82]. PEG has also been blended with PLA to make a more hydrophilic final product compared to the polyester alone^[82]. The challenge with the use of synthetic polymers *in vivo* is that cell adhesion is often low due to the lack of cell-binding sites along the polymer backbone^[82]. This issue can be overcome through alteration or treatment of the polymers, for example, PCL nanofibres displayed significantly increased cell adhesion following NaOH-soaking for 1 hour prior to cell seeding^[158].

A commercially available scaffold as a dental membrane, BioMesh® (Samyang), consists of a blend of PGA, PLA and PLGA polyesters^[115]. This was determined to be less effective for cell growth than a collagen scaffold^[115]. A further study compared three synthetic commercial products based on either poly(ethylene terephthalate) (Greiner Bio-One), PCL (Costar® (Corning)) or collagen-based scaffolds^[136]. This also found that the collagen scaffolds were superior with regards to cell growth and ECM deposition despite the faster degradation shown by the latter products^[136]. This would suggest that more work is needed to enhance the cell-scaffold interactions in

the above-mentioned synthetic scaffolds. One commonly used technique is the inclusion of peptide sequences within polymer scaffolds, such as the tripeptide Arg-Gly-Asp (RGD) or Tyr-Ile-Gly-Ser-Arg (YIGSR) sequences which are known to increase cell binding affinity^[159–167]. For example, cell growth and differentiation on PLGA films with grafted RGD/YIGSR protein motifs were shown to be significantly greater than for the native PLGA films^[168]. However, modified synthetic polymers would require additional testing before gaining regulatory approval which is likely to increase the cost and time taken before the polymer scaffold can be approved for clinical use^[169].

Despite this, nonwoven pure PGA scaffolds have been shown to successfully support cell growth of human dental pulp cells and gingival fibroblasts when implanted into mice^[170]. Scaffolds produced with degradable, hydrophobic polyurethane were also determined to be useful for repair of oral mucosa by seeding with human gingival fibroblasts^[171,172] and have been electrospun into functional biomaterials^[173].

Overall, synthetic products could be the ideal choice for tissue engineered biomaterials due to their already widespread clinical use, fine-control of macroscopic properties, with no ethical or religious implications, and the removed risk of disease transmission^[86]. They are also cost-effective and versatile as they can be highly tuneable to their applications^[174].

1.2.1.2.3 Hybrid Polymer Systems

An interesting advancement in polymer science has been the use of hybrid polymer systems consisting of synthetic and natural polymer blends^[175–177]. Hybrid polymer systems have the advantage of being highly tuneable yet displaying the necessary cell adhesion motifs and biocompatibility found with naturally derived biopolymers. Studies have been performed with a nonwoven gelatin/PCL scaffold^[178,179]. This hybrid polymer structure was found to be able to successfully mimic the ECM fibrous architecture and not stimulate an inflammatory response whilst being used to repair mini-pig oral mucosa^[178].

As these hybrid polymer systems contain ECM-mimicking sequences at the molecular scale, they would result in the same associated disadvantages

as described previously such as ethical or religious issues as well as the increased expense and time taken for regulatory approval. The production of a purely synthetic polymeric oral mucosa substitute made entirely from polymers with regulatory approval would be preferable to completely avoid these associated issues if optimisation of the desired properties was successfully achieved.

1.2.2 Desirable Properties of Polymeric Biomaterials for Oral Mucosa Regeneration

In manufacturing a new biomaterial to be used as a regenerative medical device, several factors should be taken into consideration. The biomaterial should^[180]:

- Support cell growth by having good **biocompatibility**^[181]
- Have **fibrous scaffold architecture** to allows for tissue ingrowth^[182,183]
- Be appropriately **biodegradable**^[124]
- Have suitable **mechanical properties**^[184]
- Be compliant with industrial **manufacturing processes** to allow for commercialisation^[185–187]

Each of these features will be discussed in more detail below.

1.2.2.1 Biocompatibility

It is crucially important for all medical devices to be non-toxic to the native *in vivo* environment^[174]. This is essential not only for clinical success, but also to ensure approval by the regulatory bodies prior to commercialisation^[188–190]. For any medical device, the ISO (International Organization for Standardization) 10993 standards are the main consideration, with a <30% mammalian cell cytotoxicity needed to be proven *in vitro*^[188,191,192]. For this reason, a range of *in vitro* cytotoxicity tests have been developed as an initial indicator of the tolerability of a new biomaterial in biological settings^[193]. These include quantitative measurements which involves growing a monolayer of mammalian cells (commonly L929 mouse fibroblast cells) and introducing the new biomaterial to see the effect on morphology and confluence of the cells^[192,194]. Common studies to estimate

the cytotoxicity results from these assays include the determination of the metabolic activity of the cells via MTT assays^[195], AlamarBlue™ assays^[196] or ATP (adenosine triphosphate) luminosity assays^[197,198]. These assays use either dyes which change colour, or proteins which luminesce, when they are reduced by enzymes present in living cells^[197].

Any biomaterial to be made commercially available as a medical device needs to be approved by the relevant regulatory bodies^[124]. Using FDA-approved polymers in the scaffold would facilitate the expensive and lengthy process of applying for medical device approval^[199]. The FDA-approved synthetic polymers which have previously been used for oral mucosal repair include PCL^[200], PGA^[201], PLA^[202] and PLGA^[203].

Aside from not harming the cells, it is also important that regenerative scaffolds encourage cell adhesion to promote neotissue formation^[204]. Many material properties are known to affect cell attachment, including biomaterial architecture (such as fibre diameter and pore size)^[205,206], shape^[207], environmental responsiveness^[208], mechanical properties^[209], biodegradation^[116], chemical functionality^[210] and biological motifs^[211].

1.2.2.2 Biodegradability

Biodegradation is a term used to describe polymers which lose mass over a period of time in a biological environment^[124]. There are concerns with the use of slowly degrading polymers in medical devices as these could cause adverse biological effects when present *in vivo* for prolonged periods of time and prevent full neotissue formation as cells cannot infiltrate the polymer structure^[82]. Alternatively, if the degradation occurs too quickly, there will be a rapid loss of mechanical stability at the site of regeneration before neotissue is formed which could lead to further injury^[212]. An additional concern with polymers (i.e. polyesters) degrading too quickly is that this could lead to the formation of acidic and potentially toxic degradation by-products in a localised area within the body^[154]. Therefore, the degradation profile of each polymer needs to be tailored to fall within an appropriate timescale for the proposed clinical application^[201].

In biological environments, polymers can undergo chemical degradation through hydrolysis or enzyme-catalysed cleavage^[154]. Synthetic polymers (such as polyesters) are more likely to be degraded via hydrolysis whilst biopolymers typically degrade through enzymatic reactions^[154].

Hydrolytic polymer degradation occurs through a series of events. Firstly, water enters the polymeric structure and causes swelling^[213]. Water molecules cleave covalent bonds between repeating units resulting in the formation of oligomers^[214]. This process causes the architecture of the polymer to become irregular and more porous^[215]. As these oligomers typically contain acidic functionality, a pH drop is usually observed locally within these pores, which accelerates the polyester degradation via autocatalysis^[213]. Controlled degradation of a polymeric building block is important as this will ensure that the biomaterial structure, toxicity and clearance rate is uniform and controlled^[194,216]. Hydrolysis results in the decrease in molecular weight at the molecular scale and a drop in mechanical strength at the macroscopic scale of the polymer scaffold^[217]. Both molecular weight and mechanical strength of the polymeric scaffold can be monitored *in vitro* to investigate the degradation kinetics^[154,218].

Hydrolytic reactivity of the chemical bonds present in the polymer is an important consideration with respect to degradation kinetics (**Table 1.6**)^[219].

Polymer Type	Functional Group	Relative Hydrolytic Reactivity
Polyether	-CH ₂ -O-CH ₂ -	Low
Polyurethane	-O-CO-NH-C-	↓
Polyester (aromatic)	-CO-O-C-	↓
Polyamide	-CO-NH-C	↓
Polyanhydride	-(CH ₂ -CO) ₂ -C-O-	↓
Polyester (aliphatic)	-CO-O-C-	High

Table 1.6 - The relative reactivity of different polymer types increases from the top to the bottom of the table^[219]

Aliphatic polyesters are commonly used as building blocks for medical devices as they are most hydrolytically active and their degradation products have low toxicity^[220]. It is also possible to cap end groups of polymers, chemically cross-link polymer chains or synthesise co-polymers in order to fine tune the hydrolytic degradability and hydrophilicity as well as thermal and morphological properties of the resulting material^[24,221–223].

Within a polymer structure, polymer chains can arrange into crystalline or amorphous configurations. Amorphous structures consist of randomly arranged polymer chains^[224,225]. Contrastingly, crystalline structures are highly regular, closer to the structural arrangements within a crystal structure^[224,225]. Semi-crystalline structures contain both of these structural regions^[226] (**Figure 1.2**).

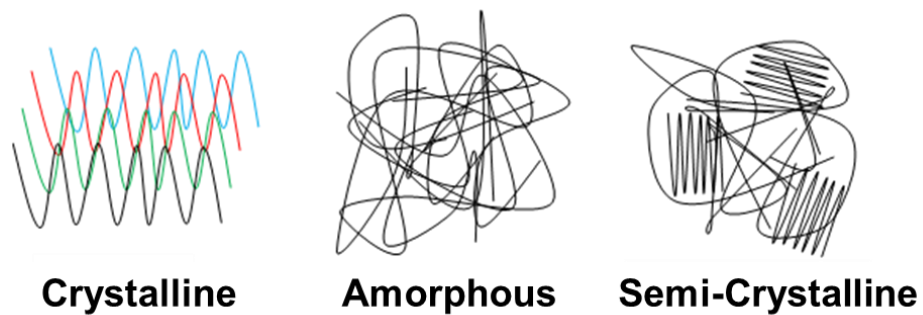


Figure 1.2 - The states of polymer arrangement: crystalline, amorphous and semi-crystalline

If a second monomer type is incorporated within the polymer backbone, a change in the morphology and thermal properties such as the crystallinity and glass transition temperatures of the resulting copolymer are expected^[154]. The different degree of crystallinity within a polymer will alter the rate of biodegradation^[227]. For example, crystalline PGA sutures are known to degrade in dental surgery within 7-10 days^[228]. Therefore, the use of pure PGA scaffolds in oral mucosal repair may be unsuitable as it could degrade too quickly (< 1 month) to support the neotissue formation^[229,230]. To overcome this problem, PGA can be copolymerised with PLA to generate PLGA copolymers^[231]. This is advantageous as the tuning of the glycolide to lactide ratio can be used to alter the crystallinity and thus tune the degradation rate to suit the desired application^[123]. It has been demonstrated that an increase in the lactide component decreases the rate at which degradation occurs^[123,232,233]. One study evaluated cell viability on electrospun scaffolds to help heal skin using the synthetic polymers PLA, PGA and PLGA^[123]. In this study, it was concluded that PLGA 85:15 (85% lactide to 15% glycolide monomers) and 75:25 (75% lactide to 25% glycolide monomers) were optimal in terms of the polymer biodegradability and biocompatibility to be used for this application^[123].

A structural characteristic which affects many properties such as degradation, mechanical properties and the water uptake (WU) is the scaffold porosity^[234]. The more porous the scaffold, the easier it would be for the scaffold to take in water, and therefore a greater surface area would be

exposed for potential hydrolytic degradation^[234]. In tissue engineered products, porosity is also important for cell infiltration^[235,236]. Another factor is the hydrophilicity of the polymer, as if the polymer is less hydrophilic, the WU will be slower and thus the degradation rate will also be decreased^[237]. Therefore, both the porosity and hydrophilicity of the scaffold need to be controlled to tune the degradation^[238].

The molecular weight of the polymer also impacts on the degradation behaviour. A polymer with an increased molecular weight displays a decrease in degradability^[239,240]. This is because a greater molecular weight polymers would require more chemical bonds to be broken during the break down of the polymer chain^[240].

1.2.2.3 Mechanical Properties

The thermal properties and crystallinity of polymers (section 1.2.2.2) have been shown to have an influence on the mechanical properties of the material^[241]. Tensile properties of polymer scaffolds are typically established via uniaxial tensile testing, which can be used to calculate the elastic modulus, toughness and percentage elongation for a particular scaffold^[242,243].

Improvements in the mechanical properties of polymers can be achieved through techniques such as heat treatments to alter the degree of crystallinity^[226].

The properties of oral biomaterials are not only important *in vivo* but also for the dental practitioner during surgery^[244,245]. If the device is difficult to handle, the product may be at increased risk of being implanted incorrectly, ultimately resulting in poor clinical performance^[90]. It is therefore desirable for the product to be pliable and relatively adhesive when moist^[246]. The adhesion here would prevent the biomaterial from 'springing back' when put in place^[246,247]. If the product was too adhesive however, it would be difficult to initially position or reposition if required^[246].

1.2.2.4 Manufacture of Fibrous Scaffolds

Nonwoven fibrous scaffolds are frequently used in regenerative scaffolds as the fibre diameter and pore size can be tuned for the desired application^[125]. Pores present within the structure are also inter-connected

which can be useful for cell infiltration^[125]. This three-dimensional porous structure produced within nonwoven scaffolds mimics the ECM of biological tissues, such as the lamina propria layer of the oral mucosa^[127,248,249].

As scientific research has progressed, it has become possible for biodegradable regenerative biomaterials to be combined with additional functionality through drug loading to aid new tissue formation^[250–254] such as antimicrobial functionality^[255,256]. Depending on the polymeric building blocks, nonwoven fibrous scaffolds generated can be used for both hydrophobic and hydrophilic drugs^[257–259]. For delivery of antimicrobials into the oral cavity, the antimicrobials would ideally be steadily released from the biomaterial until complete mucosal relining had occurred, as by this point the risk of infection would be lower^[260]. This has been shown to take up to 4 weeks^[260]. Fibrous scaffolds could be suitable for this as the release profile for the scaffolds can be highly tuned by varying the composition and porosity of the structure^[254,261].

There are a range of commonly used techniques to generate fibrous scaffolds, each with inherent advantages and disadvantages. These include wet spinning, melt spinning and electrospinning.

1.2.2.4.1 Wet Spinning

Wet spinning is a technique which involves the extrusion of a polymer solution into a coagulation reservoir, upon which solid fibres form through non-solvent induced phase separation^[193]. This is a useful technique if there are concerns about the use of high voltages (such as those used with electrospinning techniques) degrading the polymer solution or biomolecules contained within this solution^[193,262]. When using synthetic polyesters, it is unlikely that the polymer solution would be susceptible to degradation at high voltages, so this would not be a concern. Therefore, as wet spinning is a relatively complex manufacturing technique, it would not be the preferable choice of manufacturing for polyester solutions^[262].

1.2.2.4.2 Melt Electrospinning

Melt electrospinning is a technique which avoids the use of toxic solvents as a polymer solution is generated through the direct melting of the polymer into a viscous solution^[263]. Therefore, it is commonly chosen for

polymers with limited solubility in water to allow for a 'greener' manufacturing method to be chosen^[264]. However, this technique is less frequently used than electrospinning due to the increased complexities and associated costs^[264].

1.2.2.4.3 Electrospinning

Electrospinning is a relatively simple technique which is used to efficiently produce micro- to nano-scale fibres of polymer solutions at a high production rate with low associated costs^[125,265,266]. Although the principle of the technique was discovered over 120 years ago^[267], it has only become widespread in the last 10-15 years, possibly due to the increased interest in nanoscience and tissue engineering applications^[125]. The size of the fibres can be smaller than with most other techniques such as self-assembly and phase separation^[125,268].

The electrospinning apparatus consists of a syringe with metal spinneret, a voltage supply and a grounded collector (**Figure 1.3**)^[125,248].

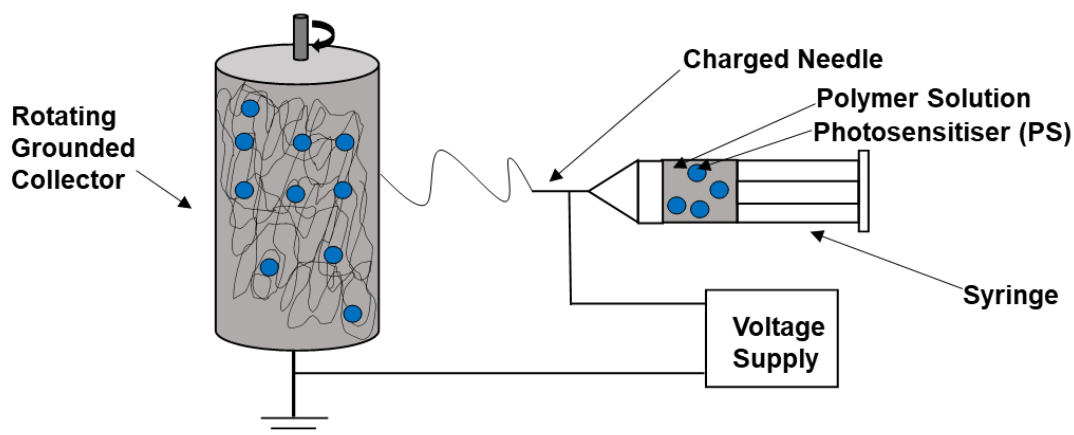


Figure 1.3 - The basic electrospinning apparatus^[125,248]

A polymer solution is fed into the needle of the syringe, and held at the tip by surface tension^[248]. A voltage is applied to the system, commonly between 10 – 50 kV, which causes charge repulsion within the polymer droplet and causes it to stretch away from the needle^[248,266]. Once a sufficient

charge repulsion has been transferred, this overcomes the electrostatic repulsion and causes the droplet to stretch into a Taylor cone (**Figure 1.4**)^[269].

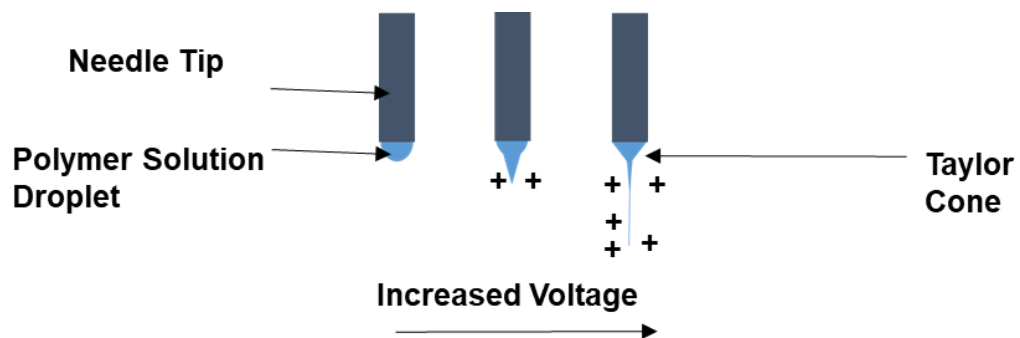


Figure 1.4 - The process of applied voltage resulting in a Taylor cone being generated at the needle tip of electrospinning apparatus^[269]

This charged cone is then pulled into a jet of polymer solution^[125,248]. As the voltage is increased this causes the charges within the polymer to repel each other^[266]. This, along with the evaporation of the solvent, causes the polymer stream to stretch from the needle tip towards the grounded collector electrode^[125,266]. This voltage gradient causes the stream to be stretched and whipped to elongate and narrow the fibres^[248,266]. The products produced therefore have inherent porosity and have a large surface area to volume ratio^[266]. It was initially hypothesised that the jet splayed into several smaller jets when the charge repulsion caused movement in the jet^[270]. The use of high speed photography has since shown that the stream remains a single jet, subject to rapid whipping^[271].

One of the most important parameters which can be altered is the polymer solution used^[272–274]. Different properties of the resulting scaffold can be a result of changes to the viscosity, conductivity, surface tension and the molecular weight of the polymer solution^[125]. The difficulty with varying these parameters is that there is often an interplay between different factors^[248].

The solvent system needs to be optimised depending on the polymer used^[125,275]. The volatility of the solvent has a key role in the process; the

more volatile the solvent, the earlier the jet will dry, and therefore the jet will have a slower speed^[248,270]. Volatile organic solvents are commonly used for the process, but the most volatile of these are often also highly flammable, which may limit their use in commercially produced scaffolds^[276]. In order to optimise the process of selecting the optimum solvent, a 'spinnability-solubility map' has been produced, but this study concluded a higher solubility does not always produce better electrospun scaffolds^[277]. Although there are concerns with the use of toxic solvents in electrospinning, vacuum drying the electrospun scaffolds for prolonged periods of time can remove any potentially toxic solvent residues^[254,263,264]. Thermogravimetric analysis (TGA) can be used to confirm the removal of all residual solvent^[254].

The electrical field applied, the type and size of needle tip used, the flow rate and the distance between the tip and the collector will also alter the product of electrospinning^[125]. Various electrospinning techniques such as coaxial, multiaxial, needleless or emulsion electrospinning could also be used to tune the final product^[125,266]. The ambient environment of the electrospinning rig can also affect the final nonwoven scaffold structure, which includes the temperature, humidity and air velocity^[278].

It has been found that the morphology and density of fibres is changed upon the incorporation of additives such as hydrophilic antibiotics due to the charge effects on the process, i.e. an increase in solution charge would result in an increased whipping action and a narrowing of resulting fibres^[254].

A key benefit of electrospinning for the production of a commercially available tissue engineered regenerative medical device is the ease and relative low cost of the apparatus setup^[248]. As only a small size is needed for the oral cavity, a large amount of the product can be produced at once, and product homogeneity is easily achieved due to the repeatability of the technique^[248]. Therefore, for oral applications, electrospinning could be the preferred choice of manufacturing technique.

1.3 Antimicrobial Strategy

Bacterial susceptibility to antimicrobials can be tested with bacteria in planktonic (suspended in solution) or biofilm form^[279,280]. Testing with planktonic bacteria is commonly used initially as it allows for faster screening of antimicrobials^[281]. The use of biofilms is a more accurate way of testing antimicrobials as bacteria commonly exist in this form *in vivo* in the oral cavity, particularly in dental plaque^[282,283]. It is worth noting that biofilms have been shown to be up to 1000 times less susceptible than planktonic bacteria to certain antimicrobials^[281,283].

There are two classes of bacteria; gram-negative and gram-positive, which are distinguished due to the cell wall structure (**Figure 1.5**).

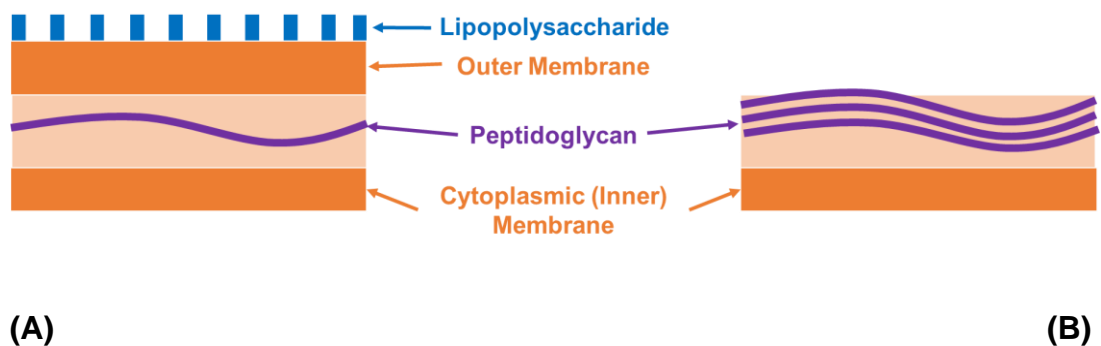


Figure 1.5 – General membrane structure of (A) Gram-negative and (B) Gram-positive bacteria^[284]

Gram-positive bacteria have a thick porous layer of peptidoglycan and an inner cytoplasmic membrane, whereas Gram-negative bacteria have both an outer and an inner membrane which are separated by a thin layer of peptidoglycan^[285]. This additional outer membrane on Gram-negative bacteria means that typically they are less permeable to uptake antimicrobials and are therefore more resistant^[284–286].

1.3.1 Types of Antimicrobials

The severe consequences of AMR (section 1.1.2) has led to research into a host of antibiotic-free antimicrobial strategies^[287–290]. These alternative antimicrobial approaches include organic substances (e.g. chitosan^[126], cinnamaldehyde^[291–293], carvacrol^[291] and manuka honey^[294], fatty acids^[295] and chlorhexidine^[296,297]) inorganic substances (e.g zinc^[255,298], titanium oxide^[299], silver nitrate^[300] and gold or silver nanoparticles^[290,301–303]), and a host of either organic or inorganic PS for use with light resulting in aPDT effect^[304–306].

There are several examples of nonwovens being used for the delivery of antimicrobial agents in the oral cavity^[307]. These include zein/chitosan blend electrospun scaffolds^[308], chlorhexidine polytetrafluoroethylene scaffolds^[297], chlorhexidine glycolide fibre scaffolds^[297], and zinc carbomer (Carbopol®) scaffolds^[298].

Chitosan is inherently antimicrobial, and this polymer has proven to be effective on oral pathogens^[309]. Common oral pathogens *Actinobacillus actinomycetemcomitans* and *Streptococcus mutans* were shown to be inactivated by a 0.1% chitosan solution with a 2-log reduction in colony forming units (CFU) after 30 minutes, which increased to 4.5-log reduction after 120 minutes^[310]. Antimicrobial activity was also demonstrated on the periodontal pathogen *Porphyromonas gingivalis* upon exposure to chitosan^[309]. However, chitosan is a naturally occurring polymer so has the associated disadvantages (section 1.2.1.2.1).

Inorganic components such as nanoparticles of silver, titanium dioxide and silica dioxide have been compared to the commonly used dental antibacterial chlorhexidine in biochemical assays to determine their use as antimicrobial agents within the oral cavity^[303]. Both silver nanoparticles and silver nitrate were shown to be more bactericidal than chlorhexidine in this case, but titanium dioxide and silica dioxide were not as effective as chlorhexidine^[303]. Similarly, silver zeolite (AgZ), silver zirconium phosphate silicate (AgZrPSi) and silver zirconium phosphate (AgZrP) were all shown to be effective at deactivating *Streptococcus mutans*, *Lactobacillus casei*,

Candida albicans and *Staphylococcus aureus*^[311]. However, in a report published by the Scientific Committee on Emerging and Newly Identified Health Risks for the European Union (EU), it was concluded that due to gaps in knowledge, it is not yet known whether nanosilver is harmful for the environment or could lead to further AMR^[312]. Another issue raised in this report was the risk of occurrence of argyria, a permanent bluish-grey skin discoloration resulting from exposure to silver^[312].

aPDT is a promising alternative strategy to the antimicrobial agents discussed above, with the additional benefit of the on-demand capability of the treatment.

1.3.1.1 Antimicrobial Photodynamic Therapy

PDT originates from observations made over 100 years ago that the combination of light and photosensitising dyes can lead to the death of microorganisms^[18,313]. It has since been used throughout medical science, predominantly for the treatment of cancer^[313–315] but also in dermatology and eye disorders^[18,316]. Recently, applications have moved back towards the original use of PDT by using PS to target bacterial infections locally^[313,317–319]. As oral infections can be treated through localised antimicrobial action, this technology would be a good alternative to antibiotics^[320].

The key advantages are that it is possible to have the same killing effect upon all bacteria, regardless of resistant strains, and that there is no further induction of resistance triggered^[18,321,322]. Another benefit of aPDT is that both the PS and the light are non-toxic alone, but when combined in the correct dose levels they can be tuned for selective toxicity to bacteria^[323].

A main issue in the use of this technology for infectious diseases is that it is yet to be fully established^[18,281]. This is due to the lack of knowledge on the delivery of the PS to bacteria, the role of uptake and the selectivity achievable between the bactericidal effect and the sparing effect upon host cells^[18].

1.3.1.1.1 Photochemical Mode of Action

In a non-activated PS, a pair of electrons exist in the PS ground state (⁰PS)^[313]. To activate a PS, light of a specific wavelength needs to be applied.

This is normally light in the visible or near-infrared region of the electromagnetic spectrum and is PS-specific^[313]. This light provides the energy to excite one of these electrons from the highest occupied molecular orbital (HOMO) into the lowest unoccupied molecular orbital (LUMO) of the excited singlet state ($^1\text{PS}^*$) (**Figure 1.6**)^[313].

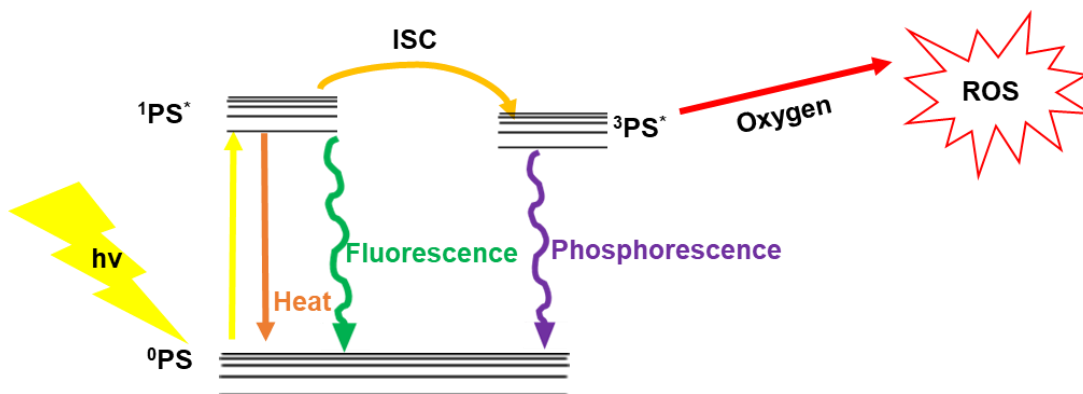


Figure 1.6 - Jablonski diagram showing the movement of electrons upon light stimulation within a photosensitiser (PS). ^0PS : PS Ground State; $^1\text{PS}^*$: PS Excited Singlet State; $^3\text{PS}^*$: PS Excited Triplet State; $h\nu$: Light Energy; ISC: Inter-System Crossing; ROS: Reactive Oxygen Species^[313]

The spin state of the electron remains unchanged^[313]. The electron is relatively unstable, so only remains in the LUMO of the $^1\text{PS}^*$ for a few nanoseconds^[313]. As this state is short-lived, it is important to localise the PS to the site of infection before activation as it will only affect cells in the immediate vicinity^[313]. From the $^1\text{PS}^*$ LUMO, there are three routes which the electron can take^[313]. The first is that it can fall back to ^0PS and release the absorbed energy as heat^[313]. The second is that this fall back to ^0PS can result in the emission of fluorescence energy as the wavelength of light emitted is slightly different to the wavelength absorbed^[313]. The third is that the electron will reverse spin, known as inter-system crossing (ISC) which will convert it to the excited triplet state ($^3\text{PS}^*$)^[313].

From the $^3\text{PS}^*$ state, the electron can fall back to ^0PS , this time with the energy being emitted as phosphorescence^[313]. The final route for the energy of this electron is the course which provides the PDT activity, which involves the electron reacting with oxygen to produce reactive oxygen species (ROS)^[313]. The interaction of this electron from the $^3\text{PS}^*$ with oxygen can occur through two different photochemical reactions: Type I PDT and Type II PDT^[313]. Both of these mechanisms occur concurrently, with the ratio of the two depending on the type of PS used and the local environment of the PS *in vivo*^[324].

Type I PDT involves an electron transfer reaction from $^3\text{PS}^*$ to generate free radicals^[313]. For example, hydrogen peroxide (H_2O_2) can diffuse easily through cell membranes, and once within cells, this molecule can use the electron from the excited triplet state of the PS to undergo homolytic fission to produce hydroxide ions inside cells^[313]. These will react with small amounts of transition metals such as Fe^{2+} or Cu^+ via homolytic fission and produces hydroxide ions (HO^-) and hydroxyl radicals ($\cdot\text{OH}$)^[325]. These hydroxyl radicals are very damaging inside cells, initiating radical chain reactions with fatty acids, cholesterol and lipids, ultimately resulting in cell death^[313].

Type II processes involve the transfer of energy from the electron in $^3\text{PS}^*$ directly to the ground triplet state of a molecule of dioxygen (O_2) to produce reactive species of singlet oxygen ($^1\text{O}_2$)^[313]. This is a highly reactive ROS which oxidises sulphur atoms or double bonds in macromolecules and can also react with DNA to create unstable and reactive products, again, resulting in cell death^[326]. The half-life of this singlet oxygen is less than 0.04 μs and it will only deactivate cells within a 0.02 μm radius^[327].

1.3.1.1.2 Photodynamic Therapy in Antimicrobial or Anticancer Strategies

Type I PDT reactions are commonly associated with the killing of microbes, and Type II reactions are typically used to target cancer cells^[328,329]. However, this is not always the case as some studies have found that Type II reactions can kill bacteria and particular PS such as a Pd-bacteriopheophorbide target cancer cells but act via a Type I mechanism^[330–332]. Attempts have been made to use one PS (such as erythrosin B) for both

anticancer and antimicrobial PDT^[55,318,333]. This PS has been tested on malignant and pre-malignant oral epithelial cells and did trigger toxicity on cancerous cells^[333]. However, erythrosin B is more commonly used in aPDT treatments^[55,334,335].

In the early stages of aPDT, the same PS being used for anticancer PDT were used for aPDT to deactivate microbes^[313]. It was then discovered that optimisation of PS could provide greater selectivity of bacteria over mammalian cells, by controlling the ratio of Type I to Type II reactions^[313]. The PS selectivity is based primarily on a PS 'dosage window', within which bacterial cells are primarily targeted over mammalian cells^[313,336]. This optimal dose applies to both the PS concentration and the light source, i.e. time and intensity of light exposure^[313,336]. Another factor to consider is that in severe infections there will be a much larger number of bacterial cells to host tissue cells, so as the PS is applied locally, it is likely to be taken up preferentially by bacterial cells^[313].

1.3.1.1.3 Choice of Photosensitiser

The main classes of PS can be grouped according to their chemical structure (**Table 1.7**).

Class	Example	Peak Wavelength (λ_{max})	Reference
Phenothiazinium	Methylene blue	610 and 670 nm	[337,338]
	Toluidine blue O	630 nm	[339,340]
Porphyrin, chlorin and phthalocyanine	5,10,15,20-tetrakis(4-sulfonatophenyl)-21 <i>H</i> ,23 <i>H</i> -porphine (TPPS) Porfimer sodium (Photofrin)	420 nm	[341]
Xanthene	Erythrosin B	530 nm	[335,342]
Fullerene	Decacationic functionalized fullerene (LC15)	Strong absorption in UV and visible region	[343,344]
Phenalenone	7-perinaphthenone (PN)	356-418 nm	[345]
Riboflavin	Riboflavin	450 nm	[346]
Curcumin	Curcumin	420 nm	[347,348]

Table 1.7 – Summary of the main classes of photosensitisers for antimicrobial photodynamic therapy

The two PS of main interest for this study were methylene blue (MB) and erythrosin B (ER) due to their being readily available and having previously been screened for use in scaffolds with aPDT functionality proposed for this project^[349]. These PS are both FDA-approved and have also been studied previously in the context of PDT for oral infections^[334].

1.3.1.2 Existing Antimicrobial Photodynamic Therapy Biomaterials

The use of PS for the treatment of infections via aPDT is established as a possible solution to treat infections whilst avoiding unnecessary antibiotic

prescriptions^[317]. However, the delivery of these PS to the site of infection is an area which is currently of interest^[350]. A steady release of PS is required, and as the activation of the PS is short-lived, the PS needs to target the site of infection whilst in the active state^[284,351]. Several research papers have reported PS-encapsulation within various scaffolds and respective PDT functionality (**Table 1.8**).

Photosensitiser	Scaffold
Curcumin	PLGA nanoparticle scaffolds ^[348]
	Alginate foams ^[244]
Methylene Blue	PVA and PEO electrospun scaffolds ^[352]
	Wool keratin films ^[353]
	Poly(siloxane) polymers ^[354]
Erythrosin B	Electrospun polyvinyl pyrrolidone/ hydroxypropyl- β -cyclodextrin (PVP/HP β CD) scaffolds ^[355]
Toluidine Blue	Poly(methyl vinyl ether/maleic anhydride) and Tripropyleneglycol methyl ether blended mucoadhesive patches ^[356]
Zinc tetraphenylporphyrin	N-isopropylacrylamide (NIPAA) and hydroxyethylmethacrylate (HEMA) hydrogels ^[357]

Table 1.8 – Examples of photosensitiser and scaffold combinations aimed to treat infections via antimicrobial photodynamic therapy

Despite several scaffold and PS systems being researched, additional attention needs to be given to oral treatment applications to ensure that both the PS-release profile and degradation of the scaffold suit the harsh and moist oral environment^[11]. One interesting additional aspect to the study in **Table 1.8** by Jones et al^[357] which loaded a porphyrin based PS into hydrogels was the addition of a thermoresponsive element to the scaffold which allowed for a

switchable release of the PS depending on the temperature of the gel^[357]. If the scaffold was adapted for use in oral applications, this 'switch' could be achieved through rinsing the oral cavity (and therefore the scaffold) with hot or cold water^[357].

1.3.1.2.1 Antimicrobial Photodynamic Therapy in Dentistry

The use of antimicrobial PS in dental surgery is the largest growth of PDT in clinical infection treatment^[18,358]. This is due to the many advantages that PDT offers over traditional routes of treating bacterial infections, both in practicality and in the effectiveness of the treatment^[18]. The inexpensive and quick to use treatment method suits dental surgery^[18,359]. The oral cavity can be easily accessed with a light source by the dental practitioner which allows specific targeting of only the affected areas of the mouth. Importantly, the use of PDT for antimicrobial activity has not been found to induce AMR^[18,360]. In terms of effectiveness, aPDT will not just kill bacteria, but can target all microbes including viruses, virulent factors, fungi and bacteria present within biofilms^[18,361,362]. This is a great advantage in the human oral cavity as the microflora is known to be complex and diverse^[11].

It has long been known that PDT could be used to target bacteria in oral biofilms^[363–366]. Over 20 years ago, an *in vitro* study demonstrated the action of toluidine blue and MB on *Streptococcus sanguis*, *Porphyromonas gingivalis*, *Fusobacterium nucleatum* and *Actinobacillus actinomycetemcomitans*^[367]. Aside from bacteria, MB has also been used to successfully destroy oral fungal infections in a murine animal model^[368].

With regards to treatment of oral diseases, aPDT activity using MB has been used to successfully treat oral mucositis infections in clinical applications^[369]. The use of PDT for the treatment of chronic periodontitis has been explored, and porphycene–poly(lysine) conjugates combined with a light source have been used to successfully kill bacteria associated with periodontal disease *in vitro*^[370,371]. A clinical study on 27 patients with periodontitis showed successful outcomes following aPDT treatment^[372]. However, it has been suggested that the use of this aPDT is particularly

effective when combined with mechanical debridement for extreme cases of periodontitis^[373,374].

A consideration for the use of PDT in dental surgery is the source of light as to purchase a new light could result in additional costs for the end user. A dental chair light is commonly set at a wavelength of 420-480 nm (blue light) to be used for curing^[246]. This blue light has the advantage of not transferring heat which could damage the periodontal tissues, and is known to be inherently bactericidal^[246,313,375]. However, a longer wavelength red light between 650-800 nm would prevent the light being absorbed by typical chromophores within the tissue so is known to have greater tissue penetration which would help to activate PS deeper in the wound bed^[322,376]. The light wavelength required will be dependent upon the requirements for the peak absorbance of the PS used.

There are several commercially available systems for treating oral infections using aPDT. Periowave™ (Ondine Biopharma) is an antimicrobial PDT system for the treatment of periodontal disease with a thin plastic light tip to be used with MB in solution form^[377]. This device has been demonstrated to be successful in the treatment of periodontal disease without the need to administer antibiotics^[57,378]. Another approved treatment on the market involves the use of a solution of the PS toluidine chloride with a SaveDent® lighting system (Denfotex)^{[379][380]}. This light system has also been used to show that bacteria can be destroyed with aPDT techniques in the oral cavity^[380]. Finally, HELBO 3D EndoProbe (HELBO Photodynamic Systems) uses the PS toluidine blue with a 635nm wavelength light to treat infected root canals^[379,381].

The main issue currently with the use of PDT to kill bacteria in regenerative products, is the difficulty in specifying the toxic effects to selectively target the microbial cells^[382]. Tissue regeneration relies on new cell proliferation, so if the PDT harms these new cells, the product will not fulfil the purpose for which it was designed^[87]. A limited number of studies in the published literature have explored mammalian cell toxicity caused by aPDT. The literature reports one preliminary study which tested the effect of aPDT

upon human periodontal ligament cells and human gingival fibroblasts, and concluded that no harmful effects were observed^[383].

There are limited recent examples in the literature of combining aPDT technology with oral hard tissue regeneration^[384,385]. However, there is presently no published research which demonstrates the use of a soft tissue regenerating scaffold designed specifically for oral applications with aPDT capability.

Chapter 2 PhD Research Aim

There is a clinical need for a regenerative medical device made from a finely tuned synthetic bioresorbable polymer which can manage infections through aPDT.

The aim of this project was to develop a prototype of a biocompatible scaffold with incorporated aPDT capability. The prototype should support cell integration and trigger optional bactericidal effect following activation with light. The loaded antimicrobial PS should be released from the scaffold through controlled release kinetics and be selectively taken up by bacteria. In a clinical setting, if the clinician sees necessary, a specific frequency of light could then be applied to activate the PS and to selectively kill any bacteria present in the wound bed (**Figure 2.1**).

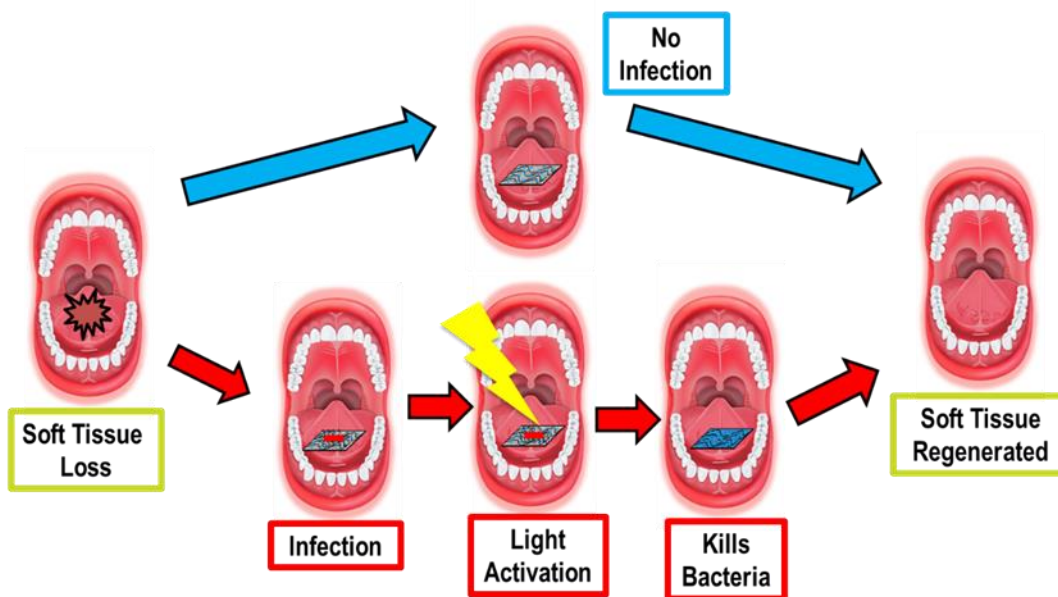


Figure 2.1 - The light activation of the incorporated PS (photosensitizer) within the biodegradable polymer scaffold initiating antimicrobial activity

If the light source is not deployed, the PS should be broken down through normal biochemical pathways and excreted harmlessly from the body^[386]. The scaffold would need to support new tissue growth for a clinically relevant period of time before it was biodegraded and removed from the body, again through normal biochemical pathways which ends in the product being released through excretion or through respiration processes as water or carbon dioxide^[386]. This would prevent the need to painfully remove the scaffold after wound healing has occurred (**Figure 2.2**).

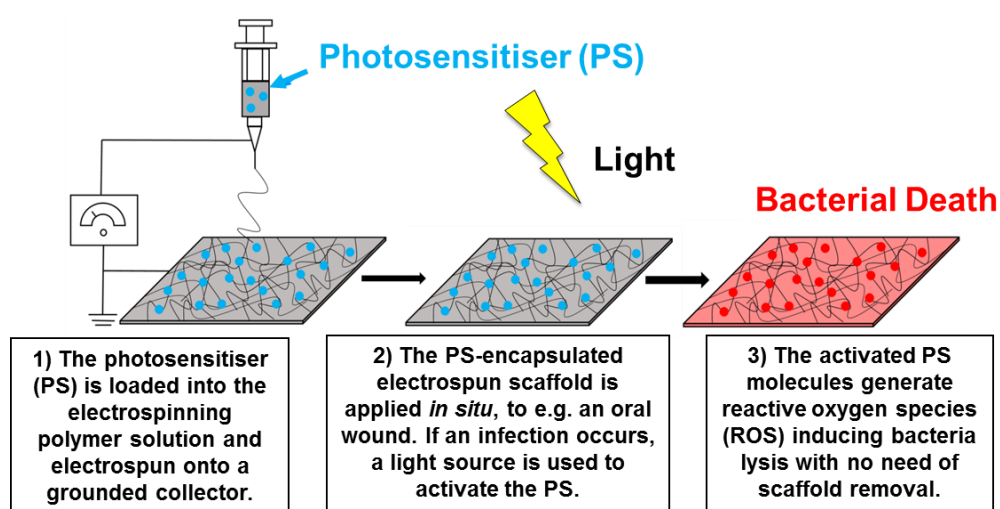


Figure 2.2 – Design and clinical applicability of photodynamically-active electrospun fibrous scaffolds for antibiotic-free infection control

2.1.1 Research Strategies

Prior to the start of this project, a proof of concept study was performed with a range of scaffolds loaded with antimicrobial PS, namely ER, tin (IV) chlorin e6, haematoporphyrin IX and MB^[387]. A patent was then filed for the concept of a polymer scaffold loaded with antimicrobial PS for use in soft tissue regeneration^[349]. From the results of this study it was concluded that the optimal product for skin regeneration was the ER-loaded PGA scaffold system for which sustained release of the PS, bactericidal

effect and cell survival upon bactericidal activation of the PS were demonstrated^[387].

However, changes need to be made to the methodology used in the initial research to optimise the scaffold for use in the oral cavity. Degradation of PGA sutures within the oral cavity has been found to take <10 days which would not be long enough to ensure full mechanical support and cell integration^[228]. Other FDA-approved polyesters (PLGA and PCL) should therefore be examined. Specific scaffold requirements identified in this literature review are summarised below (**Table 2.1**).

Scaffold Characteristic	Reason
Fibrous and porous	To allow for tissue integration
Appropriate mechanical properties for the oral mucosa (e.g. elastic modulus of 0.9-11 MPa ^[388])	For comfort of the patient and ease of implantation by the dental practitioner
Capable of loading PS and releasing steadily for up to 4 weeks	To allow for repeated activation of aPDT activity until oral mucosa epithelial layer has healed
Demonstrates stability and maintains porous structure in aqueous environments	To ensure it is suitable for implantation in moist oral environment
Maintains integrity up to 8 weeks	To support full neotissue formation
<30% cytotoxicity to mammalian cells in dark or light conditions	To ensure mammalian cells can populate the scaffold and for potential conformity with ISO 10993
Minimal bactericidal activity in dark conditions but ability to kill bacteria upon light activation	To allow for the dental practitioner to activate the aPDT in the scaffold 'on-demand' and selectively kill bacteria

Table 2.1 – Summary of scaffold requirements for oral applications

2.1.2 Research Objectives

- To determine suitable FDA-approved bioresorbable polyesters (e.g. PCL or PLGA) from which to manufacture a suitable electrospun scaffold for use in oral mucosal repair
- To investigate the effect of encapsulation within, and release of, PS (e.g. ER or MB) from the scaffold fibres on the biomaterial properties of the scaffold in an aqueous environment
- To investigate the selectivity achievable between human cells and bacterial cells
- To investigate the feasibility of commercialising the lead prototype as PhotoTherix™

Chapter 3 Manufacture and Characterisation of Photosensitiser-Loaded Electrospun Scaffolds

3.1 Introduction

The aim of the work described in this chapter was to manufacture and characterise the biomaterial properties of electrospun scaffolds with PS inclusion. This should address structure-function relationships for the desired therapeutic effects of an oral soft tissue regenerating medical device with antimicrobial capability.

3.2 Materials and Methods

3.2.1 Materials

1,1,1,3,3,3-hexafluoro-2-propanol (HFIP) solvent was sourced from Fluorochem Ltd. Poly(ϵ -caprolactone) (PCL) (M_n : 80,000 g·mol⁻¹) was sourced from Sigma Aldrich, whilst poly(*rac*-lactide-co-glycolide) (PLGA7525) (M_n : 63,000 g·mol⁻¹, 75:25 molar ratio of lactic and glycolic acid units) was purchased from Purac Biomaterials (PURASORB[®] PDLG 7507) (**Figure 3.1A** and **Figure 3.1B**). Methylene Blue (molecular mass of 319.85 g·mol⁻¹) and Erythrosin B (molecular mass of 835.90 g·mol⁻¹) PS were both sourced from Sigma Aldrich (**Figure 3.1C** and **Figure 3.1D**).

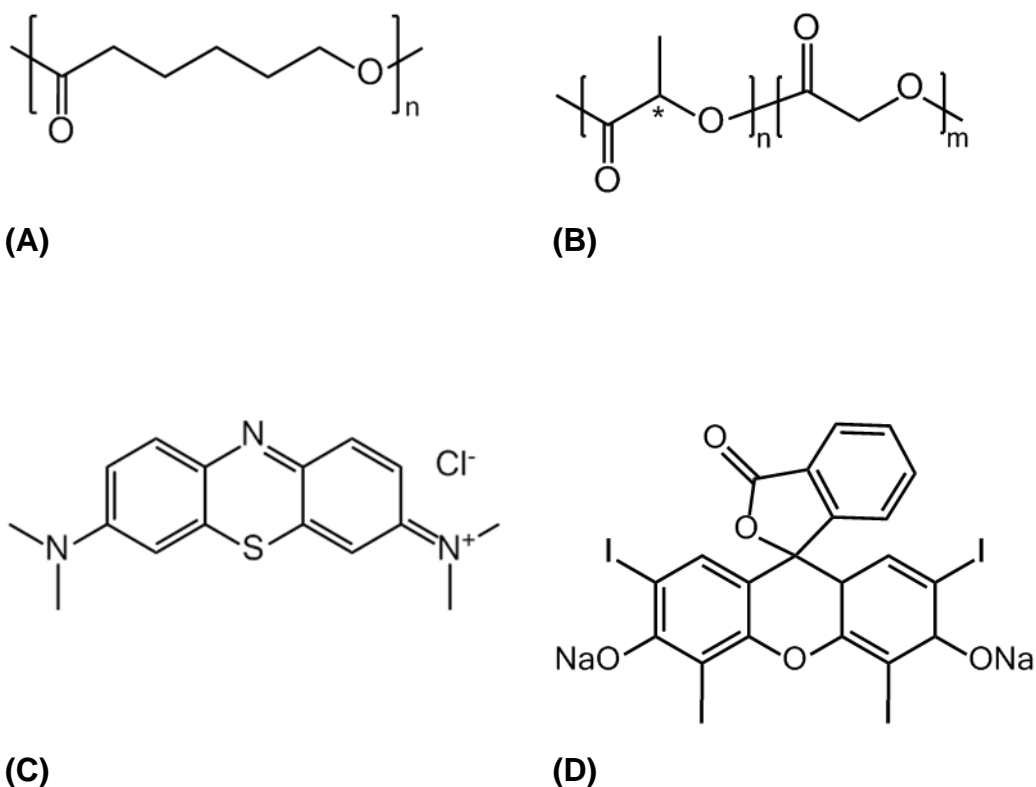


Figure 3.1 - (A-D): Chemical structure of selected polymers and PS. (A): Poly(ϵ -caprolactone) (PCL); (B): Poly[(rac-lactide)-co-glycolide] (PLGA7525) with 75:25 monomer ratio; (C): Methylene Blue (MB); (D): Erythrosin B (ER).

Sample nomenclature is as follows: samples of either fibres or electrospinning solutions were coded as Polymer-YY, whereby ‘Polymer’ identifies the type of polymer, i.e. either PCL or PLGA7525, whilst YY indicates the PS encapsulated in the sample, either MB or ER. Control samples without PS (‘No Dye’) will be called either PCL-ND or PLGA7525-ND throughout the results.

3.2.2 Electrospinning Solution Preparation

PCL and PLGA7525 were tested initially at 6 wt.%, 9 wt.% and 12 wt.% to determine the most optimal starting viscosity. Both MB and ER were used at a concentration of 2.2 mM in the electrospinning solution based on previous reports on MB and ER-induced aPDT^[334,389]. Polymer, PS and HFIP were weighed together into sealed flasks and covered with foil to protect

from ambient light. They were stirred at room temperature for 48 hours to allow for dissolution of all components.

3.2.3 Viscosity Measurements

Viscosity measurements were taken at room temperature as per manufacturer's instructions using a Brookfield DV-E bench top viscometer (Brookfield Engineering Laboratories, Inc., Middleboro, MA, US). Briefly, 9.0 ml of electrospinning solution was loaded into the sample holder, and spindle SC4-31 was placed into the solution. A steady shear stress reading was recorded from shear rates ranging from 0.68-6.8 sec⁻¹ for each sample. These were then converted to viscosity readings by dividing the shear stress value by the corresponding shear rate value.

3.2.4 Surface Tension

Density of solutions were calculated by weighing 1 ml of electrospinning solution in triplicate (and plotting mass versus volume) with the density calculated as 1.52±0.04 g/ml. Each electrospinning solution was loaded into a 2ml syringe with 18-gauge blunt-ended needle. The solution was ejected manually until a stable droplet was formed at the needle tip. KSV Pendant Drop equipment was used with Attension Theta Software Version 4.1.9.8 to analyse the droplet with 60 images taken over one minute.

3.2.5 Electrospinning

Polymer solutions were transferred into a 10 ml plastic syringe with an 18-gauge blunt-ended needle, which was then loaded into a syringe pump. A pump rate of 0.03 ml/min was used with an applied voltage of 16 kV. A cylindrical grounded mandrel (height = 125 mm, diameter = 75 mm) was coated with aluminium foil at 100 mm distance away from the needle tip and rotated at 30 RPM. Scaffolds were electrospun for 55±5 minutes, with both relative humidity (33±7%) and temperature (21±1 °C) being recorded for each experiment (88±54 µm thickness, measured using a digital fabric thickness testing gauge). Scaffolds were dried under reduced pressure in a vacuum desiccator for 72 hours to remove residual solvent. Scaffolds were

sealed in foil/poly bags (Sigma Aldrich) and frozen until use to prevent degradation.

3.2.6 Scanning Electron Microscopy

Dry samples were attached to metal stubs using carbon double-sided stickers and sputter coated with gold twice before being analysed on a 6-sample multi-stub holder on a Hitachi Scanning Electron Microscope (SEM) at 4000x magnification. Scaffolds were sensitive to high vacuum settings so VP-SEM (variable pressure-SEM) low vacuum setting was used (270 Pa) when required. Randomly selected locations were chosen to produce five images of each scaffold, and ten fibre diameters were taken from each image using ImageJ.

3.2.7 Loading Efficiency

Dry samples were cut into round discs (diameter = 1 cm) and weighed individually on an analytical balance. These were then incubated in glass vials with 5 ml of HFIP and rolled at 60 RPM for 48 hours to ensure full dissolution. A standard UV-vis (ultraviolet-visible) curve was drawn with the PS dissolved in HFIP over an appropriate concentration range using a photometric plate reader at wavelength of 610nm for MB and 530nm for ER. The loading efficiency (*LE*) value was calculated for each PS according to (Equation 3.1).

$$LE = \frac{m_d}{m_e} \times 100 \quad \text{Equation 3.1 – Loading Efficiency}$$

where m_d and m_e are the determined and expected values of PS mass loaded in the electrospun scaffold, respectively.

3.2.8 Brunauer–Emmett–Teller Analysis

To quantify the average surface area of the scaffolds and therefore give supporting information on the porosity of the scaffolds, Brunauer–Emmett–Teller (BET) analysis was performed. Micrometrics FlowPrep 060

was used to flush samples (approximately 0.4 g) with N₂ at 40 °C for 4 hours prior to analysis. Micrometrics TriStar 3000 Surface Area and Porosity Analyzer used along with complementary Tristar 3000 software to analyse the sample. A full isotherm was produced for each sample.

3.2.9 Porometry

Samples were soaked in a low surface tension Galpore125 (perfluoroether, surface tension 15.6 mNm⁻¹) solution before being displaced with air at a specific pressure within the POROLUX™ 100FM porometer. The Young-Laplace equation was used to convert this pressure into the diameter of the capillary (**Equation 3.2**).

$$\text{Pore diameter} = \frac{4 \times \cos \theta \times \gamma}{P} \qquad \text{Equation 3.2 – Young-Laplace}$$

with P representing the pressure required to displace the liquid from pore, θ representing the contact angle of the wetting fluid with the scaffold and γ representing the surface tension of Galpore125^[390].

The associated POROLUX™ software was used to calculate the largest and smallest pores, mean flow pore size, and the distribution of pore sizes in the scaffold.

3.2.10 Scaffold Colour Measurements

Further to PS-inclusion (and scaffold colouration), samples were analysed using an SF600 Plus-CT machine and the associated ColorTool © QC software. Prior to measurements being taken, the machine was calibrated using the provided white and green reference tiles. LAB readings were converted to on-screen colour using the RGB selection tool on MS Word.

3.2.11 Differential Scanning Calorimetry

A Differential Scanning Calorimeter (DSC) (Q100 – TA Instruments) was loaded with two metal cups. The first empty as a reference, and the second containing 6-12mg of sample (which was weighed out using an analytic balance). The machine was then programmed to run on a cycle from 20 °C to 200 °C for PLGA7525 scaffolds and 20 °C to 100 °C for PCL scaffolds to remove thermal history of the polymer at a heating rate of 10 °C/minute and a cooling rate of 5 °C/minute and then repeating to take the measurement. The glass transition and melting temperature were calculated using the operating software Thermal Advantage for Q Series Version 2.5.0.256 (©Thermal Instruments-Waters). The glass transition temperature was taken as the mid-point of the shift decrease in the DSC graph, and the maxima of the endothermic peak was taken as the melting point value. The DSC heat flow plots were plotted as 'exothermic up', with an increasing heat flow up the y-axis.

3.2.12 Tensile Testing

Dry scaffolds were cut into 10x30 mm strips and clamped into a James Heal™ Titan⁵ Universal Strength Testing machine with a 100 N loading cell and T27 jaw scheme. The equipment was used with TestWise 2017 test analysis software. A pretension of 0.5 N was applied to the material, and then the material was elongated at a speed of 100 mm/min until the material failed. Force against elongation measurements were recorded for each sample five times. Stress-strain curves were plotted, and the elastic modulus calculated as the slope of the linear region of the curve. The toughness was measured as the integral under the stress-strain curve.

3.2.13 Statistical Analysis

Significant differences in the results were evaluated using an unpaired Student's *t*-test. Data was deemed to be significantly different at $p < 0.05$. All data were collected in triplicate and presented as Mean \pm Standard Deviation.

3.3 Results and Discussion

3.3.1 Characterisation of Electrospinning Solutions

3.3.1.1 Initial Concentration Determination

PCL and PLGA7525 were expected to be suitable polymers for this project due to their frequent use in regenerative electrospun scaffolds and drug delivery devices in the published literature^[125,391]. PCL has been reported to biodegrade slowly in the body due to hydrophobicity^[218]. This could be advantageous for use in the harsh and moist oral environment as the polymer selected would need to resist degradation until neotissue formation has occurred. PLGA has highly tuneable properties depending on the selection of lactide to glycolide monomer ratio^[203]. The 75:25 monomer ratio used in this study has previously been used for both soft tissue regeneration and drug delivery purposes^[392–394]. A racemic mixture of D- and L-stereoisomers of the lactide component is more commonly chosen than the enantiomerically pure version of PLGA in drug delivery devices due to an increase in amorphous regions in the racemic polymer^[395]. These amorphous regions allow for greater drug dispersion resulting in a more even distribution^[395]. A commonly used volatile solvent to produce electrospinning solutions is HFIP, as it readily dissolves the polyesters through hydrogen bonding of the hydroxyl hydrogen to carbonyl groups^[396] and traces of the solvent can be removed from the finished product to safe levels with adequate drying^[195,397,398].

The viscosity of the electrospinning solution is known to affect fibre formation and to alter the resulting diameter of the electrospun fibres^[193,399], which could ultimately impact the scaffold degradation and PS release kinetics. Therefore, the viscosity of the electrospinning solutions both with and without PS for each polymer was determined. Initial screening of the polymer solutions in HFIP was performed to gain comparable viscosities and spinnability between polymer groups (**Figure 3.2**).

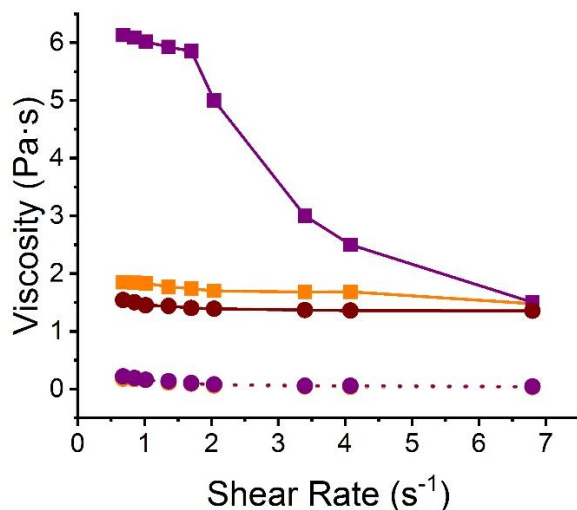


Figure 3.2 - Viscosity of electrospinning polymer solutions at different concentrations in HFIP. (■): PCL-ND-6 wt.%; (■): PCL-ND-9 wt.%; (●): PLGA7525-ND-6 wt.%; (●): PLGA7525-ND-9 wt.%; (●): PLGA7525-ND-12 wt.%. Lines are guidelines to the eye

A typical shear thinning behaviour was observed in all electrospinning solutions, whereby the solution viscosity was found to be inversely related to the shear rate, as expected for non-Newtonian liquids. The PCL and PLGA7525 polyesters were chosen for this study due to their comparable molecular weight (M_n : 63,000-80,000 g·mol⁻¹). Comparable viscosities were found between PCL-ND and PLGA7525-ND solutions at a shear rate of 6.8 s⁻¹ at concentrations of 6 wt.% PCL and 12 wt.% PLGA7525 in HFIP ($\eta = 1.5$ and 1.4 Pa·s respectively) (**Figure 3.2**). Similar polymer concentrations have been reported for the formation of electrospun fibres with or without soluble factors^[400–403].

Each of these polymer solutions were electrospun to ensure that the selected concentrations were suitable to produce bead-free fibres (**Figure 3.3**).

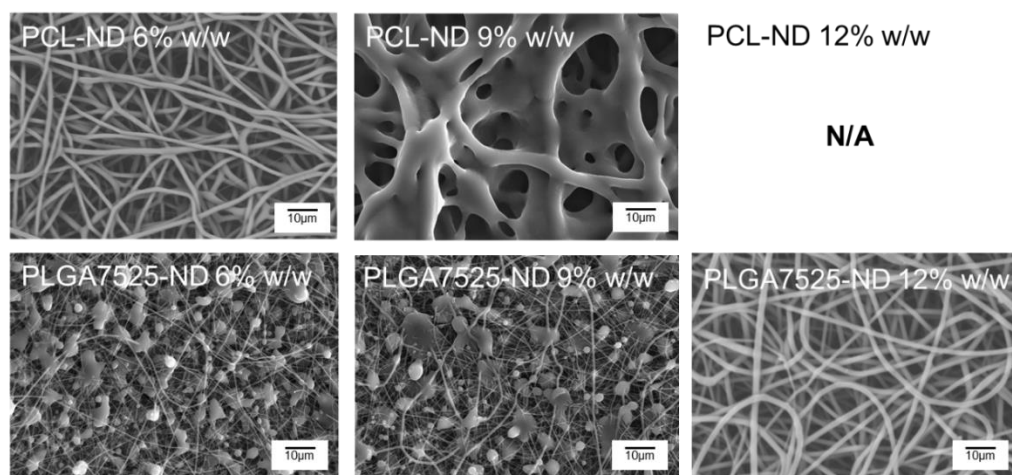


Figure 3.3 - Scanning Electron Micrographs to determine fibre morphology from electrospinning different concentrations of PLGA7525 and PCL solutions. Electrospinning was not possible for the PCL-ND 12 wt.% formulation due to high viscosity

The PCL-ND and PLGA7525-ND solutions which were chosen based on their viscosities produced smooth fibres. The increased viscosity in the PCL scaffolds produced a clumped non-fibrous structure. Any further increase in the viscosity prevented electrospinning. The reduction of the concentration and consequent viscosity of the PLGA7525 solution resulted in beaded fibre formation in the resulting scaffolds. This has been observed numerous times in previously published work^[273,277,308,404–406]. This confirmed that appropriate polymer solution concentration had been selected and the influence of PS-inclusion could be studied.

3.3.1.2 Viscosity and Surface Tension with Photosensitiser Inclusion

Following this initial decision on the concentration of the polymer in the scaffold, a concentration of 2.2 mM of either MB or ER was employed in the electrospinning solutions. The aim of this was to achieve electrospun fibres with prolonged PS release and antimicrobial effect. Each PS was combined separately with each polymer type, and the resulting solutions were electrospun (**Figure 3.4**).

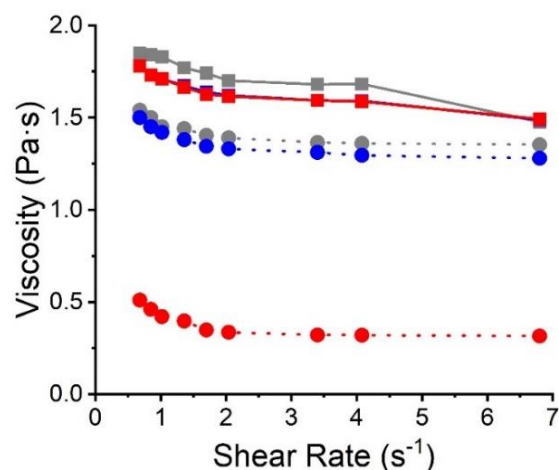


Figure 3.4 - Viscosity of native and PS-loaded electrospinning polymer solutions. (■): PCL-ND; (■): PCL-MB; (■): PCL-ER; (●): PLGA7525-ND; (●): PLGA7525-MB; (●): PLGA7525-ER. Lines are guidelines to the eye.

Again, shear thinning behaviour was observed in all electrospinning solutions regardless of the selected PS and polymer. Compared to respective PS-free polymer solutions, loading of PS did not induce detectable changes in the viscosity of the PCL-MB, PCL-ER or PLGA7525-MB polymer solutions ($p = 0.10-0.12$), whilst the viscosity of solution PLGA7525-ER proved to be significantly decreased ($p = 5.5 \times 10^{-16}$) (**Figure 3.4**). Previous studies reported that low concentrations of additives ($< 12 \text{ mg}\cdot\text{ml}^{-1}$) do not significantly change the viscosity of the electrospinning polyester solution^[407], in agreement with the majority of the results obtained in this study. The significantly-decreased value of viscosity measured in PLGA7525-ER solutions with respect to solutions PLGA7525-ND and PLGA7525-MB may hint at secondary, e.g. hydrophobic, interactions between the PS and the fibre-forming polymer, as indirectly observed in ER-loaded PLGA nanoparticles^[408]. Such secondary interactions between ER and PLGA7525 are expected to compromise the polymer chain entanglements leading to a decrease in solution viscosity, as observed previously with different polymer and additive formulations^[174,398,400,409].

The surface tension of solutions was also determined, since surface tension is expected to inversely relate to the electrospinnability of a given solution (**Table 3.1**)^[410].

Electrospinning Solution		Surface Tension (mN/m)
PCL	ND	32.0±0.6
	MB	28.2±0.5
	ER	32.2±0.3
PLGA7525	ND	32.5±2.8
	MB	32.4±0.8
	ER	33.2±1.9

Table 3.1 – Electrospinning Solution Surface Tension. Results reported as Mean±SD (n=3)

The surface tension appeared to be comparable between PCL- ($\sigma = 28\pm 1$ – 32 ± 1 mN·m⁻¹) and PLGA7525-based ($\sigma = 32\pm 1$ – 33 ± 2 mN·m⁻¹) electrospinning solutions, whilst the range of surface tension values was found to be in agreement with the one observed in previously-reported electrospinning polyester solutions^[231]. There has been great interest into elucidating the relationship between surface tension and viscosity of electrospinning solutions and their effects on scaffold microarchitecture^[411–413], since the fluid viscosity concerns the molecular interactions in the bulk of the solution, whereas the surface tension reflects the interactions of the solution at the air-liquid interface^[411]. The above-mentioned surface tension results would therefore suggest that any change in the characteristics of the electrospun scaffolds are likely due to the PS-polymer-solvent secondary interaction in the bulk of the solution rather than at the air-liquid interface of the Taylor cone and subsequent jets during electrospinning^[414].

3.3.2 Characterisation of Electrospun Scaffolds

3.3.2.1 Scaffold Formation

Obtained polymer solutions successfully led to the formation of bead-free fibrous scaffolds (**Figure 3.5**), confirming that previously-measured solution viscosities and surface tensions were compatible with the electrospinning of selected polymers and PS.

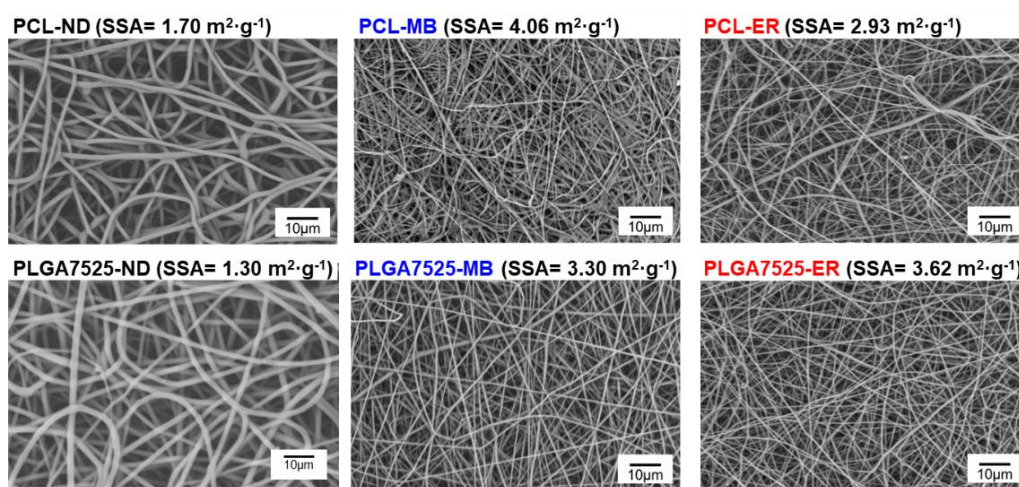


Figure 3.5 - Microstructural analysis of PS-encapsulated scaffolds and electrospun controls. SEM images taken at 1000x magnification and Specific Surface Area (SSA) measurements obtained via BET analysis.

To elucidate the scaffold loading efficiency and demonstrate the fibre encapsulation with either MB or ER, respective electrospun scaffolds were dissolved in HFIP to induce full release of incorporated PS (**Table 3.2**).

Sample ID	PCL		PLGA7525	
	MB	ER	MB	ER
LE /wt.%	103±16	103±31	110±16	97±30

Table 3.2 - Loading efficiency (LE) and percent release measured in PCL and PLGA7525 scaffolds electrospun in the presence of either MB or ER. Results reported as Mean±SD (n=3).

Photometric analysis of the resulting solution revealed a loading efficiency in the range of 97±30–110±16 wt.% therefore confirming that all the PS dissolved in the electrospinning solution was successfully encapsulated in the resulting fibres. Certain samples showed a greater than 100% loading efficiency, which would indicate that there was a greater mass of PS than would be expected. This could be due to the PS interacting strongly with the polymer.

SEM, BET analysis and porometry were performed on the scaffolds enabling quantification of fibre diameter as well as scaffold specific surface area and pore size, respectively. Despite employing the same molar concentration of PS, there was a significant reduction in fibre diameter upon encapsulation of either PS molecules in both scaffold systems (**Figure 3.5** and **Figure 3.6A**).

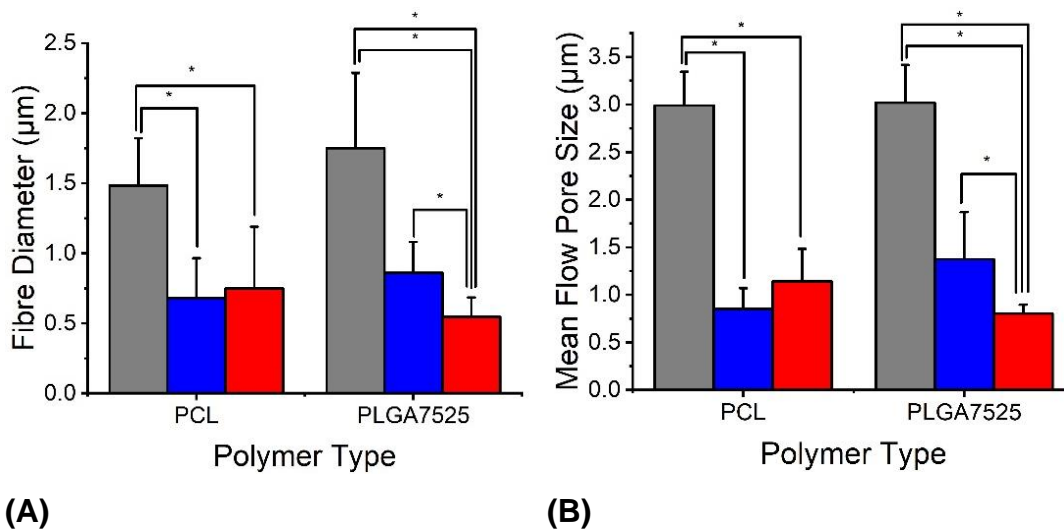


Figure 3.6 - (A) Average Fibre Diameter determined from SEM images for each electrospun scaffold. (B) Average Mean Flow Pore Size determined from porometry analysis for each electrospun scaffold. Grey bars: Control scaffolds; Blue bars: MB-included scaffolds; Red bars: ER-included scaffolds. Results reported as Mean±SD (n=3). ‘*’ denotes significantly different means ($p < 0.05$, t -test).

For PCL scaffolds, encapsulation with either MB or ER resulted in 54% and 49% averaged reduction of fibre diameter, respectively, and similar values (51-69%) were also observed with PLGA7525-based samples. Such reduction of fibre diameter has been observed in other fibrous systems, deriving from electrospinning of PCL solutions containing peptides^[415]. Introduction of ionically-charged PS, such as MB and ER, is likely to cause increased electrostatic repulsion between fibre-forming polymer jets in the electrospinning process^[416]. For the PLGA7525-ER scaffolds, there was a further significant reduction in fibre diameter with respect to PS-free and MB-encapsulated PLGA7525 scaffolds. This additional reduction in fibre diameter is in agreement with the significant decrease in viscosity observed in ER-loaded electrospinning solutions (**Figure 3.4**), since electrospinning solutions with reduced viscosity typically generate fibres with reduced diameter ^[273,417].

Porometry was next performed to determine the pore size among the fibres within the fibrous structure (**Figure 3.6B** and **Figure 3.7**).

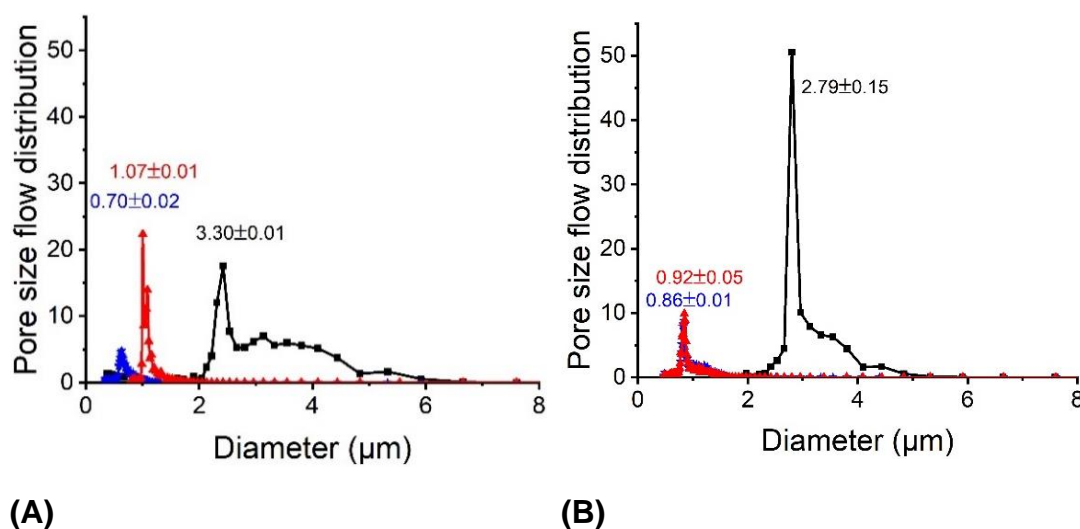


Figure 3.7 - Pore size distribution of scaffold types. (A) PCL scaffolds; (B) PLGA7525 scaffolds. Black lines: Polymer-ND scaffolds; Blue lines: Polymer-MB scaffolds; Red lines: Polymer-ER scaffolds. Values of mean flow pore size (µm) are given for each scaffold type. Results reported as Mean±SD (n=3).

The pore size between fibres is an important characteristic for a regenerative scaffold, as delivery of soluble factors, e.g. encapsulated PS, and cell infiltration have been shown to be altered by the pore size, with fibroblast cells being unable to bridge pores larger than 20 µm^[418]. A pore size in the range of 0.7-3 µm was measured among the different scaffolds, whereby the scaffold formulation proved to induce variations in pore size comparable to those found with the fibre diameter, i.e. PS-encapsulated fibres were associated with scaffolds of decreased pore size. It is expected that an increased number of fibres with decreased diameter will be required to fill the same scaffold volume compared to fibres with an increased diameter. Previous porometry measurements therefore confirm the direct relationship between the fibre diameter and pore size in electrospun scaffolds ^[4]. The observed trends in fibre diameter is consistent with the

variations in specific surface area of the scaffolds (**Figure 3.5**), since fibres with reduced diameter are expected to lead to scaffolds with increased specific surface area ^[419]. Overall, the averaged pore size was measured to be below 4 μm in all samples, suggesting that cell should be able to bridge these distances. Furthermore, this range of pore size is likely to promote the release of the PS molecule via a predominant diffusion mechanism through the scaffold, given the relatively low molecular weight of selected soluble factors ($M < 900 \text{ g}\cdot\text{mol}^{-1}$).

Interestingly, a narrow pore size distribution was found in PS-encapsulated scaffolds, in contrast to the broader range of pore size measured with the PS-free electrospun controls (**Figure 3.7**). Given the electrostatic charge of the PS molecules employed, this observation provides supporting evidence of the PS-induced electrostatic repulsion between polymer electrospinning jets. This ultimately results in PS-encapsulated scaffolds with more regular porous architectures with respect to the case of PS-free electrospun controls, as previously reported with other electrostatically-charged additives ^[416].

3.3.2.2 Polymer Scaffold Colour

Together with the photometric analysis, PS encapsulation proved to induce fibre colouration effects on the resultant scaffolds (**Figure 3.8**).



Figure 3.8 - Macroscopic images of PS-free and PS-encapsulated scaffolds.

As would be expected, PS-free and ER-encapsulated fibres appeared ‘white’ and ‘pink’ respectively. Unusually, MB-incorporated scaffolds displayed either a ‘purple’ or ‘blue’ colour depending on whether fibres were made of PCL or PLGA7525. This was quantified through the use of LAB Colour Space equipment to convert the macroscopic colour observed into LAB values to provide specific colours regardless of print or screen effects (**Table 3.3**).

	L	A	B
PCL-MB	68.55	24.6	-20.24
PCL-ER	81.66	32.03	-6.94
PLGA7525-MB	72.08	-19.95	-24.81
PLGA7525-ER	86.08	30.38	-6.24

Table 3.3 – LAB colour space results for PS-loaded scaffolds.

Colours of associated rows represent the colour of the scaffold as per the LAB result.

Although the colouration of PS-loaded materials is mainly determined by the specific PS and respective loading efficiency, as in the case of ER-encapsulated samples, the above-mentioned observations on MB-encapsulated samples suggest that secondary interactions between PS molecules and the polymer carrier may also play a role. With regards to MB, it has been described in previous publications that loading of cellulosic derivative with MB species typically results in a blue colouration; however, when the PS concentration was increased, a purple colouration was observed in respective MB-encapsulated polymer ^[420]. This is said to be due to the aggregation of MB molecules via non-covalent pi-pi stacking interactions between aromatic rings of MB (**Figure 3.9**).

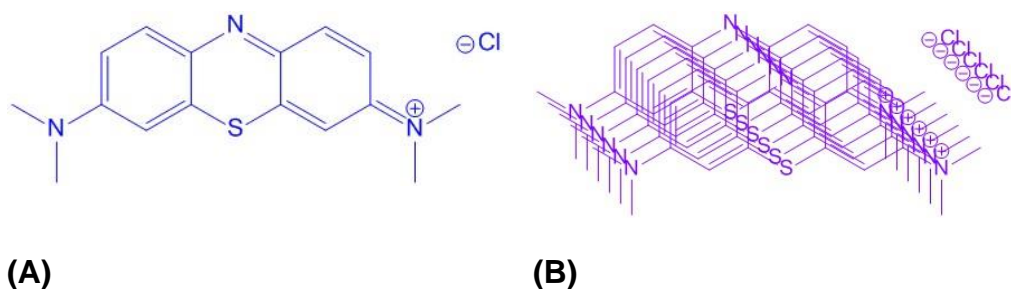
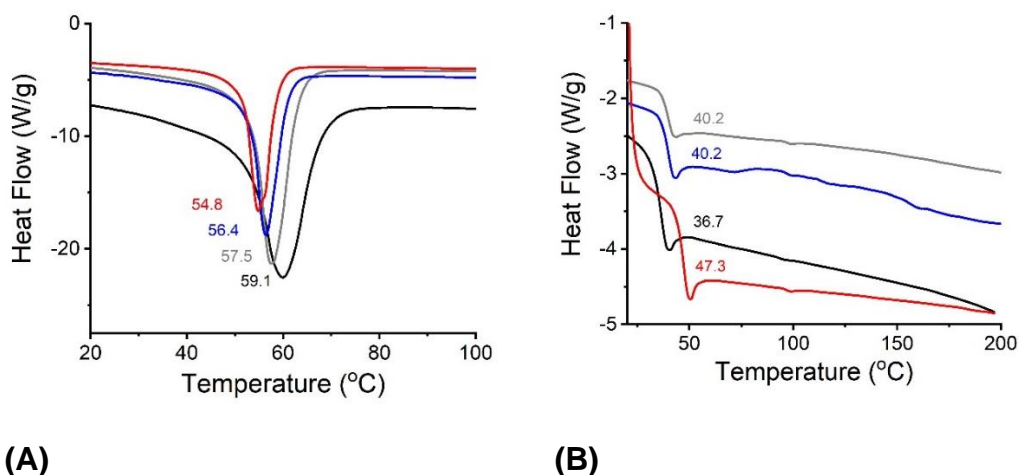


Figure 3.9 – (A) Encapsulation of MB in the monomeric state results in a blue colour of respective fibres. (B) Aggregation of MB molecules results in a purple colour of PS-encapsulated fibres^[420]

In this study, the higher viscosity measured in MB-loaded PCL solutions with respect to the corresponding PLGA7525 variant (**Figure 3.4**) suggests a different state of MB molecules in the PCL solutions and resulting fibres. In the aggregated MB configuration, a lowered energy is required for the electrons to be excited, resulting in a red shift in the wavelength of visible light being absorbed and in a distinct fibre colouration effect. It is worth noting that UV-vis spectrophotometry experiments were conducted to determine whether this change was observable in the electrospinning solution, but no differences were found prior to scaffold formation. Aggregation is therefore expected to increase upon solvent evaporation during the electrospinning process.

3.3.2.3 Crystallinity

Crystallinity is known to effect many properties of polymeric scaffolds^[241,300,421–426]. It was therefore deemed important to determine the crystallinity of the polymers prior to processing, and then once again when in scaffolds either with or without PS-inclusion (**Figure 3.10**).



(A) **(B)**
Figure 3.10 – Differential Scanning Calorimetry heat flow plots of (A) PCL scaffolds and (B) PLGA7525 scaffolds. (—): Unprocessed polymer; (—): Pol-ND scaffolds; (—): Pol-MB scaffolds; (—): Pol-ER scaffolds

The results in this study suggest that PCL samples were predominantly crystalline, as only a sharp melting peak was observed (**Table 3.4**).

Scaffold Type		T _m (°C)	ΔH _m (J/g)	T _g (°C)
PCL	Raw	59.1	187.7	-
	ND	57.5	118.2	-
	MB	56.4	89	-
	ER	54.8	71.9	-
PLGA7525	Raw	-	-	36.7
	ND	-	-	40.2
	MB	-	-	40.1
	ER	-	-	47.3

Table 3.4 – DSC Thermal Analysis Values for PCL or PLGA7525 samples of either ‘Raw’ polymer pellets, PS-free (ND) control scaffolds, MB-incorporated scaffolds or ER-incorporated scaffolds

The crystallinity of PLGA is known to be affected by the monomer ratio of the two monomer components^[427–429]. PLGA7525 samples in this study were predominantly amorphous as no melting peak was observed but there was a clear glass transition point for all samples. These characteristics have been reported previously in the literature^[430].

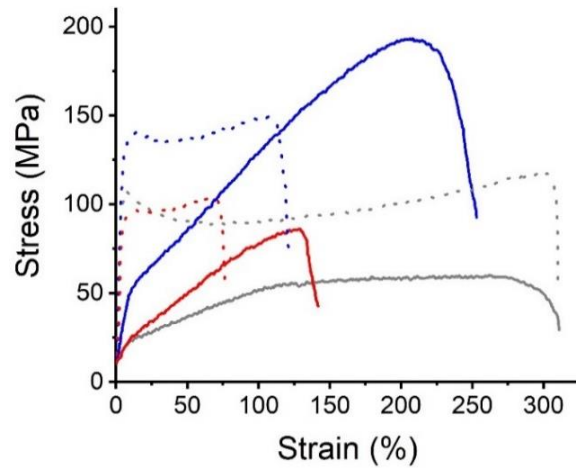
Another key observation in these results is that there was a noticeable shift in both the melting point and the glass transition state of each polymer upon inclusion of PS. In the PCL samples, the melting point decreased from unprocessed polymer ($T_m = 59.1^\circ\text{C}$), to the control electrospun PCL scaffolds ($T_m = 57.5^\circ\text{C}$), to the MB and ER PS-included scaffolds ($T_m = 56.4^\circ\text{C}$ and 54.8°C respectively). This phenomenon is commonly known as a ‘melting point depression’^[431]. The more the contaminant, i.e. PS, interacts with the polymer, the greater the depression in the melting point. This would imply that the ER is interacting most strongly with the polymer.

A similar trend was observed in the glass transition state of the PLGA7525 samples, with the unprocessed PLGA7525 having the lowest glass transition temperature ($T_g = 36.7^\circ\text{C}$), then the PLGA7525-ND and PLGA7525-MB scaffolds having the same increased glass transition temperature ($T_g = 40.2^\circ\text{C}$), and the PLGA7525-ER scaffolds having the greatest transition temperature ($T_g = 47.3^\circ\text{C}$). This increase in glass transition temperature is again normally indicative of a distinct interaction between the polymer and contaminant, in this case the PLGA7525 and the ER molecules^[432]. This is further supporting evidence towards the secondary interaction which was suggested in the increased fibre diameter reduction effect (section 3.3.2.1).

3.3.2.4 Mechanical Properties of Scaffolds

The mechanical properties of the scaffolds were measured on the samples to investigate the potential effect of PS encapsulation on tensile properties (**Figure 3.11** and **Figure 3.12**). This characteristic is important to explore as it will change the surgical handling capability and the scaffold

applicability *in vivo*, e.g. for oral soft tissue applications, because the elasticity of the fibrous matrix has been shown to alter cell adhesion^[433].



(A)

(B)

Figure 3.11 - (A): Stress-strain curve of PS-encapsulated scaffolds and electrospun controls. (—): PCL-ND; (—): PCL-MB; (—): PCL-ER; (---): PLGA7525-ND; (---): PLGA7525-MB; (---): PLGA7525-ER. (B): Experimental setup employed during tensile testing

When comparing the elastic modulus of PCL-ND ($E = 1.4 \pm 0.3$ MPa) and PLGA7525-ND ($E = 18.7 \pm 1.9$ MPa) control scaffolds, the PLGA7525-ND scaffold has a significantly greater elastic modulus ($p = 0.00005$) (**Figure 3.12A**). This comparison of the two polyester types has been observed previously in the literature^[434].

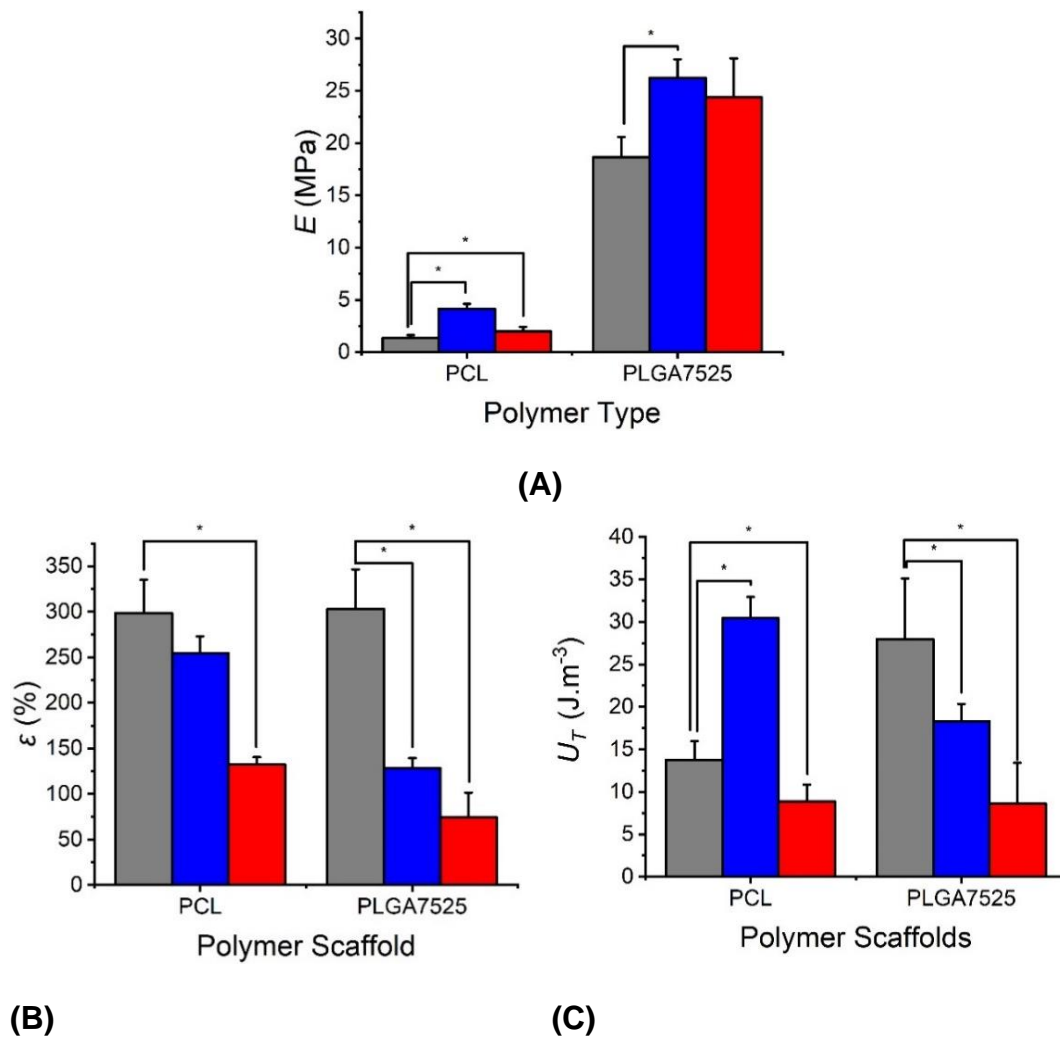


Figure 3.12 (A) Elastic Modulus (E) and (B) Strain at Break (ϵ) measured in PCL or PLGA7525 samples (C) Ultimate Toughness (U_T). Grey bars: control polymer scaffolds; Blue bars: MB-loaded scaffolds; Red bars: ER-loaded scaffolds. Results reported as Mean \pm SD (n=3). “*” denotes significantly different means ($p < 0.05$, t -test)

The elastic modulus values reported for the scaffolds are in agreement with previously reported values^[184,435]. PCL-MB ($E = 4.2 \pm 0.5$ MPa) and PCL-ER ($E = 2.0 \pm 0.4$ MPa) scaffolds both showed a significant increase in comparison to PCL-ND controls ($p = 0.00004$ and 0.04 respectively). In the literature, it has been previously reported that inclusion of drugs increases the elastic modulus of fibrous PCL scaffolds^[436]. For the

PLGA7525 samples, the PLGA7525-MB ($E = 26.2 \pm 1.8$ MPa) elastic modulus was significantly increased ($p = 0.0004$) as found with the PCL scaffolds, but the PLGA7525-ER scaffolds ($E = 24.4 \pm 3.7$ MPa) did not highlight a significant difference to the control scaffolds ($p = 0.4$).

The elastic modulus of the natural oral mucosa is thought to be approximately 3 MPa, but this varies between 0.9-11 MPa depending on the location within the oral cavity^[178,388,437]. While the PCL scaffolds exhibited a comparable modulus to that of the native tissue, PLGA7525 scaffolds displayed increased tensile modulus with respect to the natural tissue. Consequently, these electrospun fibres may prove advantageous to enable easy surgical handling of the graft material during implantation minimising risks of material breakdown. The elasticity of the scaffold will also influence the interactions with contacting tissue *in vivo*^[184].

There was no significant difference between the elongation at break (ϵ) values between the PCL-ND ($\epsilon = 299 \pm 36\%$) and PLGA7525-ND ($\epsilon = 303 \pm 44\%$) control scaffolds ($p = 0.9$) (**Figure 3.12B**).

PCL-MB scaffolds ($\epsilon = 255 \pm 18\%$) did not show a significant difference when compared to the PCL-ND control ($p = 0.08$) but PCL-ER scaffolds showed a significant reduction in elongation at break ($\epsilon = 132 \pm 8\%$) ($p = 0.001$). Comparatively, both PLGA7525-MB ($\epsilon = 128 \pm 11\%$) and PLGA7525-ER ($\epsilon = 74 \pm 27\%$) displayed a significant reduction in elongation at break ($p = 0.0009$ and 0.01 respectively) when compared to the PLGA7525-ND controls.

The difference between polymer types and the effect of PS encapsulation is also reflected in the toughness values (U_T) obtained through integrating the area under each stress-strain curve (**Figure 3.12C**). The toughness value represents the energy required to fracture the material, so the higher the value, the more tough this sample proved to be^[438]. As with the elastic modulus, PLGA7525-ND samples ($U_T = 28.0 \pm 7.1$ J.m⁻³) had a significant increase in toughness when compared to PCL-ND scaffolds ($U_T = 13.8 \pm 2.2$ J.m⁻³) ($p = 0.01$). This increase in toughness and elasticity would make the polyester desirable for use biomaterial scaffolds.

For the PCL scaffolds, interestingly, there was a large significant increase in toughness for the PCL-MB scaffolds ($U_T = 30.4 \pm 2.5 \text{ J.m}^{-3}$) ($p = 0.000009$) but a significant decrease for PCL-ER scaffolds ($U_T = 8.9 \pm 2.0 \text{ J.m}^{-3}$) ($p = 0.01$). The increase in toughness and elasticity for the PCL-MB scaffolds is unexpected, as normally an increase in one of these properties reduces the other^[439,440]. However, other reports of this phenomenon have been reported in previous literature with fibrous scaffolds^[441].

There was no significant difference in the toughness of the PLGA7525-MB scaffolds ($U_T = 18.3 \pm 2.0 \text{ J.m}^{-3}$) ($p = 0.05$) but the PLGA7525-ER scaffolds ($U_T = 8.6 \pm 4.8 \text{ J.m}^{-3}$) displayed a significant decrease in toughness ($p = 0.01$). Again, these changes in mechanical properties with the addition of soluble factors have been observed in previous studies^[434], providing further indirect evidence of the development of secondary, e.g. hydrophobic, interactions between the PS molecule and the fibre-forming polymer.

3.4 Conclusion

This study has successfully used viscosity measurements to find suitable polymer concentrations to manufacture smooth, bead-free fibrous scaffolds of two different FDA-approved polyesters via electrospinning. These polymer solutions have then been loaded with two different PS. Despite shear-thinning behaviour being observed in all electrospinning solutions, there was only a significant reduction in the PLGA7525-ER polymer solution, which suggested a secondary interaction being present between the polymer and the ER molecules.

After electrospinning these polymer solutions, it was confirmed that the loading efficiency in each scaffold was ~100%. Another key finding was that PS-inclusion significantly reduced both the fibre diameter and pore size. This was expected to have implications on cell adhesion in later studies. There was an additional reduction in both fibre diameter and pore size in the PLGA7525-ER scaffolds, which was expected to be due to the reduced viscosity of the electrospinning solution.

The macroscopic colour of the MB-containing scaffolds depended on the polymer carrier, with the PCL scaffolds being purple-like and the PLGA7525 being blue-like. This was expected to be due to the secondary interactions in the PLGA7525-MB scaffold which caused the MB to be in the monomeric form along each fibre, whereas in the PCL scaffolds, the MB had aggregated upon electrospinning resulting in the purple colouration.

The characterisation of the thermal properties of the scaffolds revealed that the PCL scaffolds were all crystalline and the PLGA7525 scaffolds were all amorphous. The inclusion of each PS in the PCL scaffolds resulted in a melting point depression, which is expected with contaminant interaction disrupting the crystal structure of the polymer chains. The increase in glass transition temperature for the PLGA7525-ER scaffold also indicates secondary interactions between the polymer and ER molecules, which confirms the finding with the reduced viscosity, fibre diameter and pore size.

Finally, the mechanical properties of the scaffolds were studied. In all scaffolds, the PLGA7525 had a greater elastic modulus than the PCL scaffolds. The inclusion of PS increased the elastic modulus between control and PS-containing scaffolds. The only exception to this was the PLGA7525-ER scaffold which showed a small but insignificant increase. These mechanical properties may affect the clinical use of the scaffold in terms of handleability and comfort for the patient.

To summarise, a number of scaffold characterisation techniques were adopted to elucidate the scaffold morphology and physical behaviour. The next stage in the study analysed these scaffolds in terms of their interactions to an aqueous environment.

Chapter 4 Interactions of Photosensitiser-Loaded Electrospun Scaffolds with Aqueous Medium

4.1 Introduction

The aim of the research in this chapter was to determine the interactions between PCL or PLGA7525 electrospun scaffolds with MB or ER PS in aqueous environments. These interactions will be influenced by the structural characteristics determined in Chapter 3. The choice of materials will affect the hydrophobicity of the scaffolds, which has been shown to influence cell integration in tissue regenerating devices^[442]. The release profile of the PS from the scaffolds will be a vital characteristic for the functionality of the antimicrobial PDT, as a slow release will prevent cytotoxic concentrations of PS from accumulating and allow for repeat activations of the PS. The degradation profile is also important as the scaffold is required to maintain integrity in an oral environment for a sufficient time to allow for new tissue formation to occur^[443].

4.2 Materials and Methods

4.2.1 Contact Angle

Static contact angle measurements were recorded in triplicate for each scaffold using an FTA 4000 Contact Angle Goniometer and the associated software package. The scaffolds were attached to glass slides to hold them flat for analysis. A microsyringe was used to drop deionised water onto the surface of the scaffold. After a few seconds, an image was taken, and the shape of the droplet was analysed to calculate the contact angle. As the scaffolds are fibrous, additional analysis was performed on films produced from the electrospinning solutions to compare contact angles without interference from pore size and fibre diameter discrepancies. To produce the films, glass slides were coated in the corresponding

electrospinning solution and left for the HFIP to evaporate for 7 days. Following this time, the films were analysed in the same way.

4.2.2 Release Kinetics

Samples were cut into discs and weighed (ca. 20 mg) before being incubated with 5 ml of phosphate-buffered saline (PBS) solution at 37°C for up to 4 weeks. At selected time points, 100 µl of the solution was collected, analysed by UV-vis spectroscopy, and added back to the sample. The collected solutions (100 µl) were analysed on a microplate reader to record peak absorbance at either 610 nm (for MB) or 530 nm (for ER). Resulting absorbance values were converted into concentration of PS in the medium via a linear absorbance-concentration calibration curve ($R^2 > 0.99$) obtained by measuring solutions whose PS concentrations covered the range used for scaffold PS encapsulation.

4.2.3 Water Uptake Analysis

Samples were cut into 1 cm² squares and weighed individually before being incubated in well plates at 37°C in 5ml of distilled water (dH₂O) for 24 hours. Samples were then removed and blotted dry on filter paper to remove non-bonded water before being weighed again on an analytical balance. The percentage water uptake (WU) of each scaffold was calculated (**Equation 4.1**).

$$\text{WU} = \frac{m_w - m_d}{m_d} \times 100 \quad \text{Equation 4.1 – Percentage Water Uptake}$$

where m_w and m_d represent the mass values of hydrated and dry scaffold discs respectively. All samples were analysed in triplicate.

4.2.4 Hydrolytic Degradation

Samples were cut into 1 cm² squares and weighed before being incubated with 5 ml of PBS solution in sealed Falcon tubes at 37°C for up to 8 weeks. At selected time points, samples were removed, washed in dH₂O

three times for 5 minutes each time on a shaker plate and blotted dry before being dried in vacuum desiccator for 1 week. All samples were analysed in triplicate. The percentage mass loss of the scaffolds was calculated (Equation 4.2).

$$\text{Mass loss} = \frac{m_t - m_d}{m_d} \times 100 \quad \text{Equation 4.2 – Percentage Mass Loss}$$

where m_t and m_d represent the mass values of either the dry partially degraded scaffold disc at the selected time point t , or the dry, freshly prepared electrospun scaffold disc, respectively.

4.2.5 Scanning Electron Microscopy

As described in Section 3.2.6

4.2.6 Statistical Analysis

Significant differences in the results were evaluated using an unpaired Student's t -test. Data was deemed to be significantly different at $p < 0.05$. All data were collected in triplicate and presented as Mean \pm Standard Deviation.

4.3 Results and Discussion

4.3.1 Wettability

4.3.1.1 Contact Angle

The contact angle measurements allow quantification of the overall wettability of the scaffold. This is relevant since either PS diffusion or cell adhesion (to the surface of biomaterials) can be significantly affected by the surface wettability [442,444]. A contact angle of over 90° indicates a low interaction between the scaffold and the water (a hydrophobic response)[445]. Since fibre and pore size within the fibrous scaffold will affect the contact angle[446,447], water contact angle measurements were carried out on both

the scaffolds and the pore-free films obtained via casting and drying of the same electrospinning solution (**Figure 4.1**).

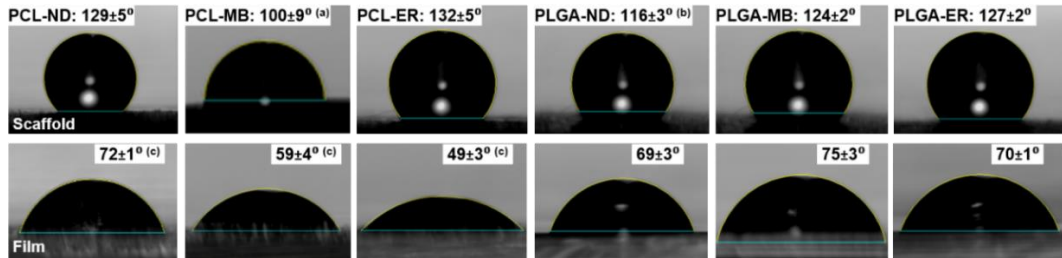


Figure 4.1 - Water contact angle (WCA) images and measurements on dry PS-encapsulated and PS-free (ND) samples in the form of electrospun scaffold (top) and film (bottom). Results reported as Mean±SD (n=3). (a)-(c): significantly different means ($p < 0.05$, t -test)

Both PLGA7525 and PCL scaffolds proved to display water contact angles higher than 90°, whereby a significant increase in contact angle was measured on PLGA7525 scaffolds containing either MB or ER when compared to the PLGA7525-ND scaffold ($p = 0.03$ and 0.008 respectively). Fibrous scaffolds with a greater surface area have been shown to have an increased contact angle to those with a smaller surface area^[446], and this trend was confirmed in this study via BET analysis and porometry on PLGA7525 scaffolds (section 3.3.2.1). PCL-MB electrospun samples displayed a significantly decreased water contact angle with respect to those of ER-encapsulated and PS-free electrospun samples, so the variation in contact angles across the different sample groups did not seem correlated to the effect of PS encapsulation on the surface of electrospun structures. In order to clarify this point, the effect of the fibre diameter and pore size was neglected, and pore-free films were analysed.

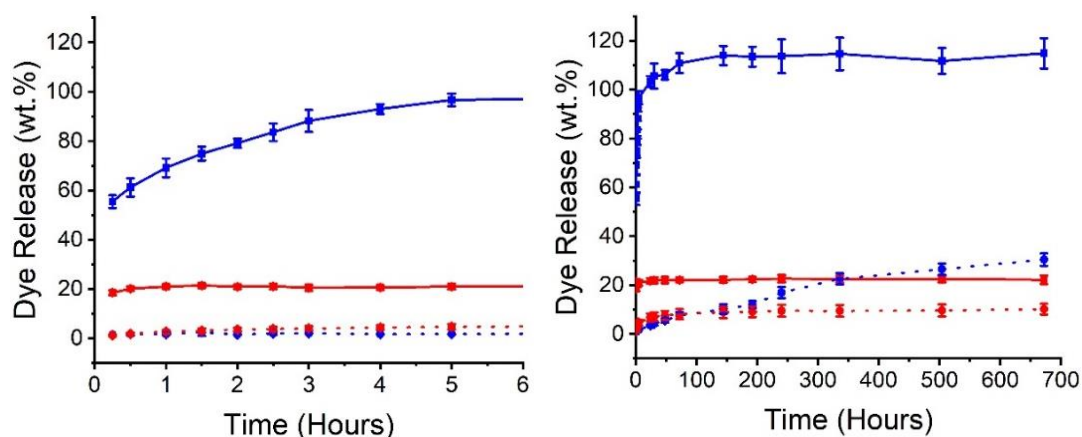
Water contact angles well below 90° were measured in pore-free films obtained from respective electrospinning solutions, indicating that all films displayed increased compatibility with water in contrast to the case of the electrospun scaffold. There was a significant reduction in contact angle in

both MB- and ER-loaded PCL films with respect to PS-free (ND) PCL controls ($p = 0.03$ and $p = 0.005$, respectively), in agreement with previous publications^[415,448,449], whilst no significant difference was found for either the PLGA7525-MB or PLGA7525-ER films ($p = 0.06$ and 0.6 respectively) with respect to the PLGA7525-ND controls. Contact angle values obtained with PCL films therefore suggest that PS molecules directly interact with the water droplet, leading to increased wettability of the polymer surface with respect to the case of electrospun fibrous structures. Electrospun scaffolds are non-homogeneous porous materials constructed from solid fibres, such that the superficial discontinuities (i.e. air in pores) appear to be responsible for the different wetting behaviour of scaffolds with respect to pore-free samples. On the other hand, it should be noted that film formation is a different process to that of electrospinning, as in film formation the polymer solution (with or without PS) is cast and air-dried.

4.3.1.2 Photosensitiser Release

The PS release profile from these scaffolds is crucial in terms of the intended clinical use of prototype scaffold described previously (section 1.3). A gradual release would allow repeated activation of the PS which would enable the dental surgeon to reactivate the antimicrobial activity of the scaffold should an infection arise requiring more than one aPDT treatment. Studies have shown post-operative oral infections are most likely to occur within the first 28 days following surgery, so it was decided that this would be the maximum time point needed to monitor the PS release as at this time point, healing of the oral mucosa should have taken place and the risk of infection should therefore be reduced^[13,47].

Electrospun PCL samples generally presented a faster PS release profile compared to equivalent PLGA7525 variants, whilst MB proved to be more readily released compared to ER, regardless of the polymer carrier employed (**Figure 4.2**).



(A) **(B)**
Figure 4.2 - Typical PS release profiles measured via UV-Vis spectroscopy of the supernatant collected during incubation (PBS, 37 °C) of MB- and ER-encapsulated scaffolds at selected time points over (A): 6 hours or (B): 672 hours (4 weeks). (-■-): PCL-MB; (-■-): PCL-ER; (·▲·): PLGA7525-MB; (·▲·): PLGA7525-ER. Lines are guidelines to the eye. Results reported as Mean±SD (n=3)

Scaffolds of PCL-MB displayed complete release following 96-hour incubation, and the cumulative mass of MB measured in the supernatant (m : 170±9 mg) was found to compare well with the mass of PS encapsulated in the electrospun fibres (m : 150±2 mg). The value is slightly higher than 100%, but this would be expected as the loading efficiency of these scaffolds was calculated to be 103±16% (section 3.3.2.1). In comparison, only a limited amount of PS was released from both PCL-ER and the PLGA7525 scaffolds, suggesting that PS is being held within the scaffold due to secondary interactions between the PS molecule and the polymer.

The different PS release profiles recorded from PCL and PLGA7525 electrospun scaffolds were somewhat surprising, given that the averaged pore size was comparable between the two scaffold architectures (section 3.3.2.1) and that the amorphous morphology of PLGA7525 should allow for increased diffusion of the PS out of the electrospun fibres compared to semi-crystalline PCL. The most likely explanation for the increased release capability of PCL with respect to PLGA7525 samples is that the

encapsulation of PS in the PCL fibres leads to increased surface hydrophilicity, as demonstrated by contact angle data (**Figure 4.1**), so that diffusion of PS molecules is promoted in the PCL samples. The higher and faster release of MB with respect to ER can on the other hand be explained considering the different solubility in water and molecular weight of the two PS. MB (*solubility* = 35.5 mg·ml⁻¹; *M* = 319.85 g·mol⁻¹) is more soluble in aqueous environment with respect to ER (*solubility* = 0.7 mg·ml⁻¹; *M* = 879.86 g·mol⁻¹), so that an increased diffusion of MB out of the scaffold is expected.

Overall, the burst release observed with these samples is commonly seen with fibrous scaffolds used in drug delivery applications [450]. A steady PS release would be preferred to allow repeated activation of the PS to treat infections which may arise. Altering the monomer ratios in PLGA7525 polymers could open up relevant avenues to induce polymer crystallisation enabling both dimensional stability and weaker PS-polymer interactions which would increase the PS-release from these scaffolds[391].

4.3.1.3 Water Uptake

As the hydrolysis of polyester is a second order reaction, the reaction rate of hydrolysis will be dependent upon the WU and swelling of the polymer with water [451]. Other than hydrolysis, the WU into the scaffold will also have an impact as shown here, on the scaffold PS-release capability as well as cytocompatibility and regenerative potential *in vivo*. Following 24-hour incubation in aqueous medium, a significantly greater WU was measured in PCL-ND compared to PLGA7525-ND scaffolds (**Figure 4.3**), and the same trends were observed in respective PS-encapsulated samples.

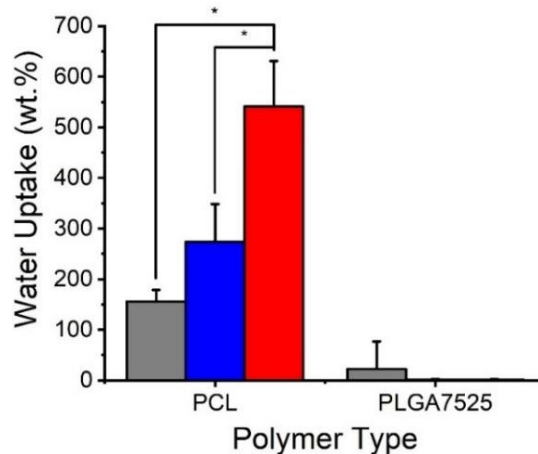


Figure 4.3 – Water uptake measured gravimetrically following incubation (H₂O, 37 °C) of either PS-loaded or electrospun control (ND) samples. Grey bars: Polymer-ND scaffolds; Blue bars: Polymer-MB scaffolds; Red bars: Polymer-ER scaffolds. Results reported as Mean±SD (n=3). “” denotes significantly different means ($p < 0.05$, *t*-test)**

Although detectable release of PS was measured within the selected WU time window (**Figure 4.2**), the mass percentage loss of PS in the electrospun fibre was minimal with respect to that of the control polymer fibres, suggesting that the measured WU was mostly ascribed to the effect of the scaffold chemical composition (e.g. polymer type) and architecture (e.g. fibre diameter) rather than the diffusion of PS out of the material.

Whilst the averaged fibre diameter and mean flow pore size measured in PCL and PLGA7525 sample groups were statistically equivalent (section 3.3.2.1), the WU results are in agreement with previous contact angle (**Figure 4.1**) and PS release (**Figure 4.2**) measurements, indicating a higher compatibility with water in PCL with respect to the PLGA7525 samples. The WU measured for PS-encapsulated PCL scaffolds was greater than the PLGA7525 samples and electrospun controls. These trends in WU were found to correlate with the decrease in fibre diameter and pore size and the increase in hydrophilicity observed in the water contact

angle experiments on the films recorded in both samples PCL-MB and PCL-ER (**Figure 4.1**) with respect to sample PCL-ND.

4.3.2 Degradation

Degradability of regenerative devices needs to be tailored for the intended tissue repair/clinical application, therefore the hydrolytic degradability of each fibrous system in this study was investigated^[401]. Furthermore, it has been experimentally determined that fibroblast attachment to polymeric scaffolds is altered by the extent of polymer degradation^[452]. Previous research performed on porcine palatal wounds found that full clinical closure of the small wounds had occurred by 14 days, and complete healing of the wound had occurred after 7 weeks^[31]. This timescale will change depending on the size of the wound and may also differ in humans. It was therefore determined that the scaffolds would need to maintain integrity for 6-8 weeks in the oral cavity to allow for support of neotissue formation to occur.

Changes in microarchitecture (**Figure 4.4** and **Figure 4.5**), sample mass (**Figure 4.6**) and macroscopic volume (**Figure 4.7**) were monitored following sample incubation in PBS for up to 8 weeks.

Minimal structural changes were observed for the retrieved PCL scaffolds at all selected time points (**Figure 4.4**), whilst both PLGA7525-ND and PLGA7525-MB scaffolds revealed a decrease in pore size between fibres after 1 week incubation in PBS (**Figure 4.5**).

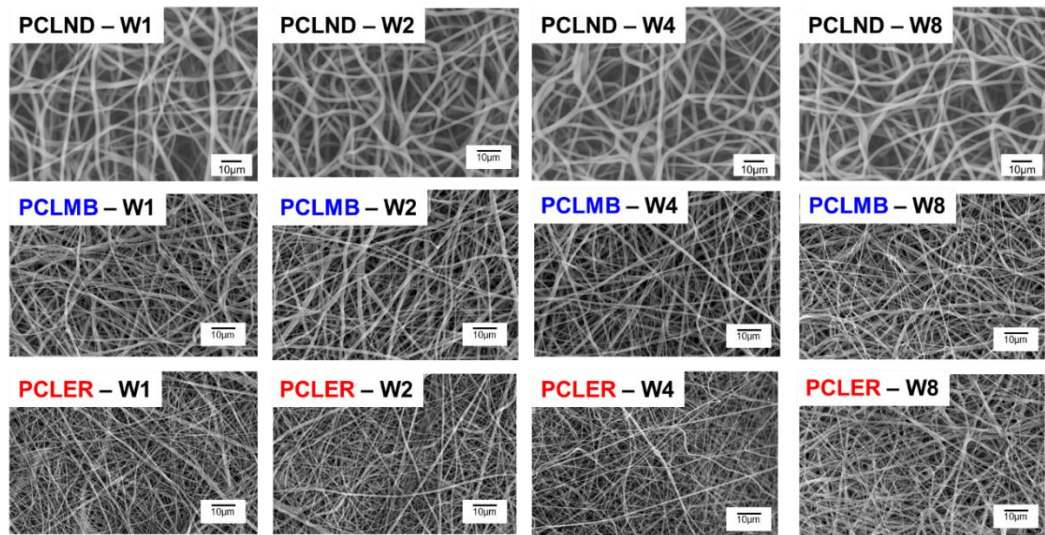


Figure 4.4 - Scanning Electron Microscopy (SEM) of electrospun PCL scaffolds following 8-week incubation in PBS at 37 °C

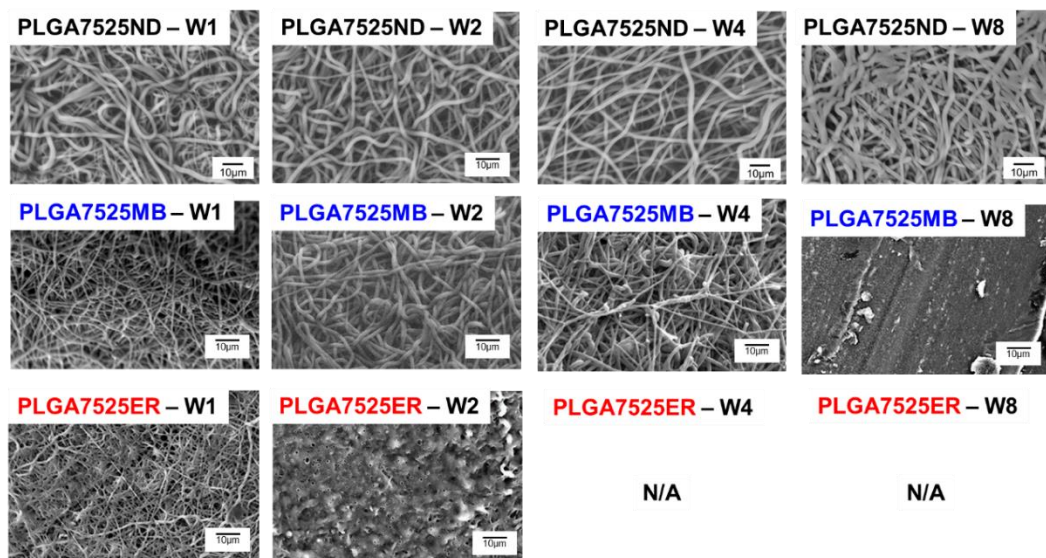


Figure 4.5 - Scanning Electron Microscopy (SEM) of electrospun PLGA7525 scaffolds following 8-week incubation in PBS at 37 °C

Following 8 weeks incubation, PLGA7525-MB scaffolds were disintegrated and a collapsed fibrous architecture was observed, in line with the observed macroscopic volume reduction (**Figure 4.5** and **Figure 4.7**). Consistent with the greater instability at both macroscopic and microscopic scales, electrospun PLGA7525 scaffolds proved to display a higher mass loss (14 ± 4 wt.%) than PCL scaffolds (4 ± 2 wt.%) following 8-weeks incubation (**Figure 4.6**).

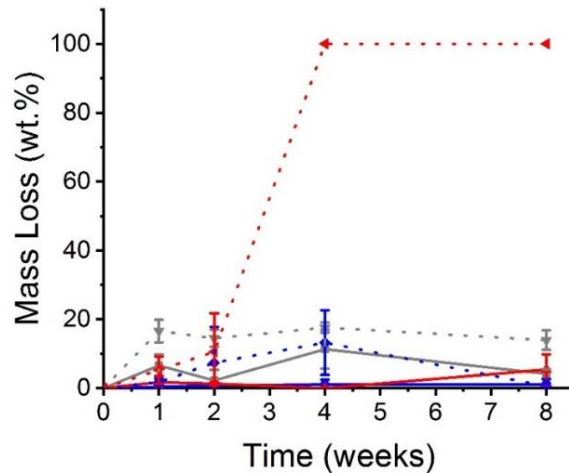


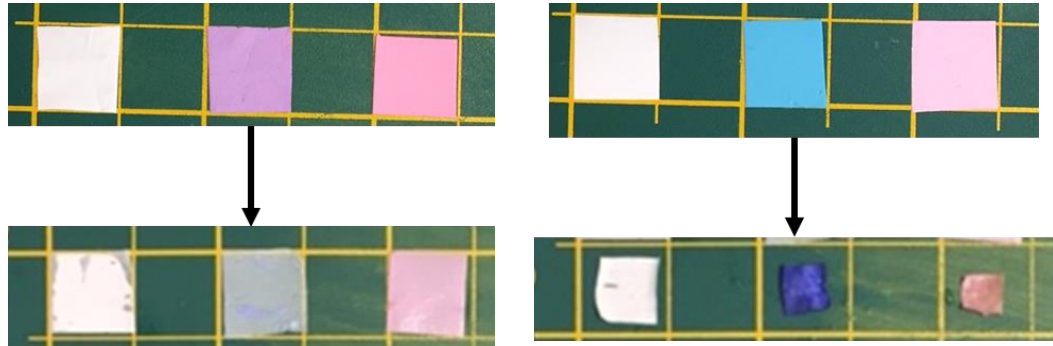
Figure 4.6 – Mass loss measured on PS-encapsulated or PS-free control (ND) samples following hydrolytic degradation (PBS, 37 °C). (-■-): PCL-ND; (-■-): PCL-MB; (-■-): PCL-ER; (·◀·): PLGA7525-ND; (·◀·): PLGA7525-MB; (·◀·): PLGA7525-ER. Lines are guidelines to the eye. Results reported as Mean±SD (n=3)

Given the increased hydrolytic degradability of PLGA7525 with respect to PCL, an increased PS release should be observed in the former with respect to the latter scaffolds, following polymer hydrolysis and breakdown of the scaffold. This was unexpectedly not the case, possibly due to the macroscopic scaffold shrinkage preventing PS release.

Previously published research has concluded that the pore size significantly alters cell adhesion within electrospun scaffold^[418,447,453]. As the scaffold becomes non-porous in a moist environment (**Figure 4.5**), cells would not be able to infiltrate so the scaffold would not function well as a regenerative device. For this reason, the PLGA7525 formulations were withdrawn from further studies.

During scaffold incubation in aqueous medium to monitor macroscopic behaviour, mass loss and PS release it was observed that none of the PS-encapsulated PCL samples showed a significant change in dimensions during the selected incubation time, whilst a drastic macroscopic

shrinkage was observed with respective PLGA7525 variants upon contact with water (**Figure 4.7**).



(A)

(B)

Figure 4.7 – Macroscopic volume change of (A) PCL scaffolds and (B) PLGA7525 scaffolds following 1 week incubation in PBS. The yellow grid has 1 cm² dimensions

PS-encapsulated PLGA7525 samples reduced in macroscopic surface area by approximately 50% when compared to the pre-incubated scaffolds. Such variation in macroscopic dimensions is likely explained by the fact that PLGA7525 fibres display an amorphous polymer morphology (section 3.3.2.3); consequently, water molecules can access relatively freely throughout the polymer chains, acting as plasticiser and inducing increased chain mobility ^[454]. In contrast, the crystalline regions in PCL fibres present limited accessibility to water molecules (section 3.3.2.3), therefore acting as physical crosslinks and preventing volumetric change in hydrated scaffold dimensions. The plasticising effect of PLGA7525 fibres in aqueous environments is dominant in PS-encapsulated samples, given that respective fibres proved to display a significantly-decreased diameter with respect to the case of electrospun control fibres (51% and 69% reduction respectively, section 3.3.2.1). In line with the PS-induced decrease of fibre diameter and increased WU, merging of fibres and collapse of the porous scaffold architecture are increasingly likely.

4.4 Conclusion

In an aqueous physiological environment, PLGA7525 scaffolds displayed significant macroscopic shrinkage upon contact with water and collapse of the fibrous structure following 8-week incubation, likely explained by the amorphous polymer morphology of PLGA7525 with respect to the semi-crystalline state of PCL fibres. This shrinkage resulted in the PLGA7525 scaffolds being deemed not suitable for use in the moist environment of the mouth, due to reduced porosity which would prevent cell infiltration and therefore neotissue formation. No observable shrinkage was found for either PCL-ND control samples or the PS-loaded PCL scaffolds. Together with results obtained from the hydrolytic degradation study (section 4.3.2), PCL scaffolds were therefore deemed to be a dimensionally-stable polymer carrier for both PS molecules. However, a burst release profile was detected for either PS from the PCL scaffolds.

Further biomaterial optimisation is needed to either slow the PS-release from the PCL scaffolds or to increase the crystallinity of the PLGA7525 scaffolds to prevent shrinkage in aqueous media. Increasing the glycolic acid monomer ratio in the PLGA7525 could lead to an increase in crystallinity and therefore a more stable polymer carrier. For example, previously published work has been performed on electrospun PLGA with a lactide to glycolide ratio of 10:90, and minimal shrinkage was observed following incubation in aqueous media^[229].

To summarise, electrospun scaffolds were characterised in terms of their behaviour in aqueous medium. The next stage of this study was to determine the optimal PS (MB or ER) for loading in the optimised polymer carrier based on a comparison of the bactericidal activity and mammalian cytotoxicity between these two PS. The lead polymer carrier at this stage, PCL, was also used as a model to test the cell survival and bactericidal capacity of the PS when loaded into and released from polymer electrospun scaffolds.

Chapter 5 Selection of Photosensitiser for Antimicrobial Photodynamic Therapy

5.1 Introduction

The aim of the research presented in this chapter was to determine the optimal PS (MB or ER) for encapsulation within polymeric electrospun scaffolds to enable aPDT activity in oral applications.

Initially, a light source was analysed to determine the irradiation intensity in comparison with lights currently used in dental applications. This was used as a guide for the temporal length of light exposure to be used in the mammalian and bacterial cell studies. Solutions of either MB or ER in PBS were then analysed for their aPDT capability against two model strains of bacteria (*Streptococcus mutans* (*S. mutans*) Ingbritt and *Escherichia coli* (*E. coli*) 11954). These bacteria were chosen as gram-negative and gram-positive strain models respectively. aPDT is most effective on gram-positive strains of bacteria due to the presence of an additional cell wall in gram-negative strains^[455].

A comparable experiment was then performed on L929 mouse fibroblast cells to provide an early indication of any mammalian cell cytotoxic effects induced by the PS when in solution.

The lead prototype polymer carrier was selected in Chapter 3 and Chapter 4 as being PCL, due to the dimensional stability of the respective scaffolds in aqueous environments. This PCL electrospun scaffold was used as a model scaffold to test the effects of scaffold-induced release of either MB or ER on either *E. coli* bacteria or L929 fibroblasts.

5.2 Materials and Methods

5.2.1 Quantification of Light Intensity

An easily accessible light source was used as a model for the preliminary purpose of this study. For this purpose, a 6000-lumen work light (50W, 135 lumen/W, 2800-3200 warm light) was selected. An ILT2400 hand-held optical meter was used (International Light Technologies NIST Traceable Light Measurement Systems) with two laser line filters (532±2 nm (ER peak absorbance) and 670±2 nm (MB peak absorbance)) (ThorLabs, Inc.) to determine the light intensity in the spectral regions of interest. The light was tested both with and without the filters, and with or without a water bath which was used to dissipate any heat which may arise from the light source in order to protect the samples during testing (section 5.2.5.1, **Figure 5.3**). The light meter was held under the light in 9 distinct locations and the light intensity (mW/cm²) associated with these were averaged together to ensure that the light output in each well under the light was consistent. The experiment was repeated three times per parameter.

5.2.2 General Cell Culture

5.2.2.1 Cell Culture Materials

Mouse fibroblast cells (L929) were chosen as a suitable model mammalian cell type according to ISO standard testing of cytotoxicity^[191,456]. PBS, Minimum Essential Media Eagle – alpha modification (α-MEM) (supplemented with L-Glutamine, 10 v.% Fetal Bovine Serum (FBS) and 1 v.% Penicillin-Streptomycin) and Trypsin were all from Lonza BioWhittaker®). All media was stored in a 4°C fridge until use and, when required, heated in a water bath to 37°C. Triton™ X-100 detergent (Alfa Aesar) was diluted in PBS to a working concentration of 10 v.%. Dimethyl sulfoxide (DMSO) and all other reagents were from Sigma Aldrich unless otherwise stated.

5.2.2.2 Cell Culture Passage

L929 cells were passaged regularly in T175 flasks to maintain 80% confluency. When passaging was required, adherent cells were washed twice in PBS (5 ml, 37°C) before Trypsin (5 ml, 37°C) was added and the flasks incubated (37°C, 5% CO₂) for 3 minutes. Following this, flasks were tapped gently on the side to detach any cells still adhering to the plastic and examined by light microscopy to ensure all cells had detached. Media (5 ml, 37°C) was then added to deactivate the trypsin enzyme and the resulting solution was centrifuged for 5 minutes at 1200 rotations per minute. The supernatant was removed, and the pellet of cells was resuspended in fresh medium (10 ml, 37°C) and the flask returned to the incubator (37°C, 5% CO₂). The passage number was monitored throughout all experiments.

5.2.2.3 Cell Culture Counting

Cells were passaged and suspended in medium (section 5.2.2.2), before an aliquot of 45 µl was taken and put into a 1.5 ml eppendorf tube. 5 µl of trypan blue was added to the cell suspension and mixed (1:10 dilution), before a 10 µl aliquot of the solution was taken and dispensed into a haemocytometer. Living cells appeared white and (when present) dead cells appeared blue due to penetration of the trypan blue into the cells. All live cells in four squares of the haemocytometer were counted and averaged. The cell concentration (cells/ml) was then calculated (**Equation 5.1**).

$$Cell\ Conc. = \frac{N_{average}}{Vol.} \times DF \quad \text{Equation 5.1 – Cell Concentration}$$

with ' $N_{average}$ ' representing the average number of living cells per square, ' $Vol.$ ' representing the volume of solution in each square (10^{-4} ml) and ' DF ' (Dilution Factor) representing the dilution of the cell solution with trypan blue. To obtain the total number of cells in the cell suspension, the value obtained was multiplied by the volume of the initial cell suspension.

5.2.2.4 Cell Culture Freezing and Thawing

Cells were periodically frozen and stored if a constant culture was not needed to be maintained. L929 cells were passaged as previously described (section 5.2.2.2) but in the final stage, they were resuspended in freezing medium rather than the normal α -MEM medium. The freezing medium was supplemented with 30 v.% FBS and 10 v.% DMSO. Vials of cells resuspended in freezing medium were placed in a Mr. Frosty™ Freezing Container (Thermo Fisher Scientific) to control the cooling rate and placed in -80°C freezers.

When cells were required again, they were thawed by removing from the -80°C freezers and defrosting for ~1 minute in a 37°C water bath. The cell suspension was then resuspended in fresh medium (5 ml, 37°C), centrifuged and the supernatant removed to remove traces of the freezing medium. The pellet of cells was then resuspended in fresh medium again.

5.2.3 General Bacterial Culture

5.2.3.1 Bacterial Culture Materials

Brain Heart Infusion (BHI) broth and Columbia Blood Agar Base (CB) were both from Oxoid. Horse Blood Oxalated was from Thermo Scientific. Crystal Violet, Gram's Iodine and Safranin used for staining were all from Pro-Lab Diagnostics. All other reagents were sourced from Sigma Aldrich unless otherwise stated.

5.2.3.2 Broth and Agar Plate Preparation

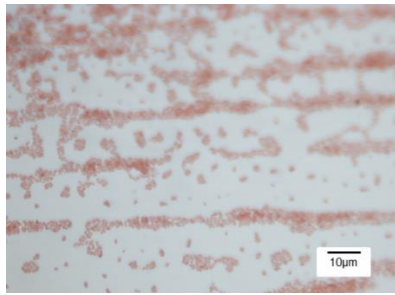
Fresh broth and agar plates were made prior to use. BHI and CB agar plates were made as per manufacturer's instructions. Briefly, 37 g of BHI was mixed with 1 L of dH_2O in a sterile Duran flask and autoclaved. The broth was cooled to room temperature overnight prior to use. CB agar plates were prepared by mixing 39 g of CB agar base with 1 L of dH_2O and autoclaving in a sterile Duran flask. The Duran flask was then placed in a 50°C water bath to cool the solution for ~1 hour, before 50 ml of oxalated horse blood was added and gently mixed to combine. Sterile plates were

then poured in aseptic conditions and left to solidify at room temperature. When set, the plates were inverted and stored in a 4°C fridge overnight.

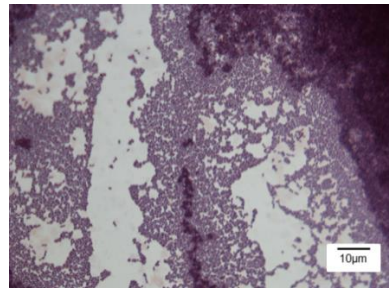
5.2.3.3 Bacterial Strain Characterisation

Bacterial strains chosen for use in this study were *S. mutans* Ingbritt (gram-positive coccus bacteria) and *E. coli* 11954 (gram-negative rod-shaped bacteria). These were chosen as model bacteria to represent a gram-negative and gram-positive bacterial strain.

Each week, a single colony was swabbed onto fresh agar plates and incubated overnight at 5% CO₂ and 37°C before being stored in a fridge. Each time a fresh agar plate was swabbed, colony morphology and gram-staining were used to confirm lack of contamination. Gram-staining was performed by taking a single colony on a sterile loop and swabbing onto a fresh glass slide. The slide was passed briefly through a Bunsen flame to fix the sample, before the slide was flooded with Crystal Violet for 1 minute. The slides were then washed briefly in water before being flooded with Gram's Iodine for 1 minute. After washing again briefly in water, the slides were washed with acetone to decolourise for 2 seconds and washed in water again. The slides were finally immersed in Safranin for 30 seconds and washed again in tap water, before being visualised by light microscopy with immersion oil. Examples of the gram-staining obtained from each bacterial strain are shown below (**Figure 5.1**). Gram-negative bacteria were stained pink and gram-positive bacteria were stained purple.



(A)



(B)

Figure 5.1 – Examples of Gram-Staining of two bacterial strains used in this study. (A) *Escherichia coli* (*E. coli*) 11954 (gram-negative); (B) *Streptococcus mutans* (*S. mutans*) Ingbritt (gram-positive)

Overnight cultures of bacteria were grown by selecting two separate colonies on sterile loops and inoculating them into 20 ml BHI in a sterile flask. The flasks were incubated in an incubator maintained at 37°C, 5% CO₂ overnight.

5.2.3.4 Growth Curve Characterisation

A growth curve was plotted for each bacterial strain of the variation of absorbance at 600 nm (OD₆₀₀) over time. This was achieved by initially growing an overnight culture of bacteria in sterile BHI broth to generate a large batch of bacteria. The following day, 25 ml of the overnight solution was added to 250 ml fresh sterile BHI, two 1 ml samples were taken and the OD₆₀₀ of each was measured (t = 0). The bacterial suspension was then incubated at 37°C and two 1 ml samples were taken every hour for up to 6 hours. The two OD₆₀₀ readings for each timepoint were averaged, and the whole experiment was repeated in triplicate for each bacterial strain. The OD₆₀₀ vs. time curve was plotted and the mid-log phase determined to be the linear region of the resulting graph representing the highest rate of growth of bacteria (**Figure 5.2**).

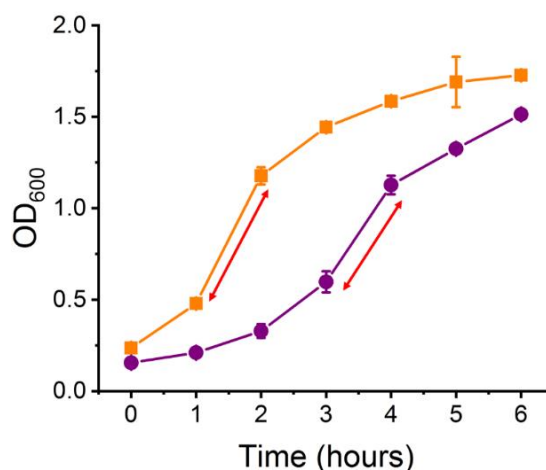


Figure 5.2 – OD₆₀₀ with respect to time of bacterial suspensions. Orange: *E. coli* 11954; Purple: *S. mutans* Ingbritt; (↔): Mid-log phase. Results reported as Mean±SD (n=3)

This graph was used to determine that mid-log phase was reached after 1.5 hours for *E. coli* and 3.5 hours for *S. mutans*.

Following this, the number of CFU per ml of solution were determined for the mid-log phase. 1 ml of overnight culture was added to 9 ml of fresh BHI and incubated for the allotted time until mid-log phase was reached (as calculated in **Figure 5.2**). A 10 µl sample was then taken and serially diluted in 90 µl of fresh BHI before 10 µl of each dilution was spread on CB agar plates in triplicate. The plates were incubated overnight at 37°C and the number of colonies counted. Only plates containing 20-100 colonies were counted. The whole experiment was repeated twice for each bacterial strain and the CFU/ml was calculated (**Equation 5.2**).

$$CFU/ml = \frac{N_{CFU} \times DF}{Vol.}$$

Equation 5.2 – Colony Forming Units

with ' N_{CFU} ' representing the number of colonies on a plate, ' DF ' representing the corresponding dilution from the initial suspension, and ' $Vol.$ ' being the volume of bacterial suspension plated up (0.1 ml). The results were used to

generate equations for determining the CFU in a particular suspension of bacteria in each study (**Equation 5.3** and **Equation 5.4**).

$$CFU_{E.Coli} = 6.2 \times 10^7 \times OD_{600}$$

Equation 5.3 - CFU *E. coli*

$$CFU_{S.Mutans} = 2.7 \times 10^8 \times OD_{600}$$

Equation 5.4 – CFU *S. mutans*

5.2.4 Photosensitiser Uptake Study

5.2.4.1 Mammalian Cells - Photosensitiser Uptake

To determine the amount of PS taken up by mammalian cells, L929 cell lines were passaged, counted and seeded into 96 well plates at a density of 5×10^3 cells/ml and left for 24 hours to allow for cell attachment. Confluent monolayers were then exposed to a range of four concentrations of either MB or ER solutions in PBS (0.2-200 $\mu\text{g/ml}$) for 2 hours to allow for PS uptake. Control wells contained either the PS solution with no cells or fresh PBS with cells. After 2 hours, the solutions were removed, and each well was washed in fresh PBS twice to remove any PS which had not been taken up by the cells. The PBS solution was then removed and replaced with a 10 v.% Triton™ X-100 in PBS solution and well plates were shaken for 5 minutes and left to incubate for 25 minutes to allow for membrane disruption and full release of any incorporated PS. The absorbance of the solution was recorded at 610nm for MB and 530nm for ER and the background interference (from the absorption values of wells containing only solubilised cells) was subtracted. This value was then compared to the absorption of the initial PS-loaded solutions (containing no cells) and the percentage uptake values were calculated (**Equation 5.5**).

$$PS \text{ Uptake} = \frac{[PS]_{cells}}{[PS]_{solution}} \times 100$$

Equation 5.5 – Percentage Cell PS Uptake

with ' $[PS]_{cells}$ ' representing the concentration of PS released from cell lysis and ' $[PS]_{solution}$ ' representing the concentration of PS in the initial PS-loaded solution.

5.2.4.2 Bacteria - Photosensitiser Uptake

To determine the amount of PS taken up by bacterial cells, an overnight culture of each bacterial strain was grown. 1 ml of overnight culture was placed in 9 ml of fresh BHI and left to incubate to mid-log phase (section 5.2.3.4). Following this time, the OD₆₀₀ of the suspension was measured and the suspension diluted in fresh BHI to result in a final concentration of 10⁸ CFU/ml. After this, the planktonic bacteria suspension was washed once in PBS and then resuspended in a range of four concentrations of either MB or ER solutions in PBS (0.2-200 µg/ml), plated into 96 well plates and incubated for 2 hours to allow for PS uptake. Control wells contained either the PS solution with no bacteria or fresh PBS with bacteria. The PS containing solution was then washed off the bacteria and the bacteria resuspended in fresh PBS, centrifuged and the supernatant removed. This process of washing the bacteria was repeated twice. The PBS solution was then replaced with a 10 v.% Triton™ X-100 in PBS solution and well plates were shaken for 5 minutes and left to incubate for 25 minutes to allow for membrane disruption and full release of any incorporated PS. The absorbance of the solution was recorded at 610 nm for MB and 530 nm for ER and the background interference (from the absorption values of wells containing only solubilised bacteria) was subtracted. This value was then compared to the absorption of the initial PS-loaded solutions (containing no bacteria) and the percentage uptake values were calculated (**Equation 5.6**).

$$PS \text{ Uptake} = \frac{[PS]_{bacteria}}{[PS]_{solution}} \times 100$$

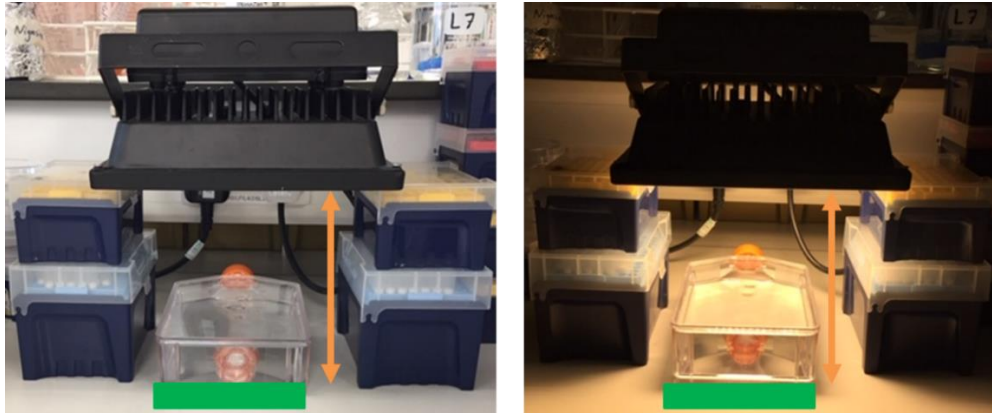
**Equation 5.6 – Percentage
Bacterial PS Uptake**

with ' $[PS]_{bacteria}$ ' representing the concentration of PS released from bacterial lysis and ' $[PS]_{solution}$ ' representing the concentration of PS in the initial PS-loaded solution.

5.2.5 Photosensitiser-Loaded Solution Toxicity

5.2.5.1 Mammalian Cells - Photosensitiser-Loaded Solution Toxicity

To determine the cytotoxicity induced by PS-loaded PBS solutions on L929 cell lines, confluent cells were passaged, counted and seeded into 96 well plates at a density of 5×10^3 cells/ml in 100 μ l of medium and left for 24 hours to allow cell attachment. Confluent monolayers were then exposed to a range of either MB or ER solutions in PBS (0.2-200 μ g/ml) for 2 hours to allow for PS uptake. Control wells contained fresh PBS with cells (negative control) and 10 v.% PBS-Triton™ X-100 solution (positive control). The well plates were then either exposed to light for 30 or 60 minutes or wrapped in foil and left under the light for the same period of time (dark control). A water bath was used to dissipate any heat which may alter the samples (**Figure 5.3**).



(A)

(B)

Figure 5.3 – Experimental setup for light activation step. Water bath was used to dissipate any heat which may arise from the light source during exposure time. (A): Light off; (B): Light on. ■: Location of well plate during experiment; ■: Arrow represents 15 cm

Following this, 100 μ l of Cell-TiterGlo® 2.0 solution (Promega) was added to each well and the well plate was covered in foil and shaken at 200 RPM on a shaker for 5 minutes, before being left to equilibrate at room temperature for 25 minutes. Well plates were then analysed on a microplate reader, with a luminosity reading being recorded for each well. The wells were all compared to the average of the negative dark control wells on each plate (fresh PBS with cells and no light exposure) to determine the percentage of cells which were killed (**Equation 5.7**).

$$\% \text{ Killing} = \frac{Lum_{test}}{Lum_{control}} \times 100$$

Equation 5.7 – Percentage Killing

with ' Lum_{test} ' representing the luminosity of the test well and ' $Lum_{control}$ ' representing the luminosity of the control well.

5.2.5.2 Bacteria - Photosensitiser-Loaded Solutions Antimicrobial Photodynamic Therapy Activity

To determine the aPDT capability of PS-PBS solutions on bacterial cells, an overnight culture of bacteria in BHI broth was grown for each bacterial strain. 1 ml of overnight culture was placed in 9 ml of fresh BHI and left to incubate to mid-log phase as determined for each bacterial strain (section 5.2.3.4). The OD₆₀₀ of the suspension was then measured and the suspension diluted in fresh BHI to an OD equivalent to 10⁸ CFU/ml. The bacteria were washed once in 1 ml of PBS and then resuspended in a range of concentrations of either MB or ER solutions in PBS (1 ml at 0.2-200 µg/ml) and 100 µl of each plated into 96 well plates and incubated for 2 hours to allow for maximum PS uptake. Control wells contained bacteria suspended in fresh PBS (negative control) and bacteria suspended in 10 v.% PBS-Triton™ X-100 solution (positive control). The well plates were then either exposed to light for 30 or 60 minutes or wrapped in foil and left under the light for the same period of time (dark control). Following this, 100 µl of Bact-TiterGlo® solution (Promega) was added to each well and the well plate was covered in foil and shaken at 200 RPM on a shaker for 1 minute before being left to equilibrate at room temperature for 4 minutes. Well plates were then analysed on a microplate reader, with a luminosity reading being recorded for each well. The wells were all compared to the average of the negative dark control wells on each plate (fresh PBS with bacteria and no light exposure) to determine the percentage of bacteria which were killed (Equation 5.7).

5.2.6 Photosensitiser-Encapsulated PCL Scaffold Toxicity

5.2.6.1 Mammalian Cells - Photosensitiser-Encapsulated PCL Scaffold Extract Toxicity

Room temperature scaffolds were cut into squares with a mass of ~20 mg before being disinfected for 15 minutes on each side using an ultraviolet light source. These were then placed in triplicate in Falcon tubes with 5 ml of PBS and incubated at 37°C for 0, 2 or 24 hours to allow for PS release to generate 'extract solutions'.

L929 cells were passaged, counted and seeded into 96-well plates at a density of 5×10^3 cells per well in 100 μ l of medium and left for 24 hours to allow for cell attachment. After this time, media was removed from the wells and they were each washed with fresh PBS to remove residual media contaminants, before the extract solution was added and left for 2 hours. Control wells contained fresh PBS with cells (negative control) and 10 v.% PBS-Triton™ X-100 solution (positive control). The well plates were then either exposed to light for 30 or 60 minutes or wrapped in foil and left under the light for the same period of time (dark control).

Following this, 100 μ l of Cell-TiterGlo® 2.0 solution was added to each well and the well plate was covered in foil and shaken at 200 RPM on a shaker for 5 minutes, before being left to equilibrate at room temperature for 25 minutes. Well plates were then analysed on a microplate reader, with a luminosity reading being recorded for each well. The wells were all compared to the average of the negative dark control wells on each plate (cells in PBS with no light activation) to determine the percentage of cells which were killed (**Equation 5.7**).

5.2.6.2 Bacteria - Photosensitiser-Encapsulated PCL Scaffolds Antibacterial Photodynamic Therapy Activity

Due to this experiment being performed during an external placement at the University of Massachusetts Amherst, a different but comparable bacterial strain was used, and different reagents were used. All reagents were purchased from Sigma Aldrich unless otherwise stated.

An overnight culture of bacteria was prepared. Briefly, 5 ml of Luria-Bertani (LB) media and 5 μ l Carbenicillin (Carb) antibiotic were added to an autoclaved test tube in aseptic conditions. A pipette tip was flame sterilised and used to collect a single colony from an agar plate containing the K12 MG1655 *E. coli* bacterial strain, which was then added to the test tube. This was then flame sterilised, sealed and incubated on a stirrer plate at 250 rotations per minute overnight at 37°C.

When ready to use, a sample of the culture solution was diluted in a cuvette with additional LB media to obtain an absorbance reading at 600 nm between 0.5 and 1 against an LB media background. An absorbance reading of 1 was taken to be equivalent to 1.6×10^8 CFU/ml according to the McFarland 0.5 standard to calculate the number of bacterial cells in the overnight culture solution^[457]. Approximately 2.5×10^7 CFU was used in each experiment.

Room temperature scaffolds were cut into round discs with a diameter of 1.27 cm (weight ~20mg) before being disinfected for 15 minutes on each side using an ultraviolet light source. These were then placed in a 6-well plate with 5ml of M9 minimal salts medium per well. Glass slides were used for the control wells, which contained either M9 minimal salts medium (negative control) or ethanol (positive control) with the same quantity of bacteria in each well. The well plates containing M9 medium and scaffolds were incubated at 37°C for 0, 2 or 24 hours to allow for PS release. After this time, overnight bacterial culture solution and 5 µl of Carb was added. The plates were then irradiated (at 1 cm distance) with the light source (3500 lumen Husky LED portable work light) for either 30 or 60 minutes. During each experiment, a duplicate plate was wrapped in foil and placed in the same incubator as a 'dark' control to measure the level of toxicity of the PS and scaffold when not activated by the light source. The temperature of the incubator was monitored to ensure that there was no significant increase of temperature for the duration of the experiment.

The *E. coli* K12 MG1655 bacteria used were engineered to fluoresce with a maximum excitation wavelength of 488nm and a maximum emission wavelength of 510nm thus eliminating the need to stain the bacteria with a 'live' green fluorescent protein (GFP) stain. PI (propidium iodide), was used to monitor the number of dead cells in each experiment. Following light exposure, the bacterial solution was removed and 2 ml of PI solution (12.5 µl per ml of deionised water) was added to each well. This was left to incubate at room temperature for 15 minutes to allow bacterial staining to occur. After

this, each sample was removed, rinsed in deionised water to remove excess stain and blotted gently on Kimwipes to remove excess water.

The samples were then placed onto a glass slide and imaged directly under a Zeiss epifluorescence microscope using GFP (488 nm) and PI (535 nm) wavelength filters and ZenPro software. Images were taken at 20x magnification in three randomly chosen areas across the scaffold. ImageJ was used with the multi-point tool to count the live or dead cells on each image. The average log reduction in live bacteria was calculated according to **(Equation 5.8)**.

$$\text{Log Reduction} = \log_{10} \frac{n_{dead} + n_{live}}{n_{dead}} \quad \text{Equation 5.8 – Log Reduction of Live Bacteria}$$

where ' n_{dead} ' and ' n_{live} ' are the number of dead (red) and live (green) bacteria, respectively, measured in the epifluorescence microscope image.

5.2.7 Statistical Analysis

Significant differences in the results were evaluated using an unpaired Student's *t*-test. Data was deemed to be significantly different at $p < 0.05$. All data were collected in triplicate and presented as Mean \pm Standard Deviation.

5.3 Results and Discussion

5.3.1 Quantification of Light Intensity

The average light intensity of the model work light was calculated either with no filter (the full spectrum of light intensity) or filters to detect the light output intensity in correspondence of the maximum absorption areas for MB (670 nm) or ER (530 nm) (**Table 5.1**).

Experimental Conditions	Light Intensity (mW/cm ²)		Energy Density (J/cm ²)	
	No Water	Water	30 mins	60 mins
No Filter	103±15	119±9	215±16	430±32
670nm Filter (MB)	3±0.4	3±1	6±1	11±2
532nm Filter (ER)	3±1	3±1	5±1	11±2

Table 5.1 – Summary of average light intensity tested in various experimental conditions. No water refers to readings taken without the presence of the water bath. The energy density values are calculated from light intensity values with water bath. Results reported as Mean±SD (n=3)

The water bath which was used to protect the samples from any light-induced heat was found to have no significant impact on the intensity readings at either 670 nm or 530 nm ($p = 0.4$ and 0.4 respectively). No significant difference was found between the light intensity at the wavelengths of interest for MB and ER ($p = 0.7$). This is important as it enabled a direct comparison of the two PS to be performed using this light system.

A handheld portable device with a non-thermal diode laser currently available on the market (Periowave™, Ondine Biopharma, Vancouver, Canada) has been specifically designed for use with MB in oral applications with a wavelength range of 650-670 nm^[458]. This product has been reported to have a maximum output of between 150-200 mW and following a 60 second light exposure, an energy density of 21 J/cm²^[458–460].

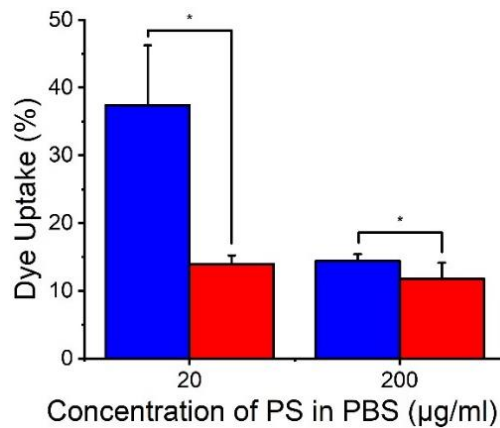
In this preliminary study, light exposure times of 30 minutes and 60 minutes were selected based on previously published studies using a similar white light source^[333,353,461]. It is important to note that research has shown that repeated smaller doses of light exposure (also known as light

fractionation) led to greater aPDT effect than an equivalent single dose of light^[462–465]. This is likely to be due to the absence of photobleaching effect on the PS. The phenomenon of light fractionation confirms that the overall light energy density is not the only factor to consider in PDT and this should be considered in the future development of this medical device.

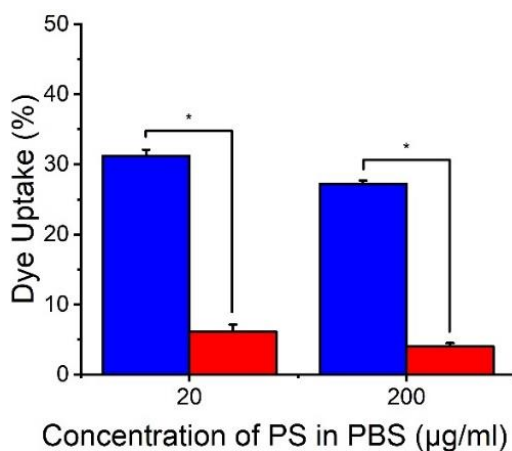
5.3.2 Photosensitiser Uptake

An experiment was designed to determine the PS uptake based on a previously published protocol^[466]. Four solution concentrations ranging from 0.2-200 µg/ml of either MB or ER in PBS were tested on L929 mammalian cells and two bacterial strains, one gram-positive (*S. mutans*) and one gram-negative (*E. coli*).

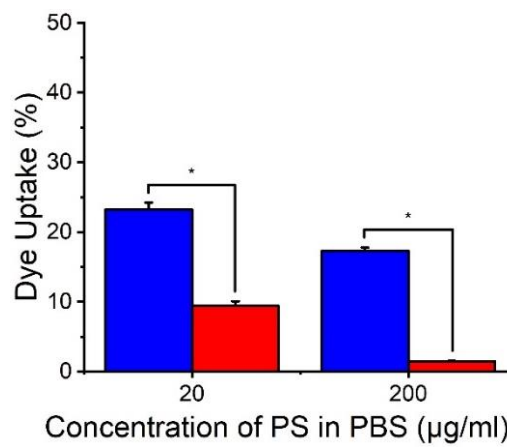
Due to the low absorbance readings of the amount of PS taken up at the lowest two concentrations (0.2 µg/ml and 2 µg/ml), there was no significant difference between the absorbance measurement and the 'cell only' controls for either PS, meaning that the result was undetectable using this experimental procedure. These results are therefore not shown here, and only the results for the two highest PS concentrations are compared (**Figure 5.4**).



(A)



(B)



(C)

Figure 5.4 – PS Uptake by either cells or bacteria during a 2 hour incubation in PS-loaded solutions. ■: MB-loaded PBS solutions; ■: ER-loaded PBS solutions. (A) L929 mammalian cells, (B) *S. mutans* Ingbritt gram-positive bacteria, (C) *E. coli* 11954 gram-negative bacteria. Results reported as Mean±SD (n=3). “*” denotes significantly different means ($p < 0.05$, *t*-test)

The overall uptake values are comparable to those found in the previously published literature^[466]. There was a significantly greater uptake of MB compared to the uptake of ER at either concentration for both the *E. coli* ($p = 2 \times 10^{-5}$ and 0.0004 respectively) and the *S. mutans* ($p = 3 \times 10^{-6}$ and 4×10^{-5}) bacterial strains and the L929 mammalian cells ($p = 0.01$ and 6×10^{-5} respectively). This is likely to be due to cationic charge of the MB enhancing

uptake by interacting more strongly with the external wall or outer membrane of the cell or microorganism^[466]. Studies have also shown that microbial efflux pumps play a role by enhancing uptake of cationic PS such as MB which was not found with anionic PS^[467].

For the cationic MB, gram-positive *S. mutans* bacteria took up significantly more PS than Gram-negative *E. coli* over the 2-hour incubation period for both the 20 µg/ml and 200 µg/ml concentrations ($p = 4 \times 10^{-5}$ and 0.003 respectively). It is expected that this is due to the need to penetrate the outer membrane which acts as a barrier to uptake of PS in gram-negative bacteria.

These results would suggest that at comparable concentrations, more MB will be moved intracellularly than ER and therefore it could be more active as a PS for aPDT.

5.3.3 *In vitro* testing with Photosensitiser-Loaded Solutions

5.3.3.1 Mammalian Cell Photosensitiser-Loaded Solution Testing

Testing was performed by incubating a confluent mammalian fibroblast cell line (L929) in either MB-loaded or ER-loaded PBS solutions at four concentrations (0.2 µg/ml to 200 µg/ml) for 2 hours to allow for PS uptake. The viability of the cells was determined using an ATP detection assay, 'Cell-Titre Glo® 2.0'. ATP was used as an indicator of metabolically active (living) cells. Briefly, the assay involved the full lysis of cells to release any intracellular ATP. The ATP was then reacted with luciferin and the Ultra-Glo™ rLuciferase enzyme to generate oxyluciferin which was luminescent. The RLU (relative light units) measured correlates to cell survival: the greater RLU reading, the greater the number of living cells present in the sample^[197]. The negative dark control with cells in fresh PBS and no light activation was assumed to be representative of the RLU for 100% cell survival. The average RLU reading of these control samples was used to calculate the percentage killing of the other test samples, based on a percentage reduction in RLU.

In each experiment, PBS was selected as a negative control and a solution of PBS containing 10 v.% Triton™ X-100 detergent to lyophilise all the cells was selected as a positive control (Figure 5.5).

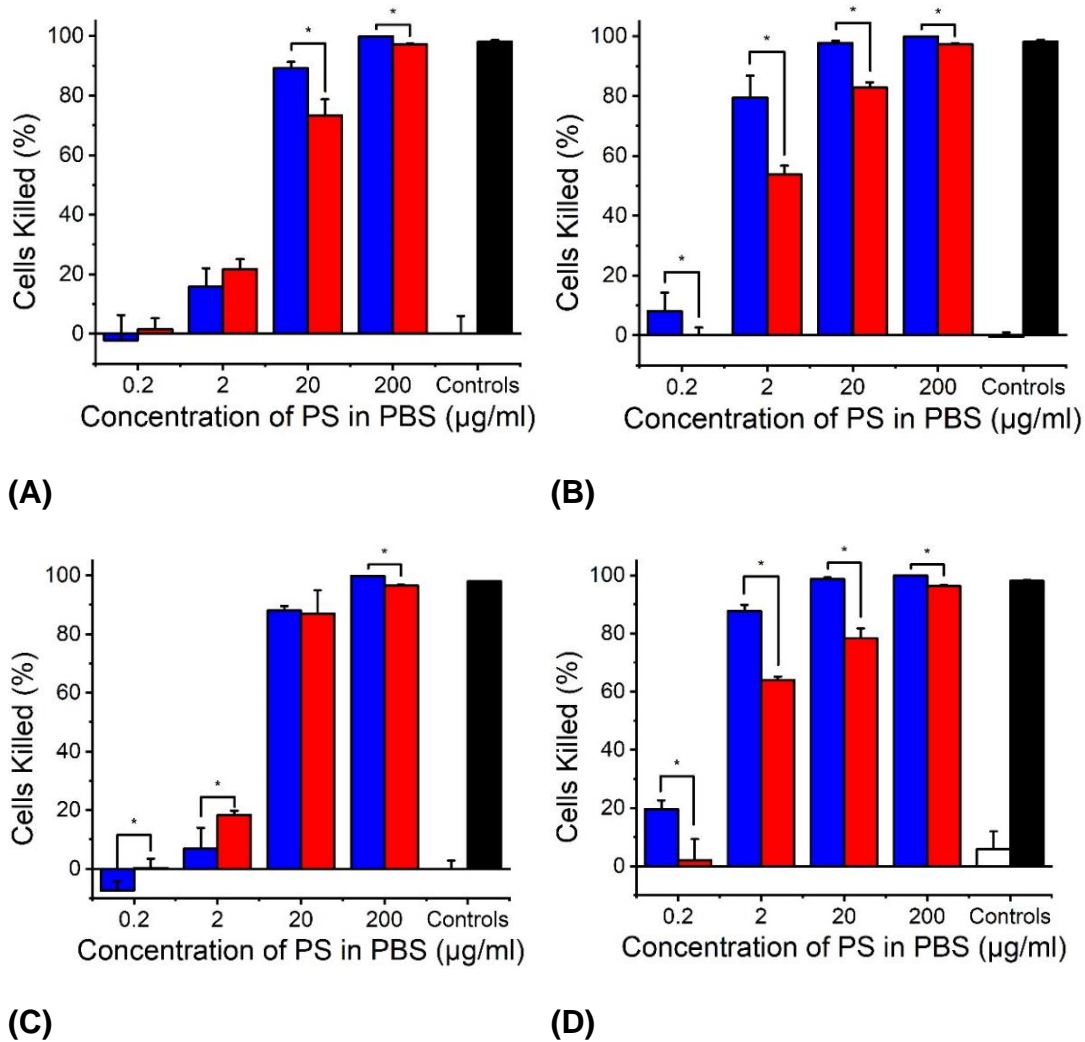


Figure 5.5 - L929 Solution Toxicity. (A) 30 min 'dark' control; (B) 30 min light exposure. (C) 60 min 'dark' control; (D) 60 min light exposure. ■: MB-loaded PBS solutions; ■: ER-loaded PBS solutions; □: fresh PBS negative control; ■: PBS-Triton™ X-100 solution positive control. Results reported as Mean±SD (n=3). “*” denotes significantly different means ($p < 0.05$, t -test)

The cell killing produced by the positive control of PBS containing 10 v.% Triton™ X-100 was found to indicate cell killing of $98\pm 0.4\%$ over all experiments, and cell killing in PBS alone was $-0.2\pm 0.6\%$, providing evidence that the cells could be killed, but that without treatment the cells were able to survive.

An important consideration in the use of PS is the 'dark toxicity' of the PS, which describes the toxicity induced by the PS without light activation^[389,468]. This is primarily controlled by the concentration of the PS within the PS-loaded solution. Upon optimisation of the PS polymer carrier, an ideal release profile is sought which will provide a controlled release of the PS. This steady release should avoid high, potentially toxic concentrations of PS accumulating at any point in time. To determine the concentration suitable for a non-toxic release profile of PS, testing of PS-loaded PBS solutions was performed on monolayers of mammalian cells and bacteria to identify the PS concentration causing minimal 'dark toxicity' (i.e. 30% cell death).

For 100 μ l of a PS concentration of 200 μ g/ml and 20 μ g/ml with no light activation, MB killed significantly more L929 cells than ER after 60 minute incubation times ($p = 1\times 10^{-11}$ and $p = 0.01$ respectively) (**Figure 5.5C**). However, both PS killed >85% of the cells at either of these concentrations, which indicates that these concentrations would be too toxic for use in a tissue regenerating scaffold product. The initial loading of PS into the scaffold and the consequent release profile will need to be tuned to avoid these concentrations being reached.

At 2 μ g/ml, the average dark toxicity for the 60 minute timepoint was $14\pm 11\%$, and the maximum dark toxicity for ER was $20\pm 3\%$, with no significant difference between the two PS ($p = 0.1$) (**Figure 5.5C**). At the lowest concentration of 0.2 μ g/ml, the average dark toxicity was <1% for either PS ($-2\pm 10\%$ and $1\pm 3\%$ for MB or ER respectively) and again, there was no significant difference between the two PS ($p = 0.4$) (**Figure 5.5C**). Therefore, either 2 or 0.2 μ g/ml were tolerated by the cells and could therefore be encapsulated in the electrospun scaffold.

It is worth noting that although comparisons can be made between the concentrations of PS in PBS, the molarity of these solutions is different as the molecular weight of MB (319.85 g·mol⁻¹) is approximately 2.6 times less than that of ER (835.90 g·mol⁻¹). Conversions of these mass concentrations into molarity concentrations is summarised below for clarity (**Table 5.2**).

Concentration of PS in PBS (µg/ml)	Molarity of MB (mol/L)	Molarity of ER (mol/L)
0.2	6.3 x10 ⁻⁷	2.4x10 ⁻⁷
2	6.3 x10 ⁻⁶	2.4x10 ⁻⁶
20	6.3 x10 ⁻⁵	2.4x10 ⁻⁵
200	6.3 x10 ⁻⁴	2.4x10 ⁻⁴

Table 5.2 – Conversion of concentration of photosensitiser in solution into molarity

Therefore, at comparable mass concentrations, a smaller number of molecules of ER would be available, which may be the cause of the increased toxicity found with the MB-loaded solutions of PBS in comparison to the ER-loaded solutions.

Although the target for the aPDT effect (the toxicity associated with the combination of PS and light) will be oral pathogenic bacteria, it was important to also determine the extent of mammalian cell toxicity induced upon light activation of these PS solutions in the presence of monolayers of cells to determine whether normal tissue would be damaged at a PS dose which would be toxic to bacteria.

Following 30 minute light exposure, MB killed significantly more L929 cells at each concentration (200, 20, 2 and 0.2 µg/ml) than ER ($p = 1.0 \times 10^{-6}$, 5.3×10^{-7} , 2.9×10^{-4} and 0.03 respectively) (**Figure 5.5B**). The same trend was

observed for the 60 minute light exposure ($p = 4.6 \times 10^{-6}$, 3.1×10^{-5} , 6.5×10^{-8} and 0.002 respectively) (**Figure 5.5D**). This could be due to the significantly greater uptake of MB over ER (**Figure 5.4**), and may have implications for the cytotoxicity of the scaffold *in vivo*. However, it is important to note that this experiment is not fully reflective of the clinical application of the scaffold. The results here are an indication as to what could happen should all the PS be taken up by mammalian cells. If bacterial cells were present and the desired concentration was slowly released over a suitable period of time, these unacceptable levels of toxicity could be avoided.

For further assurance that this test would be more 'extreme' than the clinical scenario, it was decided to test two other commonly used PS in a comparable experimental set-up to compare to the cytotoxicity found with MB. These were Toluidine Blue O (TB)^[52,329,350,367,469] and New Methylene Blue (NMB)^[470-472] (**Figure 5.6**).

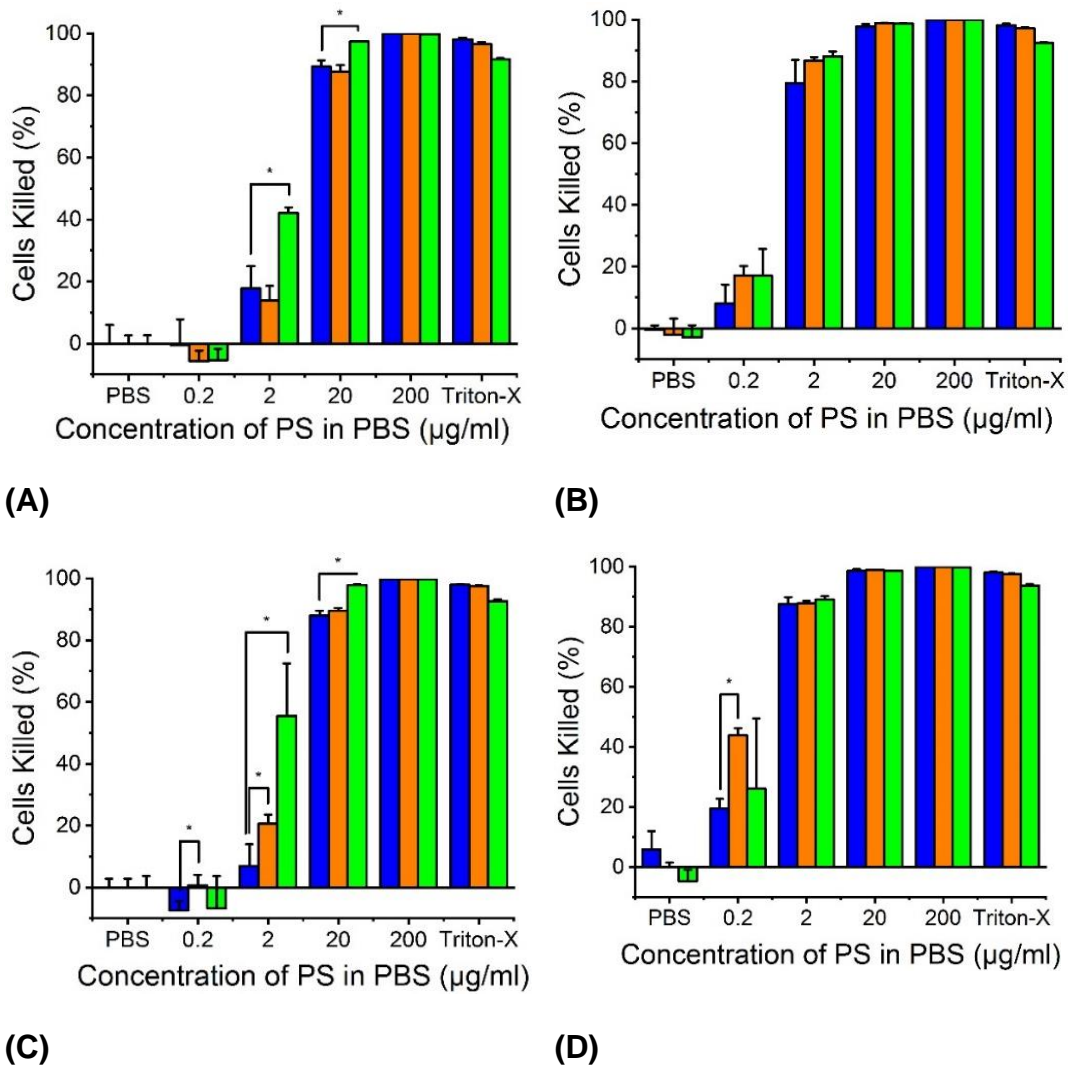


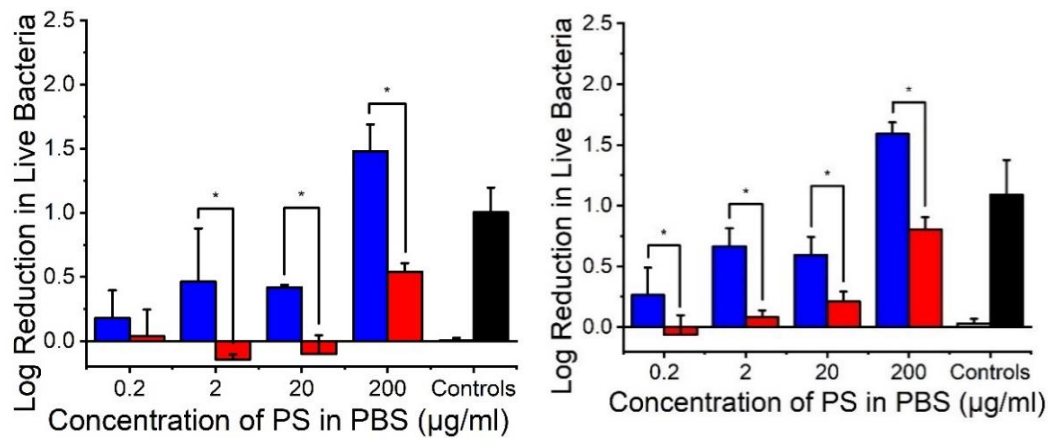
Figure 5.6 - L929 Solution Toxicity Comparison with three photosensitisers. (A) 30 min 'dark' control; (B) 30 min light exposure. (C) 60 min 'dark' control; (D) 60 min light exposure. ■: MB-loaded PBS solutions; ■: TB-loaded PBS solutions; ■: NMB-loaded PBS solutions. Results reported as Mean±SD (n=3). '' denotes significantly different means ($p < 0.05$, t -test)**

In all cases, the mammalian cell killing for TB or NMB was either not significantly different or was significantly greater than that of MB. This experiment supports the hypothesis that the mammalian cell killing is greater in this system than would be expected in a clinical setting, as it has previously been published that all three of these PS have limited mammalian

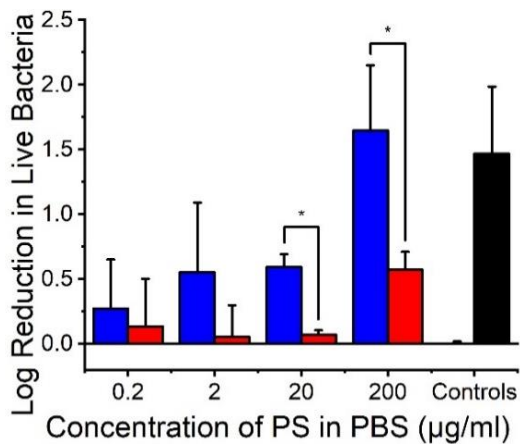
cell cytotoxicity^[473–476]. In a clinical setting, the cells are unlikely to be incubated in this high concentration of PS for a prolonged period of time due to the turnover of saliva in the oral cavity.

5.3.3.2 Antimicrobial Photodynamic Therapy Capability of Photosensitiser-Loaded Solutions

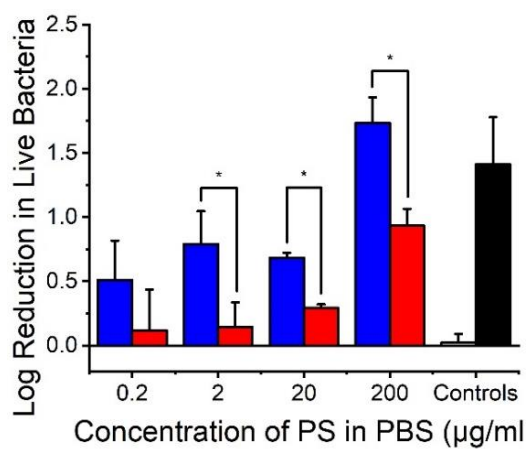
A comparable experiment to the mammalian cell toxicity determination (section 5.2.5.1) was performed with planktonic bacteria to determine the bactericidal capacity of each PS solution. The use of an ATP bioluminescence assay for determining the antimicrobial activity of a compound has been used in previously published literature^[477]. The initial ‘dark toxicity’ of the solutions towards each bacterial strain was first determined experimentally before quantifying the toxicity of the same solutions following application of light (**Figure 5.7** and **Figure 5.8**).



(A)



(B)



(C)

(D)

Figure 5.7 – Bactericidal toxicity of *S. mutans* following incubation in PBS solutions containing PS. (A) 30 min 'dark' control; (B) 30 min light exposure. (C) 60 min 'dark' control; (D) 60 min light exposure.

■: MB-loaded PBS solutions; ■: ER-loaded PBS solutions; □: fresh PBS negative control; ■: PBS-Triton™ X-100 solution positive control. Results reported as Mean±SD (n=3). '*' denotes significantly different means ($p < 0.05$, t -test)

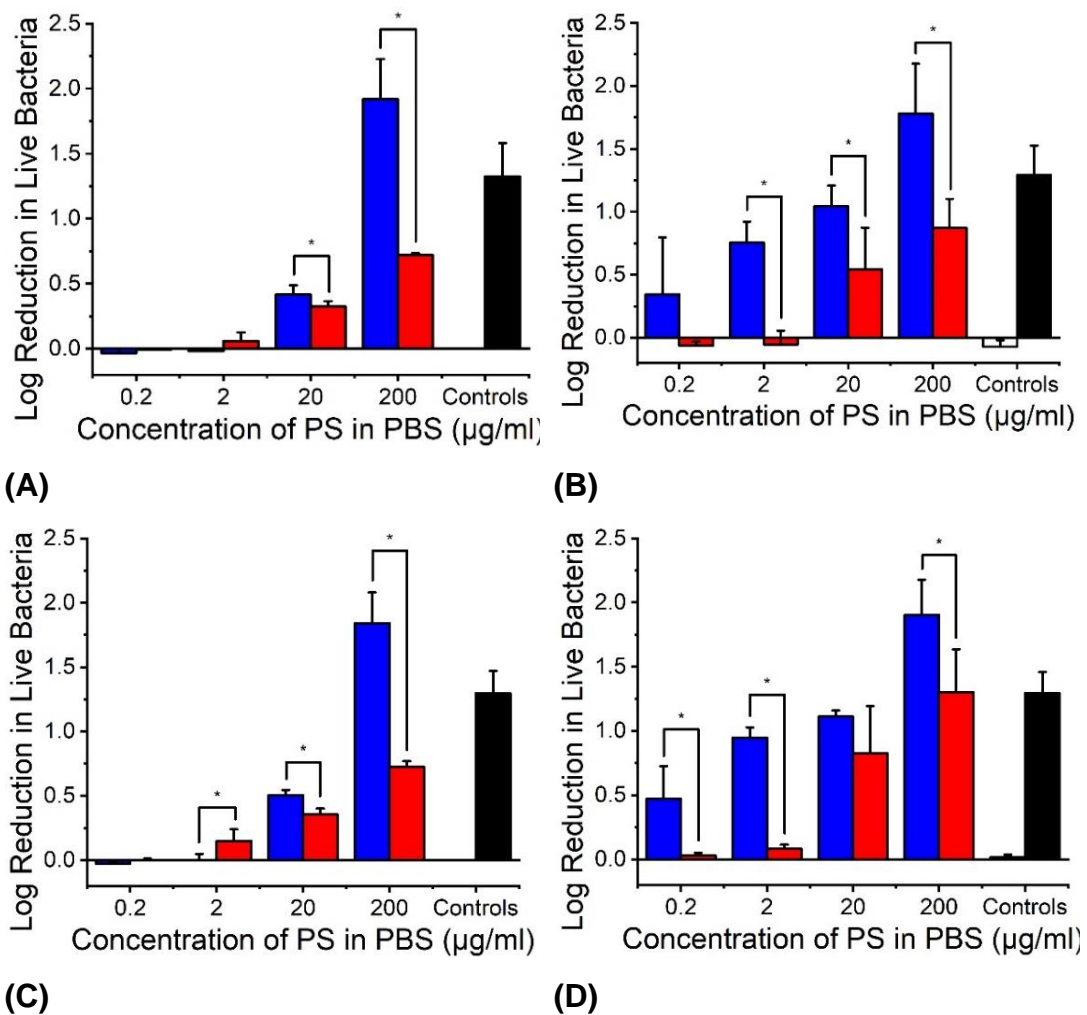


Figure 5.8 – Bactericidal toxicity of *E. coli* following incubation in PBS solutions containing PS. (A) 30 min 'dark' control; (B) 30 min light exposure. (C) 60 min 'dark' control; (D) 60 min light exposure. ■: MB-loaded PBS solutions; ■: ER-loaded PBS solutions; □: fresh PBS negative control; ■: PBS-Triton™ X-100 solution positive control. Results reported as Mean±SD (n=3). "*" denotes significantly different means ($p < 0.05$, t -test)

As with the mammalian cell data (section 5.3.3.1), it was first confirmed that the control samples demonstrated that both the *S. mutans* and *E. coli* bacteria survived in PBS alone (log reductions of 0.01 ± 0.9 and -0.01 ± 0.7 respectively) and were killed in the Triton™ X-100 solution (log reductions of 1.4 ± 0.6 and 1.3 ± 0.4 respectively).

Following this, the 'dark toxicity' of the solutions was evaluated across both 30- and 60-minute exposure times. For the 'on-demand' aPDT capability of the scaffold to be achieved, a low dark toxicity would be expected (<0.5 log reduction), which would increase significantly upon light activation. It was found that at the two highest concentrations (200 and 20 µg/ml), MB-loaded solutions (log reductions of 1.9 ± 0.3 and 0.5 ± 0.1 respectively) proved more bactericidal against *E. coli* than corresponding ER-loaded solutions (log reduction of 0.7 ± 0.03 and 0.3 ± 0.05 respectively) ($p = 2.2 \times 10^{-8}$ and 0.0002). At the lower concentrations of (2 and 0.2 µg/ml), the dark toxicity was minimal with the highest observed log reduction in bacteria being for ER at 2 µg/ml (0.1 ± 0.09).

For *S. mutans* bacteria, the same trend was observed. The two highest concentrations (200 and 20 µg/ml) of MB had log reductions of 1.6 ± 0.4 and 0.5 ± 0.1 respectively, which was significantly greater than the log reductions for ER of 0.6 ± 0.1 and -0.02 ± 0.1 respectively ($p = 2 \times 10^{-6}$ and 3×10^{-9}). At the lower two concentrations of MB (2 and 0.2 µg/ml) the toxicity was 0.5 ± 0.4 and 0.2 ± 0.3 respectively, and for ER this was -0.05 ± 0.2 and 0.1 ± 0.3 respectively.

For *E. coli* after 30 minutes light activation, a log reduction of >1 was achieved by the two highest concentrations of MB (1.8 ± 0.4 and 1.0 ± 0.2 respectively) but not for the two lower concentrations of MB tested (0.8 ± 0.2 and 0.2 ± 0.5 respectively). After 60 minutes light activation, again, the two highest concentrations displayed a >1 log reduction in live bacteria (1.9 ± 0.3 and 1.1 ± 0.05 respectively) but not for the lower concentrations (0.9 ± 0.1 and 0.5 ± 0.3 respectively).

For *E. coli* tested with the ER solutions, the minimum threshold required was not met by any of the concentrations (200, 20, 2 or 0.2 µg/ml) tested following 30 minutes light exposure (0.9 ± 0.2 , 0.5 ± 0.3 , -0.1 ± 0.1 and -0.1 ± 0.03 respectively). After 60 minutes light exposure, only the 200 µg/ml solution showed a >1 log reduction of live bacteria (1.3 ± 0.3) with all other concentrations being below this threshold. We conclude that against *E. coli* bacteria, MB was shown to be more effective at comparable concentrations.

A similar trend was found in the results from the *S. mutans* experiments. After 30 minutes light exposure, a 1.6 ± 0.1 log reduction in live bacteria was recorded for the 200 $\mu\text{g/ml}$ concentration of MB-loaded PBS solution, but less than 1 log reduction (0.6 ± 0.1 , 0.7 ± 0.1 and 0.3 ± 0.2 respectively) was recorded for the other concentrations. For each of the tested concentrations for ER, a log reduction below 1 (0.8 ± 0.1 , 0.2 ± 0.1 , 0.1 ± 0.1 and -0.1 ± 0.2 respectively) was measured. After 60 minutes light exposure, again, the greatest concentration of MB caused a 1.7 ± 0.2 log reduction in bacterial numbers, but all other concentrations recorded less than 1 log reduction of bacteria (0.7 ± 0.04 , 0.8 ± 0.3 and 0.5 ± 0.3). For ER, no concentration tested met or exceeded 1 log of bactericidal activity following 60 minutes of light exposure (0.9 ± 0.1 , 0.3 ± 0.03 , 0.1 ± 0.2 and 0.1 ± 0.3 at 0.2-200 $\mu\text{g/ml}$ respectively). This again highlights that MB was more effective at killing bacteria than ER. Cationic PS such as MB have been shown to be more effective than anionic PS such as ER due to the charge interactions with the bacterial cell wall^[281,478].

Contrasting the log reductions for the two bacterial strains, it was interesting to find that for MB, there was no significant difference between the killing of gram-negative *E. coli* and gram-positive *S. mutans* for all concentrations tested, except that of 20 $\mu\text{g/ml}$ where significantly more *E. coli* was killed than *S. mutans* ($p = 0.001$ and 5×10^{-8} after 30 and 60 minute light exposures respectively). For ER at the same concentration, again significantly more *E. coli* was killed than *S. mutans* ($p = 0.04$ and 0.02 after 30- and 60-minute light exposures respectively). This would be a particular advantage in the oral cavity, where gram-negative bacteria in biofilms are the main target as these are most difficult to destroy^[58,479].

5.3.4 *In vitro* testing with Photosensitiser-Encapsulated PCL Scaffolds

The next stage of this study was to test the effects of the PS released from the polymer carrier on the bacteria and cells. The PCL scaffolds were selected over PLGA7525 scaffolds as a model PS-carrier at this stage due to their dimensional stability in an aqueous environment (section 4.3.2).

5.3.4.1 *In vitro* Testing of Photosensitiser-Encapsulated PCL Scaffolds on Mammalian Cells

As these scaffolds are designed for use as regenerative devices, it was important to determine initially whether the scaffolds were toxic to mammalian cells. Samples containing approximately 20 mg of PCL-ND, PCL-MB (containing approximately 4.4×10^{-7} moles equivalent to 0.14 mg of MB) and PCL-ER (containing approximately 4.4×10^{-7} moles equivalent to 0.38 mg of ER) scaffolds were irradiated under UV light for 30 minutes and then incubated in 5 ml of PBS for either 1 minute (0 hours), 2 hours or 24 hours to allow for PS release. These times were chosen as they may be clinically relevant, as the oral surgeon could decide to activate the PS immediately in high risk patients, or wait 2 hours to allow for release from the scaffold, or request the patient return a day after surgery for a 'check-up' where they then may decide to light activate the PS. These 'extract' solutions were then added to monolayers of confluent L929 cells and incubated for 2 hours to allow for PS uptake. As in the solutions testing (section 5.2.5.1), the dark toxicity was determined first (**Figure 5.9**).

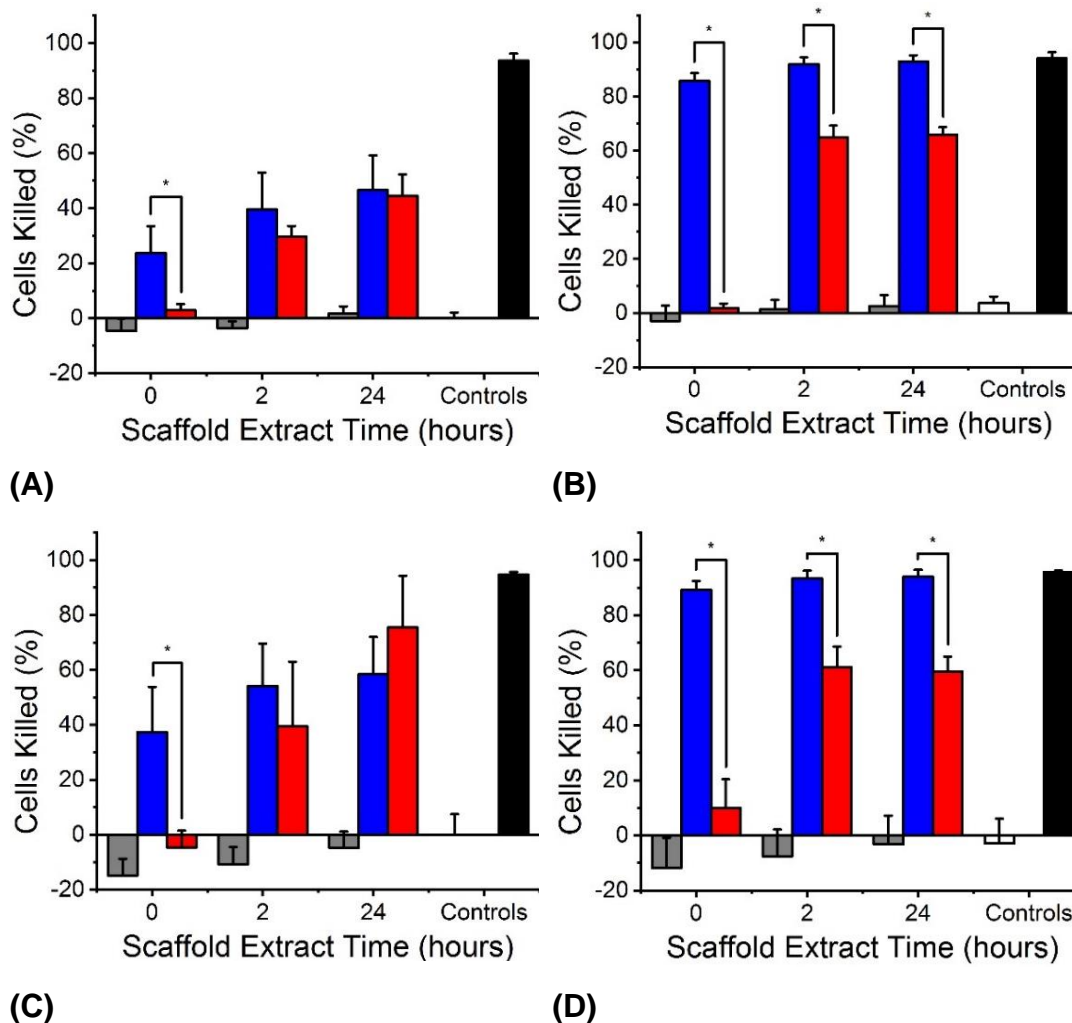


Figure 5.9 – L929 monolayer cytotoxicity following application of PCL scaffold PBS extract solution. (A) 30 min 'dark' control; (B) 30 min light exposure. (C) 60 min 'dark' control; (D) 60 min light exposure. ■: PCL-ND control scaffold extract solutions; ■: PCL-MB scaffold extract solutions; ■: PCL-ER scaffold extract solutions; □: fresh PBS negative control; ■: PBS-Triton™ X-100 solution positive control. Results reported as Mean±SD (n=3). "*" denotes significantly different means ($p < 0.05$, t -test)

This experiment highlighted that the PCL-ND scaffolds were non-toxic as cell killing was below 6% in all experiments. In some cases, the PCL-ND scaffolds appeared to aid proliferation of cells with a negative value being observed, particularly in the 60-minute timepoint experiments.

The dark toxicity of scaffold extract solutions across both 30- and 60-minute exposure times was above 30% for 0-, 2- and 24-hour incubation times of MB scaffolds (31 ± 15 , 47 ± 16 and $53\pm 14\%$ respectively). The toxicity of the 0-hour incubation time for ER scaffolds was low ($-0.9\pm 6\%$) but increased to $>30\%$ after 2- or 24-hours incubation (35 ± 18 and $60\pm 21\%$ respectively).

There was a significant increase in cell killing for all PS-included samples upon light activation, apart from the PCL-ER samples following 60-minute light activation where there was no significant difference. This confirms that the combination of light and PS causes killing of mammalian cells.

There was an increase in the percentage of cells killed between the 0- and 2-hour incubation times for MB after 30 minutes light exposure ($p = 0.005$) but not after 60 minutes light exposure ($p = 0.05$). There was also no significant increase in killing between 2- and 24-hour incubation times for either 30- or 60-minute light exposure times ($p = 0.6$ and 0.7 respectively). This is likely to be due to the cell killing being close to maximal after this point and therefore an increase in PS release does not significantly impact the cell killing. This correlates with the PS-release data (section 4.3.1.2) as $\sim 100\%$ of MB was found to be released during the first 2 hours incubation in PBS.

For ER, there was a significant increase between 0- and 2-hour incubation times for both 30- and 60-minutes light exposure ($p = 4\times 10^{-8}$ and 9×10^{-6} respectively). However, there was no significant difference between the 2- and 24-hour incubation time for the two different light exposure times ($p = 0.7$ and 0.7 respectively).

Again, these results indicate an unacceptably high mammalian cell toxicity for either PS used in the tissue regenerating scaffolds, which exemplifies the importance of slowing the release from the scaffold and potentially reducing the amount of PS loaded into the electrospun scaffold during production.

5.3.4.2 *In vitro* Testing of Photosensitiser-encapsulated PCL Scaffolds with Bacteria

The antibacterial activity of the PS-encapsulated PCL scaffolds was determined during an external placement to the University of Massachusetts Amherst in the Chemical Engineering department under the supervision of Prof. Jessica Schiffman. Due to the time-constraints of this placement, only one bacterial strain was able to be tested. The aPDT effect has been shown in previously published data to be more effective against Gram-positive bacteria^[480]; consequently, only *E. coli* was used in these studies to test the effect of aPDT scaffolds on a model Gram-negative bacteria.

This experiment was performed by directly imaging the bacteria populating the scaffold with fluorescence microscopy (**Table 5.3**).

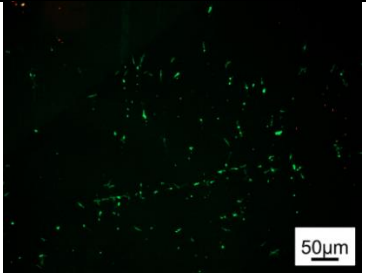
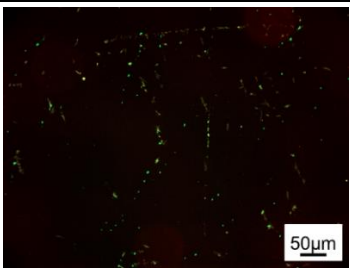
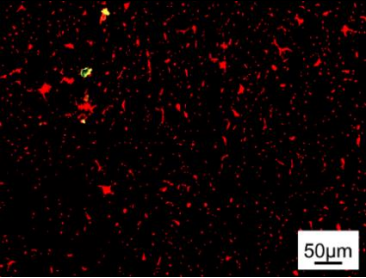
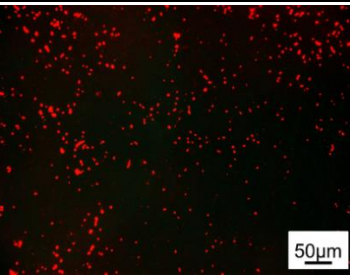
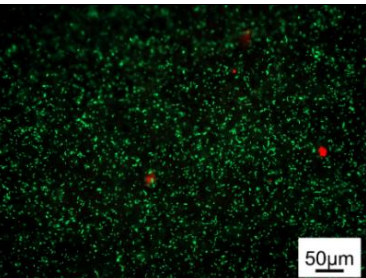
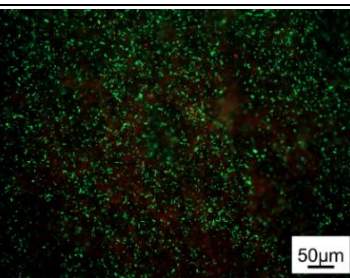
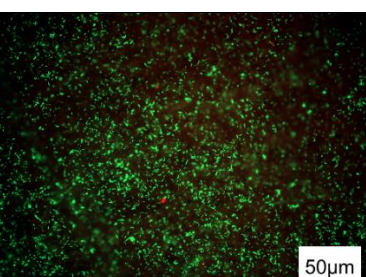
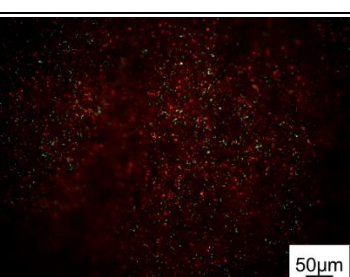
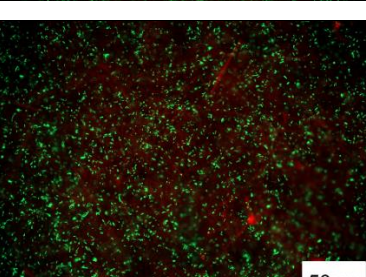
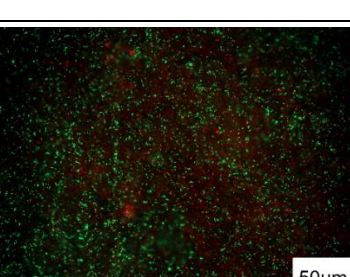
	Dark	Light
Bacteria in fresh M9 salts solution (Negative Control)		
Bacteria in Ethanol (Positive Control)		
PCL-ND		
PCL-MB		
PCL-ER		

Table 5.3 – A set of live/dead images showing an example set of the data from testing *E. coli* bacteria on PCL-PS scaffolds following 60 minute light exposure

Initially, the scaffolds were incubated in medium for 2 hours to allow for PS release. Following this time *E. coli* bacteria were added to the scaffolds (section 5.2.6.2). These scaffolds were then light activated for 30 or 60 minutes and live/dead images were collected for each scaffold and the log reduction calculated based on these results (Figure 5.10).

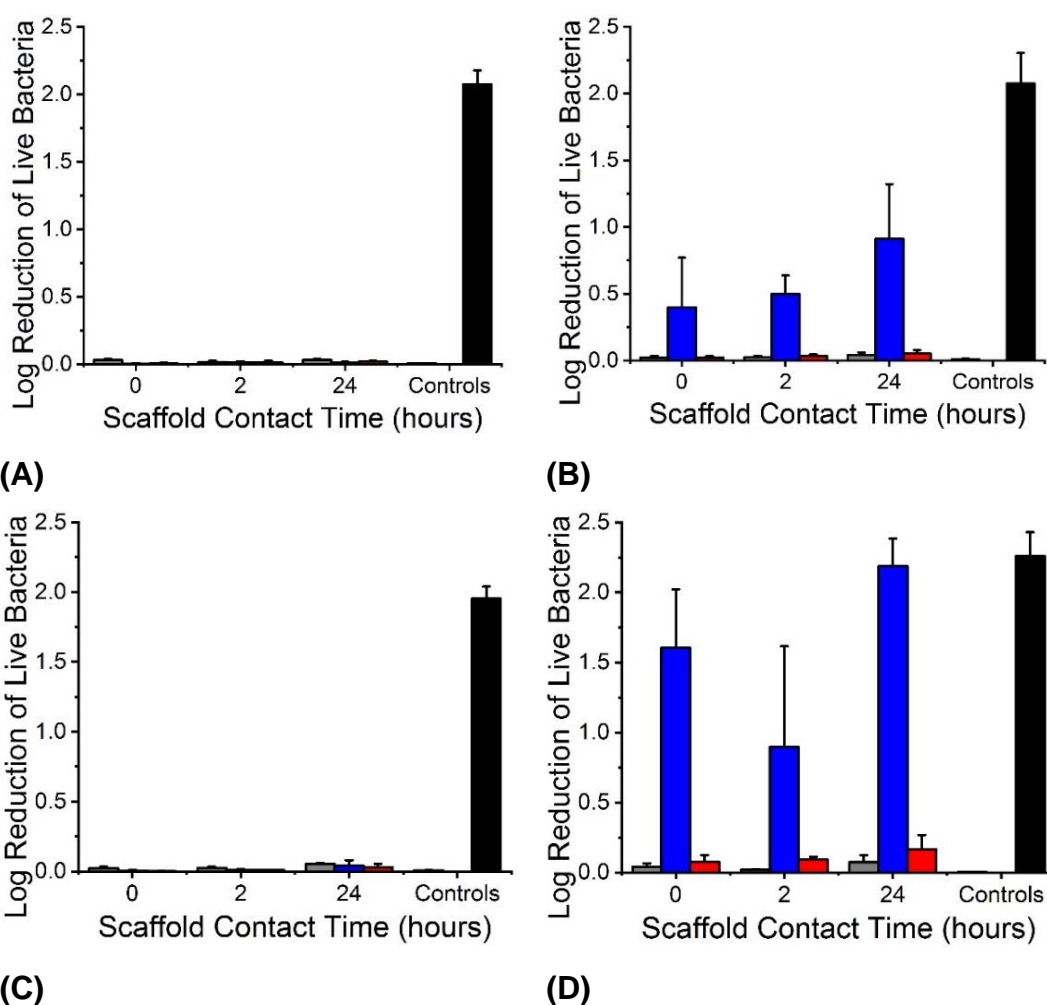


Figure 5.10 – Log reductions of *E. coli* bacteria on PCL scaffolds. (A) 30 min 'dark' control; (B) 30 min light exposure. (C) 60 min 'dark' control; (D) 60 min light exposure. ■: PCL-ND control scaffolds; ■: PCL-MB scaffolds; ■: PCL-ER scaffolds; □: Fresh M9 medium negative control; ■: Ethanol positive control. Results reported as Mean±SD (n=3)

A key observation from these results was that there was minimal killing observed for the control scaffolds with no PS inclusion. This implies that the PS is responsible for the bacterial death, and that the scaffolds themselves are not inherently bactericidal.

To verify that the selected PS molecules were not toxic prior to light activation, an identical set of foil-covered scaffold samples were analysed in each experiment to calculate the 'dark toxicity' of the scaffolds. In all experiments, the dark toxicity of the PS-encapsulated scaffolds was below 0.05 log reductions. These results should be compared to the light activated PS-free electrospun scaffold controls (■, **Figure 5.10**) which confirms that the PS and the light combination is needed to deactivate the bacteria.

A key observation seen across all PS-containing scaffold formulations, was that the longer the light exposure, the more bacteria were killed, e.g. for PCL-MB scaffolds following 30- or 60-minute light exposure, the log reductions were 0.5 and 0.9 respectively. This finding is in agreement with previous reports that the greater the dose of light, the more toxic reactive species are generated and the more active the PS is^[353].

Following this initial study, samples were incubated in medium for 1 minute (0 hours) and 24 hours prior to bacterial addition. This was to determine whether the greater PS concentration available increased the bacterial killing.

It can clearly be seen from these results that the MB-encapsulated scaffolds with the same PS concentration were found to kill significantly more *E. coli* than ER-encapsulated scaffolds across all incubation times and with both light exposure times. This observation is in agreement with the increased release of MB from the scaffold with respect to ER (section 4.3.1.2) resulting in an expected increase in cellular MB uptake. The increased aPDT effect of MB-encapsulated fibres may also be due to the fact that MB is cationic, which would result in greater interaction with the Gram-negative *E. coli* cell membranes and therefore more damage to the outer membrane^[313].

5.4 Conclusion

These experiments were conducted to identify an optimal PS dose for loading of and releasing from a polymer scaffold for use in oral applications. They were used to quantify the aPDT capability of the scaffold and provide an indication of how either MB or ER would behave *in vivo*. However, it is important to note that in a clinical setting, results would vary as the mammalian cells would not be present in monolayers and bacteria will be mainly growing as biofilms rather than in planktonic form. Additionally, the cell types would effectively be present as a mixed population rather than each in isolation. However, the experiments here were a suitable model for comparing the effects of MB or ER on bacteria and mammalian cells in order to determine the most suitable PS for continued analysis.

In this study, MB was shown to be more readily taken up by both bacterial and mammalian cells than ER (**Figure 5.4**). This is likely to be due to MB being cationic and ER being anionic. Cationic PS have previously been found to be more readily taken up by bacteria due to the increased interaction between PS and bacterial cell wall, which has the advantage of limiting the amount of damage to surrounding mammalian tissue^[481].

When testing solutions of PS on monolayers of mammalian cells and planktonic bacteria, the dark toxicity of MB and ER were similar. When light activated, at lower concentrations of PS, an increase in cell or bacterial killing was observed which indicates that both the light and PS combination is needed in aPDT. This would also suggest that both PS act in a drug- and light- dose dependent manner. This study provides evidence that MB is more effective against both gram-positive and gram-negative bacteria than ER at comparable concentrations, which is potentially advantageous for the desired application of this biomaterial.

As this study aims to conclude with the production of a clinically relevant medical device, it is important to consider regulation and approval of each PS for use in clinical applications. MB is currently clinically approved for aPDT in dentistry, which will aid the regulatory hurdles needed to take

the product to market^[281]. In contrast, ER was de-listed in the US in 1990 for use in either externally applied drugs or cosmetic products due to findings of carcinogenicity in rat models^[482].

A discussion on the light source is also important for clinical translation. Blue light has the advantages of being inherently antimicrobial, but red light is a greater tissue penetration range^[281]. As this scaffold will be used for tissue regeneration, light may be required to penetrate new tissue which has formed on the surface of the scaffold to activate PS taken up by bacteria which may be populating the scaffold below this. Therefore, the red light required to activate MB may be advantageous for the product.

Aside from the PS comparison, a conclusion to be drawn from the results presented here was that PCL control scaffolds were confirmed to be non-toxic to both mammalian cells and bacterial cells. This is important as the scaffold will be required to support neotissue formation and this would be limited if the scaffold was inherently cytotoxic.

To conclude, of the two PS tested in this study with light activation, MB was shown to be more effective at killing bacteria than ER in all studies. Combined with the unusual secondary interactions found with the ER-loaded scaffolds (section 3.3.1.2), it was decided at this point in the project to discontinue the use of ER and focus on optimising the biomaterial properties of MB-loaded polymeric electrospun scaffolds. Although these studies provide evidence that the MB from the PCL scaffolds is toxic to cells, further studies will be performed to elucidate the selectivity achieved relative to the concentration of PS introduced into the scaffold system.

Chapter 6 Optimisation of Polymer Carrier with Methylene Blue for Use as a Regenerative Electrospun Scaffold in Oral Environments

6.1 Introduction

This chapter was aimed to describe the work conducted to characterise and optimise a polymer carrier for use as a regenerative scaffold. Chapter 3 and Chapter 4 of this thesis discussed the use of PCL and PLGA7525 as the polymer carrier, with either MB or ER PS. From these chapters, it was concluded that PLGA7525 was not suitable for the intended application as the resulting scaffold shrunk upon incubation in aqueous media. PCL proved to be a stable polymer carrier over the 8-week incubation period, but the PS was released in a 'burst' within the first 2 hours which resulted in toxic levels of PS being reached, which would prevent neotissue formation.

Chapter 5 then compared MB and ER with both mammalian and bacterial cell types to determine the optimal PS for use in the final prototype scaffold. From this study, MB was taken up more readily into the bacteria and was found to be more toxic to the tested bacterial cells at comparable concentrations in comparison to ER. Also in Chapter 5, PCL scaffolds were used as a model carrier as an additional test for comparison of the activity of the PS. This study confirmed that MB was being released too quickly from the scaffold as toxic concentrations for mammalian cells were reached almost immediately upon incubation.

Therefore, this chapter presents evidence aimed at characterising a new polymer carrier that will maintain integrity over approximately 8 weeks in oral environments and not show signs of macroscopic shrinkage or fibrous microstructure collapse upon incubation in aqueous media. The scaffold should also be capable of controlled release of MB over approximately 4 weeks to allow for long-lasting activation of antimicrobial PDT when required but prevent toxic levels of MB from being reached for the mammalian cells populating the scaffold. There are many examples in the literature of the use

of coaxial electrospinning^[483], hybrid electrospinning^[484] or chemically-bonding drugs into the scaffold^[485] in order to achieve controlled release profiles.

Due to limitations in access to equipment and the desire to keep the processing of the polymer system as simple as possible for regulatory purposes, it was decided to try a different monomer ratio of PLGA initially. It has previously been published that the lactic acid component of the PLGA is responsible for the amorphousness (and consequent water-induced shrinkage) of the PLGA copolymer^[421,486,487]. PGA is also known to be a semi-crystalline polymer and so increasing the percentage of this monomer in the polymer ratio should lead to increased crystallinity in the copolymer^[488]. With respect to the previous PLGA formulation, it was therefore decided to use a polymer with a higher glycolide and lower lactide monomer ratio, i.e. PLGA1090 with 10% poly(lactic acid) and 90% poly(glycolic acid).

6.2 Materials and Methods

6.2.1 Materials

Poly(*rac*-lactide-co-glycolide) (PLGA1090) (M_n : 63,000 g·mol⁻¹, 10:90 molar ratio of lactic and glycolic acid units) was purchased from Purac Biomaterials (PURASORB PLG 1017). All other materials are as listed previously (section 3.2.1).

6.2.2 Electrospinning Solution Preparation

As described previously (section 3.2.2). Where polymers were blended, each polymer was weighed out as a mass percentage of either 80:20, 50:50 or 20:80 of PCL to PLGA1090. The total concentration of polymer in HFIP remained unchanged from previous electrospinning solutions at 6 wt.%.

For reduced concentration electrospinning solutions, 1.1mM or 0.2mM concentrations of MB were added to each polymer solution. These were referred to as 50% and 10% respectively.

6.2.3 Viscosity Measurements

As described previously (section 3.2.3).

6.2.4 Electrospinning

As described previously (section 3.2.5).

6.2.5 Scanning Electron Microscopy

As described previously (section 3.2.6).

6.2.6 Loading Efficiency

As described previously (section 3.2.7).

6.2.7 Scaffold Colour Measurements

As described previously (section 3.2.10).

6.2.8 Differential Scanning Calorimetry

As described previously (section 3.2.11).

6.2.9 Tensile Testing

As described previously (section 3.2.12).

6.2.10 Water Uptake Analysis

As described previously (section 4.2.3).

6.2.11 pH Testing

The pH of the aqueous supernatant was recorded at regular time points over the course of the experiment using a Mettler Toledo 'FiveEasy™ FE20' pH meter with a VWR pH electrode (DJ 113). Prior to use, the pH meter was calibrated using Buffer reference standards (Sigma Aldrich) at pH 4, 7 and 10. Between each sample, the pH electrode was rinsed thoroughly in d_4H_2O to remove traces of the previous testing solution. The probe was placed into each testing solution, stirred, and left until a stable reading was reached.

6.2.12 Hydrolytic Degradation

6.2.12.1 Hydrolytic Degradation Trial with Controlled pH in Tris Buffer

A 1M Tris buffer was made by dissolving Tris base (Sigma Aldrich, M_w : 121.14 g/mol) in d_4H_2O before adjusting the pH to 7.4 using concentrated

hydrochloric acid (HCl, Sigma Aldrich). Prior to use, this was diluted 1:100 to reach a 10mM Tris-HCl solution.

Samples were cut into 1 cm² squares and weighed before being incubated with 5 ml of Tris buffer solution in sealed falcon tubes at 37°C for 1 week. Following this time, the pH of the solutions was recorded to determine if there had been a significant decrease.

6.2.12.2 Modified Hydrolytic Degradation

As described previously (section 4.2.4) but with additional monitoring of the pH. pH was monitored at least every 3 days during the 8-week experiment, and if necessary, fresh PBS solution was added until the pH ~7.4 was achieved.

6.2.13 Modified Release Kinetics

As described previously (4.2.2) but with additional monitoring of the pH. pH was monitored at least every 3 days during the 8-week experiment, and if necessary, fresh PBS solution was added until the pH ~7.4 was achieved.

6.2.14 Statistical Analysis

Significant differences in the results were evaluated using an unpaired Student's *t*-test. Data was deemed to be significantly different at $p < 0.05$. All data were collected in triplicate and presented as Mean \pm Standard Deviation.

6.3 Results and Discussion

A new polymer carrier, PLGA1090, with comparable molecular weight to the previously tested polymers (PCL and PLGA7525) was obtained as fibre a building block to evaluate the potential structure-property relationships of the scaffolds. Electrospun polymer constructs were first analysed in terms of fibrous architecture and then with regards to the scaffold behaviour in aqueous medium.

6.3.1 PLGA1090 Characterisation

6.3.1.1 PLGA1090 Polymer Solution Characteristics

To allow direct comparison of results, an initial screen of three different PLGA1090 polymer concentrations (6, 9 and 12 wt.%) was first performed to determine which concentration would yield measurements most similar to the two previous polymer carriers used in this study (**Figure 6.1**).

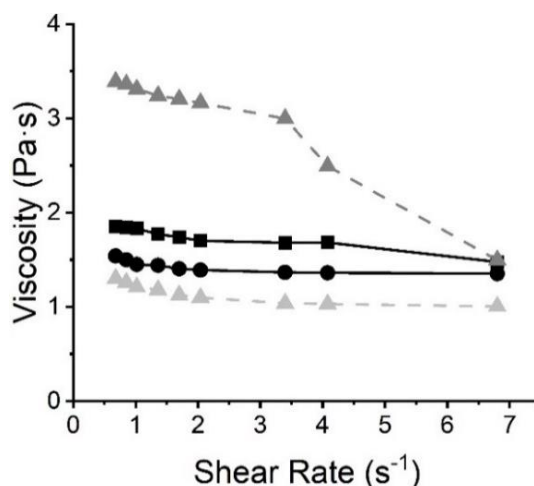


Figure 6.1 – Viscosity of PS-free (ND) electrospinning polymer solutions at different concentrations in HFIP. (▲): PLGA1090-ND-6 wt.%; (▲): PLGA1090-ND-9 wt.%; (■): PCL-ND-6 wt.%; (●): PLGA7525-ND-12 wt.%. Lines are guidelines to the eye

Each PLGA1090 solution concentration tested was found to display the same shear-thinning as observed with PCL and PLGA7525 (section 3.3.1). PLGA1090 was found yield solutions with increased viscosity with respect to PLGA7525 solutions at the same concentration. At 12 wt.%, the PLGA1090 solution was too viscous to handle and a viscosity reading could not be taken, as was the situation with the PCL solutions at 12 wt.% concentration. The most similar viscosity with respect to the PLGA7525 12 wt.% and PCL 6 wt.% solutions was measured with 6 wt.% PLGA1090 solutions. Therefore, this polymer concentration was chosen to be carried forward into the remainder of the study.

As discussed in Chapter 5, MB was found to be the most effective PS to use in this study with respect to aPDT capability, so the viscosity a 6 wt.% PLGA1090 solution doped with 2.2 mM MB was determined (**Figure 6.2**).

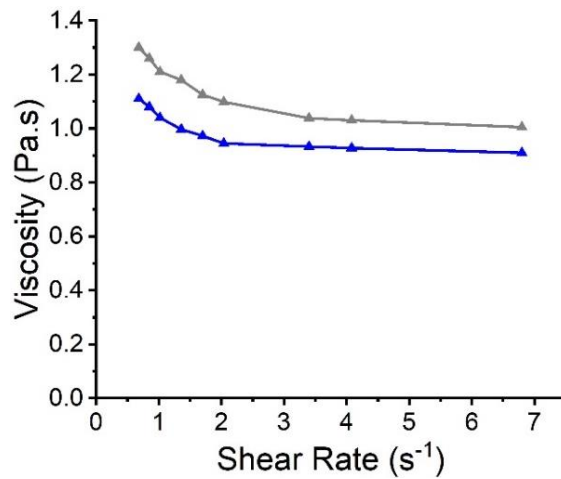


Figure 6.2 – Viscosity of electrospinning polymer solutions at different concentrations in HFIP at 6 wt.% polymer concentration with or without 2.2mM MB. (▲): PLGA1090-ND; (▲): PLGA1090-MB. Lines are guidelines to the eye

In previously tested PCL and PLGA7525 polymer, there was a decrease in viscosity following inclusion of MB, but this was not statistically significant. In contrast, the viscosity of the PLGA1090-MB solution was significantly reduced in comparison to the PLGA1090-ND solution control ($p = 0.004$, **Figure 6.2**). The observed decrease in solution viscosity could suggest that there is an additional interaction between the polymer chains of PLGA1090 and MB in solution, which may have an impact on the material properties and microarchitecture of the electrospun scaffolds. This was found (more severely) with the PLGA7525 and ER interaction, which resulted in a significant decrease in fibre diameter (section 3.3.2.1) and an increase in scaffold degradability (section 4.3.2).

6.3.1.2 PLGA1090 Electrospun Scaffold Characteristics

The polymer solutions were electrospun and resulting electrospun scaffolds analysed using SEM (**Figure 6.3**).

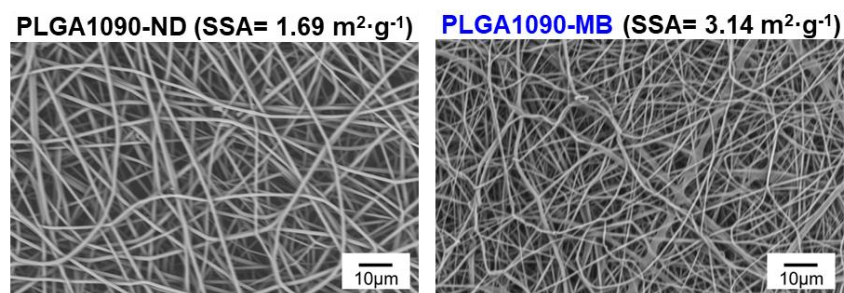


Figure 6.3 – Microstructural analysis of MB-encapsulated scaffolds and electrospun ‘ND’ controls. SEM images taken at 1000x magnification and Specific Surface Area (SSA) measurements obtained via BET analysis

Both PLGA1090-ND and PLGA1090-MB solutions produced bead-free fibrous scaffolds. Macroscopically, the PLGA7525-MB scaffolds, the PLGA1090-MB scaffolds were blue coloured as opposed to the purple coloured PCL-MB scaffold as discussed previously (section 3.3.2.2). This would suggest that the MB molecules are present in monomeric form.

To ensure that all the PS had been transferred from the electrospinning solution into the resultant scaffolds, the loading efficiency of the scaffolds was calculated. This was calculated to be $97\pm 6\%$, which confirms that the PS loading efficiency is equal to that of the previously characterised polymer carriers at approximately 100% efficiency.

The fibre diameters were measured from the SEM images (**Figure 6.4**).

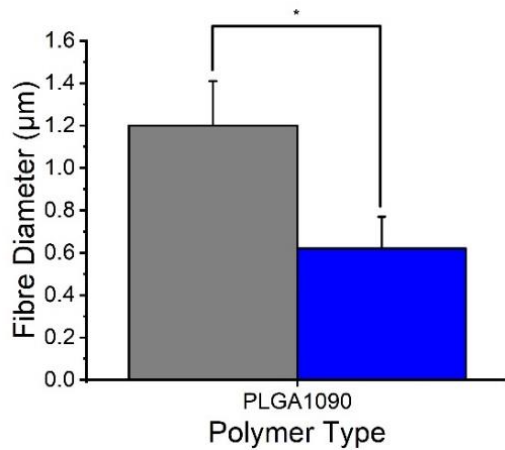


Figure 6.4 – Average Fibre Diameter determined from SEM images for each PLGA1090 electrospun scaffold. Grey bars: Control scaffolds; Blue bars: MB-included scaffolds. Results reported as Mean±SD (n=3). ‘*’ denotes significantly different means ($p < 0.05$, t -test)

There was found to be a significant reduction between the PLGA1090-ND and the PLGA1090-MB scaffolds in fibre diameter of 48% ($p = 2.5 \times 10^{-27}$). This is comparable to the reductions of the fibre diameter in PCL-MB and PLGA7525-MB fibres previously observed results (54% and 51% respectively, section 3.3.2.1).

Following the scaffold characterisation, it was important to ensure that the crystallinity of the polymer had been increased as the presence of crystallites is expected to enhance macroscopic stability of the scaffolds in aqueous environments^[489]. Therefore, DSC analysis was carried out (**Figure 6.5**).

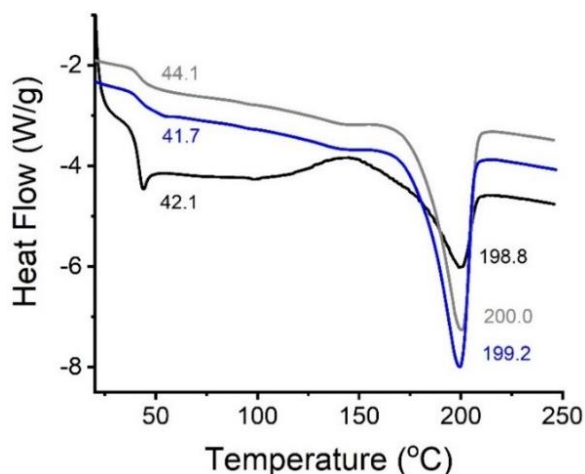


Figure 6.5 – Differential Scanning Calorimetry heat flow plots. (—): Unprocessed PLGA1090 polymer; (—): PLGA1090-ND scaffolds; (—): PLGA1090-MB scaffolds

The DSC plot highlights both a glass transition (T_g) (related to the amorphous regions of the polymer) and a melting transition (related to the crystalline regions of the polymer) for both the polymer and respective electrospun scaffolds (**Table 6.1**).

		T_m (°C)	ΔH_m (J/g)	T_g (°C)
PLGA1090	Raw	198.8	49.3	42.1
	ND	200.0	76.4	44.1
	MB	199.2	67.9	44.7

Table 6.1 – DSC Thermal Analysis Values for PLGA1090 samples of either ‘Raw’ polymer pellets, PS-free (ND) control scaffold samples or MB-incorporated scaffold samples

This indicates that the semi-crystalline structure is maintained following electrospinning. PCL scaffolds were found to be predominately crystalline and the PLGA7525 was found to be predominately amorphous as discussed previously (section 3.3.2.3). As this new polymer possess both a T_g and a T_m in the heat flow plot generated during DSC analysis, this would suggest that

the new polymer may be a 'mid-way' point in crystallinity between the two previously tested polymers.

The inclusion of MB with PLGA1090 reduced the T_g from 44.1°C for the control (ND) scaffold to 41.7°C. This effect of a small molecule included in PLGA fibrous polymers reducing the T_g has been previously published^[490] and is thought to be due to the molecule inclusion increasing mobility of polymer chains, thus lowering the temperature required^[491].

As it is known that the crystallinity of a scaffold affects the mechanical properties of a scaffold^[492–494], tensile testing was performed on samples of each of these scaffold types (**Figure 6.6** and **Figure 6.7**).

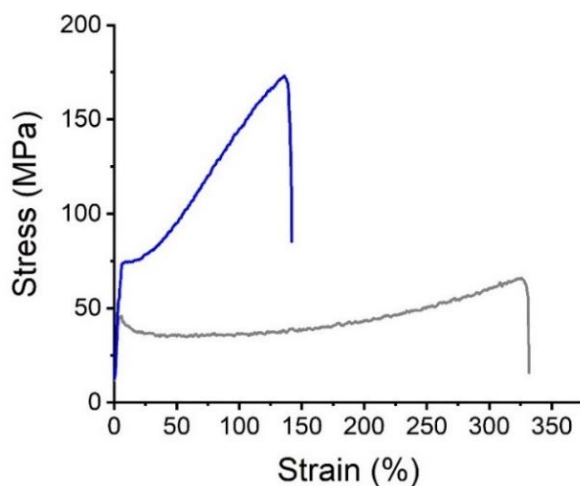


Figure 6.6 – Stress-strain curve of PS-encapsulated PLGA1090 polymer scaffolds. (—): PLGA1090-ND; (—): PLGA1090-MB

The stress-strain curve of the PLGA1090-ND and PLGA1090-MB was used to quantify the elastic modulus (E), percentage strain (ϵ) and toughness (U_T) (**Figure 6.7**).

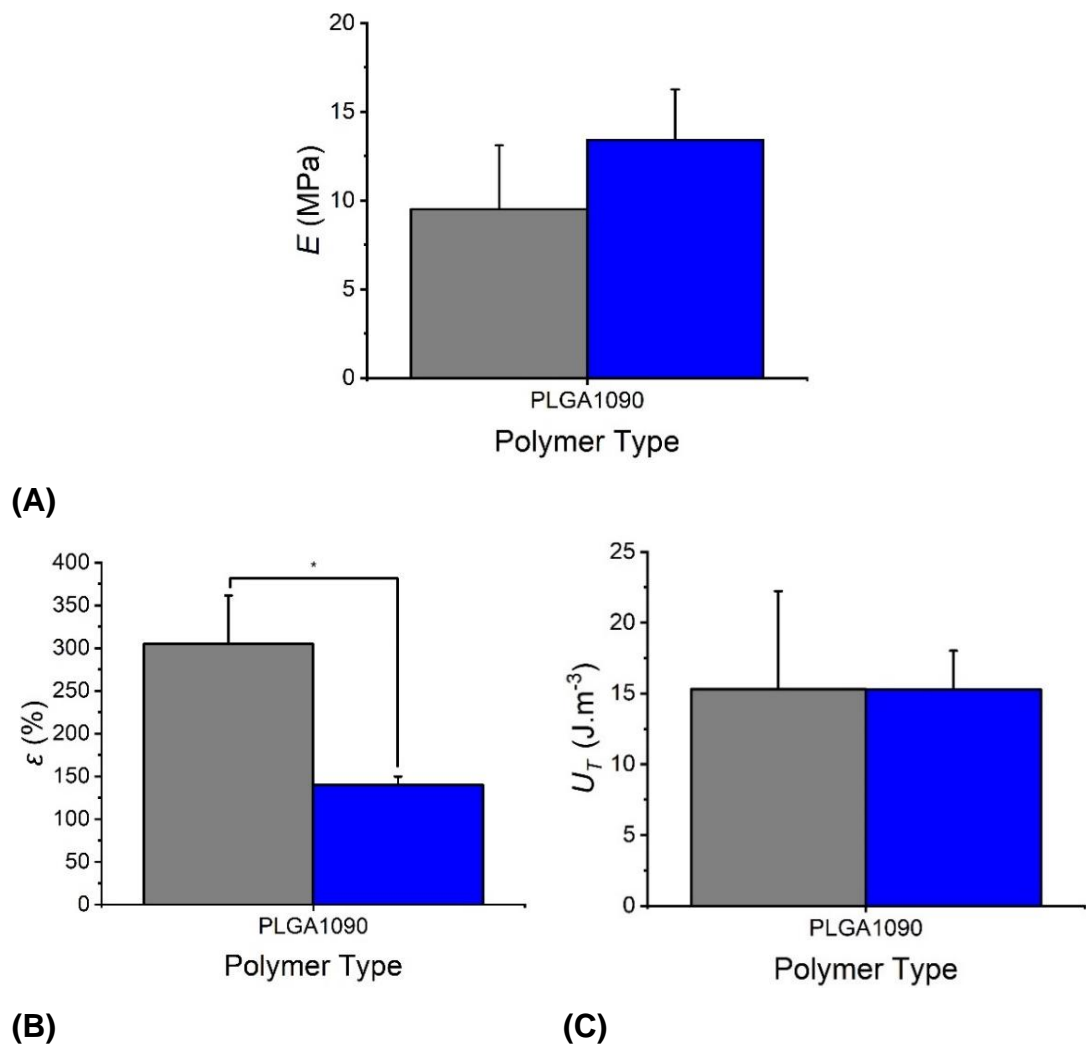


Figure 6.7 – Mechanical properties measured in PLGA1090 samples. (A) Elastic Modulus (E); (B) Strain at Break (ϵ) and (C) Ultimate Toughness (U_T). Grey bars: control polymer scaffolds; Blue bars: MB-loaded scaffolds. Results reported as Mean \pm SD (n=3). “*” denotes significantly different means ($p < 0.05$, t -test)

The elastic modulus of the control PLGA1090 samples was 9.5 ± 3.6 MPa, this was significantly greater than the PCL sample controls at 1.4 ± 0.3 MPa ($p = 0.01$). The PLGA1090-MB scaffolds had a significantly decreased elastic modulus in comparison to the PLGA7525-ND control scaffolds (18.7 ± 1.9 MPa, $p = 0.004$). This could be related to the crystallinity of the scaffolds, as this polymer type was found to be at a mid-way point between the two polymers in terms of crystallinity as well as elastic modulus.

There was no significant difference between the PLGA1090-ND and the PCL-ND or PLGA7525-ND controls in relation to the calculated strain at failure ($p = 0.9$ and 0.9 respectively). The PLGA1090 and PCL controls had comparable ultimate toughness values ($p = 0.7$), but significantly lower values than the PLGA7525 control ($p = 0.03$).

The inclusion of MB in the scaffold did not significantly change the elastic modulus or the toughness of the electrospun scaffold ($p = 0.1$ and 1.0 respectively). However, the elongation at break was significantly decreased ($p = 0.004$). This reflects the same result as with the PLGA7525-MB scaffolds in comparison to the control samples.

6.3.1.3 PLGA1090 Electrospun Scaffold Interactions in Aqueous Medium

It was discussed previously in this thesis that the crystallinity of the scaffolds impacts on the interaction of the scaffold with water molecules and WU of the scaffolds (section 3.3.2.3 and section 4.3.1). To confirm this point with the polymer system, the wet-state behaviour of the new PLGA1090 scaffolds was quantified.

The WU for all samples was found to be over 100% for both the control and the PS-included samples (**Figure 6.8**).

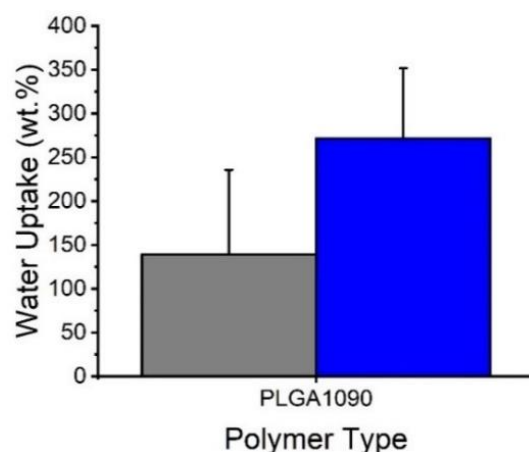


Figure 6.8 – Water uptake measured gravimetrically following incubation (H_2O , $37\ ^\circ C$) of either PS-loaded or electrospun control PLGA1090 samples. Grey bars: Pol-ND scaffolds; Blue bars: Pol-MB scaffolds. Results reported as Mean \pm SD (n=3)

Although an increase in the mean WU was observed for the PLGA1090-MB scaffolds, this was not a statistically significantly different result ($p = 0.1$). This was also found with the PCL polymer scaffolds, in which there was a non-significant increase between the PCL-ND and PCL-MB WU measurements ($p = 0.1$).

Importantly, no macroscopic shrinkage occurred during this experiment. This was a crucial result as the PLGA7525 polymer scaffolds were found to significantly shrink over this time period, which highlights the impact of glycolide/lactide monomer ratio on the interaction of resulting copolymers with water.

The scaffolds were next incubated in PBS at 37°C for up to 8 weeks to ensure that the scaffold maintained the fibrous morphology over this time (Figure 6.10 and Figure 6.10).

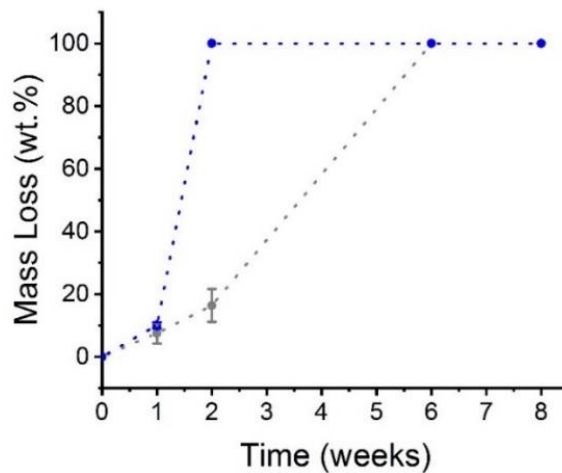


Figure 6.9 – Mass loss measured on samples following hydrolytic degradation in PBS (PBS, 37 °C). (-●-): PLGA1090-ND; (-●-): PLGA1090-MB. Lines are guidelines to the eye. Results reported as Mean±SD (n=3)

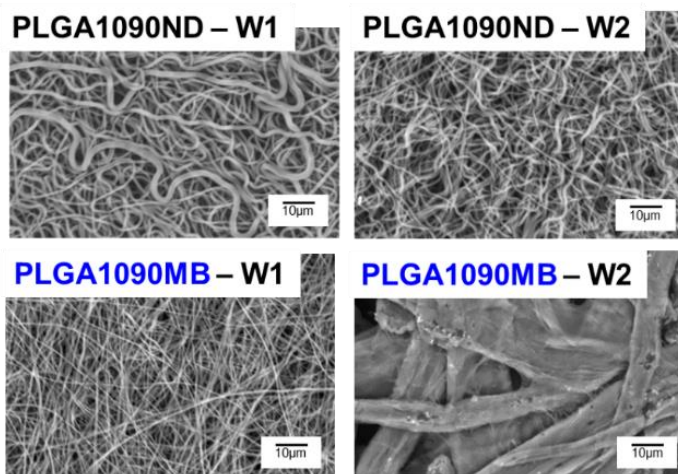


Figure 6.10 – Scanning Electron Microscopy (SEM) of electrospun PLGA1090 scaffolds. W1 and W2 refer to 1 week and 2 weeks incubation time points

After 1 week incubation both the PLGA1090-ND and PLGA1090-MB scaffolds had lost integrity and could not be handled as a complete scaffold but only as fragments (**Figure 6.10**). The SEM micrographs of the fragments at week 2 confirm the loss of structure during this time (**Figure 6.10**). The PLGA1090-ND scaffold were fibrous but compact during this time, but the PLGA1090-MB scaffolds had a collapsed structure which would not be suitable for use in this medical device. Although the more crystalline, PLGA1090 polymer scaffolds were observed to degrade more quickly than the PLGA7525 scaffolds (section 6.3.1.3), this finding is likely due to the decreased lactide content of the polymer, as the glycolide component is more hydrophilic and will therefore increase the degradation when a greater ratio is present in the copolymer^[495].

As the polymer degraded rapidly, acidic monomer residues were expected to be released into the 5ml of PBS. The accumulation of these could cause an autocatalytic effect on the degradation of the polymer and result in a rapid degradation profile which would not be found *in vivo*^[496–498]. When implanted in the oral cavity, the turnover of the aqueous medium (saliva) is likely to carry some of these acidic monomers away from the scaffold. It was therefore decided to determine the pH of the solutions to ensure that the ‘buffering’ ability of the PBS was sufficiently minimising the acidic effect of the

monomers being released. This was done by incubating each of the polymer scaffolds with incorporated MB in 5ml of PBS and measuring the pH value of the solution at the 4-week time point (**Table 6.2**).

Scaffold Type	Average
PCL-MB	7.3±0.005
PLGA7525-MB	6.7±0.02
PLGA1090-MB	3.0±0.008

Table 6.2 – pH Values of the PBS supernatant containing the Pol-MB scaffold following 4-weeks incubation at 37°C. Results reported as Mean±SD (n=3)

The results show that although the PCL and PLGA7525 scaffolds maintain a pH of ~7, the scaffolds containing the rapidly degrading PLGA1090 had a large reduction in pH. It was therefore decided to use a higher buffer capacity with these samples to determine whether a control of the pH could be achieved.

Samples of PCL-MB and PLGA1090-MB were incubated in 5 ml of 10 mM Tris-buffer for 1 week and the pH values were recorded after this time to determine whether this buffer could minimise the pH change. The PCL-MB scaffold solution was found to have a pH of 7.4 but the PLGA1090-MB scaffold supernatant had a pH of 3.8. This trial highlighted the that the higher buffer capacity was still not able to control the pH reduction.

Although a simple solution would be to start with a larger volume of PBS, this would result in low absorbance values being reached for the MB release study. The MB release and the hydrolytic degradation are known to be linked, so although this methodology would work for the mass loss study, it would not be appropriate for the release kinetics. An additional trial was conducted by performing the mass loss in 5 ml of PBS but then monitoring the pH every other day and adding further PBS upon a drop in pH to sustain a pH of ~7. This technique was found to be successful as it could be used to achieve a controlled pH but with an initial monitoring of the sample in 5 ml of

PBS. After an initial study, a full 8-week hydrolytic degradation study was performed on all PLGA1090 scaffolds with pH monitoring. The pH of the solution in this study did not reduce below pH 6.5 at any time point (**Figure 6.11** and **Figure 6.12**).

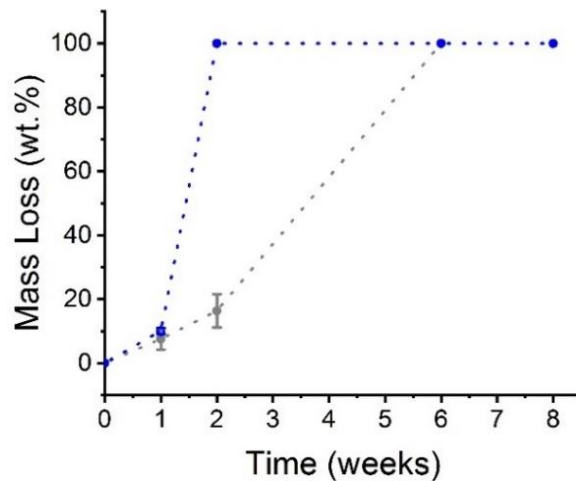


Figure 6.11 - Mass loss measured on samples following hydrolytic degradation in PBS with controlled pH (PBS, 37 °C, pH ~7.4). (●): PLGA1090-ND; (●): PLGA1090-MB. Lines are guidelines to the eye. Results reported as Mean±SD (n=3)

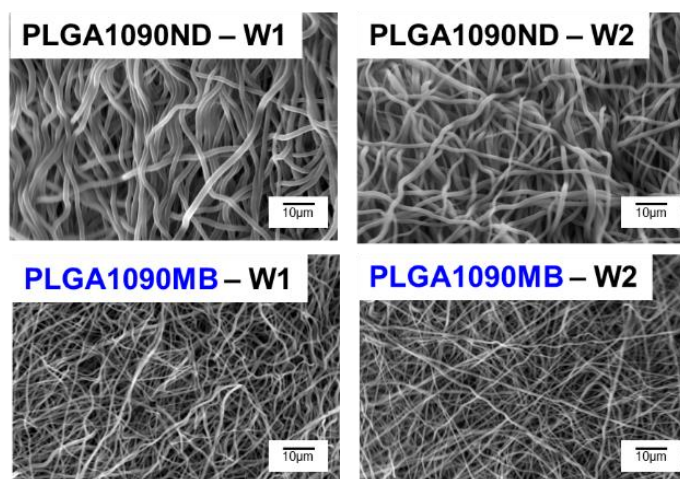


Figure 6.12 - Scanning Electron Microscopy (SEM) of electrospun PLGA1090 scaffolds. W1 and W2 refer to 1 week and 2 weeks incubation time points

This study showed that the scaffolds were more stable in the non-acidic environment, but that the PLGA1090-MB samples had still lost integrity at week 2 so were unsuitable for the intended use.

Besides the wet-state scaffold integrity, one of the two primary reasons for the choice of polymer carrier was to manufacture a scaffold capable of gradually releasing the PS over several weeks. The scaffolds were incubated initially in 5 ml of PBS for 24 hours and extracts were taken and analysed at regular timepoints. This was to ensure that the absorbance readings from the PS release were large enough to detect accurately. Following this, the pH was regularly monitored and additional PBS was added to ensure that the solution remained at pH ~7 at all times (to reflect the hydrolytic degradation study) (Figure 6.13).

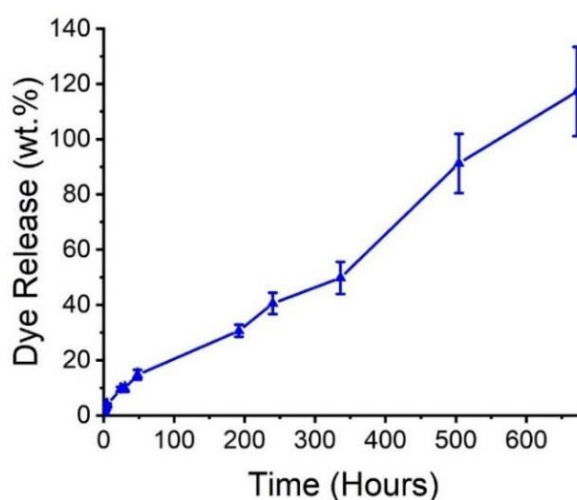


Figure 6.13 – Typical PS release profile measured via UV-Vis spectroscopy of the supernatant collected during incubation with controlled pH (PBS, 37 °C, pH ~7.4) from PLGA1090-MB scaffolds at selected time points over 672 hours (4 weeks). Line is guideline to the eye. Results reported as Mean±SD (n=3)

The release profile suggests that the polymer is suitable to deliver sustained release of PS over this time frame. Although the scaffolds lost integrity and became fragments after two weeks incubation, it is likely that the

PS release continues to increase over this time due to fragments of the scaffold being broken down.

6.3.2 Blended PCL and PLGA1090 Scaffold Characterisation

From the initial study, it was found that PLGA1090 polymer scaffolds had the advantage of gradually releasing the PS over the timeframe, but the sample lost integrity over 2 weeks, which would restrict scaffold functionality with time. The PCL polymer carrier characterised in Chapter 3 and Chapter 4 had the advantages of being stable in aqueous environments and displaying controlled degradation over the 8 week time-frame required by the medical device. However, PCL scaffolds proved to release the PS in a burst release. The desired polymer carrier therefore needed specific qualities of each of these two polymers. One way of possibly achieving the desirable properties of two different polymers is to combine them.

There are four main techniques to combine two polymers when electrospinning: blend, emulsion, co-axial and hybrid electrospinning^[499,500]. Blend electrospinning is arguably the simplest method as it involves mixing two electrospinning solutions together and then using the same apparatus as with a single solution to produce a scaffold. Emulsion electrospinning involves similar apparatus but requires the use of two immiscible solvents such as an organic and an inorganic solvent. The solutions are vortexed together prior to electrospinning to produce an emulsion. Co-axial electrospinning involves a different experimental set up by attaching an additional syringe to a dual needle, with one solution being at the 'core' of the needle tip and one being around the outside as the 'shell'. Finally, hybrid electrospinning involves the use of two separate electrospinning solutions being used in two different syringes separately but aimed at the same grounded collector^[501].

As blend electrospinning requires no change of solvent or experimental setup, this was the most logical first choice to try. A previous study had used blend electrospinning of these two polymers demonstrating that resulting electrospun materials displayed increase stability in water and decreased degradability as well as controlled drug release and improved mechanical properties such as Young's modulus and tensile strength^[434]. It was therefore

decided to combine the two polymer types in formulation to determine whether this would improve the PS-release capability and wet-state electrospun architecture of resulting PS-encapsulated scaffolds.

6.3.2.1 Polymer Blend Solution Characteristics

The polymer solutions were mixed in three different ratios of PCL:PLGA1090 at various wt.%, i.e. 80:20, 50:50 and 20:80. From this point onwards, these scaffolds are referred to as 0000-ND or 0000-MB, where 0000 represents the four digits of the polymer ratio, and ND and MB represent 'No Dye' or 'Methylene Blue' incorporated samples as previously reported.

Initially, a screening of the viscosity of each polymer formulation was performed to ensure that electrospinning was still possible (**Figure 6.14**).

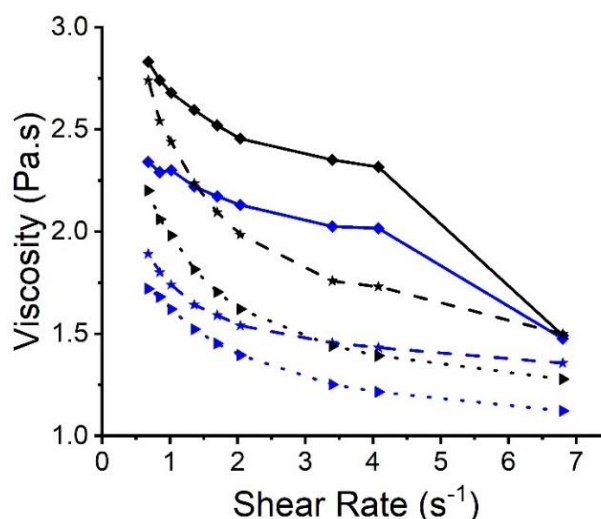


Figure 6.14 – Viscosity of electrospinning PCL and PLGA1090 polymer blend solutions at different concentrations in HFIP. (◆):8020-ND; (◆):8020-MB; (★):5050-ND; (★):5050-MB; (▶):2080-ND; (▶): 2080-MB. Lines are guidelines to the eye

As expected, the same shear-thinning behaviour of the polymer solutions was observed, as found with each of the polymers in isolation (section 3.3.1 and section 6.3.1.1). There was a small decrease in MB-incorporated scaffolds viscosity for all polymer blends with respect to the related PS-free control scaffolds. However, the decrease from MB-doped to

PS-free scaffold viscosity was not significant for the 8020 and the 2080 blends ($p = 0.05$ and 0.05), but statistically significant for the 5050 sample ($p = 0.006$).

6.3.2.2 Polymer Blend Scaffold Characteristics

The PLGA1090 polymer solutions were electrospun into scaffolds for further analysis (**Figure 6.15**).

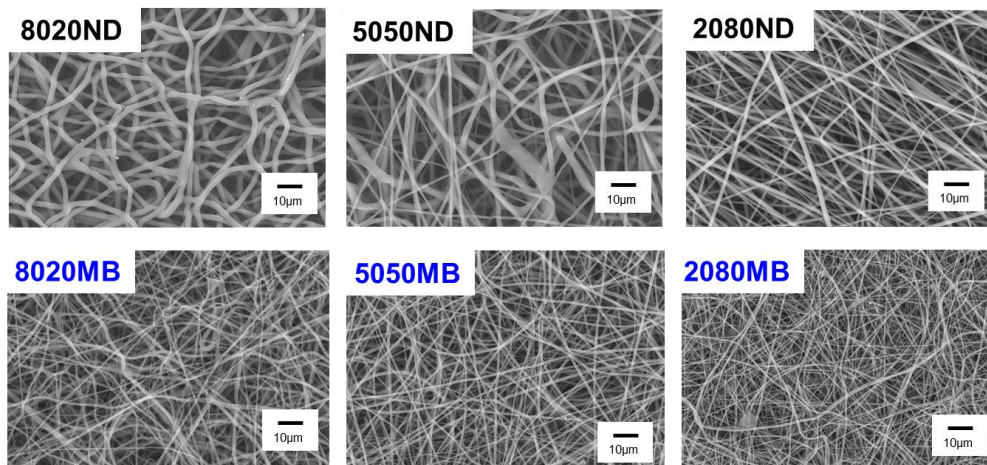


Figure 6.15 – Microstructural analysis of PS-encapsulated PCL and PLGA1090 electrospun polymer blend scaffolds and controls. SEM images taken at 1000x magnification

The electrospinning polymer blend solutions each produced smooth bead-free fibres. Upon blending purple PCL-MB and blue PLGA1090-MB polymer solutions, a gradient in colouration of the resulting scaffolds was observed. This was quantified as per LAB colour space measurements (**Table 3.3**).

	L	A	B
PCL-MB	68.55	24.6	-20.24
8020-MB	68.45	17.51	-19.69
5050-MB	69.73	11.41	-18.24
2080-MB	68.93	-12.32	-28.55
PLGA1090-MB	67.64	-7.22	-30.85

Table 6.3 – LAB colour space results for PS-loaded scaffolds.

Colours of associated rows of the table represent the colour of the scaffold as per the LAB result

When MB was electrospun with pure PCL, the resulting scaffolds were purple in colour (section 3.3.2.2). When MB was electrospun with pure PLGA7525 or pure PLGA1090, the resulting scaffolds were blue in colour (section 3.3.2.2 and section 6.3.1.2). When PCL-MB and PLGA1090-MB were mixed and the solutions electrospun, the resulting scaffolds displayed a gradient in colour from a purple to a blue/purple to a blue colour. These results were taken as a visual indicator that the electrospinning solutions had been successfully mixed and the resulting scaffolds were a blend of the two polymer types.

The loading efficiency of each of these polymer blends was calculated again to ensure that full transfer of MB from solution to electrospun scaffold had been achieved. For the 8020-MB, 5050-MB and 2080-MB scaffolds, the loading efficiency was calculated at $100\pm 1\%$, $104\pm 7\%$ and $103\pm 1\%$ respectively, indicating successful fibre PS-encapsulation.

The SEM images were analysed to determine the fibre diameters of each scaffold (**Figure 6.16**).

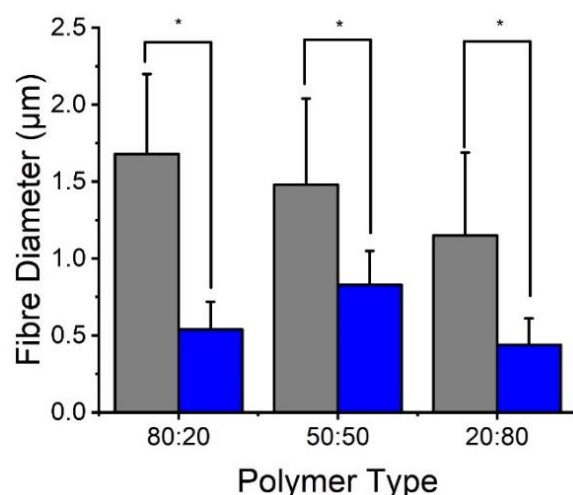
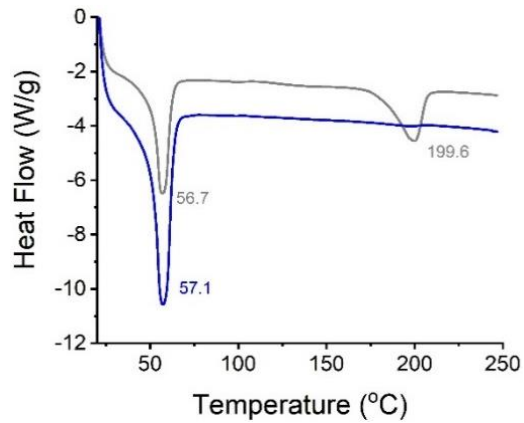


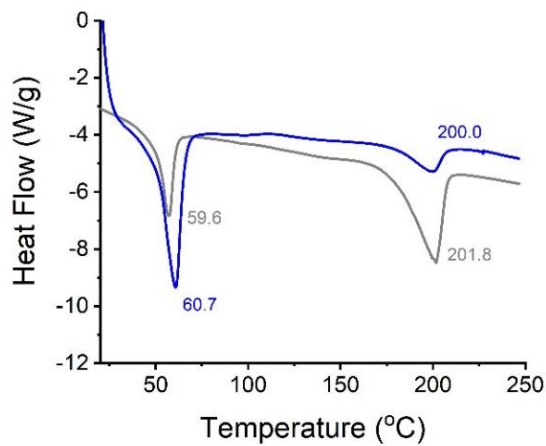
Figure 6.16 – Average Fibre Diameter determined from SEM images for each PCL and PLGA1090 polymer blend electrospun scaffold. Grey bars: Control scaffolds; Blue bars: MB-included scaffolds. Results reported as Mean±SD (n=3). ‘*’ denotes significantly different means ($p < 0.05$, t -test)

Each of the 8020, 5050 and 2080 scaffolds showed a significant decrease between the control and MB-incorporated scaffolds ($p = 9.8 \times 10^{-46}$, 1.8×10^{-10} and 2.7×10^{-13} respectively). The average reduction in fibre diameters (68%, 44% and 53% respectively), which was comparable to those found with the previous scaffold formulations from the polymers in isolation.

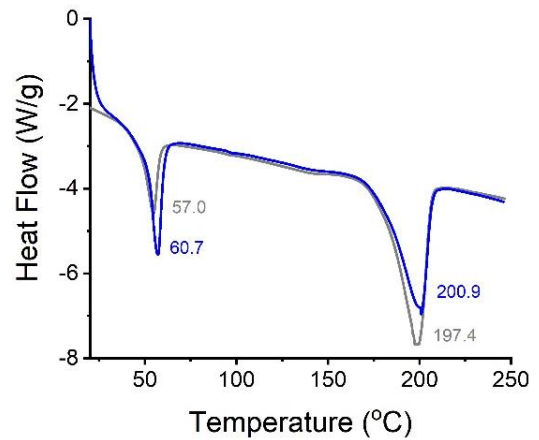
As discussed previously (section 6.3.1.2), DSC analysis of the polymer is important to ensure that the semi-crystalline structure of the polymer scaffold has been maintained upon electrospinning. Therefore, the DSC profiles of the polymer scaffolds were analysed (**Figure 6.17**).



(A)



(B)



(C)

Figure 6.17 - Differential Scanning Calorimetry heat flow plots of PCL:PLGA1090 blended polymer scaffolds. (A) 80:20, (B) 50:50, (C) 20:80 polymer blends. (—): Polymer-ND scaffolds; (—): Polymer-MB scaffolds

The melting transition temperatures at 56.7-60.7 °C are due to the presence of the PCL polymer (section 3.3.2.3), and the melting transition temperatures at 199.6-201.8 °C are due to the presence of the PLGA1090 polymer (section 6.3.1.2). A summary of the thermal properties of the blends in comparison to the pure polymers is given to allow for direct comparison (**Table 6.4** and **Table 6.5**).

	PCL	8020	5050	2080	PLGA1090
T_m (PCL) (°C)	57.5	56.7	56.9	54.5	-
ΔH_m (PCL) (J/g)	118.2	33.4	21.8	10.1	-
T_m (PLGA1090) (°C)	-	199.6	201.8	197.4	200.0
ΔH_m (PLGA1090) (J/g)	-	37.1	43.9	58.4	76.4
T_g (PLGA1090) (°C)	-	-	-	-	44.1

Table 6.4 – DSC Thermal Analysis Values for pure and blended scaffolds for PS-free (ND) control samples

	PCL	8020	5050	2080	PLGA1090
T_m (PCL) (°C)	56.4	57.1	60.7	57.0	-
ΔH_m (PCL) (J/g)	89.0	71.6	59.1	16.3	-
T_m (PLGA1090) (°C)	-	-	200.0	200.9	199.2
ΔH_m (PLGA1090) (J/g)	-	-	20.3	47.2	67.9
T_g (PLGA1090) (°C)	-	-	-	-	44.7

Table 6.5 – DSC Thermal Analysis Values for pure and blended scaffolds with MB inclusion

Each of these DSC plots indicates the presence of only melting transition temperatures, and no glass transition temperatures were found to be present. This would suggest that the polymers in each scaffold type exist in a predominantly crystalline form.

Previously published reports on the thermal properties of polymer blends conclude that fully miscible blends display one transition temperature, but if polymers were not fully miscible then the transition temperatures of each individual polymer were present^[502–504]. Two melting transition peaks are present for all samples except for that of the 8020-MB polymer blend, which exclusively displayed a T_m in the region which would be expected for the melting temperature of PCL (57.1 °C). This was initially thought to suggest that the polymer forms are miscible in this sample, as the melting peak has also shifted towards that of the PLGA1090 polymer which would occur if the different polymer types within the blend which have interacted^[505]. However, when analysing the full data set obtained from running the DSC analysis on

the 8020MB sample, it can be seen that both melting points are observed in the first cycle which was used to remove the thermal history of the polymers (**Figure 6.18**).

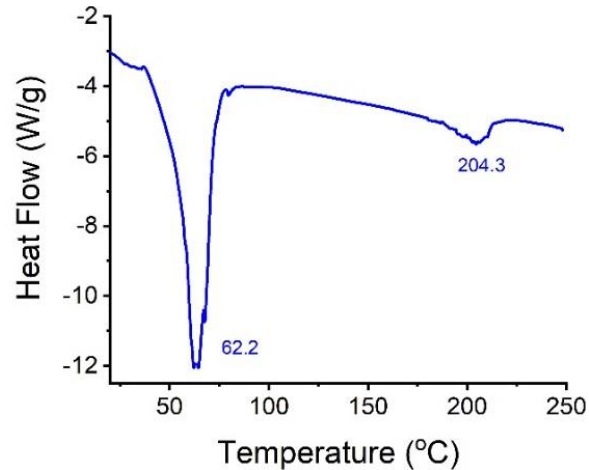


Figure 6.18 - Differential Scanning Calorimetry heat flow plots of the first cycle from PCL:PLGA1090 blended polymer scaffolds at 80:20 ratio and MB (—)

It is only when the thermal history has been removed that the PLGA1090 peak does not appear on the heat flow plot. Therefore, the presence of two melting peaks in each of these samples would suggest that the polymers are immiscible. A surfactant could be used to increase miscibility if this causes adverse properties for the scaffolds^[502].

In previous studies, the mechanical properties of blended scaffolds have been reported to change in comparison to the pure polymers from either constituent scaffold^[502,506,507]. The tensile properties of the blended scaffolds in this study were analysed either without PS or with PS inclusion (**Figure 6.19** and **Figure 6.20**).

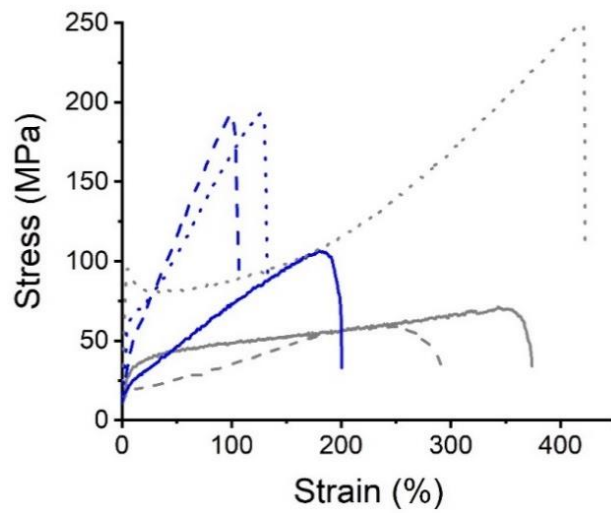
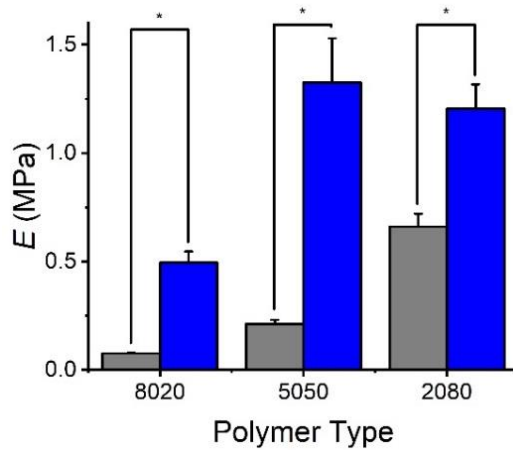
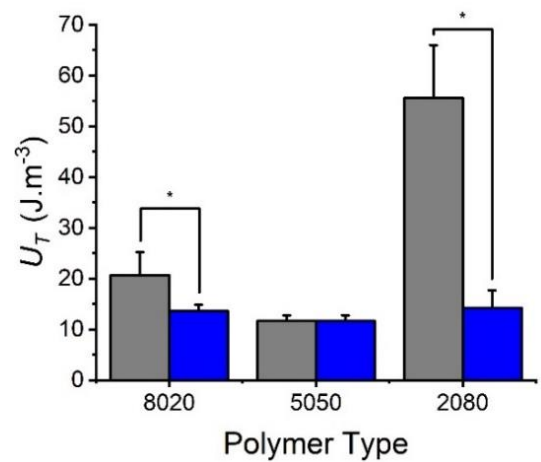
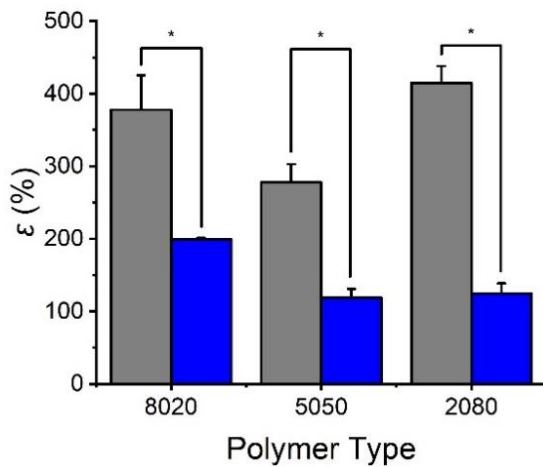


Figure 6.19 - Stress-strain curve of PS-encapsulated PCL and PLGA1090 polymer blend scaffolds. (—): 8020-ND; (—): 8020-MB; (---): 5050-ND; (---): 5050-MB; (...): 2080-ND; (...): 2080-MB

The PS-included and PS-free control stress-strain graphs of each polymer scaffold type was used to quantify the mechanical behaviour of the blended polymer scaffolds (**Figure 6.20**).



(A)



(B)

(C)

Figure 6.20 – Mechanical properties measured in PCL and PLGA1090 polymer blend samples. (A) Elastic Modulus (E); (B) Strain at Break (ϵ) and (C) Ultimate Toughness (U_T). Grey bars: control polymer scaffolds; Blue bars: MB-loaded scaffolds. Results reported as Mean \pm SD ($n=3$). “*” denotes significantly different means ($p < 0.05$, t -test)

Comparing the elastic modulus of the control samples without PS inclusion of the polymer blends, there was a significant increase with an increased ratio of PLGA1090 to PCL (from 8020-ND to 5050-ND, $p = 0.0001$ and from 5050-ND to 2080-ND, $p = 4 \times 10^{-5}$). This has been observed previously in the literature^[434,506,508,509]. This incremental increase in mechanical properties with increasing ratio suggests that the two polymers have been successfully combined^[434].

Studying the effect of MB-incorporation on the elastic modulus, there was found to be a significant increase between the control and the MB-incorporated samples in each 8020-MB, 5050-MB and 2080-MB polymer blend ratio ($p = 0.0001$, 0.0004 and 0.0001 respectively). This decrease in flexibility is also reflected in the elongation at break values, which reduces significantly for each of the PS-included scaffolds in comparison to the control samples ($p = 0.002$, 0.00004 and 3×10^{-7} respectively).

The toughness of the polymer scaffolds significantly decreased for the 8020 and the 2080 ratio blends (0.03 and 0.0007 respectively), but no significant difference was found for the 5050 ratio of polymer electrospinning solutions ($p = 0.9$).

6.3.2.3 Polymer Blend Scaffold Interactions in Aqueous Medium

The main purpose of blending the polymers in these scaffolds was to control the degradation of the polymer scaffolds when incubated in aqueous medium whilst enabling sustained release of MB from the PLGA1090 polymer fibres. Initially, this was tested through the ability of the scaffold to take up water over 24 hours (**Figure 6.21**).

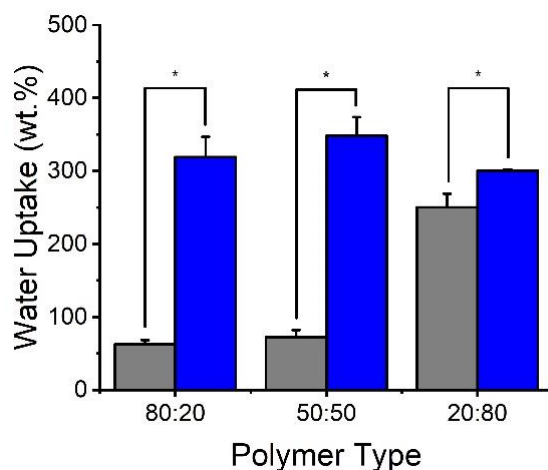


Figure 6.21 – Water uptake measured gravimetrically following incubation (H_2O , $37^\circ C$) of either PS-loaded or electrospun control PCL and PLGA1090 polymer blend samples. Grey bars: ND scaffolds; Blue bars: MB scaffolds. Results reported as Mean \pm SD ($n=3$). ‘*’ denotes significantly different means ($p < 0.05$, t -test)

As with the PLGA1090 and PCL scaffolds, there was not found to be any shrinkage over the 24-hour incubation period for any of the polymer blended scaffolds.

There was a significant increase in WU for each of the polymer scaffolds with MB incorporation when compared to the control samples ($p = 0.003, 0.00009, 0.04$). The WU values for each of the MB-encapsulated samples was greater than 200% which would be advantageous for both MB release and in allowing exchange for the nutrients of cells populating the scaffold.

As with the PLGA1090 scaffolds, it was determined to be more clinically applicable to regularly change the aqueous media to ensure that the autocatalytic hydrolytic effect would be minimised, and to more closely replicate the biological environment. Therefore, degradability experimental analysis was performed with this modification (**Figure 6.22** and **Figure 6.23**).

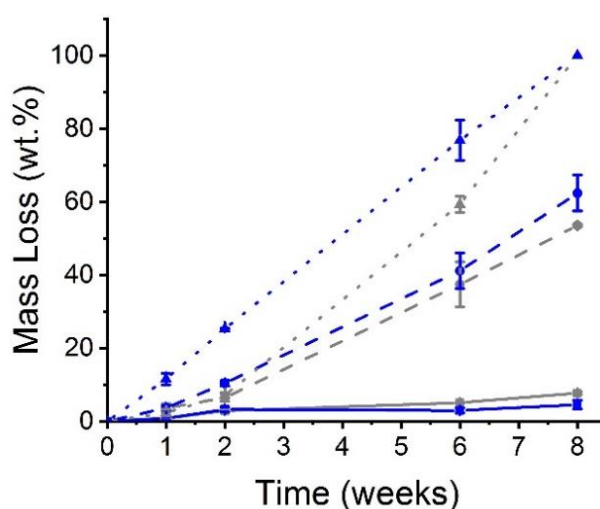
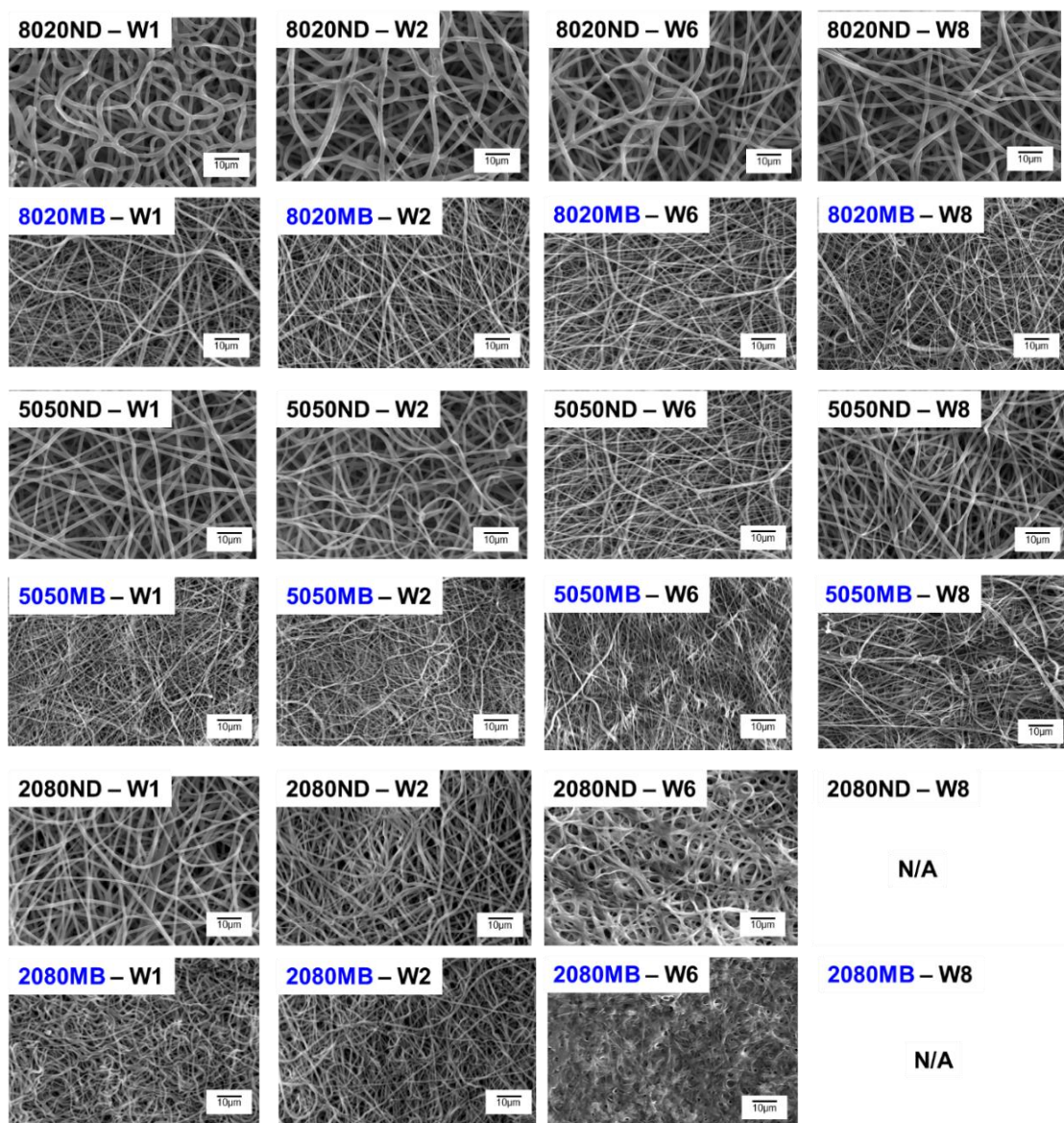


Figure 6.22 – Mass loss measured on PCL and PLGA1090 polymer blend samples following hydrolytic degradation in PBS with controlled pH (PBS, 37 °C, pH ~7.4). (■):8020-ND; (■):8020-MB; (●):5050-ND; (●):5050-MB; (▲):2080-ND; (▲):2080-MB. Lines are guidelines to the eye. Results reported as Mean±SD (n=3)



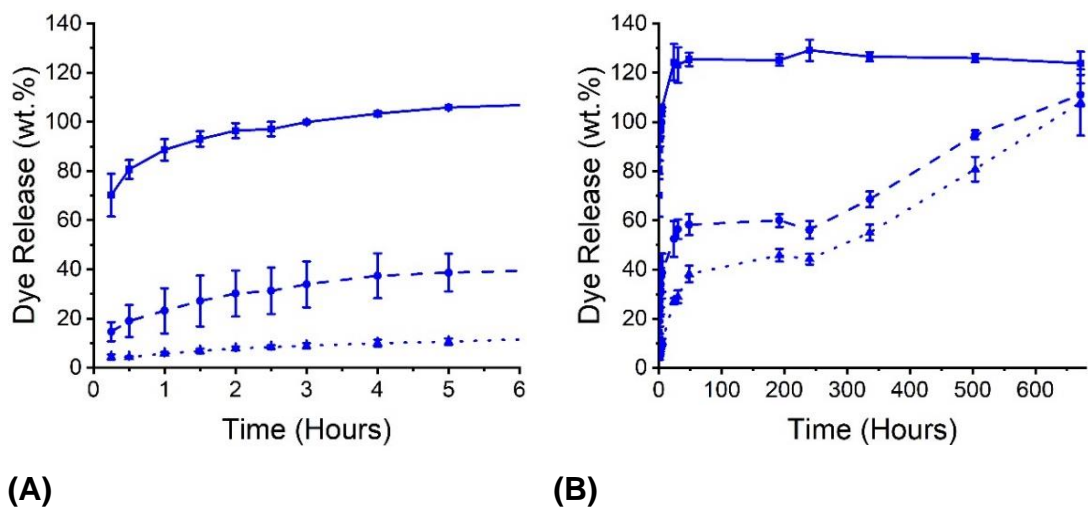
(B)

Figure 6.23 – Scanning Electron Microscopy (SEM) of electrospun PLGA1090 scaffolds. W1, W2, W6 and W8 refers to 1, 2, 6 and 8 week incubation time points respectively. N/A samples had degraded so were unable to be analysed

The 8020 scaffolds which contain a higher ratio of PCL showed the least mass loss over the 8-week period. Both the control and MB-incorporated 2080 electrospun scaffolds which had a higher ratio of PLGA1090 showed the fastest degradation profiles, with both the 2080-MB scaffolds losing integrity after 2 weeks incubation. From the SEM image at the 6-week timepoint, it can be observed that a loss of fibrous structure has occurred. As discussed

previously (section 3.3.2.1) for the PLGA7525 scaffolds, a narrowing of pore size could result in cells being unable to penetrate the scaffold and this would limit the scaffold performance as a neotissue-encouraging regenerative device.

The final property to analyse was the PS release profiles of the blended scaffolds types. The scaffolds were analysed in the same way as with the PLGA1090MB scaffolds (section 6.3.1.3) (**Figure 6.24**).



(A) **(B)**
Figure 6.24 – Typical PS release profiles measured via UV-Vis spectroscopy of the supernatant collected during incubation with controlled pH (PBS, 37 °C, pH ~7.4) from MB-incorporated scaffolds at selected time points over (A) 6 hours or (B) 672 hours (4 weeks). (■):8020-MB; (●):5050-MB; (▲):2080-MB. Lines are guidelines to the eye. Results reported as Mean±SD (n=3)

The 8020-MB scaffold, which degraded the least over the 8-week window, also had the highest concentration of PCL and therefore had the greatest ‘burst’ release of MB. This appears to be consistent with the result from the DSC (**Figure 6.17**) which suggested that the 8020-MB scaffolds are predominately crystalline and therefore the MB was unable to penetrate the polymer chains and is therefore more freely available upon scaffold incubation in PBS. Both 5050-MB and 2080-MB scaffolds had the ability to gradually release the PS into the aqueous media over 4 weeks. However, the 2080-MB

sample had lost integrity over the course of the experiment, and only the fragments remained after 2 weeks incubation. 5050-MB gradually released the PS but also maintained integrity for the duration of the 8-week mass loss experiment which would suggest that it would be suitable for use as a regenerative scaffold in the desired application.

6.3.2.4 5050 Polymer Blend Scaffold with Reduced Methylene Blue Concentrations

The next stage of this study involved testing the lead prototype polymer carrier for MB (a 50:50 blend of PCL and PLGA1090 with a total polymer concentration of 6 wt.%) with both mammalian cells and bacteria. Prior to *in vitro* analysis, new scaffolds were electrospun with a lower concentration of MB in the electrospinning solution to provide a comparison in cytotoxic and bactericidal properties. The selected concentrations were either the full '100%' concentration (100%-MB, 2.2 mM), 50% of the initial MB concentration (50%-MB, 1.1 mM) or 10% of the initial MB concentration (10%-MB, 0.2 mM). These solutions were made as previously described and electrospun into scaffold samples. As this concentration change was relatively small, it was not expected to cause any changes to the biomaterial properties of the scaffolds. To confirm this, the new range of scaffold samples were analysed via SEM to calculate the average fibre diameter of the scaffolds (**Figure 6.25**).

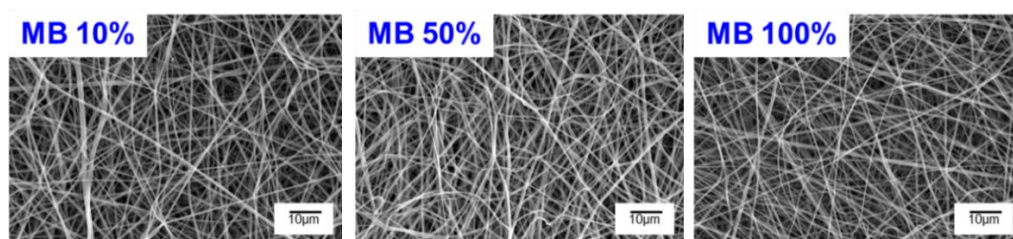


Figure 6.25 – Microstructural analysis of MB-encapsulated electrospun polymer blend (5050) scaffolds from electrospinning solutions with various concentrations of MB. 0.2mM: 10% MB; 1.1mM: 50% MB; 2.2mM: 100% MB. SEM images taken at 1000x magnification

SEM images were analysed with ImageJ as previously described (section 3.3.2.1) to determine the average fibre diameter. This was then compared to the average fibre diameter of the 100%-MB 5050 polymer blend scaffolds to determine whether the reduction in MB has led to a different scaffold morphology (**Figure 6.26**).

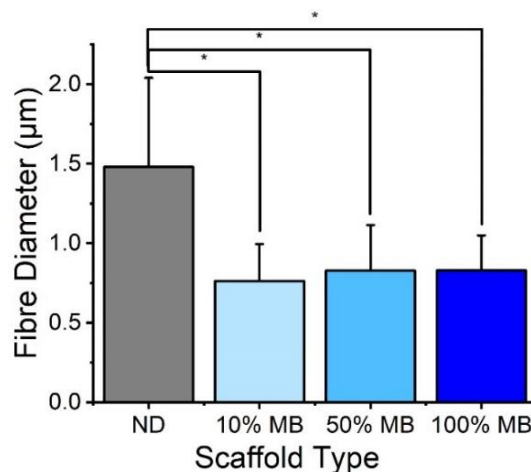


Figure 6.26 - Average Fibre Diameter determined from SEM images for each MB concentration of 5050 polymer blend electrospun scaffold. Results reported as Mean±SD (n=3). “*” denotes significantly different means ($p < 0.05$, *t*-test)

This data confirms that there is a comparable significant decrease in average fibre diameter between the ND control and each of the 10%, 50% and 100% MB-included 5050 blend scaffolds ($p = 7 \times 10^{-12}$, 4×10^{-5} and 2×10^{-10} respectively). There was no significant difference between the 100%-MB scaffolds and either the 10%-MB or 50%-MB scaffolds ($p = 0.12$ and 0.9 respectively). This data suggests that a decrease in MB within this range of MB concentrations (2.2 mM – 0.2 mM) does not significantly change the physical characteristics of the scaffold.

To ensure that the crystallinity of the polymer had not changed with a reduction of MB, DSC analysis was performed on the 10%-MB scaffolds as

this scaffold has the greatest reduction in MB so would represent the largest change if there was to be one (**Figure 6.27**).

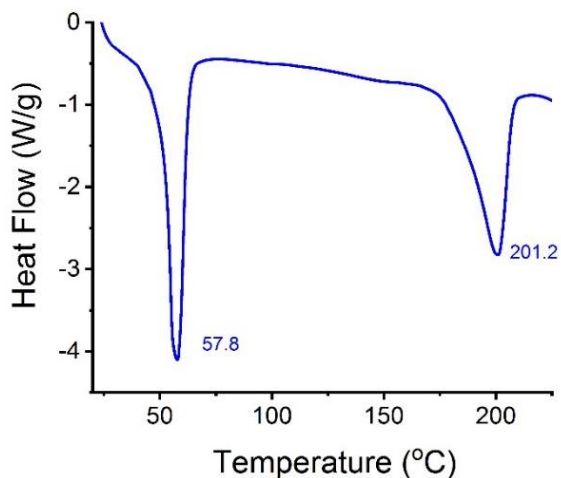


Figure 6.27 - Differential Scanning Calorimetry heat flow plots of 5050 PCL:PLGA1090 blended polymer scaffolds with a reduced MB concentration. (—): 10%-MB 5050 scaffolds

These DSC plots are similar to that of 5050-MB with a 2.2 mM concentration, with both melting transition temperatures for the presence of PCL and PLGA1090 polymers present (**Table 6.6**).

	10%-MB 5050	100%-MB 5050
T_m (PCL) (°C)	57.8	60.7
ΔH_m (PCL) (J/g)	32.4	59.1
T_m (PLGA1090) (°C)	201.2	200.0
ΔH_m (PLGA1090) (J/g)	30.0	20.3

Table 6.6 – Comparison of DSC Thermal Analysis Values for 5050 polymer blended scaffolds with MB inclusion at a higher and lower concentration

As the fibre diameter of these scaffolds were found to be comparable, and there was no apparent change in the crystallinity of the scaffold caused by reducing the MB concentration, it was therefore decided that there was no significant change in the characteristics of the 5050-MB scaffold. Further characterisation was therefore not needed, and all properties were assumed to follow the same trends as the characterised 100%-MB 5050 polymer scaffolds characterised previously in this chapter.

6.4 Conclusion

Initially, a 10% lactide and 90% glycolide copolymer (PLGA1090) was explored for suitability as a polymer carrier for MB which could maintain integrity over an 8-week period in aqueous medium. After initial characterisation, a 6 wt.% polymer concentration electrospinning solution was electrospun into bead-free fibrous scaffolds either with or without 2.2 mM concentration of MB. The MB containing scaffolds had a 48% reduction in average fibre diameter to the control samples. DSC analysis confirmed the presence of both a glass transition temperature and a melting point peak in PLGA1090 polymer scaffolds, which suggests the polymer arrangement is of increased crystallinity in comparison to the PLGA7525 polymer carrier which shrunk macroscopically in solution.

The mechanical properties of the MB-containing and control PLGA1090 scaffold samples were comparable in all properties except elongation at break, which was significantly lower for the PLGA1090-MB scaffold. The WU analysis was comparable to that of the PCL polymer scaffolds, and importantly, there was no shrinkage of the PLGA1090 scaffolds in solution. Despite a desirable gradual release of MB over a 4-week timeframe, the polymer scaffolds lost integrity after 2 weeks incubation and were therefore deemed unsuitable for use in this application.

To obtain the desirable degradation profile of PCL and gradual PS release of PLGA1090, blending of these two electrospinning solutions was performed in ratios of 80:20, 50:50 and 20:80.

The resulting electrospinning solutions were characterised in terms of their viscosity, before being electrospun and confirming the presence of bead-free fibres. Again, a reduction in fibre diameter was confirmed for the MB-containing scaffolds in comparison to the control scaffolds.

Miscibility of the polymer solutions was suggested visually with a colour gradient of the scaffolds from purple (PCL) to blue (PLGA1090) scaffolds, but the polymers were shown to be immiscible through DSC analysis. Mechanical characterisation highlighted an increase in elastic modulus and a decrease in elongation at break for the MB-containing scaffolds for all polymer blend ratios.

Upon degradation studies, 2080-MB ratio blend was found to degrade too quickly and lost fibrous structure after 6 weeks in solution. Both the 8020-MB and 5050-MB formulations proved promising in terms of their stability in the aqueous environments over 8 weeks.

The MB release profile for 8020-MB scaffolds was similar to that of the PCL scaffolds, in that the MB was released quickly upon scaffold incubation in PBS. However, the 5050-MB scaffolds demonstrated the ability to gradually release MB. In combination with the desirable degradation profile, this was identified as the lead prototype to move on into the next and final stages of this study.

Finally, to allow for comparison in the *in vitro* studies with the lead prototype, two lower concentration 5050-MB scaffolds were electrospun. These were confirmed via SEM and DSC analysis to have comparable characteristics to the 5050-MB original concentration scaffolds.

Chapter 7 *In vitro* Testing of Prototype Scaffolds

7.1 Introduction

The aim of the work presented in this chapter was to determine a lead prototype regenerative medical device using *in vitro* testing techniques. A range of three scaffolds were electrospun using a 50:50 polymer blend of PCL and PLGA1090 which were characterised in Chapter 6. These were '5050-ND' (a control scaffold with no MB-encapsulation) and then three different concentrations of MB. The original concentration of MB was 2.2 mM, and these scaffolds are referred to as 100%-MB. The two lower dose scaffolds contained 1.1 mM and 0.2 mM, referred to as 50%-MB and 10%-MB respectively.

In vitro methods for determining cytotoxicity are categorised into two main groups; extract and contact assays^[456]. Both of these methods are described in '*ISO 10993 Biological evaluation of medical devices - Part 5: Tests for in vitro cytotoxicity*' (2018), which is the international standard used to determine whether medical devices are cytotoxic against mammalian cells^[192,510]. Any medical device will need to have been shown to comply to these standards prior to commercialisation.

The tests initially determine whether an extract solution taken from the sample causes a cytotoxic response. In ISO 10993, it is stated that a reduction in cell viability of up to 30% is commonly used as an acceptable value for cell tolerance^[192]. Therefore, this threshold was used in this chapter. Additionally, direct visualisation of cells in contact with the medical device was used to determine whether the cell morphology would be altered. A summary of the grading system used in the ISO 10993 report was used, and is given below for reference (**Table 7.1**).

Grade	Reactivity	Conditions
0	None	No limited cell growth
1	Slight	Slight growth inhibition <20% cells round and loosely attached
2	Mild	<50% growth inhibition <50% cells round and loosely attached
3	Moderate	<50% growth inhibition <70% cells round and loosely attached
4	Severe	Nearly complete or complete destruction of cells

Table 7.1 – ISO 10993 morphological grading of cells ^[192]

After the determination of the lead scaffold prototype with an acceptable level of cytotoxicity, experiments were performed with model bacteria strains to determine the extent to which this scaffold formulation could be used to kill bacteria following aPDT principles. This was initially performed using a comparable extract testing experiment, which involved producing extract solutions from the scaffold and using a luminosity assay to determine the log reduction in metabolically active bacteria^[511,512]. Following this, another commonly used microbiology test was used to determine the growth limiting effect of the treatment^[366,368,513,514]. This involved exposing a bacterial suspension to PDT using the extract solutions, and then diluting and plating the resulting bacteria onto agar plates. After allowing for bacterial growth (typically over incubation at 37°C, 5% CO₂ for 24 hours), the reduction in CFU as a result of PDT was compared to non-treated bacterial samples^[63,515–517].

Finally, antibacterial tests based upon ISO 20645 standards (*Textile Fabrics Determination of Antibacterial Activity - Agar Diffusion Plate Test*) were used to determine the bactericidal effect of the scaffolds in direct contact with the model bacteria^[294]. UV-treated scaffolds were placed on agar plates, light-activated and then incubated overnight. A ‘zone of inhibition’ (ZOI) was measured as the diameter of the area of no growth around the sample (**Figure 7.1**).

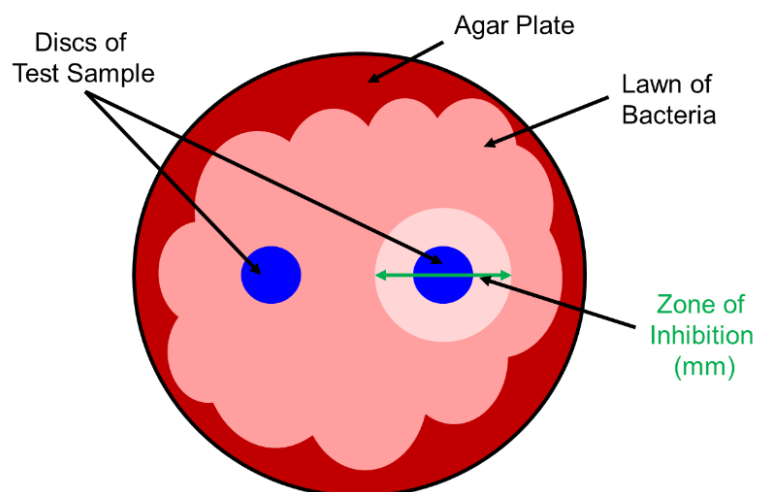


Figure 7.1 – Experimental setup schematic for ‘Zone of Inhibition’ microbiological testing

7.2 Materials and Methods

7.2.1 Mammalian Cell Toxicity Testing

L929 cells were cultured as previously described (section 5.2.2).

7.2.1.1 Mammalian Cell Extract Testing – Luminosity Assay

As previously described (section 5.2.6.1) but with new scaffolds (section 6.3.2.4).

7.2.1.2 Mammalian Cell Contact Testing – Scanning Electron Microscopy Morphology

SEM was used to visualise the morphology of L929 cells in contact with the scaffolds. Scaffolds were cut into 20 mg squares and placed in 48 well plates. These scaffolds were exposed to UV light for 15 minutes in the tissue culture hoods on each side for disinfection purposes, before 0.5 ml of sterile cell culture medium was added and the samples placed in an incubator (37°C, 5% CO₂) for 1 hour to allow for the scaffolds become moist. Confluent L929 cells were passaged, counted and seeded onto the centre of each scaffold sample in 0.5 ml of media to result in a final seeding density on each scaffold of 5x10³ cells/ml. The samples were then either exposed to light for 30 or 60 minutes or kept in the dark for the same period of time. Following this,

samples were incubated for either 24 hours or 7 days (with media changed for fresh media every other day). At the selected time, samples were removed from cell culture medium, washed twice in fresh PBS and placed in formalin for 24 hours. The scaffolds were then removed and dehydrated in a series of ethanol concentrations (**Table 7.2**).

Ethanol Concentration in Distilled Water (v.%)	Time (minutes)
25	5
50	5
70	5
80	10
95	10
100	10
100	10

Table 7.2 – Series of Solutions and Incubation Times for Dehydrating Cells on Scaffold Samples prior to Scanning Electron Microscopy

Following dehydration, samples were each placed in 24-well plates and left at 4 °C for 48 hours to dry. Dry samples were attached to metal stubs using carbon double-sided stickers and sputter coated with gold (x2) before being visualised using a 6-sample multi-stub holder on a Hitachi Scanning Electron Microscope at 1000x and 4000x magnification.

7.2.2 Antibacterial Photodynamic Therapy Activity Testing

7.2.2.1 Bacteria Extract Testing – Luminosity Assay

Overnight *E. coli* or *S. mutans* cultures were produced by inoculating a single colony of bacteria in 20 ml of BHI overnight. The following day, 1 ml of this broth was added to 9 ml of fresh BHI and the solution incubated until mid-log phase (section 5.2.3.4). Bacteria numbers were then estimated using OD₆₀₀ (section 5.2.3.4) and the concentration altered to reach a final concentration of 10⁸ CFU/ml. Bacteria were then washed once in PBS before

being resuspended in each of the same extract solutions as previously used in the mammalian cell testing (section 7.2.1.1). Controls of Triton X-100™ (10 v.%) and fresh PBS were used with each well plate. 100 µl of each solution was then plated in triplicate into opaque walled 96-well plates and either exposed to light for 30 or 60 minutes or kept wrapped in foil as a dark control.

Following the allotted light exposure time, 100 µl of Bact-TiterGlo® solution was added to each well, the plate was shaken for 1 minute and then left at room temperature for 4 minutes. A multiplate reader was then used to analyse the luminosity reading from each well, and the percentage bacterial killing was calculated (**Equation 5.7**).

7.2.2.2 Bacteria Extract Testing – Colony Counting

Overnight bacterial cultures were produced by inoculating a single colony of bacteria in 20 ml of BHI overnight. The following day, 1 ml of this broth was added to 9 ml of fresh BHI and the solution incubated until mid-log phase (section 5.2.3.4). Bacterial numbers were then estimated using OD₆₀₀ (section 5.2.3.4) and the concentration altered to reach a final concentration of 5×10^8 CFU/ml. Bacteria were washed once in PBS before being resuspended in 10% extract solutions. They were then immediately exposed to light for 30 or 60 minutes or kept in the dark as described previously (section 7.2.2.1). Following this treatment, the solutions were serially diluted and 100 µl spread on fresh agar plates. The plates were then incubated at 37 °C for 24 hours. The following day, manual counting of colonies was performed and the number of CFU for each solution was calculated and compared to the initial inoculation. The experiment was performed in triplicate to allow for statistical significance to be calculated

7.2.2.3 Bacteria Contact Testing - Zone of Inhibition

Fresh agar plates were made as described previously (section 5.2.3) a day prior to testing. Overnight cultures were produced by inoculating a single colony of bacteria in 20 ml of BHI overnight. Three replicate samples of each scaffold type were cut into discs using a biopsy punch (diameter of 10 mm) and disinfected for 15 minutes on each side under UV light.

The following day, 1 ml of overnight bacterial culture was added to 9 ml of fresh BHI and the solution incubated until mid-log phase (section 5.2.3.4). Lawns of bacteria were spread by using a sterile swab dipped in bacterial broth and streaking across a fresh agar plate. Sterile tweezers were used to place disinfected scaffold discs onto the agar plate inoculated with bacteria in triplicate. The plates were then incubated for 1 hour to allow for MB release, before being exposed to light for 30 or 60 minutes (or wrapped in foil as the dark control). Agar plates were then incubated at 37 °C overnight to allow for bacterial growth. The following day, images were taken of each plate. Zones of inhibition were calculated using the straight-line tool on ImageJ® to count the number of pixels in a known section of the image to produce a scale, and then to measure the zone size for each image.

7.2.3 Statistical Analysis

Significant differences in the results were evaluated using an unpaired Student's *t*-test. Data was deemed to be significantly different at $p < 0.05$. All data were collected in triplicate and presented as Mean \pm Standard Deviation.

7.3 Results and Discussion

7.3.1 Mammalian Cell Cytotoxicity Testing

7.3.1.1 Mammalian Cell Extract Testing

Initially, the scaffolds were examined in a similar way to the testing performed with extract solutions described previously (section 5.3.4.1). In this chapter, the experimental setup was used to distinguish between two PS (MB or ER). Here, it was used initially as a 'worst case scenario' testing method (i.e. it was expected to have a more severe effect on the cells than *in vivo*).

Initially the extract solutions were generated by incubating 20 mg of scaffold in PBS for 0, 2 and 24 hours. From the data in collected in Chapter 6, these solutions were expected to contain the concentrations of MB given in **Table 7.3**.

Collection Time (hours)	Expected MB Concentration ($\mu\text{g/ml}$)		
	10%-MB	50%-MB	100%-MB
0	0.4 \pm 0.1	2.1 \pm 0.7	4.3 \pm 1.4
2	0.9 \pm 0.3	4.4 \pm 1.6	8.8 \pm 3.2
24	1.5 \pm 0.3	7.6 \pm 1.5	15.2 \pm 2.9

Table 7.3 – Expected concentrations of MB in extract solutions collected following 0, 2 or 24 hour incubations times

These solutions were applied to the monolayers of L929 cells and incubated for 2 hours prior to light activation (**Figure 7.2**).

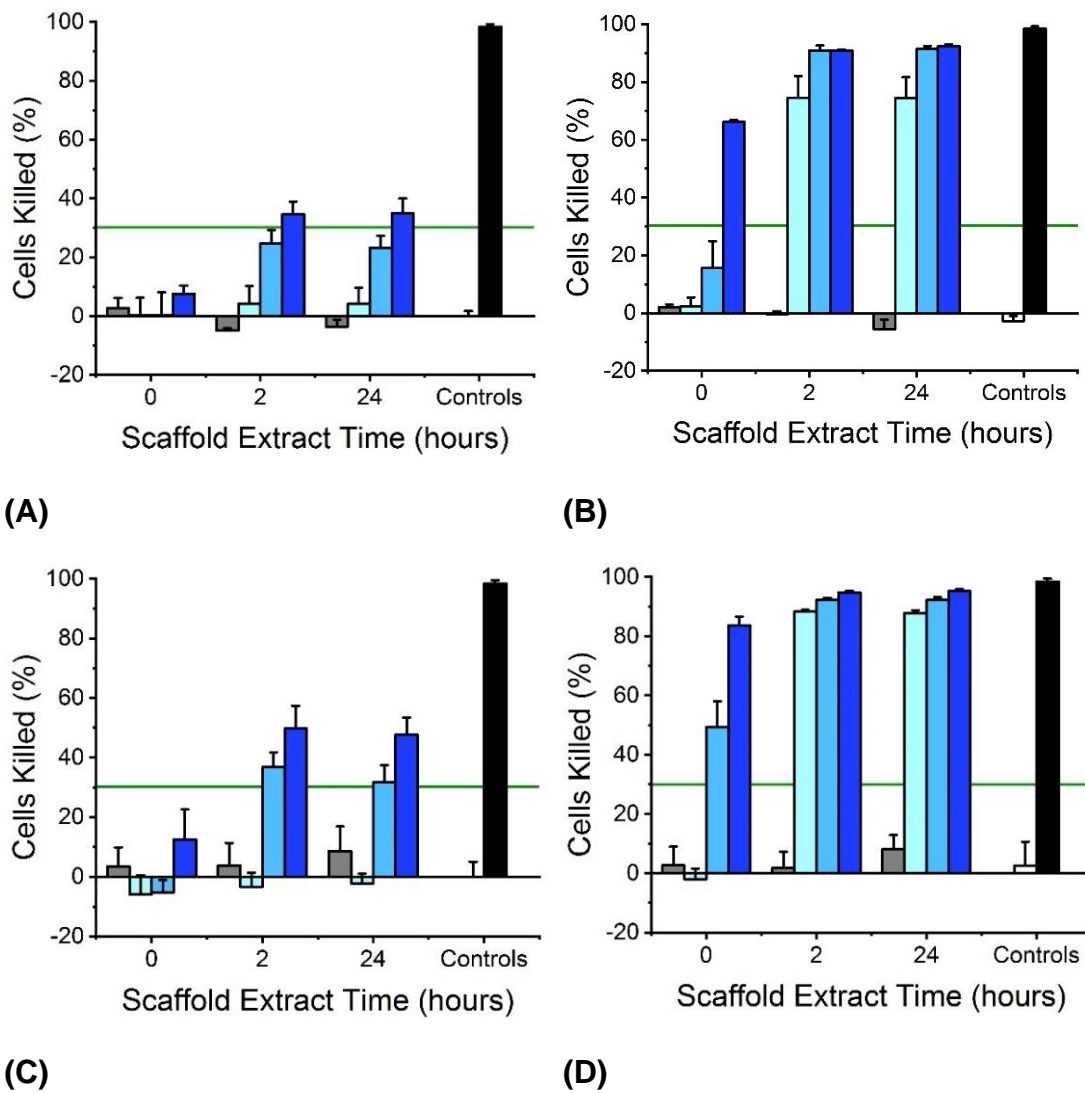


Figure 7.2 - L929 extract solution toxicity. (A) 30 min 'dark' control; (B) 30 min light exposure. (C) 60 min 'dark' control; (D) 60 min light exposure. Solutions extracted from various 5050 polymeric electrospun scaffolds. ■: MB-free (ND) controls; ■: 100%-MB; ■: 50%-MB; ■: 10%-MB; □: fresh PBS negative control; ■: PBS-Triton™ X-100 solution positive control; (--) : 30% reduction in cell viability. Results below this line are accepted as 'non-cytotoxic' in line with ISO 10993. Results reported as Mean±SD (n=3)

A value of <30% cytotoxicity was selected as an acceptable level of cell tolerance in line with ISO 10993 standards^[192]. In all experiments, the control

without MB-encapsulation resulted in minimal cell killing ($2.7\pm 4.9\%$) confirming that the scaffolds were non-cytotoxic.

In the non-light activated control experiments, none of the scaffolds tested were cytotoxic for the 0-hour extract solution. These extract solutions all had MB concentrations of $<4.3\ \mu\text{g/ml}$. This is in agreement with comparable toxicity study described previously (section 5.3.3.1) where all MB solutions with a concentration of the most similar concentration tests ($2\ \mu\text{g/ml}$) in 'dark control' samples also resulted in $<30\%$ cytotoxicity. For 2- and 24-hour extract solutions, 100%-MB scaffolds proved to be cytotoxic following both 30 minute ($34.5\pm 4.4\%$ and $34.9\pm 5.1\%$ respectively) and 60 minute ($49.7\pm 7.7\%$ and $47.6\pm 5.8\%$ respectively) 'dark' control time points. These extract solutions contained $8.8\pm 3.2\ \mu\text{g/ml}$ and $15.2\pm 2.9\ \mu\text{g/ml}$ respectively. The corresponding 50%-MB scaffold sample solutions for 2 and 24 hour extract times (concentrations of $4.4\pm 1.6\ \mu\text{g/ml}$ and $7.6\pm 1.5\ \mu\text{g/ml}$ respectively) were shown to induce $<30\%$ cell viability after 30 minutes light activation ($24.8\pm 3.5\%$ and $23.2\pm 4.1\%$ respectively) whilst $>30\%$ cell viability reduction was recorded after 60 minute light activation ($36.8\pm 5.0\%$ and $31.6\pm 5.8\%$ respectively). This would suggest that the concentration for the 'dark' cytotoxicity threshold is approximately $4\text{-}8\ \mu\text{g/ml}$. Each of the 10%-MB scaffolds extract solutions had a concentration of $<1.5\ \mu\text{g/ml}$ and were found to be non-cytotoxic without light activation ($<4.2\%$).

Upon light activation for either 30 or 60 minutes, all MB-incorporated scaffolds resulted in a $>70\%$ cell killing value for both the 2 and 24-hour extract scaffold solutions. This would indicate that all scaffolds are too cytotoxic for use with mammalian cells in agreement with the results described previously (section 5.2.5.1) as all MB-loaded PBS solutions of $2\ \mu\text{g/ml}$ following 30 or 60 minutes of light activation resulted in $>30\%$ cytotoxicity. However, upon a review of the literature it was determined that other experimental setups test cytotoxicity with <10 minutes pre-incubation time in a particular PS solution prior to light activation^[474,518,519]. In the experiments used to generate the results in **Figure 7.2**, pre-incubation of 2 hours was used prior to light exposure. A pre-incubation time of <2 hours can be justified in oral applications as the high turnover of saliva in the oral cavity is likely to

prevent localised accumulation of MB over time. Therefore, the full experiment was repeated with <10 minutes pre-incubation time (**Figure 7.3**).

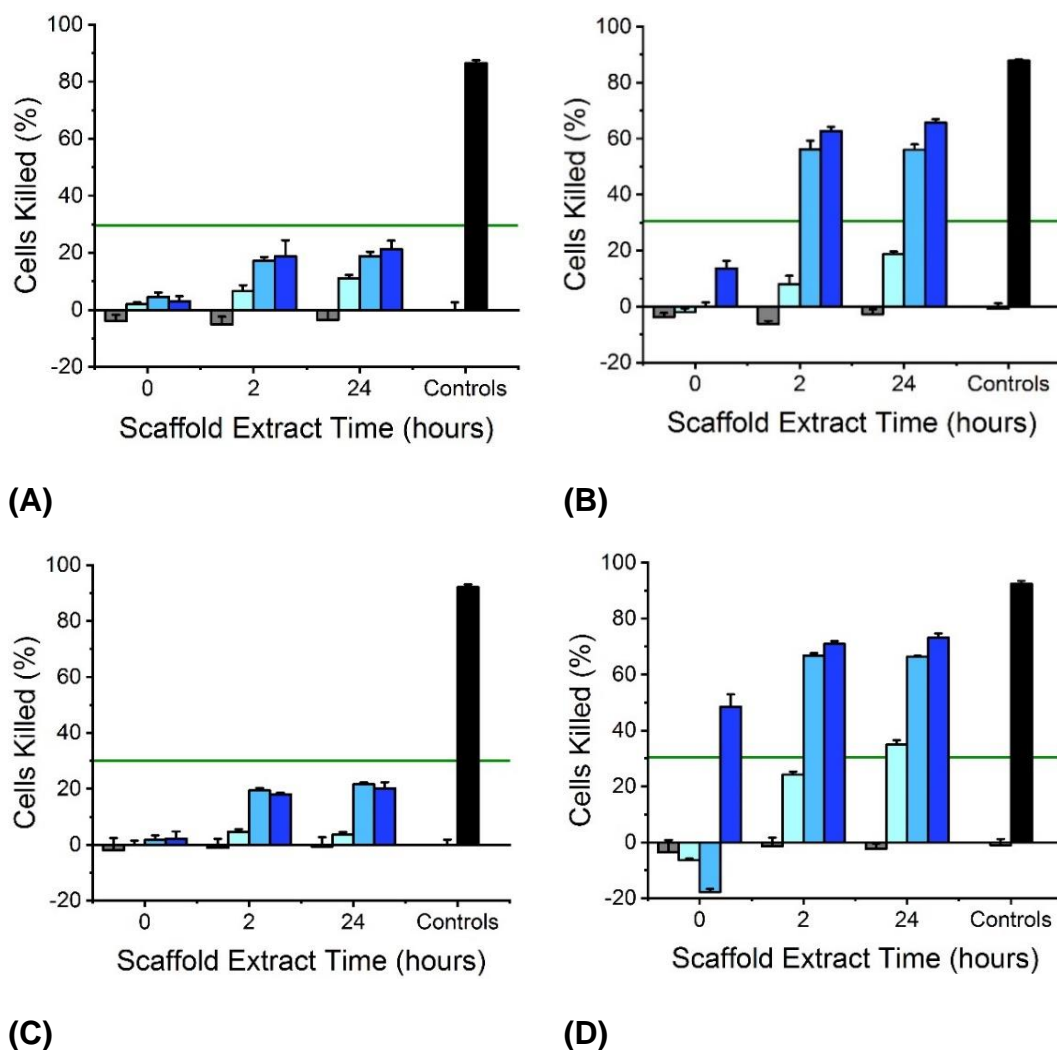


Figure 7.3 - L929 Extract Solution Toxicity with no pre-incubation prior to light activation. L929 Extract Solution Toxicity. (A) 30 min 'dark' control; (B) 30 min light exposure. (C) 60 min 'dark' control; (D) 60 min light exposure. Solutions extracted from various 5050 polymeric electrospun scaffolds. ■: MB-free (ND) controls; ■: 100%-MB; ■: 50%-MB; ■: 10%-MB; □: fresh PBS negative control; ■: PBS-Triton™ X-100 solution positive control; (- -): 30% reduction in cell viability. Results below this line are accepted as 'non-cytotoxic' in line with ISO 10993. Results reported as Mean±SD (n=3)

In this optimised experiment, all samples with or without MB-encapsulation were non-cytotoxic (<30% reduction in cell viability) in the absence of light activation. Therefore, the new 'dark' cytotoxicity threshold for this experiment was $>15.2 \pm 2.9$ $\mu\text{g/ml}$.

Upon light activation for 30 minutes none of the scaffolds tested as 'cytotoxic' for the 0-hour extract solutions. However, for the 2- and 24-hour extract solutions, both 50%-MB ($56.2 \pm 3.1\%$ and $56.0 \pm 1.9\%$ respectively) and 100%-MB scaffolds ($62.7 \pm 1.5\%$ and $65.7 \pm 1.3\%$ respectively) exceeded the 30% cell killing threshold. Alternatively, 10%-MB scaffold extract solutions obtained with an extraction time of 0, 2 or 24 hours were found to be non-cytotoxic ($-2.0 \pm 1.3\%$, $8.0 \pm 3.1\%$ and $18.7 \pm 1.0\%$ respectively) following 30 minutes of light activation. Therefore, MB concentrations of $>4.4 \pm 1.6$ $\mu\text{g/ml}$ were cytotoxic following 30 minutes light exposure, but $<2.1 \pm 0.7$ $\mu\text{g/ml}$ were below the cytotoxicity threshold. Therefore, the MB concentration released from the scaffold would need to stay below ~ 4 $\mu\text{g/ml}$ to be non-cytotoxic.

After 60 minutes light activation, the 100%-MB scaffolds were cytotoxic for each of the scaffold extract solutions ($48.4 \pm 4.5\%$, $70.9 \pm 1.0\%$ and $73.1 \pm 1.6\%$ respectively). The 50%-MB scaffolds were non-cytotoxic for the 0-hour extract solutions but exceeded 30% cell killing for the 2- and 24-hour extract solutions ($66.8 \pm 0.9\%$ and $66.3 \pm 0.3\%$ respectively). The 0- and 2-hour solutions from the 10%-MB scaffolds were non-cytotoxic ($-6.4 \pm 0.6\%$ and $24.2 \pm 1.2\%$), but the 24-hour extract solutions were marginally above the 30% killing threshold ($34.9 \pm 2\%$). The concentration of the extract solution collected here (1.5 ± 0.3 $\mu\text{g/ml}$) is likely to be at the threshold of cytotoxicity following 60 minutes light exposure. Despite this fact, the 10%-MB was the most optimal scaffold out of the range of scaffolds tested.

7.3.1.2 Mammalian Cell Contact Testing

Morphological examination of cells cultured in contact with the scaffolds was conducted. Cells were added to UV-treated scaffold samples, allowed to attach for 2 hours, before being exposed to 30 or 60 minutes of light activation (or kept in the dark as controls). The scaffolds were incubated to allow for cell proliferation for either 24 hours or 7 days. Samples were then fixed in

formalin, dehydrated with ethanol treatments and visualised using SEM
(**Figure 7.4** and **Figure 7.5**) ^[520].

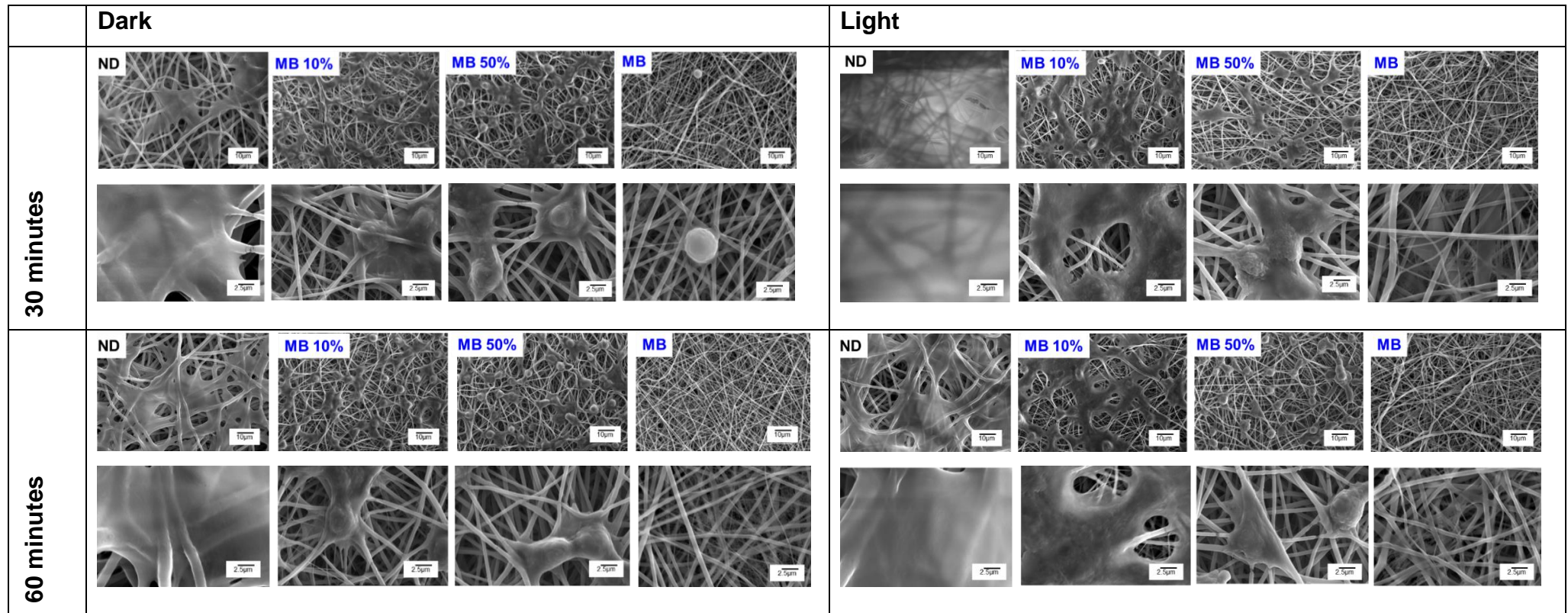


Figure 7.4 - L929 Cell Morphology following 30 or 60 minutes light activation (or kept in the dark as a control) and then 24 hours incubation on electrospun scaffolds. Scanning electron micrographs taken at 1000x or 4000x magnification

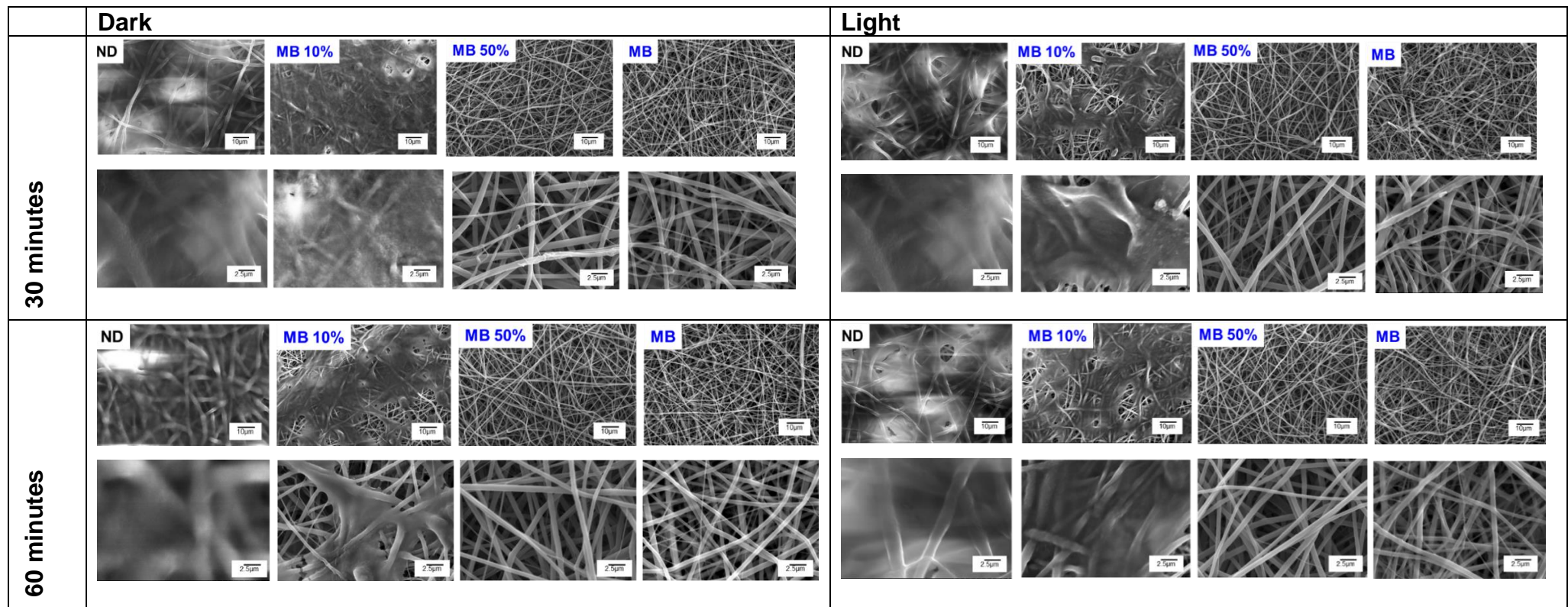


Figure 7.5 - L929 Cell Morphology following 30 or 60 minutes light activation (or kept in the dark as a control) and then 7 days incubation on electrospun scaffolds. Scanning electron micrographs taken at 1000x or 4000x magnification

The ISO 10993 grading system given in **Table 7.1** was used to analyse the images shown in **Figure 7.4** and **Figure 7.5**. The cells populating the control samples with no MB-incorporation displayed good proliferation, with evidence of ECM deposition. After 24 hours, cells appeared to have spread between fibres, and following 7-day incubation, cells with or without light activation appeared to have formed a full 'sheet' across the fibres. These samples were valued at Grade 0 as there was no visual limitation to cell growth (**Table 7.1**).

In the scaffold samples with MB-incorporation, the 100%-MB scaffolds appeared to be cytotoxic, as cells had not attached to the scaffold. These samples were marked as 'Grade 4 (i.e. Severe 'reactivity)'), with near complete destruction of cells being seen. One cell was visualised in 24-hour samples for the 30-minute dark control, but it was spherical and did not appear to be attached. This sample was valued as being 'Grade 3 - Moderate' reactivity. The results in this study support the results described previously (section 7.3.1.1) which suggested that the 100%-MB scaffolds were too cytotoxic to support neotissue formation.

After 24 hours, cells appeared to have attached to the 50%-MB scaffolds in either dark or light activation conditions, but they presented a rounded appearance in most places, and there had been obvious growth inhibition in comparison to the 'ND' control samples. These were scored as 'Grade 3 – Moderate' reactivity. There was no major difference seen between the light activated and the dark control samples. After 7 days, the samples for the 50%-MB scaffolds had increased to 'Grade 4 – Severe' reactivity, as no cells could be seen on the scaffolds suggesting that the MB within the scaffold had killed the L929 cells. Along with the results described previously (section 7.3.1.1), these scaffolds were also determined to be too cytotoxic to support tissue growth in a regenerative scaffold.

Finally, the dark controls of the 10%-MB scaffolds for the 24-hour incubation time were graded as 'Grade 3 – Moderate' reactivity, as the cells populating the scaffold appeared rounded. Interestingly, upon light activation, the cells appeared less rounded. Here the scaffolds were graded as 'Grade 2 – Mild' reactivity. This effect has been found in previous studies, with Ayuk et

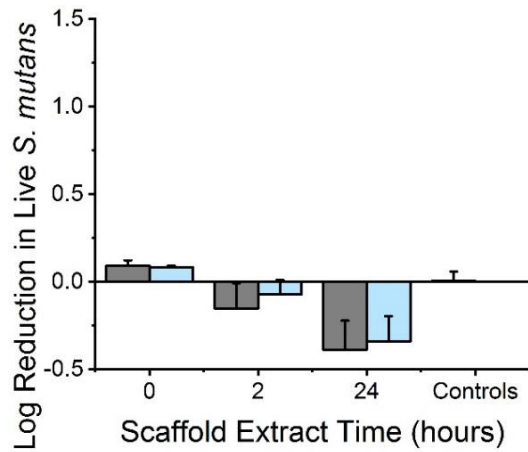
al. reporting that light exposure can increase viability and proliferation of cells^[521]. In 'stressed' cell states this response was enhanced, which could be occurring in these test samples as well due to the 'stress' induced by the MB exposure^[521]. Jin et al. also found a similar increase in proliferation with the growth of human dermal fibroblasts on electrospun fibres when exposed to light^[522].

After 7 days of incubation, the cells populating the 10%-MB scaffolds appeared to have deposited a layer of ECM. As <20% of cells were round and loosely attached, these samples were graded as 'Grade 1 – Slight' reactivity when compared to the control samples. This would again support the conclusion from previously described results (section 7.3.1.1), and these scaffolds were therefore concluded to be suitable to support neotissue formation in a regenerative device from these preliminary cytotoxicity assays.

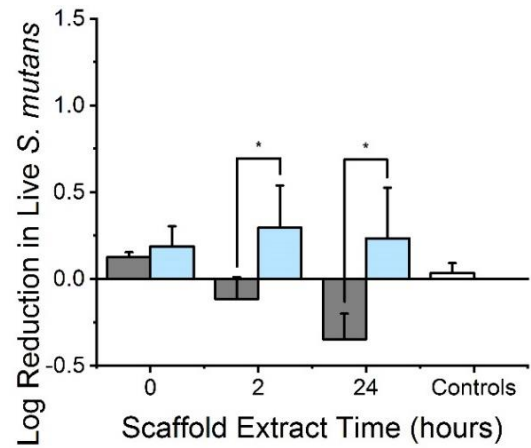
7.3.2 Antibacterial Photodynamic Therapy Activity of Lead Prototype

7.3.2.1 Bacteria Extract Testing

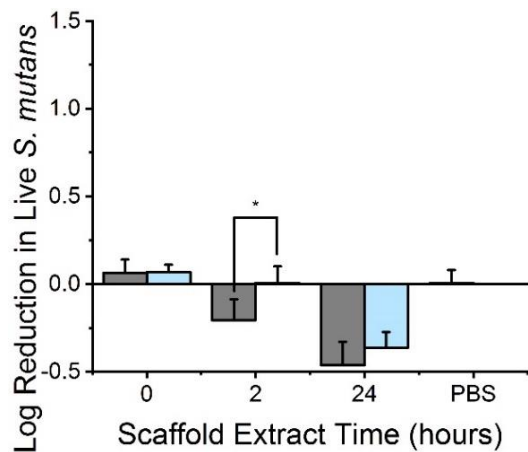
As the scaffold was required to display both tissue regenerating and antimicrobial functionality, only the 10%-MB scaffold was tested with *E. coli* and *S. mutans* bacteria as it was the only MB-encapsulated scaffold with acceptable levels of cytotoxicity towards L929 cells following light activation for either 30 or 60 minutes. Initial screening was performed using the extract solutions collected from the experiment described previously (section 7.3.1.1) with a luminosity assay to detect ATP activity from each bacterial strain. As the protocol with no incubation time was deemed most similar to the clinical situation in the mammalian cell assay, this was also used to quantify bacterial killing so that comparative data could be collected (**Figure 7.6** and **Figure 7.7**).



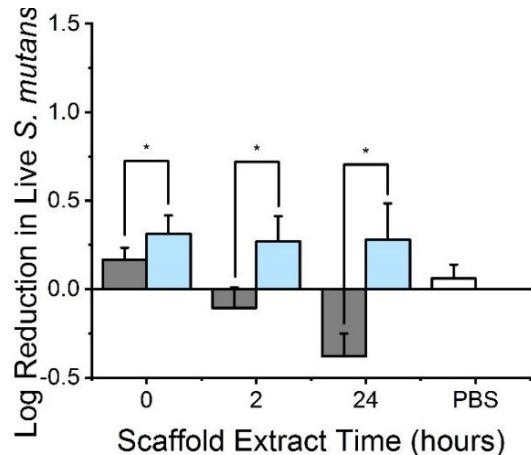
(A)



(B)



(C)



(D)

Figure 7.6 – *S. mutans* Extract Solution Toxicity with no pre-incubation time prior to light activation. (A) 30 min ‘dark’ control; (B) 30 min light exposure. (C) 60 min ‘dark’ control; (D) 60 min light exposure.

Solutions extracted from various 5050 polymeric electrospun scaffolds. ■: MB-free (ND) controls; ■: 10%-MB; □: fresh PBS negative control; ■: PBS-Triton™ X-100 solution positive control.

Results reported as Mean±SD (n=3). ‘*’ denotes significantly different means ($p < 0.05$, *t*-test)

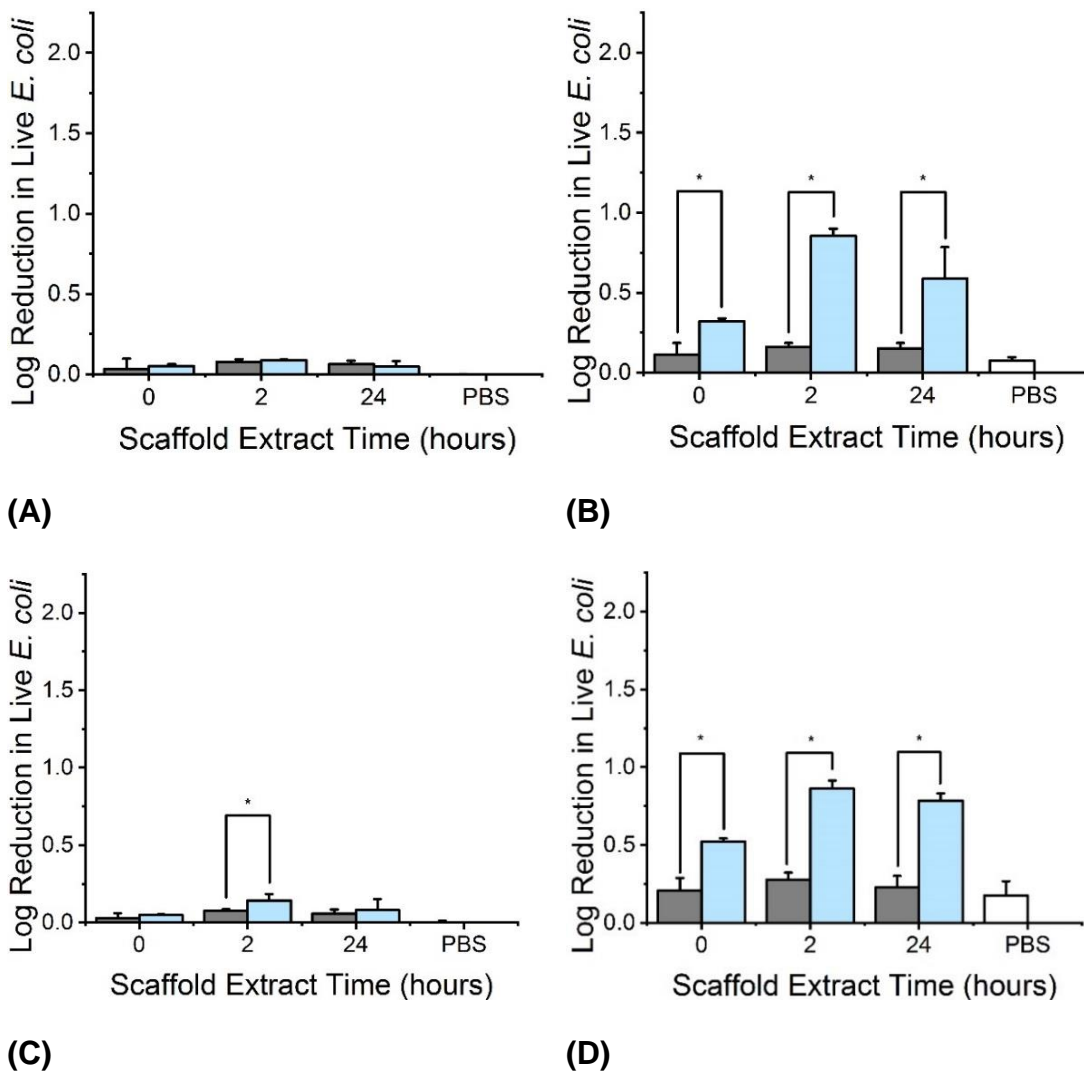


Figure 7.7 – *E. coli* Extract Solution Toxicity with no pre-incubation time prior to light activation. (A) 30 min 'dark' control; (B) 30 min light exposure. (C) 60 min 'dark' control; (D) 60 min light exposure. Solutions extracted from various 5050 polymeric electrospun scaffolds. ■: MB-free (ND) controls; ■: 10%-MB; □: fresh PBS negative control; ■: PBS-Triton™ X-100 solution positive control. Results reported as Mean±SD (n=3). "*" denotes significantly different means ($p < 0.05$, *t*-test)

When bacteria were exposed to extract solutions collected at 0-, 2- and 24-hour time points, there was no significant reduction in live bacteria for either *S. mutans* or *E. coli* bacterial strains in comparison to the ND control scaffolds without light activation ('dark' controls). The only exception to this

was the 2-hour extract solutions after 60 minutes incubation which did produce a small but significant reduction in the bacterial count for either bacteria ($p = 0.01$ and 0.01 for *S. mutans* or *E. coli* respectively). This confirms that without light activation, the PS exposure will not kill bacteria which is crucial for the 'on-demand' aspect of the scaffold to be achieved.

Upon 30 minutes of light activation with the *S. mutans* bacteria, the 2- and 24-hour extract solutions significantly reduced the bacterial viability ($p = 0.01$ and 0.005 respectively). After 60 minutes of light activation, all three extract solutions reduced the bacterial viability ($p = 0.03$, 0.001 , 0.0002 respectively). The viability of *E. coli* bacteria was significantly reduced for all extract solutions at either 30 minute ($p = 0.008$, 5×10^{-9} and 0.004 respectively) or 60 minutes light activation ($p = 0.0002$, 4×10^{-9} and 4×10^{-7} respectively). These results indicate that the combination of light and MB led to a reduction in the viability of bacteria. However, the log reductions in living bacteria for either bacterial strain were low, with the maximum reduction for *S. mutans* bacteria being 0.3 ± 0.2 , and the maximum reduction for *E. coli* being 0.9 ± 0.1 log reductions.

As the ATP assay described previously was used to determine metabolic activity of the bacteria (section 5.3.3), a comparable experiment was performed but the extract solutions containing bacteria were swabbed onto agar plates and incubated overnight to determine whether the bacteria could reproduce (**Figure 7.8**).

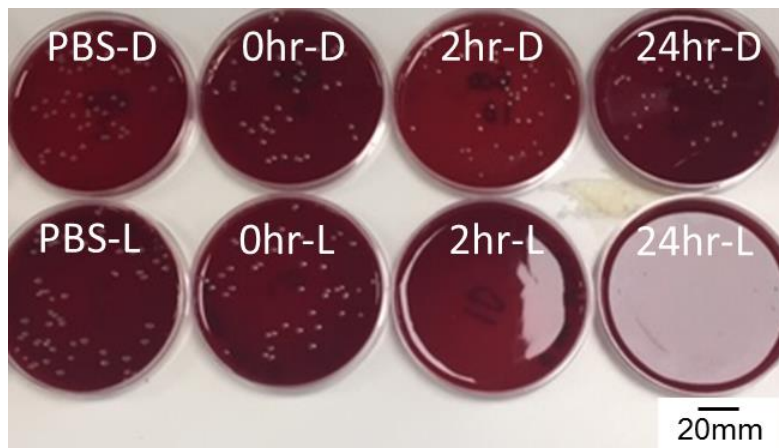
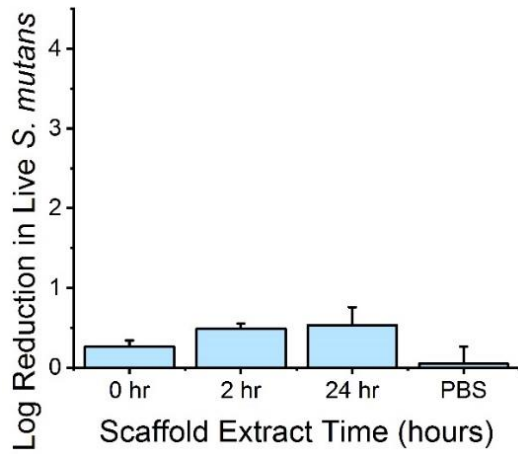
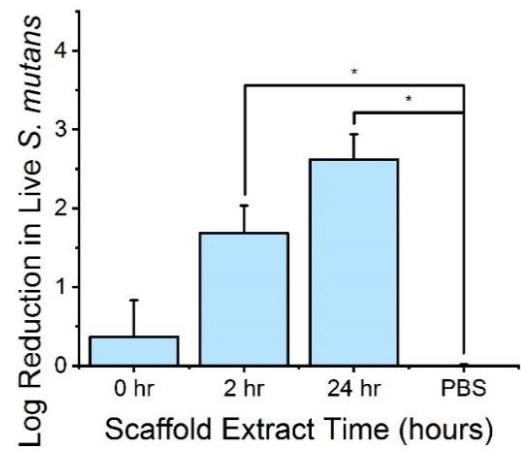


Figure 7.8 – Example set of plates grown overnight of *E. coli* suspended in extract solutions from 10% MB scaffolds. D: Dark controls; L: Light controls; PBS: Positive control; 0hr, 2hr, 24hr: Time of incubation prior to extract solution collection. All plates presented are 10^{-6} dilution from the original inoculation to allow for direct visual comparison

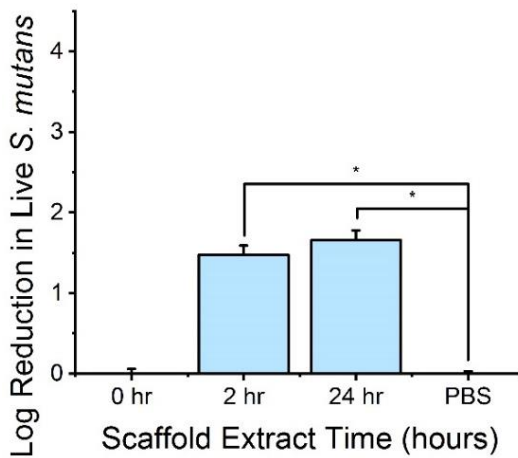
Following incubation, the counting of bacterial colonies was used to determine the reduction in CFU obtained after treatments (**Figure 7.9** and **Figure 7.10**).



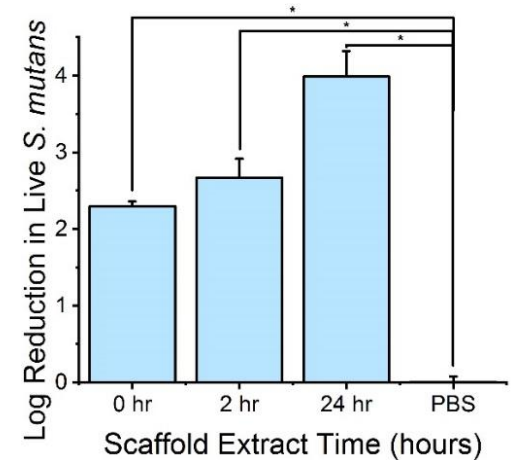
(A)



(B)



(C)



(D)

Figure 7.9 – *S. mutans* Extract Solution Toxicity with Agar Plate Testing for 10%-MB Scaffolds. (A) 30 min ‘dark’ control; (B) 30 min light exposure. (C) 60 min ‘dark’ control; (D) 60 min light exposure. Solutions extracted from various 5050 polymeric electrospun scaffolds. Results reported as Mean±SD (n=3). ‘*’ denotes significantly different means ($p < 0.05$, t -test)

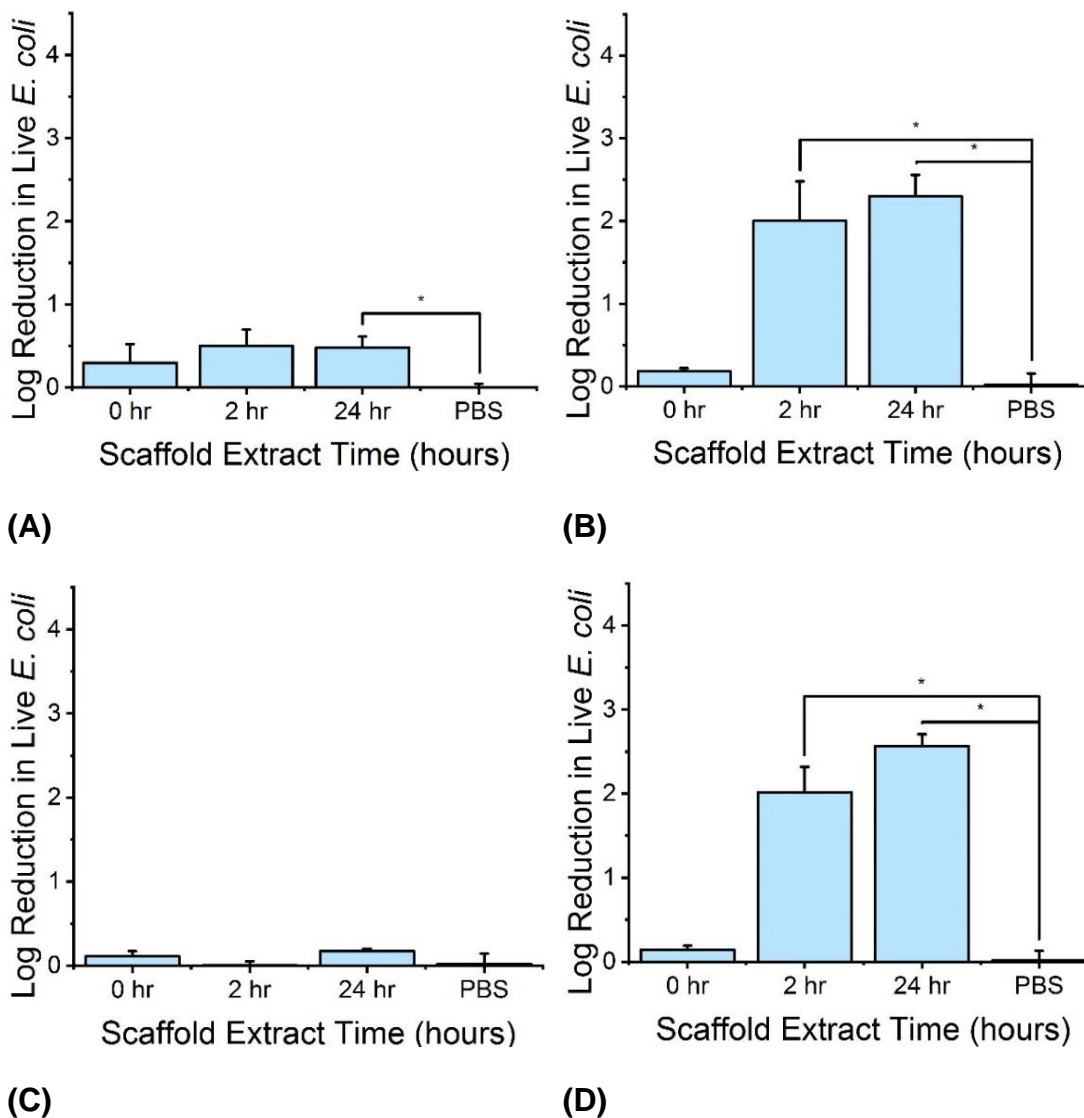


Figure 7.10 – *E. coli* Extract Solution Toxicity with Agar Plate Testing for 10%-MB Scaffolds. (A) 30 min 'dark' control; (B) 30 min light exposure. (C) 60 min 'dark' control; (D) 60 min light exposure. Solutions extracted from various 5050 polymeric electrospun scaffolds. Results reported as Mean±SD (n=3). '*' denotes significantly different means ($p < 0.05$, *t*-test)

This data shows significantly higher rates of killing than that from the ATP detection study (Figure 7.6 and Figure 7.7). The ATP assay detects how metabolically active the bacteria are and uses this as an estimate of their survival. The method based on bacterial CFU counting involved plating up the bacteria and allowing time for reproduction and so directly detects if the

bacteria can replicate. This is a more traditional and commonly used method in microbiological studies^[523]. The results presented here therefore suggest that the bacteria are metabolically active immediately after treatment with extract solutions and light but are unable to reproduce given the opportunity.

The dark controls for the 30-minute experiments did not result in a significant reduction in CFU with *S. mutans* bacteria, but the 60-minute dark controls did result in a significant reduction in CFU for both the 2- and 24-hour extract solutions ($p = 0.002$ and 0.001). The increased exposure time of the bacteria to the MB was likely to be the cause of this.

Following 30 minutes of light activation, the *S. mutans* CFU count was significantly reduced for both 2 hour and 24-hour extract solutions ($p = 0.02$ and 0.007 respectively) with average log reductions of 1.7 ± 0.4 and 2.6 ± 0.4 respectively. After 60 minutes of light exposure, there was a significant reduction in CFU/ml for each of the 0-, 2- and 24-hour extract solutions ($p = 6 \times 10^{-6}$, 0.002 and 0.002 respectively) with average log reductions of 2.3 ± 0.08 , 2.7 ± 0.3 and 4.0 ± 0.4 respectively. These results indicate that after 2 hours post-implantation, the scaffolds should be capable of killing a significant amount of gram-positive bacteria.

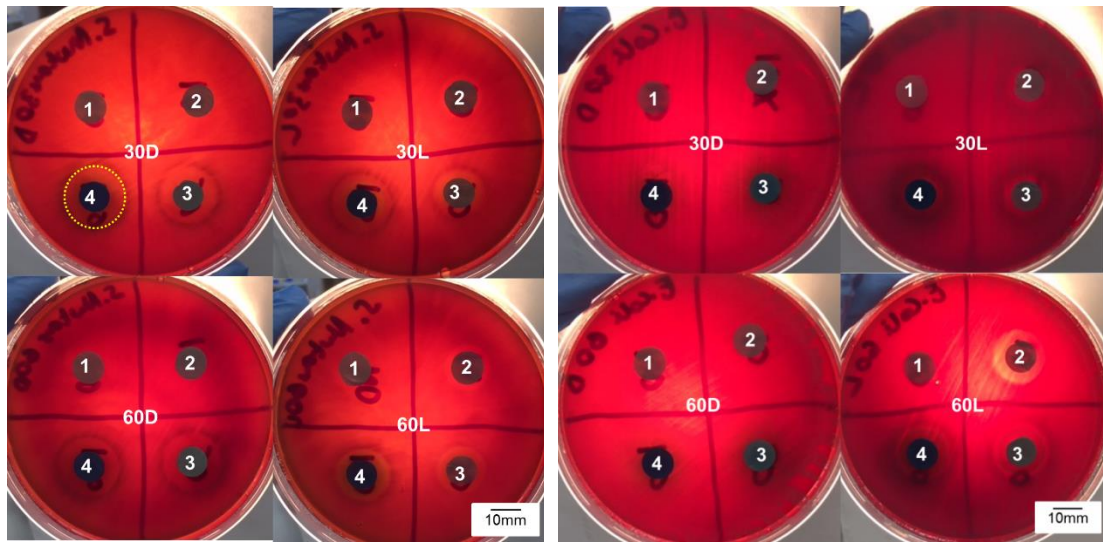
There was found to be a small significant reduction in the colonies counted for the dark control of the 30-minute *E coli* samples for the 24-hour extract solutions ($p = 0.03$) but no significant decreases were found with the 60-minute dark control samples. Upon 30 minutes of light activation, both the 2- and 24-hour extract solutions were found to significantly reduce the CFU ($p = 0.02$ and 0.002 respectively) with average log reductions calculated to be 2.0 ± 0.6 and 2.3 ± 0.3 respectively. After 60 minutes light exposure, these reductions for the 2- and 24-hour extract solutions were also observed ($p = 0.006$ and 5×10^{-5}) with average log reductions of 2.0 ± 0.4 and 2.6 ± 0.2 .

There were not found to be a significant difference in the log reduction of each bacteria at comparable time points and extract solution treatments for most of the test conditions. However, this study indicated that after 60 minutes of light activation of both the 0 hour and the 24 hour scaffold extract solutions, significantly more *S. mutans* was killed in comparison to *E. coli* bacteria ($p =$

5×10^{-6} and 0.02 respectively) with an average difference of 2.2 ± 0.2 and 1.4 ± 0.3 log reductions respectively. Additionally, the extract solutions for 2- and 24-hour time points killed both bacteria after 30- and 60-minutes light activation, however, the 0-hour extract solutions only killed *S. mutans* bacteria after 60 minutes of light activation. As discussed previously (section 5.2.5.2), gram-positive bacteria (such as *S. mutans*) has been previously found to be more susceptible to aPDT than gram-negative bacteria strains (such as *E. coli*) which has been confirmed with these results.

7.3.2.2 Bacteria Contact Testing

Finally, ZOI screening was used to assess the bactericidal capacity of the scaffolds when in direct contact with bacteria (as opposed to testing the extract solutions on planktonic bacteria)^[524,525]. The full range of scaffolds (ND control, 10%-MB, 50%-MB and 100%-MB) was tested to allow for the non-cytotoxic lead prototype (10%-MB) to be compared relatively to the scaffolds with increased doses of MB. ZOI determination was based on previously published protocols for electrospun scaffolds^[416]. Images were taken of plates in order to accurately calculate the ZOI area which was measured as the diameter of the sphere of inhibited growth (as described in **Figure 7.1**) (**Figure 7.11**).



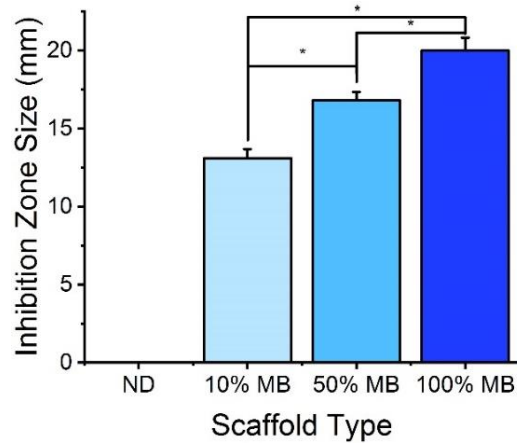
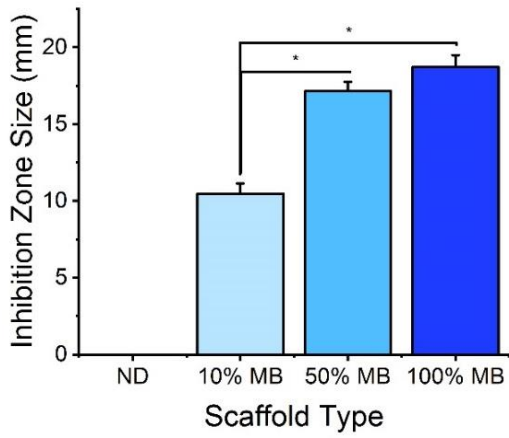
(A)

(B)

Figure 7.11 – Zone of Inhibition Plates for (A) *S. mutans* or (B) *E. coli*.

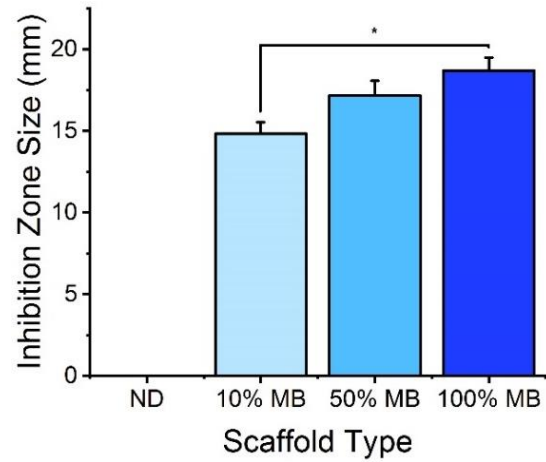
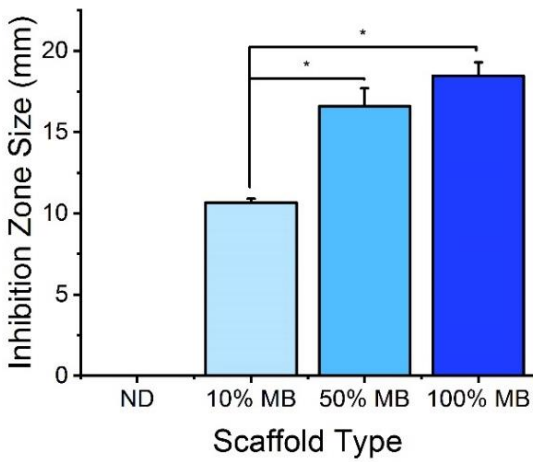
(---): Example zone of inhibition measured; (1): ND (MB-free) control scaffold; (2): 10%-MB; (3): 50%-MB; (4): 100%-MB; (30D) 30 min ‘dark’ control; (30L): 30 min light exposure; (60D): 60 min ‘dark’ control; (60L): 60 min light exposure

ZOI were measured on the images taken (where present) using ImageJ and the results collated (**Figure 7.12** and **Figure 7.13**).



(A)

(B)



(C)

(D)

Figure 7.12 – *S. mutans* Zone of Inhibition Testing. (A) 30 min ‘dark’ control; (B) 30 min light exposure. (C) 60 min ‘dark’ control; (D) 60 min light exposure. Results reported as Mean±SD (n=3). ‘*’ denotes significantly different means ($p < 0.05$, *t*-test)

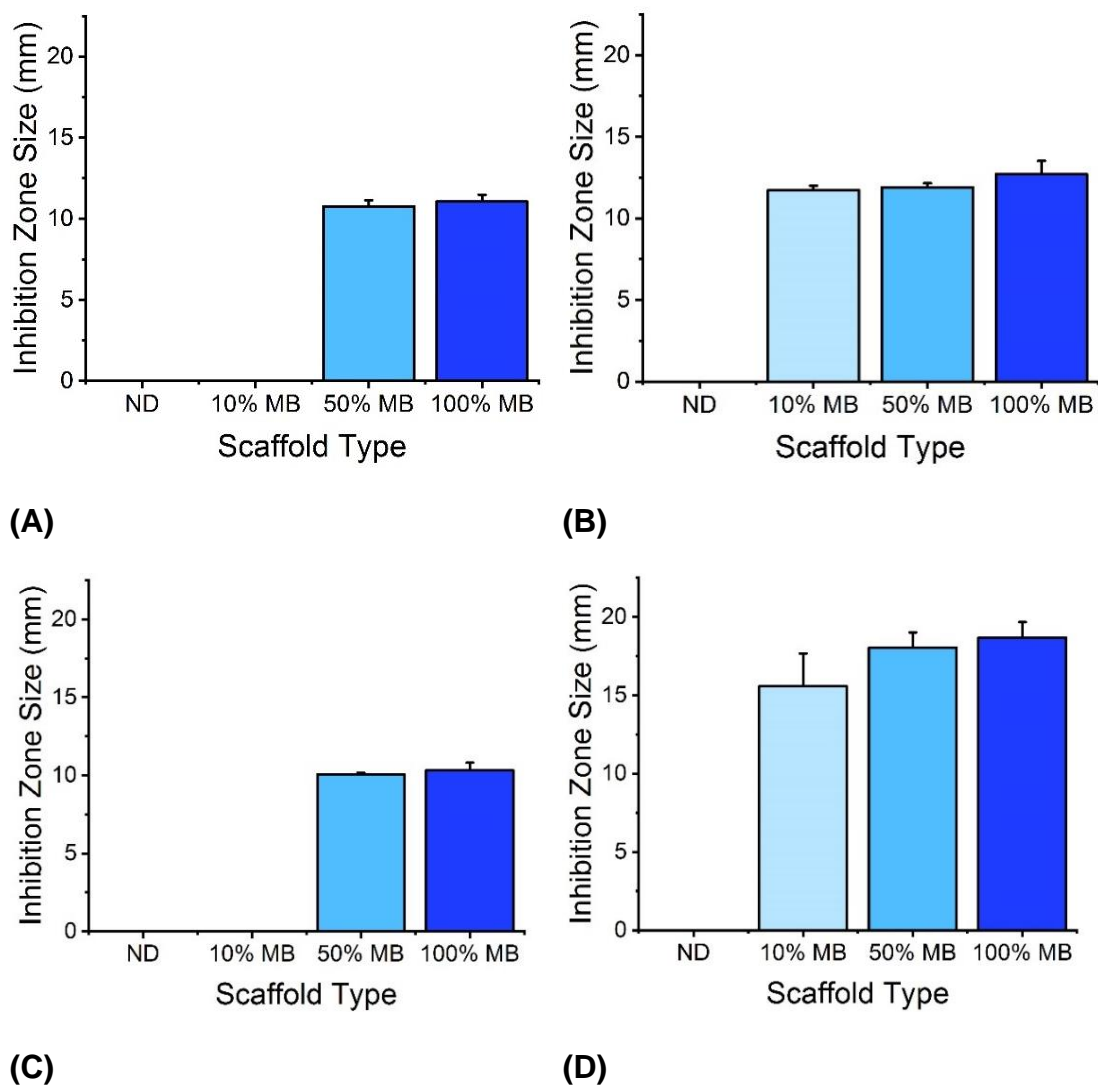


Figure 7.13 – *E. coli* Zone of Inhibition Testing. (A) 30 min ‘dark’ control; (B) 30 min light exposure. (C) 60 min ‘dark’ control; (D) 60 min light exposure. Results reported as Mean±SD (n=3). ‘’ denotes significantly different means ($p < 0.05$, *t*-test)**

For both the *S. mutans* and the *E. coli* bacteria, both in dark controls and with light activation, there was no detectable ZOI for the ND control scaffolds without MB-incorporation. This would indicate that MB is responsible for the bactericidal capacity of the scaffold. These results agree with the results presented previously in this thesis (section 5.2.6.2, section 7.2.2.1 and section 7.2.2.2) as well as with the literature^[524].

In all samples with MB-incorporation which were light activated (regardless of the concentration of MB, the time of light activation or the bacterial strain), ZOI were found to be present. Each of these zones had a defined perimeter, however, a 'blue haze' can be seen outside the ZOI (**Figure 7.11**). This could suggest that the MB has been released further than the boundary of the inhibition zone, but the concentration of MB is not enough to kill bacteria outside of the zone for the light exposure times used.

The size of the zone is known to be indicative of the level of antibacterial activity^[301]. The 10%-MB scaffolds showed a small ZOI when tested with *S. mutans* bacteria in the dark controls at 30 and 60-minute timepoints (10.5 ± 0.7 and 10.7 ± 0.2 mm). This significantly increased upon light activation for either 30 (13.1 ± 0.6 mm, $p = 0.01$) or 60 minutes (14.8 ± 0.7 mm, $p = 0.008$). There was no detectable ZOI for the 10%-MB scaffolds in the dark against *E. coli* bacteria at either the 30- or 60-minute time points. Following 30 or 60 minutes of light activation, a ZOI was apparent (11.7 ± 0.3 and 15.6 ± 2.1 respectively). These results indicate that the lead prototype scaffolds have limited bactericidal capability in the dark but are able of killing bacteria upon light activation. Again, this conclusion supports the results previously discussed in this thesis (section 7.2.2.1 and section 7.2.2.2) and suggests that the scaffold can be activated 'on-demand' to trigger the bactericidal activity of the MB.

For the *S. mutans* bacteria experiments, following 30 minutes light exposure there was a significant increase in the ZOI between the 10%-MB lead prototype and the increased MB concentrations in both the 50%-MB and 100%-MB samples ($p = 0.003$ and 0.001 respectively). After 60 minutes light exposure, there was no significant difference between 10%-MB and 50%-MB zones of inhibition ($p = 0.05$) but there was still a significant difference between the lead prototype and the 100%-MB scaffolds ($p = 0.007$). Therefore, the lower concentration of MB in 10%-MB is incapable of killing as much bacteria as the 50%-MB scaffolds after only 30 minutes light exposure, but a greater dose of light is capable of eradicating the concentration effect and the killing effects become comparable following 60 minutes light exposure.

Interestingly, in the *E. coli* experiments, no significant difference was found between the three MB-incorporated scaffolds for either 30 minutes light activation ($p = 0.55$ and 0.23 respectively) or 60 minutes light activation ($p = 0.23$ and 0.16 respectively). This suggests that the amount of MB released from any of the scaffolds is enough to kill the bacteria, and an increase in MB release does not correlate to a greater bactericidal effect. This is advantageous as the results previously discussed (**Figure 7.4** and **Figure 7.5**) confirm that a lower concentration of MB is less toxic to mammalian cells. Therefore the 10%-MB scaffolds can be used in the lead prototype which would have an acceptable level of cytotoxicity to mammalian cells but would be capable of killing as much bacteria as the 100%-MB scaffolds.

7.4 Conclusion

In vitro tests were performed on a range of control and MB-encapsulated electrospun scaffolds to determine the level of cytotoxicity on L929 cell lines of the scaffolds both with and without MB-inclusion. Initial testing was performed using an extract solution collected from incubated scaffolds at 0-, 2- or 24-hour timepoints in PBS. These tests confirmed that all ND control scaffolds were non-cytotoxic in the dark or light conditions, which confirms that the ND-polymeric scaffold and the light source are non-cytotoxic without the inclusion of MB. Initial toxicity testing involving pre-incubation of the cells with the scaffolds for 2 hours prior to light activation of either 30 or 60 minutes produced >30% cell death with any of the MB-encapsulated scaffolds. Upon an adaptation of experimental procedure to align with other experiments which did not involve a pre-incubation time, the cell death was reduced to <30% for all scaffolds in the dark controls. The 50%-MB and 100%-MB scaffolds were found to be above the threshold for cytotoxicity. However, the 10%-MB scaffold killed <30% after 30 minutes light activation and <35% following 60 minutes of light activation. Although this result was over the 30% threshold in the latter case, this scaffold formulation was the least cytotoxic to mammalian cells out of the three MB-included scaffolds.

In the L929 contact assays, 10%-MB scaffolds demonstrated the ability to support cell growth with 'mild' reactivity after 24 hours incubation and 'slight'

reactivity after 7-day incubation in comparison to the ND control samples. Considering these results, it was decided to move these scaffolds on into further tests to determine whether they could kill bacteria when combined with light.

The initial testing with the same scaffold extract solutions used in the L929 cytotoxicity assay did show a significant decrease in bacterial metabolic activity when compared to the ND control scaffolds, but the log reduction in metabolic activity was <1 log for either bacterial strain, indicating a non-bactericidal effect.

Other than bacterial metabolic activity, an alternative analysis was developed to directly count bacterial CFU and determine whether the bacteria were able to reproduce after treatment with the extract solutions and light activation. This experiment confirmed that a >1.5 log reduction was being achieved by the extract solutions. Together with the previous experiments based on the ATP assay, this data therefore suggests that although the bacteria have only had a small, but significant reduction in metabolic activity immediately after treatment, they are unable to replicate.

Other than extract assays, ZOI analysis was performed to compare the bactericidal capacity of the scaffolds when in direct contact with the bacteria. This confirmed that the combination of both light and MB were needed to kill the bacteria, as the ND controls and the 'dark' controls had significantly smaller ZOI or no zone was present. This provides further confirmation of the 'on-demand' antibacterial capacity of the scaffolds. With increased MB concentration in the 50%-MB and 100%-MB scaffolds, significantly more *S. mutans* bacteria were killed in comparison to the 10%-MB scaffold, but no significant difference was found against the *E. coli* bacteria. As the 10%-MB scaffolds were the only scaffolds with an acceptable level of mammalian cell cytotoxicity, these were selected as the most acceptable prototype.

To conclude, electrospun scaffolds manufactured from a blend of 50% PCL and 50% PLGA1090 with 0.2 mM concentration of MB (10%-MB scaffolds) were shown to successfully support L929 cell growth and result in a >1.5 log reduction in live bacteria after 30 or 60 minutes of light activation. These scaffolds therefore present a promising strategy towards the

regeneration of oral soft tissue whilst treating bacterial infections without the need to prescribe antibiotics. A general discussion of the results presented in this thesis and the next stages to be considered in the development and commercialisation of this medical device are presented in the following chapter.

Chapter 8 Discussion

8.1 General Discussion

8.1.1 Project Rationale

AMR remains a prominent healthcare concern with significant medical and financial burdens expected in the future^[526,527]. There is a currently unmet need to treat oral infections through antibiotic-free techniques to minimise the spread of AMR^[528,529].

Advancements are continuously being made in the field of regenerative medicine, such as the use of 3D bioprinting to manufacture scaffolds populated with cells^[530]. Despite this, we are currently still unable to generate synthetic functional replacement tissue and organs for transplantation into the body. Throughout the duration of this project, a number of interesting research articles aiming to meet this clinical need have been published which emphasises the importance of regenerative medicine, particularly in the field of dentistry^[531,532]. The most recent research articles aimed at regenerating oral mucosa focus on the use of cell sheet technologies^[533,534]. However, despite reports of successful research using *in vitro* systems, commercialised medical products relying on cell-based techniques are likely to be subject to a lengthy regulatory process and great expense for both the patient and the healthcare economy. Therefore, an acellular scaffold (such as the prototype proposed in this thesis) would be preferable.

The aim of this project was to determine the feasibility of designing and manufacturing a commercially relevant prototype scaffold which is capable of being activated on-demand to selectively kill bacteria through aPDT technology whilst supporting oral soft tissue regeneration.

8.1.2 Key Findings

Following a review of the preliminary research on this product concept and of commonly used FDA-approved polyesters and PS, a series of formulations for the prototype polymer scaffold were initially selected.

Throughout this research project, these formulations have been systematically characterised and optimised for use in the desired application (**Figure 8.1**).

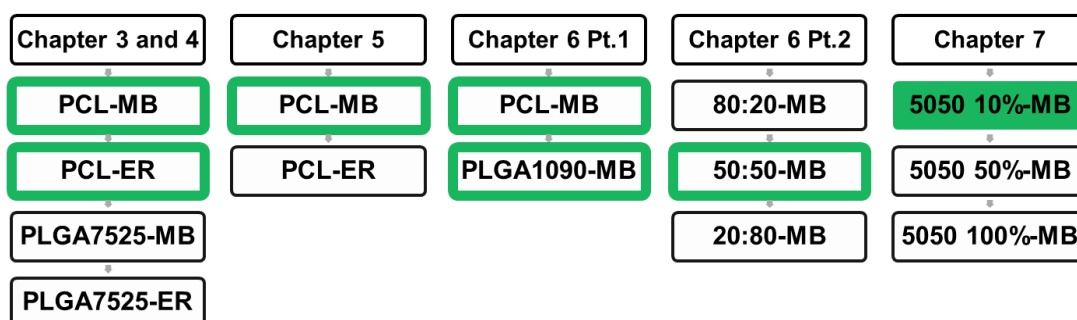


Figure 8.1 – A collection of the formulations discussed in each chapter of this thesis. □: successful formulations following that stage of development; ■: final formulation (lead prototype). Abbreviations were explained in the relevant chapter.

8.1.2.1 Initial Choice of Polymers for Scaffolds

The aim of Chapter 3 was the initial manufacture and characterisation of the biomaterial properties of scaffolds electrospun from two FDA-approved polymers (PCL and PLGA7525) along with two FDA-approved PS (MB and ER). After an initial screening of polymer concentrations (section 3.3.1.1), a range of scaffolds were successfully electrospun containing ~100% of the expected mass of PS (section 3.3.2.1). A significant reduction in fibre diameter (and consequently the pore size) upon inclusion of either PS was found, which was likely to be due to the charge repulsion in the polymer jet during electrospinning (section 3.3.2.1).

Chapter 4 contains a range of characterisation methods aimed at describing the interactions between this range of scaffolds and aqueous environments. The scaffolds proved to be hydrophilic as demonstrated by WU (section 4.3.1.3) and contact angle (section 4.3.1.1) analyses. This hydrophilicity was further enhanced with PS encapsulation. *In vitro* PS release profiles indicated that PLGA7525-PS scaffolds released a minimal amount of PS over the 4-week timeframe (section 4.3.1.2). However, during the 8-week

hydrolytic degradation study, PLGA7525 scaffolds shrunk macroscopically in solution and collapsed microscopically, resulting in a lack of porosity of the structure which would prevent cell integration *in vivo* (section 4.3.2).

PCL-ER scaffolds only released ~20% of ER included within the scaffold, which was in contrast to the PCL-MB scaffolds which displayed a typical burst release profile with 100% of MB being released during the first 24 hours of incubation (section 4.3.1.2). Neither of these profiles were ideal, as a gradual release of the PS was desired to be achieved over the first 4 weeks post-implantation in a clinical setting to allow for repeated photoinduced activation of the PS if required. The hydrolytic degradation study indicated that PCL scaffolds displayed minimal microstructure alteration and minimal mass loss (section 4.3.2).

Therefore, PLGA7525-MB and PLGA7525-ER scaffolds were withdrawn from further analysis and PCL-MB and PCL-ER scaffolds were taken forward into the next stage of the project.

8.1.2.2 Selection of Photosensitiser for Antimicrobial Photodynamic Therapy

The aim of Chapter 5 was to determine which PS was most suitable for the desired antimicrobial effect out of two FDA-approved PS; MB and ER. Initially, MB uptake was found to be greater than ER uptake into L929 mammalian cells and *S. mutans* and *E. coli* bacterial cells (section 5.3.2). This is likely to be a contributing factor to the increased toxicity of MB-loaded solutions against both mammalian and bacterial cells in comparison to ER-loaded solutions (section 5.3.3). However, solutions of PS were compared with regards to mass concentrations (mg/ml) rather than molarity concentrations, so although the results of these studies suggested that MB was more effective than ER, the molarity concentrations compared were approximately 3 times greater for the MB than ER. It is worth noting that many published research papers have compared the effectiveness of PS based on mass concentrations rather than molarity concentrations so both data sets are valuable to allow for comparisons to be made between this research and previous studies^[365,535,536].

Finally, the toxicity of two selected prototypes (PCL-MB and PCL-ER) was determined for both mammalian and bacterial cell types (section 5.3.4). PCL-MB scaffolds were found to be more effective at deactivating *E. coli* bacteria populating the scaffolds *in vitro* than the corresponding PCL-ER scaffold variant with the same molarity of PS. These results, along with a review of the literature confirming the advantages of the use of MB in dental aPDT, lead to MB being chosen as the optimal PS to be used in the intended aPDT system.

8.1.2.3 Optimisation of Polymers of Polymer Building Blocks for Electrospun Scaffolds

The data presented in Chapter 6 were the result of a series of experiments performed to determine whether biomaterial properties could be improved through altering the polymer used to manufacture the scaffolds with MB. Due to the amorphous nature of PLGA7525 resulting in scaffold shrinkage upon contact with water (sections 3.3.2.3 and 4.3.2), a new monomer ratio of PLGA (PLGA1090) was selected for analysis (section 6.3.1). These new scaffolds were found to have a greater degree of crystallinity (section 6.3.1.2) which contributed to the demonstrated optimised properties such as no detectable shrinkage in aqueous media and desirable release profiles with MB-encapsulation. However, they did degrade too quickly for the intended purpose (following 1-2 weeks incubated in PBS) (section 6.3.1.3).

A combination of the desirable properties of PCL (resistance to hydrolytic degradation) and PLGA1090 (sustained MB release) were needed. Therefore, the remainder of Chapter 6 was used to characterise blends of these two polymers in three ratios (80:20, 50:50 and 20:80) with MB-encapsulation (section 6.3.2.1). Characterisation of these scaffolds concluded that the 50:50 blend had the optimised properties from both of these systems (section 6.3.2.3).

Finally, in preparation for the final '*in vitro* testing', the 50:50 polymer blend was electrospun with three different concentrations of MB (10%-MB, 50%-MB and 100%-MB) (section 6.3.2.4). No significant changes to the fibre diameter and crystallinity of the scaffolds were found upon the reduction in MB within this range.

8.1.2.4 *In vitro* Testing of Optimised Prototype Scaffold

Chapter 7 used a series of experimental tests on the optimised scaffold with a range of three MB concentrations in order to determine whether selective aPDT effect could be achieved i.e. toxicity to bacteria but mammalian cell tolerance.

Both extract (section 7.3.1.1) and contact assays (section 7.3.1.2) were performed with L929 mouse fibroblasts. 50:50 10%-MB scaffolds proved to be non-toxic to cells in each of these tests in accordance with ISO 10993 standards. Therefore, this formulation was also tested with model gram-negative and gram-positive bacteria (i.e. *E. coli* and *S. mutans*) to determine the selectivity achievable between mouse fibroblast and bacterial cells (section 7.3.2). In both extract and contact *in vitro* assays, 50:50 10%-MB scaffolds demonstrated the ability to deactivate both bacterial strains in the light activated samples with minimal toxicity being found in the 'dark' control samples. Therefore, it was concluded that this scaffold had the required aPDT selectivity for the lead prototype at the conclusion of this project.

8.2 Commercialisation Discussion

This research has been conducted as the result of an iCASE collaboration between the University of Leeds and an industry sponsor, Neotherix Ltd. Therefore, one of the objectives of the research was to determine the potential commercial feasibility of this prototype in dental markets. For the remainder of this thesis, the prototype medical device will be referred to as 'PhotoTherix™'.

8.2.1 Technology Readiness Levels

Technology Readiness Level (TRL) descriptions were developed by NASA in 1995 as a way to describe and monitor the progression of new technologies within the organisation^[537]. The TRL scale has now been adopted for the research and development of a wide range of technological advancements. Typically, a scale from TRL 1 (foundation level research) through to the final TRL 10 stage (the technology is being used commercially) is adopted (**Table 8.1**)^[538].

1	2	3	4	5	6	7	8	9	10
Science	Technology			Commercialisation			Market		
Research Idea	Proof of Market	Proof of Concept	Proof of Validation	Market Validation	Proof of Concept	Pathway	Develop Product	Market Launch	Monitor
Basic science	Search for novelty and compare to market leaders	Evidence of inventive concept	Prove advantage compared to market leaders	Develop strategy, protect IP, engage partners	Meet industry standards	Perform IP sale, license or spin-out	Industry partner develops product for launch	Launch product	Monitor impact and finance

Table 8.1 – Technology Readiness Level (TRL) description^[538]

At the beginning of this project, a design concept for the technology had been hypothesised (TRL 1) and a preliminary market search had been performed (TRL 2) in the form of an external report produced by BITECIC Ltd^[246]. Proof of concept research had been performed for PhotoTherix™ with regards to a skin application. The research performed as part of the research project presented in this thesis was aimed to progress the technology from TRL 2 to TRL 3 for specific use in oral applications.

This project has concluded with a prototype PhotoTherix™ medical device being proposed. Through a range of *in vitro* experimental techniques, the scaffold demonstrated the ability to be stable in an aqueous environment for up to 8 weeks, to gradually release PS over 4 weeks and to selectively deactivate bacteria but sustain fibroblast cell growth following light activation. These had been determined as the minimum criteria required to demonstrate that the prototype had the potential to be an effective clinically used product. Therefore, the technology has been progressed to the 'Proof of Concept' TRL 3 stage.

Regulatory considerations have been implemented during the project to 'future proof' the prototype. For example, FDA-approved polyesters and PS were chosen to simplify the approval process. Also, awareness of the regulatory approval processes (i.e. test procedures of the ISO standard) were implemented during the design of the experiments in Chapter 7. The aim of this was to de-risk the technological design and determine whether this product concept could overcome the 'valley of death' following proof of feasibility stage towards a proof of commercial concept study^[539]. If a product works perfectly in the laboratory but the design is too complex to be approved by the regulatory bodies in a cost-effective fashion, the research is unlikely to result in innovation and a patient/end-user benefit or attract the investment funding necessary for commercial development.

The next steps on the TRL scale would be to develop the research further into TRL 4, which would require PhotoTherix™ to be compared to market leaders to ensure that the device has benefits with respect to the current commercially available products in either effectiveness or cost in

order to identify potential unique selling points. This could involve activities such as consulting clinicians and the use of animal models to indicate safety and efficacy *in vivo*. For this next stage of development, additional investment would be needed, so potential funding sources should also be considered.

8.2.2 Regulation and Classification

The Medical Device Directive (MDD) was introduced in 1993 to help regulate new medical devices in the EU to provide a way of ensuring that commercially available products were safe for use^[540]. Notified bodies such as the British Standards Institute (BSI) in the UK were nominated to help enforce these directives on behalf of the competent authority, which in the UK is the Medicines & Healthcare Products Regulatory Agency (MHRA)^[541]. As such, they assess new devices based on their safety for CE marking purposes. Part of this process involves classifying medical devices by examining their end use duration, and what risk this would pose to a patient if failure of the device were to occur^[542]. If approval is sought in one geographical area, this can often aid the process of applying for approval in another. An increased risk to health and length of exposure results in increased rigorousness in the testing protocols (**Table 8.2**).

EU Medical Devices	FDA Medical Devices	Risk Level	Example
Class I	Class I	Low	Hospital beds
Class IIa	Class II	Medium	Hearing aids
Class IIb	Class III	Higher	Infusion pumps
Class III		Highest	Prosthetic joints
Active Implantable Medical Devices (AIMD)		Very high	Spinal cord stimulators

Table 8.2 – Medical device classifications^[542]

In May 2017, a new set of directives were announced by the EU for medical device regulation, known as the Medical Device Regulations (MDR)^[543]. The main differences between the MDD and the new MDR include more stringent checks being required for most devices, cosmetic and ‘non-medical’ devices such as coloured contact lenses are now included in the regulations, and a new Unique Device Identification (UDI) has been introduced which will be required on all devices^[543]. When announcing the new MDR, a 3 year ‘transition period’ was stated in which both the MDD and MDR are active^[544]. However, this transition period finishes in May 2020, so with regards to the future commercialisation of PhotoTherix™, approval from the MDR will be of more importance than the MDD.

It is worth noting that due to the uncertainty surrounding the UK leaving the EU at the time of writing this thesis, it may be that these classification systems leading to approval will be different for the UK and the EU. However, for selling PhotoTherix™ in international markets, adhering to these systems will be required anyway.

Although flow charts are widely available online to predict which classification applies to a new medical device, official advice from relevant notified bodies should be sought out during prototype development. Due to

the large size of the market in the US for dental products, it is likely that PhotoTherix™ will be aimed for sale in both the EU and the US. Therefore, it would be useful for the device to adhere to both regulatory systems for approval by the EU and the FDA^[542].

In the US, many companies aim for their devices to be approved through the 510(k) process, which is a 90-day review procedure in which a company will submit documentation to explain that the new device is comparable to a currently approved device and would therefore not be required to go through the lengthy and expensive procedure of seeking additional approval^[542]. Unfortunately, as there is no device like PhotoTherix™ on the market currently, it is unlikely that a 510(k) approval will be possible. Therefore, in the US, pre-market approval from the FDA would need to be sought out.

It is important to note that PhotoTherix™ is a borderline product, as it is not clear whether it would be classified as a medical device or a medicinal product. As PhotoTherix™ is designed to be fully resorbed by the body, it would be classified as a Class III medical device. However, this relies on the assumption that the primary function of PhotoTherix™ is as a regenerative scaffold, with an additional functionality of the bactericidal effect. If PhotoTherix™ were to be primarily a delivery device for the PS, it would be more likely to be classified as a medicinal product. In order to be approved as medicinal product a different set of directives are relevant, which require even more stringent testing. This would be more costly in both time and expense to continue the development of this concept into a commercial product so this should be avoided if possible. Due to the difficulty in distinguishing the classification of borderline products, official advice would need to be gained from the relevant authorities.

8.2.3 Use in Dental Surgery

The prototype of PhotoTherix™ has been designed to be used by a dental practitioner in oral surgeries to help regeneration of oral soft tissue whilst treating localised oral infections. Questions remain as to how the device should be implanted, and in which types of surgical dental

procedures it would be most useful. Literature searches and informal discussions with dental practitioners in the department of Oral Biology at the University of Leeds led to the following suggested uses for the scaffold.

8.2.3.1 Gingival Recession treatment

Gingival recession is the erosion of the gingiva resulting in the exposure of the tooth root surface to the oral environment^[545]. It can be caused by many factors such as abrasion from aggressive brushing of the teeth, periodontal disease and surgery^[545]. Gingival recession often results in aesthetic and functional issues (e.g. root hypersensitivity)^[546]. Traditionally, autologous tissue harvested from elsewhere in the oral cavity (e.g. the palate) can be used during root covering surgeries. Currently, bioresorbable porcine collagen membranes such as Geistlich Mucograft® (Geistlich Pharma Inc.) are commonly used to prevent the need for two surgical sites and to decrease operation times^[547]. The use of PhotoTherix™ in place of the porcine collagen could be advantageous due to some patients being exempt from treatment with porcine tissue because of ethical or moral reasons. An additional benefit would be the extra protection from infection provided by the antimicrobial functionality of PhotoTherix™. However, oral tissue staining resulting from the use of MB may be a potential disadvantage and should be explored with customers (both end-user clinicians and patients).

8.2.3.2 Split Thickness Tissue Grafting

Split thickness grafts are used to treat large defects to the oral mucosa^[548]. They involve the extraction of a sublayer of autologous oral tissue, and the combination of this split-thickness tissue with a membrane to form a new layer of oral mucosa e.g. around implants or for patients with dental bone loss^[549]. Briefly, this surgery involves the withdrawal of the tissues surrounding the tooth and the debridement of bone tissue in the cavity^[549]. Bone stock is then taken (commonly from the third molar) and packed into the cavity with some blood to increase healing^[549]. The gap is then sealed over with a biodegradable scaffold to hold it all in place^[549]. PhotoTherix™ would be a good alternative to current membranes, as the

site would be easily accessible for light activation and the antimicrobial aspect would be an additional advantage.

8.2.3.3 Closure of Extraction Socket

PhotoTherix™ could also be used as a periodontal ligament membrane to close an extraction socket (socket seal technique)^[20]. Currently, an antimicrobial membrane is used in root extraction surgery for 1 week to seal over the site around the tooth which is then removed, prior to implantology surgery being performed^[550]. Currently, cement loaded with zinc oxide-eugenol is a common choice to cover this site^[551]. Although this works well as an antimicrobial, patients can be sensitive to the use of eugenol so this treatment cannot be used in certain patient populations^[551]. An alternative scaffold is 'CoE-Pak' (GC America Inc.) which is eugenol free^[552]. The use of PhotoTherix™ would allow for universal treatment and the on-demand antimicrobial aspect of the scaffold would be advantageous. This use of this product would allow for repeated light activation within the week in which the scaffold is in situ. However, this proposed use would not require the scaffold to function as a tissue regenerating device. In fact, this would be a disadvantage as the scaffold would need to be removed.

8.2.3.4 Surgical Technique

As described above, some suggested uses of the scaffold would involve the incorporation of an autograft or additional membrane along with the scaffold. This would require implanting the scaffold either underneath or on top of the autograft.

If the scaffold were to be placed on top of the membrane, PhotoTherix™ would be easily accessible for the dental practitioner to light activate. However, the scaffold may not fully integrate with the tissue if placed on top. If 'sandwiched' between the autograft and the wound bed, PhotoTherix™ would be in a good position for tissue integration, but it may have limited accessibility for the light source. The light required to activate MB is 610-665 nm which is in the 'red' region of the visible light spectrum. Red light has been found to have greater tissue penetration (of up to 1-2 mm^[553])

compared to other wavelengths within the visible light spectrum due to its shorter wavelength^[336].

A final consideration for this product would be the fixation of the product during placement in the oral cavity. Two possible methods include sutures or mucoadhesion. Sutures are the current most commonly used method for securing grafts in the oral cavity^[228]. Single button^[554] or cross^[178] resorbable sutures can be used.

However, many interesting research articles have been published which explore a variety of new methods to generate mucoadhesive compounds^[555–557]. Despite further research being required before these techniques become the ‘gold standard’, with scientific advancements these could be used in combination with this product during oral surgery.

8.2.4 Competitor Analysis

Successful products are currently available on the market either for oral soft tissue regeneration (e.g. mucoderm® (Botiss Dental)) or the treatment of oral infections through aPDT (e.g. Periowave™ with advanced formulation syringes (Ondine Biomedical)). For PhotoTherix™ to be a commercially viable option, there would need to be a unique selling point (USP) for there to be an advantage of purchasing and using this product over the currently used products. This could include being a more cost-effective option, proving to be more clinically effective or proving to have a unique additional feature. At the time of the publication of this thesis, there is no other medical device commercially available (to the best of the author’s knowledge) which combines a synthetic polymer scaffold for the regeneration of oral soft tissue with the release of PS designed for use with aPDT technology. This could prove to be the additional unique feature which gives a commercial advantage to this product as it would be the ‘first to market’. Further to this, electrospinning is a relatively cheap technique which has the potential to generate large sheets of product. As only a small amount of product would be required per operation, the device could also be sold at a competitive price in comparison to the other products available. For example, online prices for mucoderm® are reported as between £105-£189

per matrix (www.straumann.co.uk) depending on the size of requested (although costs are likely to vary depending on order quantity and source).

8.2.5 Patentability

Patents are legal documents which allow a monopoly of the rights of a specific invention to be obtained for up to 20 years^[558]. Obtaining a patent is seen by many as key in order to protect intellectual property and allow commercialisation of a new product as without doing so, larger companies could launch an identical product at a more competitive price. It has been reported that SMEs (Small and Medium Enterprises), such as Neotherix Ltd., are more likely to exploit their patent portfolio for monetary gains than larger firms^[559]. This is because larger firms have a greater abundance of financial resources, so they can afford to strategically patent a host of inventions to hide their main product or to prevent competition. This contrasts SMEs who are unlikely to patent an invention unless they intend to exploit the intellectual property rights through licensing to a larger company or developing the invention into a viable product.

In 2010, a patent was filed for the research concept of PhotoTherix™, jointly between the University of Leeds, the University of Bradford and Neotherix Ltd. Unfortunately, the increasing annual payments required to sustain the enforcement of the patent were not maintained and the patent was abandoned. This could be a potential disadvantage when applying for future investment into the technology to develop it further, as investment may rely on the security associated with a patent.

However, the existence of the expired patent may be enough to deter other market leaders from competing commercially. Another factor to consider is that the device could still be commercialised if a full set of data were to be obtained as the 'first to market' advantage. If the device were to be established as the leading product prior to a similar product being commercialised, it could deter competitors in the same market.

Chapter 9 Future Work

9.1 Choice of Light Source and Exposure Time

In this study, a broad spectrum 'security light' was used as a model system for PS activation due to dental lasers being too expensive to purchase at this stage in the study. Laser light of a higher intensity is likely to result in a greater activation of the PS and therefore a higher rate of bacterial cell death^[560–562].

As discussed previously (section 5.3.1), the Periowave™ handheld laser light source is a commercial product designed to activate PS such as MB in oral applications. One interesting future study would be to use this device with the proposed prototype in order to determine whether the light exposure time could be reduced to a clinically relevant timescale (30- or 60-seconds) whilst still killing enough bacteria. The reduced light exposure time may also reduce the mammalian cytotoxicity, so selectivity should be reassessed following these experiments with a different light source.

Another interesting future study would be to look into the effects of light fractionation^[320], e.g. by exposing the scaffolds to a 30 second light exposure from Periowave™ or three 10 second light exposure time points to see whether this changes the level of bacterial death.

9.2 Photosensitiser Release Profile Accuracy

The oral cavity is a notoriously difficult environment for which to predict accurate drug release profiles due to the variation in pH, saliva and the range of bacterial strains possible between patients^[563]. Research has been performed aimed at measuring the average volume of the saliva in the oral cavity^[564] but this does not account for the vast differences in composition, particularly in the case of infected oral cavities^[565]. As with the majority of the published literature, a simplified *in vitro* PS release experiment using PBS has been used in this thesis to model drug release in

the oral cavity (section 4.2.2). However, future experiments should focus on a more accurate prediction of the drug release behaviour specifically in the oral mucosa. This could be done either through *in vivo* studies or the use of an *ex vivo* diffusion model, such as the Franz diffusion cell system with rabbit oral mucosa tissue^[566].

9.3 Mammalian Cell Cytotoxicity

The scaffold system has currently only been tested on L929 cells as these are most frequently used in the regulatory approval process^[191]. However, future experiments should be designed with primary cells which are taken from the oral mucosa of patients.

An external placement was performed at the University of Sheffield under the supervision of Dr Helen Colley and Dr Craig Murdoch to determine the mammalian cell cytotoxicity using an *in vitro* infected oral mucosal disease model which they have developed^[39,567]. General details of the placement are given in the **Appendix A**. Unfortunately, the time given for the project was not sufficient to yield results due to the optimisation needed to the oral mucosal model prior to the application of the prototype scaffolds. However, the model does provide a potential future direction for this project and could be used to test the system whilst utilising the first of the '3Rs' (Replace, Reduce, Refine) in animal testing^[568]. The use of this system prior to animal testing should prevent unnecessary animal testing being performed if the results suggest that further optimisation is required. However, if this model can be used to further demonstrate that the system is non-cytotoxic, progression should then be made to test the scaffold in an *in vivo* animal model study. From this point onwards, clinical trials could be designed to validate the safety of the product for use in clinical applications.

9.4 Antimicrobial Photodynamic Therapy Capability Against Oral Bacteria

This initial prototype has only been tested on model strains of planktonic bacteria during this study. Prior to commercialisation, there is a need to confirm that the product is also effective against biofilms of anaerobic oral bacteria commonly found in oral infections. These could include *P. gingivalis* which is known to be involved in the progression of periodontal diseases^[287]. However, there are already a vast amount of studies published on the use of aPDT with MB to deactivate biofilms, so this study will be to confirm the model system is effective at delivery of the PS as opposed to the efficacy of the PS itself^[279,569,570].

9.5 Sterilisation Methods

It is vital that any regenerative medical device to be made commercially available can be proven to be sterile. In this thesis, disinfection was achieved via UV-treatment of the scaffolds. This proved to be effective for the purpose of the *in vitro* studies, evidenced by the cell growth observed via SEM (section 7.3.1.2). However, although UV-treatment is known for disinfection^[571], it is not approved as a sterilisation method in industrial applications. Alternative suitable sterilisation techniques commonly used in the medical device industry include heat treatment, gamma irradiation, electron beam irradiation, plasma treatment or ethylene oxide chemical treatment. Dai *et al* published a comprehensive review on these techniques and the consequences of use with biodegradable polymers^[572]. This review concludes that there is no ideal sterilisation technique currently available, so one should be selected with the minimal structural effects on the scaffold. Gamma or electron beam irradiation could be potentially suitable techniques due to the low temperature and the ability to control the lack of residual particles from these methods.

An additional consideration is that sterilisation of polymer scaffolds is known to lead to changes in the mechanical properties^[572–574]. Therefore, following the selection of a suitable sterilisation technique, the mechanical properties as well as the resulting degradation and PS release profiles of the

post-sterilised scaffolds should be reanalysed to ensure that the scaffolds are still suitable for the intended application.

9.5.1 Additional Use in Chronic Wound Applications

Chronic wounds are commonly defined as topical skin wounds which have not healed after 4-6 weeks^[575]. It is estimated that 2.2 million people per year in the UK need treatments for chronic wounds, costing the NHS £5.3 billion^[576]. Infection in chronic wounds is a frequent complication, and prevents the wound from healing^[575]. As this device aims to regenerate soft tissue whilst treating localised infections, the prototype produced from this research project could be expanded for use in chronic wounds as well. A research project at the University of Bradford has recently been performed with the same product concept but with the intended application of skin regeneration in chronic wounds.

Chapter 10 Conclusions

To conclude this thesis, the initial table of characteristics (**Table 2.1**) was re-examined to determine whether the development and characterisation of a prototype device has been achieved (**Table 10.1**).

Scaffold Characteristic	Achieved?
Fibrous and porous	Yes – section 6.3.2.2
Appropriate mechanical properties for the oral mucosa (e.g. elastic modulus of 0.9-11 MPa ^[388])	Yes – section 6.3.2.2
Capable of loading PS and releasing steadily over 4 weeks	Yes – section 6.3.2.3
Demonstrates stability and maintains porous structure in aqueous environments	Yes – section 6.3.2.3
Maintains integrity up to 8 weeks	Yes – section 6.3.2.3
<30% cytotoxicity to mammalian cells in dark or light conditions	Yes – section 7.3.1
Minimal bactericidal activity in dark conditions but ability to prevent growth of bacteria upon light activation	Yes – section 7.3.2

Table 10.1 – Summary of scaffold requirements for oral applications

This project has systematically determined a scaffold formulation which demonstrates the desirable characteristics which were initially identified (**Table 2.1**). A promising prototype has been developed which, with the further research described, has the potential to be developed into a commercially relevant medical device capable of improving patient outcomes, benefitting the healthcare economy, and minimising the spread of AMR.

Bibliography

- [1] E. Yuksel, J. Choo, M. Wettergreen, M. Liebschner, *Semin. Plast. Surg.* **2005**, *1*, 261.
- [2] Lady Espinosa, A. Sosnik, M. R. Fontanilla, *Tissue Eng. Part A* **2010**, *16*, 1667.
- [3] I. Wu, Z. Nahas, K. A. Kimmerling, G. D. Rosson, J. H. Elisseeff, *Plast. Reconstr. Surg.* **2012**, *129*, 1247.
- [4] M. T. Nelson, J. P. Keith, B. B. Li, D. L. Stocum, J. Li, *Proc. Inst. Mech. Eng. Part N J. Nanoeng. Nanosyst.* **2012**, *226*, 111.
- [5] F. Qi, T. Yoshida, T. Koike, H. Aizawa, T. Shimane, Y. Li, S. Yamada, M. Okabe, T. Nikaido, H. Kurita, *Arch. Oral Biol.* **2016**, *65*, 26.
- [6] H. M. Powell, D. M. Supp, S. T. Boyce, *Biomaterials* **2008**, *29*, 834.
- [7] C. E. P. Aronin, S. J. Shin, K. B. Naden, P. D. Rios Jr, L. S. Sefcik, S. R. Zawodny, N. D. Bagayoko, Q. Cui, Y. Khan, E. A. Botchwey, *Biomaterials* **2010**, *31*, 6417.
- [8] R. E. Jung, D. S. Thoma, C. H. F. Hammerle, *J. Clin. Periodontol.* **2008**, *35*, 255.
- [9] E. A. Abou Neel, W. Chrzanowski, V. M. Salih, H. W. Kim, J. C. Knowles, *J. Dent.* **2014**, *42*, 915.
- [10] K. Izumi, H. Kato, S. E. Feinberg, *Stem Cell Biol. Tissue Eng. Dent. Sci.* **2015**, 721.
- [11] J. a Aas, B. J. Paster, L. N. Stokes, I. Olsen, F. E. Dewhirst, *J. Clin. Microbiol.* **2005**, *43*, 5721.
- [12] M. Zafar, S. Najeeb, Z. Khurshid, M. Vazirzadeh, S. Zohaib, B. Najeeb, F. Sefat, *Materials (Basel)*. **2016**, *9*, 1.
- [13] O. Camps-Font, R. Figueiredo, E. Valmaseda-Castellón, C. Gay-Escoda, *Implant Dent.* **2015**, *24*, 713.
- [14] M. Godoy-Gallardo, M. C. Manzanares-Céspedes, P. Sevilla, J. Nart, N. Manzanares, J. M. Manero, F. J. Gil, S. K. Boyd, D. Rodríguez, *Mater. Sci. Eng. C* **2016**, *69*, 538.
- [15] A. Y. Hwang, J. G. Gums, *Bioorg. Med. Chem.* **2016**, *24*, 6440.

- [16] C. Nathan, O. Cars, *N. Engl. J. Med.* **2014**, 371, 1761.
- [17] U. S. Barreras, F. T. Méndez, R. E. M. Martínez, C. S. Valencia, P. R. M. Rodríguez, J. P. L. Rodríguez, *Mater. Sci. Eng. C* **2016**, 58, 1182.
- [18] T. Dai, Y. Y. Huang, M. R. Hamblin, *Photodiagnosis Photodyn. Ther.* **2009**, 6, 170.
- [19] C. A. Squier, M. J. Kremer, *J. Natl. Cancer Inst. Monogr.* **2001**, 29, 7.
- [20] O. Zuhr, D. Baumer, M. Hurzeler, *J. Clin. Periodontol.* **2014**, 41, S123.
- [21] S. K. Jindal, M. Kiamehr, W. Sun, X. B. Yang, *Silk Scaffolds for Dental Tissue Engineering*, Woodhead Publishing Limited, **2014**.
- [22] B. Kinikoglu, O. Damour, V. Hasirci, *J. Artif. Organs* **2015**, 18, 8.
- [23] B. Kinikoglu, *Tissue Engineering of Full-Thickness Human Oral Mucosa*, Universite de Lyon, **2010**.
- [24] T. A. Winning, G. C. Townsend, *Clin. Dermatol.* **2000**, 18, 499.
- [25] S. Johnstone, R. M. Logan, *Int. J. Oral Maxillofac. Surg.* **2007**, 36, 263.
- [26] E. L. McGinley, G. P. Moran, G. J. P. Fleming, *J. Dent.* **2013**, 41, 1091.
- [27] I. Atsuta, Y. Ayukawa, R. Kondo, W. Oshiro, Y. Matsuura, A. Furuhashi, Y. Tsukiyama, K. Koyano, *J. Prosthodont. Res.* **2016**, 60, 3.
- [28] R. B. Presland, R. J. Jurevic, *J. Dent. Educ.* **2002**, 66, 564.
- [29] V. F. Patel, F. Liu, M. B. Brown, *J. Control. Release* **2012**, 161, 746.
- [30] H. Inoue, K. Ono, W. Masuda, T. Inagaki, M. Yokota, K. Inenaga, *J. Oral Biosci.* **2008**, 50, 134.
- [31] J. W. Wong, C. Gallant-Behm, C. Wiebe, K. Mak, D. A. Hart, H. Larjava, L. Häkkinen, *Wound Repair Regen.* **2009**, 17, 717.
- [32] P. Batchelor, *Br. Dent. J.* **2014**, 217, 405.
- [33] L. Larsson, A. . Decker, L. Nibali, S. . Pilipchuk, T. Berglundh, W. . Giannobile, *J. Dent. Res.* **2016**, 95, 255.
- [34] D. Kaigler, D. Mooney, *J. Dent. Educ.* **2001**, 65, 456.
- [35] P. A. Mossey, J. Little, R. G. Munger, M. J. Dixon, W. C. Shaw, *Lancet* **2009**, 374, 1773.
- [36] A. Peramo, C. L. Marcelo, S. E. Feinberg, *Tissue Eng. Part C*.

Methods **2012**, *18*, 273.

- [37] M. Rouabhia, P. Allaire, *Biomaterials* **2010**, *31*, 5798.
- [38] E. L. Scheller, P. H. Krebsbach, D. H. Kohn, *J. Oral Rehabil.* **2009**, *36*, 368.
- [39] K. Moharamzadeh, H. Colley, C. Murdoch, V. Hearnden, W. L. Chai, I. M. Brook, M. H. Thornhill, S. MacNeil, *J. Dent. Res.* **2012**, *91*, 642.
- [40] P. E. Bottura, J. Milanezi, L. A. Fernandes, H. C. Caldas, M. Abbud-Filho, V. G. Garcia, M. A. S. F. Baptista, *Transplant. Proc.* **2011**, *43*, 2009.
- [41] T. Crossman, F. Warburton, M. A. Richards, H. Smith, A. Ramirez, L. J. L. Forbes, *Br. J. Oral Maxillofac. Surg.* **2016**, *54*, 208.
- [42] Cancer Research UK, “Oral Cancer Statistics,” can be found under <https://www.cancerresearchuk.org/health-professional/cancer-statistics/statistics-by-cancer-type/head-and-neck-cancers/incidence>, **2013**.
- [43] A. Gulland, *BMJ* **2016**, *355*, i6369.
- [44] M. Belusic-gobic, M. Car, M. Juretic, R. Cerovic, D. Gobic, V. Golubovic, *Oral Oncol.* **2007**, *43*, 77.
- [45] A. S. Waghmare, P. B. Vhanmane, B. Savitha, R. L. Chawla, H. S. Bagde, *J Indian Soc Periodontol* **2013**, *17*, 725.
- [46] A. Benítez-Páez, M. Álvarez, P. Belda-Ferre, S. Rubido, A. Mira, I. Tomás, *PLoS One* **2013**, *8*.
- [47] W. L. Adeyemo, A. A. Ibikunle, O. James, O. A. Taiwo, *J. Maxillofac. Oral Surg.* **2018**, *18*, 40.
- [48] J. Van Dyck, M. Cadenas de Llano-Pérula, G. Willems, A. Verdonck, *Forensic Sci. Int.* **2019**, *300*, 63.
- [49] J. Liu, J. J. Mao, L. Chen, *Tissue Eng. Part B. Rev.* **2011**, *17*, 25.
- [50] K. M. Brouwer, D. M. Lundvig, E. Middelkoop, F. A. Wagener, J. W. Von den Hoff, *Wound Repair Regen* **2015**, *23*, 302.
- [51] H. Algraffee, F. Borumandi, L. Cascarini, *Br. J. Oral Maxillofac. Surg.* **2012**, *50*, 689.
- [52] M. Taghi Chitsazi, B. Adileh Shirmohammadi, B. Reza Pourabbas, B. Nader Abolfazli, B. Ilnaz Farhoudi, B. Behrouz Daghigh Azar, B.

- Farrokh Farhadi, *J. Dent. Res. Dent. Clin Dent Prospect* **2014**, 8, 153.
- [53] P. I. Eke, X. Zhang, H. Lu, L. Wei, G. Thornton-Evans, K. J. Greenlund, J. B. Holt, J. B. Croft, *J. Dent. Res.* **2016**, 95, 515.
- [54] N. Aoyama, N. Kobayashi, T. Hanatani, N. Ashigaki, A. Yoshida, Y. Shiheido, H. Sato, C. Takamura, S. Yoshikawa, K. Matsuo, Y. Izumi, M. Isobe, *J. Periodontal Res.* **2019**, 54, 259.
- [55] S. Wood, D. Metcalf, D. Devine, C. Robinson, *J. Antimicrob. Chemother.* **2006**, 57, 680.
- [56] H. A. Alwaeli, S. N. Al-Khateeb, A. Al-Sadi, *Lasers Med. Sci.* **2015**, 30, 801.
- [57] R. Andersen, N. Loebel, D. Hammond, M. Wilson, *J. Clin. Dent.* **2007**, 18, 34.
- [58] T. Larsen, N. E. Fiehn, *Apmis* **2017**, 125, 376.
- [59] NHS England, *Adult Dental Health Survey (ADHS) - Health and Social Care Information Centre*, **2009**.
- [60] A. Mombelli, N. Müller, N. Cionca, *Clin. Oral Implants Res.* **2012**, 23, 67.
- [61] K. F. B. Payne, I. Balasundaram, S. Deb, L. Di Silvio, K. F. M. Fan, *Br. J. Oral Maxillofac. Surg.* **2014**, 52, 7.
- [62] F. Vohra, M. Q. Al-Rifaiy, G. Lillywhite, M. I. Abu Hassan, F. Javed, *Photochem. Photobiol. Sci.* **2014**, 13, 1160.
- [63] A. Al-Ahmad, C. Tennert, L. Karygianni, K. T. Wrbas, E. Hellwig, M. J. Altenburger, *J. Med. Microbiol.* **2013**, 62, 467.
- [64] R. López-Píriz, B. Cabal, L. Goyos-Ball, A. Fernández, J. F. Bartolomé, J. S. Moya, R. Torrecillas, *J. Biomed. Mater. Res. - Part A* **2019**, 1466.
- [65] L. Ding, P. Zhang, X. Wang, S. Kasugai, *Clin. Implant Dent. Relat. Res.* **2019**, 21, 154.
- [66] S. Llames, I. Recuero, A. Romance, E. Garcia, I. Pena, A. F. Del Valle, A. Meana, F. Larcher, M. Del Rio, *Cleft Palate-Craniofacial J.* **2014**, 51, 246.
- [67] M. Trimarchi, A. Galli, P. Capparè, S. Dababou, R. Vinci, M. Bussi, E. F. Gherlone, *J. Osseointegration* **2019**, 11, 29.

- [68] O. Camps-Font, P. Martín-Fatás, A. Clé-Ovejero, R. Figueiredo, C. Gay-Escoda, E. Valmaseda-Castellón, *J. Periodontol.* **2018**, 89, 1165.
- [69] J. Antonovics, *Glob. Policy* **2014**, 7, 1.
- [70] N. Dar-Odeh, H. Fadel, S. Abu-Hammad, R. Abdeljawad, O. Abu-Hammad, *Antibiotics* **2018**, 7, 38.
- [71] R. Wise, T. Hart, O. Cars, M. Streulens, R. Helmuth, P. Huovinen, M. Sprenger, *BMJ* **1998**, 317, 609.
- [72] P. S. Jorgensen, D. Wernli, *Nature* **2016**, 537, 159.
- [73] Centers for Disease Control and Prevention, *Antibiotic Resistance Threats in the United States, 2013*, **2013**.
- [74] J. O'Neill, *Rev. Antimicrob. Resist.* **2014**, 1.
- [75] S. B. Levy, M. Bonnie, *Nat. Med.* **2004**, 10, S122.
- [76] D. J. Miner, in *Ther. Drug Monit. Toxicol. by Liq. Chromatogr.*, Routledge, New York, **2017**, pp. 269–308.
- [77] H. Ullah, S. Ali, *Classification of Anti-Bacterial Agents and Their Functions*, **2017**.
- [78] P. F. McDermott, R. D. Walker, D. G. White, *Int. J. Toxicol.* **2003**, 22, 135.
- [79] A. H. Holmes, L. S. P. Moore, A. Sundsfjord, M. Steinbakk, S. Regmi, A. Karkey, P. J. Guerin, L. J. V Piddock, *Lancet* **2016**, 387, 176.
- [80] R. Laxminarayan, A. Duse, C. Wattal, A. K. M. Zaidi, H. F. L. Wertheim, N. Sumpradit, E. Vlieghe, G. L. Hara, I. M. Gould, H. Goossens, C. Greko, A. D. So, M. Bigdeli, G. Tomson, W. Woodhouse, E. Ombaka, A. Q. Peralta, *Lancet Infect. Dis.* **2013**, 3099, 1.
- [81] C. A. Michael, D. Dominey-Howes, M. Labbate, *Front. Public Heal.* **2014**, 2, 1.
- [82] C. Deng, X. Chen, H. Yu, J. Sun, T. Lu, X. Jing, *Polymer (Guildf)*. **2007**, 48, 139.
- [83] U. Hersel, C. Dahmen, H. Kessler, *Biomaterials* **2003**, 24, 4385.
- [84] A. Nauta, G. C. Gurtner, M. T. Longaker, *Oral Dis.* **2011**, 17, 541.
- [85] A. Sculean, D. Nikolidakis, F. Schwarz, *J. Clin. Periodontol.* **2008**, 35, 106.

- [86] M. Tallawi, E. Rosellini, N. Barbani, M. G. Cascone, R. Rai, G. Saint-Pierre, A. R. Boccaccini, *J. R. Soc. Interface* **2015**, *12*, 20150254.
- [87] H. Jhaveri-Desai, S. Khetarpal, *J. Healthc. Eng.* **2011**, *2*, 405.
- [88] A. S. Herford, L. Akin, M. Cicciu, C. Maiorana, P. J. Boyne, *J. Oral Maxillofac. Surg.* **2010**, *68*, 1463.
- [89] E. T. Scheyer, M. L. Nevins, R. Neiva, D. L. Cochran, W. V. Giannobile, S. B. Woo, W. N. King, J. K. Spitznagel Jr, D. Bates, M. K. McGuire, *J. Periodontol.* **2014**, *85*, e57.
- [90] C. Luitaud, C. Laflamme, A. Semlali, S. Saidi, G. Grenier, A. Zakrzewski, M. Rouabhia, *J. Biomed. Mater. Res. Part B Appl. Biomater.* **2007**, *83B*, 554.
- [91] R. E. Jung, M. B. Hürzeler, D. S. Thoma, A. Khraisat, *J. Clin. Periodontol.* **2011**, *38*, 173.
- [92] H. M. Jhaveri, M. S. Chavan, G. B. Tomar, V. L. Deshmukh, M. R. Wani, P. D. Miller, *J. Periodontol.* **2010**, *81*, 616.
- [93] Y. Yoshimura, S. Matsuda, S. Obara, *J. Oral Maxillofac. Surg.* **1995**, *53*, 998.
- [94] K. Izumi, H. Terashi, C. L. Marcelo, S. E. Feinberg, *J. Dent. Res.* **2000**, *79*, 798.
- [95] U. K. Nayak, B. Swain, *Indian J Otolaryngol Head Neck Surg* **1997**, *56*, 96.
- [96] D. J. Pearce, R. R. Hall, T. Brown, A. J. McMichael, *J. Dermatolog. Treat.* **2009**, *20*, 149.
- [97] K. Izumi, S. E. Feinberg, H. Terashi, C. L. Marcelo, *Tissue Eng.* **2003**, *9*, 163.
- [98] K. Izumi, S. E. Feinberg, A. Iida, M. Yoshizawa, *Int. J. Oral Maxillofac. Surg.* **2003**, *32*, 188.
- [99] K. K. K. Oo, W. C. Ong, A. H. C. Ang, D. W. Hutmacher, L. K. S. Tan, *Head Neck* **2007**, *29*, 458.
- [100] W. M. W. Tra, J. W. Van Neck, S. E. R. Hovius, G. J. V. M. Van Osch, S. Perez-Amodio, *Cells Tissues Organs* **2012**, *195*, 185.
- [101] M. Yoshizawa, T. Koyama, T. Kojima, H. Kato, Y. Ono, C. Saito, *J. Oral Maxillofac. Surg.* **2012**, *70*, 1199.

- [102] K. Izumi, R. F. Neiva, S. E. Feinberg, *Int. J. Oral Maxillofac. Implants* **2013**, *28*, e295.
- [103] A. P. Vriens, T. Waaijman, H. M. Van Den Hoogenband, E. M. DeBoer, R. J. Scheper, S. Gibbs, *Cell Transplant.* **2008**, *17*, 1199.
- [104] Z. M. Taufique, N. Bhatt, D. Zagzag, R. A. Lebowitz, S. M. Lieberman, *J. Neurol. Surgery, Part B Skull Base* **2018**, *80*, 46.
- [105] F. M. Chen, X. Liu, *Prog. Polym. Sci.* **2016**, *53*, 86.
- [106] F. Winterroth, J. Lee, S. Kuo, J. B. Fowlkes, S. E. Feinberg, S. J. Hollister, K. W. Hollman, *Ann. Biomed. Eng.* **2011**, *39*, 44.
- [107] K. Izumi, G. Takacs, H. Terashi, S. E. Feinberg, *J. Oral Maxillofac. Surg.* **1999**, *57*, 571.
- [108] A. Khmaladze, S. Kuo, R. Y. Kim, R. V. Matthews, C. L. Marcelo, S. E. Feinberg, M. D. Morris, *Tissue Eng. Part C Methods* **2015**, *21*, 46.
- [109] S. Kuo, Y. Zhou, H. M. Kim, H. Kato, R. Y. Kim, G. R. Bayar, C. L. Marcelo, R. T. Kennedy, S. E. Feinberg, *J. Dent. Res.* **2015**, *94*, 78.
- [110] Y. Nakanishi, K. Izumi, M. Yoshizawa, C. Saito, Y. Kawano, T. Maeda, *Int. J. Oral Maxillofac. Surg.* **2007**, *36*, 928.
- [111] R. Ophof, J. C. Maltha, A. M. Kuijpers-Jagtman, J. W. Von Den Hoff, *Eur. J. Orthod.* **2008**, *30*, 1.
- [112] W. M. W. Tra, B. Tuk, J. W. Van Neck, S. E. R. Hovius, S. Perez-Amodio, *Int. J. Oral Maxillofac. Surg.* **2013**, *42*, 939.
- [113] S. MacNeil, *Nature* **2007**, *445*, 874.
- [114] Z. Rong, M. Wang, Z. Hu, M. Stradner, S. Zhu, H. Kong, H. Yi, A. Goldrath, Y. G. Yang, Y. Xu, X. Fu, *Cell Stem Cell* **2014**, *14*, 121.
- [115] S. Köseoğlu, İ. Duran, M. Sağlam, S. B. Bozkurt, O. S. Kırtıloğlu, S. S. Hakki, *J. Periodontol.* **2013**, *84*, 1416.
- [116] S. S. Hakki, P. Korkusuz, N. Purali, B. Bozkurt, M. Kus, I. Duran, *Connect. Tissue Res.* **2013**, *54*, 260.
- [117] I. B. Kar, A. K. Singh, P. C. Mohapatra, P. K. Mohanty, S. Misra, *Int. J. Oral Maxillofac. Surg.* **2014**, *43*, 1339.
- [118] K. M. Ahn, J. H. Lee, S. J. Hwang, P. H. Choung, M. J. Kim, H. J. Park, J. K. Park, J. Jahng, E. K. Yang, *Artif. Organs* **2006**, *30*, 411.
- [119] M. A. Maksoud, K. A. Guze, *Clin. Adv. Periodontics* **2018**, *8*, 111.

- [120] D. Flesch, E. Frerick-Ochs, C. Pfeifer, R. E. Unger, A. Schröder, R. Stein, J. W. Thüroff, W. Brenner, *J. Urol.* **2012**, *187*, e301.
- [121] F. Camacho-Alonso, M. R. Torralba-Ruiz, N. García-Carrillo, J. Lacal-Luján, F. Martínez-Díaz, M. Sánchez-Siles, *Clin. Oral Investig.* **2019**, *23*, 2083.
- [122] X. Labres, A. Camps, *Biomimetics Biomater. Tissue Eng.* **2014**, *19*, 1.
- [123] K. A. Blackwood, R. McKean, I. Canton, C. O. Freeman, K. L. Franklin, D. Cole, I. Brook, P. Farthing, S. Rimmer, J. W. Haycock, A. J. Ryan, S. MacNeil, *Biomaterials* **2008**, *29*, 3091.
- [124] Y. Ikada, H. Tsuji, *Macromol. Rapid Commun.* **2000**, *21*, 117.
- [125] M. Hasan, K. A. Nayem, M. B. Hossain, S. Nahar, *Int. J. Text. Sci.* **2014**, *3*, 39.
- [126] R. Onnainty, B. Onida, P. Páez, M. Longhi, A. Barresi, G. Granero, *Int. J. Pharm.* **2016**, *509*, 408.
- [127] B. Kinikoglu, J. C. Rodriguez-Cabello, O. Damour, V. Hasirci, *Biomaterials* **2011**, *32*, 5756.
- [128] M. K. McGuire, E. T. Scheyer, *J. Periodontol.* **2014**, *85*, 1333.
- [129] M. K. McGuire, E. T. Scheyer, M. E. Nunn, P. T. Lavin, *J. Periodontol.* **2008**, *79*, 1847.
- [130] I. Milinkovic, Z. Aleksic, S. Jankovic, O. Popovic, M. Bajic, S. Cakic, V. Lekovic, *J. Periodontal Res.* **2015**, *50*, 363.
- [131] S. Rastogi, M. Modi, B. Sathian, *J. Oral Maxillofac. Surg.* **2009**, *67*, 1600.
- [132] P. F. Nocini, G. Zanotti, R. Castellani, S. Grasso, M. G. Cristofaro, D. De Santis, *Clin. Oral Implants Res.* **2013**, *24*, 612.
- [133] M. . McGuire, M. . Nunn, *J. Periodontol.* **2005**, *76*, 867.
- [134] T. Almela, I. M. Brook, K. Moharamzadeh, *J. Mater. Sci. Mater. Med.* **2016**, *27*, 1.
- [135] K. H. Lee, B. O. Kim, H. S. Jang, *J. Periodontal Implant Sci.* **2010**, *40*, 96.
- [136] K. Moharamzadeh, I. M. Brook, R. Van Noort, A. M. Scutt, K. G. Smith, M. H. Thornhill, *J. Mater. Sci. Mater. Med.* **2008**, *19*, 1793.
- [137] U. Kriegebaum, M. Mildenberger, U. D. A. Mueller-Richter, U.

Klammert, A. C. Kuebler, T. Reuther, *Oral Surg. Oral Med. Oral Pathol. Oral Radiol.* **2012**, *114*, S190.

- [138] M. L. Nevins, *Int. J. Periodontics Restorative Dent.* **2010**, *30*, 31.
- [139] B. Kinikoglu, C. Auxenfans, P. Pierrillas, V. Justin, P. Breton, C. Burillon, V. Hasirci, O. Damour, *Biomaterials* **2009**, *30*, 6418.
- [140] M. Terada, K. Izumi, H. Ohnuki, T. Saito, H. Kato, M. Yamamoto, Y. Kawano, K. Nozawa-Inoue, H. Kashiwazaki, T. Ikoma, J. Tanaka, T. Maeda, *J. Biomed. Mater. Res. - Part B Appl. Biomater.* **2012**, *100 B*, 1792.
- [141] P. A. Golinski, S. Groger, J. M. Herrmann, A. Bernd, J. Meyle, *J. Periodontal Res.* **2011**, *46*, 704.
- [142] G. Lotfi, M. A. Shokrgozar, R. Mofid, F. M. Abbas, F. Ghanavati, A. A. Bagheban, R. P. Shariati, *J. Periodontol.* **2011**, *82*, 1367.
- [143] J. D. Schiffman, C. L. Schauer, *Biomacromolecules* **2007**, *8*, 2665.
- [144] F. Croisier, C. Jérôme, *Eur. Polym. J.* **2013**, *49*, 780.
- [145] A. Sachar, A. T. Strom, S. San Miguel, M. J. Serrano, K. K. H. Svoboda, X. Liu, *J. Tissue Eng. Regen. Med.* **2014**, *8*, 862.
- [146] R. Fernández-Valadés-Gámez, I. Garzón, E. Liceras-Liceras, A. España-López, V. Carriel, M.-Á. Martín-Piedra, M.-Á. Muñoz-Miguelsanz, M.-C. Sánchez-Quevedo, M. Alaminos, R. Fernández-Valadés, *Biomed. Mater.* **2016**, *11*.
- [147] I. Pena, L. M. Junquera, A. Meana, E. Garcia, C. Aguilar, M. F. Fresno, *J. Periodontal Res.* **2011**, *46*, 214.
- [148] I. Garzón, M. C. Sánchez-Quevedo, G. Moreu, M. González-Jaranay, M. González-Andrades, A. Montalvo, A. Campos, M. Alaminos, *J. Periodontal Res.* **2009**, *44*, 588.
- [149] M. Alaminos, I. Garzon, M. . Sanchez-Quevedo, G. Moreu, M. Gonzalez-Andrades, A. Fernandez-Montoya, A. Campos, *J. Tissue Eng. Regen. Med.* **2007**, *1*, 350.
- [150] M. C. Sanchez-Quevedo, M. Alaminos, L. M. Capitan, G. Moreu, I. Garzon, P. V. Crespo, A. Campos, *Histol. Histopathol.* **2007**, *22*, 631.
- [151] J. M. Viñuela-Prieto, M. C. Sánchez-Quevedo, C. A. Alfonso-Rodríguez, A. C. Oliveira, G. Scionti, M. A. Martín-Piedra, G. Moreu,

- A. Campos, M. Alaminos, I. Garzón, *J. Periodontal Res.* **2015**, *50*, 658.
- [152] Y. Li, H. Meng, Y. Liu, B. P. Lee, *Sci. World J.* **2015**, 2015.
- [153] R. Sieira Gil, C. M. Pages, E. G. Diez, S. Llamas, A. F. Fuertes, J. L. Vilagran, *J. Oral Maxillofac. Surg.* **2015**, *73*, 195.e1.
- [154] A. Göpferich, *Biomaterials* **1996**, *17*, 103.
- [155] N. Salehi-Nik, M. Rezai Rad, P. Nazeman, A. Khojasteh, *Polymers for Oral and Dental Tissue Engineering*, Elsevier, **2017**.
- [156] M. Martín-Del-Campo, R. Rosales-Ibañez, L. Rojo, *Int. J. Mol. Sci.* **2019**, *20*.
- [157] R. Conte, A. Di Salle, F. Riccitiello, O. Petillo, G. Peluso, A. Calarco, *AIMS Mater. Sci.* **2018**, *5*, 1073.
- [158] B. Mijovic, M. T. Trcin, A. Agic, E. Zdraveva, M. Bujic, I. Spoljaric, V. Kosec, *J. Fiber Bioeng. Informatics* **2012**, *5*, 33.
- [159] W. Yao, P. Xu, J. Zhao, L. Ling, X. Li, B. Zhang, N. Cheng, Z. Pang, *J. Colloid Interface Sci.* **2015**, *458*, 14.
- [160] Y. Shin, J. Lee, L. Jin, M. Kim, J.-W. Oh, T. Kim, D.-W. Han, *Biomater. Res.* **2014**, *18*, 14.
- [161] S. H. Lee, H. M. Chung, Y. H. Kim, S. H. Kim, *Key Eng. Mater.* **2007**, *342–343*, 157.
- [162] E. Ruoslahti, *Annu. Rev. Cell Dev. Biol.* **1996**, *12*, 697.
- [163] T. Boxus, R. Touillaux, G. Dive, J. Marchand-Brynaert, *Bioorganic Med. Chem.* **1998**, *6*, 1577.
- [164] Z. Zhang, Y. Lai, L. Yu, J. Ding, *Biomaterials* **2010**, *31*, 7873.
- [165] F. Danhier, V. Pourcelle, J. Marchand-Brynaert, C. Jérôme, O. Feron, V. Préat, *Methods Enzymol.* **2012**, *508*, 157.
- [166] W. B. Tsai, Y. R. Chen, H. L. Liu, J. Y. Lai, *Carbohydr. Polym.* **2011**, *85*, 129.
- [167] R. A. Stile, K. E. Healy, *Biomacromolecules* **2001**, *2*, 185.
- [168] P. Y. Wang, T. H. Wu, W. B. Tsai, W. H. Kuo, M. J. Wang, *Colloids Surfaces B Biointerfaces* **2013**, *110*, 88.
- [169] L. Bosworth, S. Downes, *Electrospinning for Tissue Regeneration*, Woodhead Publishing Limited, **2011**.

- [170] B. Buurma, K. Gu, R. B. Rutherford, *Eur. J. Oral Sci.* **1999**, *107*, 282.
- [171] J. W. C. Cheung, E. E. Rose, J. Paul Santerre, *Acta Biomater.* **2013**, *9*, 6867.
- [172] P. H. Blit, Y. H. Shen, M. J. Ernsting, K. A. Woodhouse, J. P. Santerre, *J. Biomed. Mater. Res. - Part A* **2010**, *94*, 1226.
- [173] C. Zandén, N. Hellström Erkenstam, T. Padel, J. Wittgenstein, J. Liu, H. G. Kuhn, *Nanomedicine Nanotechnology, Biol. Med.* **2014**, *10*, 949.
- [174] P. Gunatillake, R. Mayadunne, R. Adhikari, *Biotechnol. Annu. Rev.* **2006**, *12*, 301.
- [175] Z. Xie, X. Hu, X. Guan, J. Li, Q. Pei, M. Liu, X. Jing, *Chem. Commun.* **2014**, *9*, 2731.
- [176] S. A. Bencherif, T. M. Braschler, P. Renaud, *J. Periodontal Implant Sci.* **2013**, *43*, 251.
- [177] W. Fu, W. Liu, B. Feng, R. Hu, H. X, H. Wang, M. Yin, H. Huang, H. Zhang, W. Wang, *Int. J. Nanomedicine* **2014**, *9*, 2335.
- [178] S. Schulz, M. Angarano, M. Fabritius, R. Mülhaupt, M. Dard, M. Obrecht, P. Tomakidi, T. Steinberg, *Tissue Eng. Part A* **2014**, *20*, 1935.
- [179] P. Denis, J. Dulnik, P. Sajkiewicz, *Int. J. Polym. Mater. Polym. Biomater.* **2015**, *64*, 354.
- [180] F. J. O'Brien, *Mater. Today* **2011**, *14*, 88.
- [181] E. D. Boland, T. A. Telemeco, D. G. Simpson, G. E. Wnek, G. L. Bowlin, *J. Biomed. Mater. Res. - Part B Appl. Biomater.* **2004**, *71*, 144.
- [182] V. Karageorgiou, D. Kaplan, *Biomaterials* **2005**, *26*, 5474.
- [183] H.-I. Chang, Y. Wang, in *Regen. Med. Tissue Eng. - Cells Biomater.* (Ed: D. Eberli), InTech, **2011**, pp. 569–588.
- [184] K. O. van der Werf, C. Jérôme, A. F. Léonard, A.-S. Duwez, P. J. Dijkstra, F. Croisier, M. L. Bennink, *Acta Biomater.* **2012**, *8*, 218.
- [185] N. Bhardwaj, S. C. Kundu, *Biotechnol. Adv.* **2010**, *28*, 325.
- [186] S. Şenel, G. İkinci, S. Kaş, A. Yousefi-Rad, M. F. Sargon, A. A. Hincal, *Int. J. Pharm.* **2000**, *193*, 197.
- [187] A. Repanas, S. Andriopoulou, B. Glasmacher, *J. Drug Deliv. Sci. Technol.* **2016**, *31*, 137.

- [188] M. P. Messenger, P. E. Tomlins, *Adv. Mater.* **2011**, 23, DOI 10.1002/adma.201100254.
- [189] S. Inayat-Hussain, N. F. Rajab, E. L. Siew, *In Vitro Testing of Biomaterials Toxicity and Biocompatibility*, Woodhead Publishing Limited, **2008**.
- [190] W. Li, J. Zhou, Y. Xu, *Biomed. Reports* **2015**, 3, 617.
- [191] International Organization for Standardization, *ISO 10993 Biological Evaluation of Medical Devices — Part 1: Evaluation and Testing within a Risk Management Process*, **2009**.
- [192] International Organization for Standardization, *ISO 10993 Biological Evaluation of Medical Devices — Part 5: Tests for in Vitro Cytotoxicity*, **2009**.
- [193] M. T. Arafat, G. Tronci, J. Yin, D. J. Wood, S. J. Russell, *Polym. (United Kingdom)* **2015**, 77, 102.
- [194] B. Parrish, R. B. Breitenkamp, T. Emrick, *J. Am. Chem. Soc.* **2005**, 127, 7404.
- [195] S. B. MacKintosh, L. P. Serino, P. D. Iddon, R. A. Brown, R. S. Conlan, C. Wright, T. G. Maffei, M. J. Raxworthy, I. M. Sheldon, *Biofabrication* **2015**, 7, 25010.
- [196] K. W. Ng, W. Tham, T. C. Lim, D. W. Huttmacher, *J. Biomed. Mater. Res. - Part A* **2005**, 75, 425.
- [197] Promega, *Data Sheet* **2013**, 138, 1.
- [198] A. M. Pabst, A. Happe, A. Callaway, T. Ziebart, S. I. Stratul, M. Ackermann, M. A. Konerding, B. Willershausen, A. Kasaj, *J. Periodontal Res.* **2014**, 49, 371.
- [199] K. Izumi, J. Song, S. E. Feinberg, *Cells Tissues Organs* **2004**, 176, 134.
- [200] B. D. Ulery, L. S. Nair, C. T. Laurencin, *J. Environ. Polym. Degrad.* **1993**, 1, 65.
- [201] A. Sadeghi-Avalshahr, S. Nokhasteh, A. M. Molavi, M. Khorsand-Ghayeni, M. Mahdavi-Shahri, *Regen. Biomater.* **2017**, 4, 309.
- [202] L. Xiao, B. Wang, G. Yang, M. Gauthier, *Biomed. Sci. Eng. Technol.* **2006**, 247.

- [203] H. . Makadia, S. . Siegel, *Polymers (Basel)*. **2011**, 3, 1377.
- [204] J. R. Jones, *Mater. Today* **2006**, 9, 34.
- [205] S. J. Lee, J. S. Choi, K. S. Park, G. Khang, Y. M. Lee, H. B. Lee, *Biomaterials* **2004**, 25, 4699.
- [206] J. K. Hong, J. Y. Bang, G. Xu, J. H. Lee, Y. J. Kim, H. J. Lee, H. S. Kim, S. M. Kwon, *Int. J. Nanomedicine* **2015**, 10, 1189.
- [207] T. C. Von Erlach, S. Bertazzo, M. A. Wozniak, C. M. Horejs, S. A. Maynard, S. Attwood, B. K. Robinson, H. Autefage, C. Kallepitis, A. Del Río Hernández, C. S. Chen, S. Goldoni, M. M. Stevens, *Nat. Mater.* **2018**, 17, 237.
- [208] C. M. Madl, B. L. Lesavage, R. E. Dewi, C. B. Dinh, R. S. Stowers, M. Khariton, K. J. Lampe, D. Nguyen, O. Chaudhuri, A. Enejder, S. C. Heilshorn, *Nat. Mater.* **2017**, 16, 1233.
- [209] Y. C. Yeh, J. Y. Ling, W. C. Chen, H. H. Lin, M. J. Tang, *Sci. Rep.* **2017**, 7, 1.
- [210] R. A. D'Sa, G. A. Burke, B. J. Meenan, *J. Mater. Sci. Mater. Med.* **2010**, 21, 1703.
- [211] J. Boekhoven, C. M. Rubertpérez, S. Sur, A. Worthy, S. I. Stupp, *Angew. Chemie - Int. Ed.* **2013**, 52, 12077.
- [212] I. Engelberg, J. Kohn, *Biomaterials* **1991**, 12, 292.
- [213] C. Engineer, J. Parikh, A. Raval, *Trends Biomater. Artif. Organs* **2011**, 25, 79.
- [214] I. Grizzi, H. Garreau, S. Li, M. Vert, *Biomaterials* **1995**, 16, 305.
- [215] E. J. Semler, J. S. Tjia, P. V Moghe, *Biotechnol. Prog.* **1997**, 13, 630.
- [216] O. L. Padilla De Jesus, H. R. Ihre, L. Gagne, J. M. J. Frechet, F. C. Szoka, *Bioconjug. Chem.* **2002**, 13, 453.
- [217] A. L. Sisson, M. Schroeter, A. Lendlein, *Polyesters*, John Wiley & Sons, **2011**.
- [218] H. Sun, L. Mei, C. Song, X. Cui, P. Wang, *Biomaterials* **2006**, 27, 1735.
- [219] S. Lyu, D. Untereker, *Int. J. Mol. Sci.* **2009**, 10, 4033.
- [220] S. K. Pandey, D. K. Patel, A. K. Maurya, R. Thakur, D. P. Mishra, M. Vinayak, C. Haldar, P. Maiti, *Int. J. Biol. Macromol.* **2016**, 89, 99.

- [221] Y. Han, D. Tang, G. Wang, Y. Zhang, Y. Guo, H. Zhou, W. Qiu, T. Zhao, *Polymer (Guildf)*. **2019**, 173, 88.
- [222] J. P. Chesterman, T. C. Hughes, B. G. Amsden, *Eur. Polym. J.* **2018**, 105, 186.
- [223] T. Fan, W. Ye, B. Du, Q. Zhang, L. Gong, J. Li, S. Lin, Z. Fan, Q. Liu, *J. Appl. Polym. Sci.* **2019**, 136, 47887.
- [224] S. Kavesh, J. M. Schultz, *Polym. Eng. Sci.* **1969**, 9, 452.
- [225] G. Allen, *Eur. Rev.* **1993**, 1, 197.
- [226] A. A. Aly, *Int. J. Mater. Chem. Phys.* **2015**, 1, 132.
- [227] M. Sandor, N. A. Bailey, E. Mathiowitz, *Polymer (Guildf)*. **2002**, 43, 279.
- [228] L. H. Silverstein, G. M. Kurtzman, P. C. Shatz, *J. Oral Implantol.* **2009**, 35, 82.
- [229] X. Zong, S. Ran, K. S. Kim, D. Fang, B. S. Hsiao, B. Chu, *Biomacromolecules* **2003**, 4, 416.
- [230] A. C. R. Grayson, G. Voskerician, A. Lynn, J. M. Anderson, M. J. Cima, R. Langer, *J. Biomater. Sci. Polym. Ed.* **2004**, 15, 1281.
- [231] X. Liu, S. G. Baldursdottir, J. Aho, H. Qu, L. P. Christensen, J. Rantanen, M. Yang, *Pharm. Res.* **2017**, 34, 738.
- [232] R. a Miller, J. M. Brady, D. E. Cutright, *J. Biomed. Mater. Res.* **1977**, 11, 711.
- [233] S. M. Li, G. M. Vert, *J. Mater. Sci. Mater. Med.* **1990**, 1, 131.
- [234] A. Abdal-hay, K. A. Khalil, A. S. Hamdy, F. F. Al-Jassir, *Arab. J. Chem.* **2017**, 10, 240.
- [235] S. Moscato, L. Mattii, D. D'Alessandro, M. G. Cascone, L. Lazzeri, L. P. Serino, A. Dolfi, N. Bernardini, *Micron* **2008**, 39, 569.
- [236] V. H. Fragal, D. M. Catori, E. H. Fragal, F. P. Garcia, C. V. Nakamura, A. F. Rubira, R. Silva, *J. Colloid Interface Sci.* **2019**, 547, 78.
- [237] E. Ron, T. Turek, E. Mathiowitz, M. Chasin, M. Hageman, R. Langer, *Proc. Natl. Acad. Sci. U. S. A.* **1993**, 90, 4176.
- [238] D. Liang, B. S. Hsiao, B. Chu, *Drug Deliv.* **2009**, 59, 1392.
- [239] K. Leja, G. Lewandowicz, *Polish J. Environ. Stud.* **2010**, 19, 255.
- [240] M. A. Tracy, K. L. Ward, L. Firouzabadian, Y. Wang, N. Dong, R. Qian,

- Y. Zhang, *Biomaterials* **1999**, *20*, 1057.
- [241] A. Askadskii, M. Popova, T. Matseevich, E. Afanasyev, *Adv. Mater. Res.* **2013**, *864–867*, 640.
- [242] S. Maïza, X. Lefebvre, M. Klopffer, L. Cangémi, S. Castagnet, *J. Appl. Polym. Sci.* **2019**, *136*, 47628.
- [243] S. R. Baker, S. Banerjee, K. Bonin, M. Guthold, *Mater. Sci. Eng. C* **2016**, *59*, 203.
- [244] A. B. Hegge, T. Andersen, J. E. Melvik, S. Kristensen, H. H. Tønnesen, *J. Pharm. Sci.* **2010**, *99*, 3499.
- [245] X. Zong, S. Li, E. Chen, B. Garlick, K.-S. Kim, D. Fang, J. Chiu, T. Zimmerman, C. Brathwaite, B. S. Hsiao, B. Chu, *Ann. Surg.* **2004**, *240*, 910.
- [246] C. Green, *PhotoTherix Concept Definition - BITECIC*, **2011**.
- [247] C. Cavallari, P. Brigidi, A. Fini, *Int. J. Pharm.* **2015**, *496*, 593.
- [248] Q. Pham, U. Sharma, A. Mikos, *Tissue Eng.* **2006**, *12*, 1.
- [249] I. Jun, H. S. Han, J. R. Edwards, H. Jeon, *Int. J. Mol. Sci.* **2018**, *19*.
- [250] V. Sankar, V. Hearnden, K. Hull, D. V. Juras, M. Greenberg, A. Kerr, P. Lockhart, L. Patton, S. Porter, M. Thornhill, *Oral Dis.* **2011**, *17*, 73.
- [251] C. Paderni, D. Compilato, L. I. Giannola, G. Campisi, *Oral Surg. Oral Med. Oral Pathol. Oral Radiol.* **2012**, *114*, e25.
- [252] A. K. Mathew, *Pharm. Pharmacol. Res.* **2015**, *3*, 1.
- [253] A. K. Sah, M. Dewangan, P. K. Suresh, *Colloids Surfaces B Biointerfaces* **2019**, *178*, 185.
- [254] K. Kim, Y. K. Luu, C. Chang, D. Fang, B. S. Hsiao, B. Chu, M. Hadjiargyrou, *J. Control. Release* **2004**, *98*, 47.
- [255] E. A. Münchow, M. T. P. Albuquerque, B. Zero, K. Kamocki, E. Piva, R. L. Gregory, M. C. Bottino, *Dent. Mater.* **2015**, *31*, 1038.
- [256] K. Ye, H. Kuang, Z. You, Y. Morsi, X. Mo, *Pharmaceutics* **2019**, *11*, 182.
- [257] F. R. Boroojeni, S. Mashayekhan, H. A. Abbaszadeh, *Iran. J. Pharm. Res.* **2019**, *18*, 111.
- [258] N. Pan, J. Qin, Y. Fan, Z. Li, B. Song, *J. Appl. Polym. Sci.* **2019**, *47922*, 1.

- [259] C. Hu, W. Cui, *Adv. Healthc. Mater.* **2012**, *1*, 809.
- [260] G. Lauer, R. Schimming, *J. Oral Maxillofac. Surg.* **2001**, *59*, 169.
- [261] S. Ravichandran, J. Radhakrishnan, P. Jayabal, G. D. Venkatasubbu, *Appl. Surf. Sci.* **2019**, *484*, 676.
- [262] E. Mathiowitz, D. M. Lavin, R. A. Hopkins, *Ther. Deliv.* **2013**, *4*, 1075.
- [263] A. Fuchs, A. Youssef, A. Seher, S. Hartmann, R. C. Brands, U. D. A. Müller-Richter, A. C. Kübler, C. Linz, *J. Cranio-Maxillofacial Surg.* **2019**, *47*, 695.
- [264] Z. K. Nagy, A. Balogh, G. Dravavolgyi, J. Ferguson, H. Pataki, B. Vajna, G. Marosi, *J. Pharm. Sci.* **2013**, *102*, 508.
- [265] H. Albetran, Y. Dong, I. M. Low, *J. Asian Ceram. Soc.* **2015**, *3*, 292.
- [266] J. Vonch, A. Yarin, C. M. Megaridis, *J. Undergrad. Res.* **2007**, *1*, 1.
- [267] Lord Rayleigh, *London, Edinburgh Dublin Philos. Mag. J. Sci.* **1882**, *14*, 184.
- [268] T. Subbiah, G. S. Bhat, R. W. Tock, S. Parameswaran, S. S. Ramkumar, *J. Appl. Polym. Sci.* **2005**, *96*, 557.
- [269] G. Taylor, *Proc. R. Soc. London, Ser. A, Math. Phys. Sci.* **1969**, *313*, 453.
- [270] D. H. Reneker, I. Chun, *Nanotechnology* **1996**, *7*, 216.
- [271] Y. M. Shin, M. M. Hohman, M. P. Brenner, G. C. Rutledge, *Appl. Phys. Lett.* **2001**, *78*, 1149.
- [272] M. G. McKee, G. L. Wilkes, R. H. Colby, T. E. Long, *Macromolecules* **2004**, *37*, 1760.
- [273] J. . Deitzel, J. Kleinmeyer, D. Harris, N. . Beck Tan, *Polymer (Guildf).* **2001**, *42*, 261.
- [274] S. L. Shenoy, W. D. Bates, H. L. Frisch, G. E. Wnek, *Polymer (Guildf).* **2005**, *46*, 3372.
- [275] B. A. Miller-Chou, J. L. Koenig, *Prog. Polym. Sci.* **2003**, *28*, 1223.
- [276] W.-E. Teo, R. Inai, S. Ramakrishna, *Sci. Technol. Adv. Mater.* **2011**, *12*, 013002.
- [277] C. J. Luo, M. Nangrejo, M. Edirisinghe, *Polymer (Guildf).* **2010**, *51*, 1654.
- [278] H. Li, W. Yang, in *Non-Woven Fabr.*, InTech Open, **2016**, pp. 33–54.

- [279] C. R. Fontana, A. D. Abernethy, S. Som, K. Ruggiero, S. Doucette, R. C. Marcantonio, C. I. Boussios, R. Kent, J. M. Goodson, A. C. R. Tanner, N. S. Soukos, *J. Periodontal Res.* **2009**, *44*, 751.
- [280] A. C. Voos, S. Kranz, S. Tonndorf-Martini, A. Voelpel, H. Sigusch, H. Staudte, V. Albrecht, B. W. Sigusch, *Lasers Surg. Med.* **2014**, *46*, 235.
- [281] F. Cieplik, D. Deng, W. Crielaard, W. Buchalla, E. Hellwig, A. Al-Ahmad, T. Maisch, *Crit. Rev. Microbiol.* **2018**, *44*, 1.
- [282] A. H. Teixeira, E. S. Pereira, L. K. A. Rodrigues, D. Saxena, S. Duarte, I. C. J. Zanin, *Caries Res.* **2012**, *46*, 549.
- [283] P. D. Marsh, A. Moter, D. A. Devine, *Periodontol. 2000* **2011**, *55*, 16.
- [284] N. Kashef, Y.-Y. Huang, M. R. Hamblin, *Nanophotonics* **2017**, *6*, 853.
- [285] F. Sperandio, Y.-Y. Huang, M. Hamblin, *Recent Pat. Antiinfect. Drug Discov.* **2013**, *8*, 108.
- [286] J. Walther, M. J. Bröcker, D. Wätzlich, M. Nimtz, M. Rohde, D. Jahn, J. Moser, *FEMS Microbiol. Lett.* **2009**, *290*, 156.
- [287] E.-M. Decker, V. Bartha, C. Von Ohle, *Photomed. Laser Surg.* **2017**, *35*, 1.
- [288] S. Jin, K. Li, C. Xia, J. Li, *Ind. Crops Prod.* **2019**, *135*, 271.
- [289] M. Cobos, I. De-La-Pinta, G. Quindós, M. J. Fernández, M. D. Fernández, *Carbon N. Y.* **2019**, *150*, 101.
- [290] B. Christianah Adebayo-Tayo, S. A. Inem, O. A. Olaniyi, *Int. J. Nano Dimens* **2019**, *10*, 37.
- [291] K. R. Zodrow, J. D. Schiffman, M. Elimelech, *Langmuir* **2012**, *28*, 13993.
- [292] K. A. Rieger, N. P. Birch, J. D. Schiffman, *Carbohydr. Polym.* **2016**, *139*, 131.
- [293] K. A. Rieger, N. M. Eagan, J. D. Schiffman, *J. Appl. Polym. Sci.* **2015**, *132*, 1.
- [294] S. E. L. Bulman, G. Tronci, P. Goswami, C. Carr, S. J. Russell, *Materials (Basel)*. **2017**, *10*.
- [295] C. P. Churchward, R. G. Alany, L. A. S. Snyder, *Crit. Rev. Microbiol.* **2018**, *44*, 561.

- [296] J. Gajdziok, S. Holešová, J. Štembírek, E. Pazdziora, H. Landová, P. D. D. Vetchý, *Biomed Res. Int.* **2015**, 2015, 1.
- [297] Y.-T. Chen, S.-L. Hung, L.-W. Lin, L.-Y. Chi, L.-J. Ling, *J. Periodontol.* **2003**, 74, 1652.
- [298] G. Keegan, J. Smart, M. Ingram, L. Barnes, G. Rees, G. Burnett, *Int. J. Pharm.* **2007**, 340, 92.
- [299] W. Deng, S. Ning, Q. Lin, H. Zhang, T. Zhou, H. Lin, J. Long, Q. Lin, X. Wang, *Colloids Surfaces B Biointerfaces* **2016**, 144, 196.
- [300] K. H. Hong, *Polym. Eng. Sci.* **2007**, 47, 43.
- [301] M. A. Al-Omair, *Polymers (Basel)*. **2015**, 7, 1464.
- [302] J. M. Corrêa, M. Mori, H. L. Sanches, A. D. Da Cruz, E. Poiate, I. A. V. P. Poiate, *Int. J. Biomater.* **2015**, 2015, 1.
- [303] A. Besinis, T. De Peralta, R. D. Handy, *Nanotoxicology* **2012**, 8, 1.
- [304] M. Grinholc, J. Nakonieczna, G. Fila, A. Taraszkiwicz, A. Kawiak, G. Szewczyk, T. Sarna, L. Lilge, K. P. Bielawski, *Appl. Microbiol. Biotechnol.* **2015**, 99, 4031.
- [305] C. R. L. Leal, L. H. Alvarenga, T. Oliveira-Silva, I. T. Kato, B. Godoy-Miranda, S. K. Bussadori, M. S. Ribeiro, R. A. Prates, *Photodiagnosis Photodyn. Ther.* **2017**, 19, 1.
- [306] M. L. Frade, S. R. de Annunzio, G. M. F. Calixto, F. D. Victorelli, M. Chorilli, C. R. Fontana, *Molecules* **2018**, 23.
- [307] A. W. Smith, *Adv. Drug Deliv. Rev.* **2005**, 57, 1539.
- [308] S. Torres-Giner, M. J. Ocio, J. M. Lagaron, *Carbohydr. Polym.* **2009**, 77, 261.
- [309] G. İkinci, S. Şenel, H. Akincibay, S. Kaş, S. Erciş, C. G. Wilson, A. A. Hincal, *Int. J. Pharm.* **2002**, 235, 121.
- [310] B. K. Choi, K. Y. Kim, Y. J. Yoo, S. J. Oh, J. H. Choi, C. Y. Kim, *Int. J. Antimicrob. Agents* **2001**, 18, 553.
- [311] S. Saengmee-anupharb, T. Srihirin, B. Thaweboon, S. Thaweboon, T. Amornsakchai, S. Dechkunakorn, T. Suddhasthira, *Asian Pac. J. Trop. Biomed.* **2013**, 3, 47.
- [312] SCENIHR, *EU Opinion on Nanosilver: Safety, Health and Environmental Effects and Role in Antimicrobial Resistance*, **2013**.

- [313] S. K. Sharma, P. Mroz, T. Dai, Y. Huang, G. Tyler, *Isr. J. Chem.* **2013**, 52, 691.
- [314] S. Wang, J. Li, Z. Ye, J. Li, A. Wang, J. Hu, S. Bai, J. Yin, *Colloids Surfaces A Physicochem. Eng. Asp.* **2019**, 574, 44.
- [315] D. E. J. G. . Dolmans, D. Fukumura, R. K. Jain, *Nat. Rev. Cancer* **2003**, 3, 380.
- [316] S. Y. Chan, C. T. Pan, Q. Wang, X. H. Shi, J. B. Jonas, W. Bin Wei, *Graefe's Arch. Clin. Exp. Ophthalmol.* **2019**, 1365.
- [317] S. Rajesh, E. Koshi, K. Philip, A. Mohan, *J. Indian Soc. Periodontol.* **2011**, 15, 323.
- [318] J. P. M. L. Rolim, M. A. S. De-Melo, S. F. Guedes, F. B. Albuquerque-Filho, J. R. De Souza, N. A. P. Nogueira, I. C. J. Zanin, L. K. A. Rodrigues, *J. Photochem. Photobiol. B Biol.* **2012**, 106, 40.
- [319] M. N. Alasqah, *Photodiagnosis Photodyn. Ther.* **2019**, 25, 349.
- [320] K. Konopka, T. Goslinski, *J. Dent. Res.* **2007**, 86, 694.
- [321] H. Mahmoudi, A. Bahador, M. Pourhajibagher, M. Y. Alikhani, *J. Lasers Med. Sci.* **2018**, 9, 154.
- [322] N. Kashef, M. R. Hamblin, *Drug Resist. Updat.* **2017**, 31, 31.
- [323] L. Huang, T. Dai, M. R. Hamblin, *Methods Mol. Biol.* **2010**, 635, 155.
- [324] L. Huang, Y. Xuan, Y. Koide, T. Zhiyentayev, *Lasers Surg. Med.* **2013**, 44, 490.
- [325] M. Valko, H. Morris, M. T. D. Cronin, *Curr. Top. Med. Chem.* **2005**, 12, 1161.
- [326] J. Cadet, J. Ravanat, G. R. Martinez, M. H. G. Medeiros, P. Di Mascio, L. Lesions, D. S. N. Cenujf, D. Bioquimica, D. Quimica, U. D. S. Paulo, C. E. P. S. Paulo, *Photochem. Photobiol.* **2006**, 82, 1219.
- [327] J. Moan, K. Berg, *Photochem. Photobiol.* **1991**, 53, 549.
- [328] J. P. Martin, N. Logsdon, *J. Biol. Chem.* **1987**, 262, 7213.
- [329] J. P. Martin Jr., P. E. Burch, *Oxy-Radicals Mol. Biol. Pathol.* **1988**, 256, 39.
- [330] I. Ashur, R. Goldschmidt, I. Pinkas, Y. Salomon, G. Szewczyk, T. Sarna, A. Scherz, *J. Phys. Chem. A* **2009**, 113, 8027.
- [331] P. Mroz, J. Bhaumik, D. K. Dogutan, Z. Aly, Z. Kamal, L. Khalid, H. L.

- Kee, D. F. Bocian, D. Holten, J. S. Lindsey, M. R. Hamblin, *Cancer Lett.* **2009**, *282*, 63.
- [332] T. Maisch, J. Baier, B. Franz, M. Maier, M. Landthaler, R.-M. Szeimies, W. Bäumlner, *Proc. Natl. Acad. Sci. U. S. A.* **2007**, *104*, 7223.
- [333] A. D. Garg, M. Bose, M. I. Ahmed, W. A. Bonass, S. R. Wood, *PLoS One* **2012**, *7*, 1.
- [334] R. D. C. Goulart, G. Thedei, S. L. S. Souza, A. C. Tedesco, P. Ciancaglini, *Photomed. Laser Surg.* **2010**, *28 Suppl 1*, S85.
- [335] J. F. Tahmassebi, E. Drogkari, S. R. Wood, *Eur. Arch. Paediatr. Dent.* **2015**, *16*, 433.
- [336] S. K. Sharma, T. Dai, G. B. Kharkwal, Y.-Y. Huang, L. Huang, V. J. B. De Arce, G. P. Tegos, M. R. Hamblin, *Curr. Pharm. Des.* **2011**, *17*, 1303.
- [337] B. Pourakbari, F. Rezaei, M. Pourhajibagher, N. Hosseini, H. Kazemian, A. Bahador, A. Azizollahi, N. Chiniforush, *Photodiagnosis Photodyn. Ther.* **2018**, *24*, 206.
- [338] A. Simões, B. M. Benites, C. Benassi, G. Torres-Schroter, J. R. de Castro, L. Campos, *Photodiagnosis Photodyn. Ther.* **2017**, *20*, 18.
- [339] I. C. J. Zanin, M. M. Lobo, L. K. A. Rodrigues, L. A. F. Pimenta, J. F. Höfling, R. B. Gonçalves, *Eur. J. Oral Sci.* **2006**, *114*, 64.
- [340] C. Chui, A. Aoki, Y. Takeuchi, Y. Sasaki, K. Hiratsuka, Y. Abiko, Y. Izumi, *J. Periodontal Res.* **2013**, *48*, 696.
- [341] M. A. Castriciano, R. Zagami, M. P. Casaletto, B. Martel, M. Trapani, A. Romeo, V. Villari, M. T. Sciortino, L. Grasso, S. Guglielmino, L. M. Scolaro, A. Mazzaglia, *Biomacromolecules* **2017**, *18*, 1134.
- [342] A. C. B. P. Costa, V. M. Campos Rasteiro, E. S. H. Da Silva Hashimoto, C. F. Araújo, C. A. Pereira, J. C. Junqueira, A. O. C. Jorge, *Oral Surg. Oral Med. Oral Pathol. Oral Radiol.* **2012**, *114*, 67.
- [343] P. J. Rajda, L. Y. Chiang, Y.-Y. Huang, B. Bhayana, T. Sarna, M. R. Hamblin, G. Szewczyk, *Photochem. Photobiol. Sci.* **2019**, *18*, 505.
- [344] P. Mroz, G. P. Tegos, H. Gali, T. Wharton, T. Sarna, M. R. Hamblin, *Photochem Photobiol Sci.* **2007**, *6*, 1139.
- [345] A. Späth, C. Leibl, F. Cieplik, K. Lehner, J. Regensburger, K. A. Hiller,

- W. Bäumlner, G. Schmalz, T. Maisch, *J. Med. Chem.* **2014**, *57*, 5157.
- [346] T. Maisch, A. Eichner, A. Späth, A. Gollmer, B. König, J. Regensburger, W. Bäumlner, *PLoS One* **2014**, *9*, DOI 10.1371/journal.pone.0111792.
- [347] Y. Kuthati, R. K. Kankala, P. Busa, S. X. Lin, J. P. Deng, C. Y. Mou, C. H. Lee, *J. Photochem. Photobiol. B Biol.* **2017**, *169*, 124.
- [348] I. L. Suzuki, N. M. Inada, V. S. Marangoni, T. Q. Correa, *Prog. Biomed. Opt. Imaging* **2016**, *9694*, 1.
- [349] S. Wood, X. Yang, M. De Matas, P. Iddon, M. Raxworthy, *WO2010109226 (A2) Scaffold*, **2010**.
- [350] R. A. Craig, C. P. McCoy, S. P. Gorman, D. S. Jones, *Expert Opin. Drug Deliv.* **2015**, *12*, 85.
- [351] M. R. Hamblin, *Curr. Opin. Microbiol.* **2016**, *33*, 67.
- [352] O. F. Sarioglu, N. O. S. Keskin, A. Celebioglu, T. Tekinay, T. Uyar, *Colloids Surfaces B Biointerfaces* **2017**, *152*, 245.
- [353] A. Aluigi, G. Sotgiu, A. Torreggiani, A. Guerrini, V. T. Orlandi, F. Corticelli, G. Varchi, *ACS Appl. Mater. Interfaces* **2015**, *7*, 17416.
- [354] S. Perni, C. Piccirillo, J. Pratten, P. Prokopovich, W. Chrzanowski, I. P. Parkin, M. Wilson, *Biomaterials* **2009**, *30*, 89.
- [355] P. Tonglairoum, T. Rojanarata, T. Ngawhirunpat, *Adv. Pharmacol. Pharm.* **2017**, *5*, 12.
- [356] R. F. Donnelly, P. A. McCarron, M. M. Tunney, A. David Woolfson, *J. Photochem. Photobiol. B Biol.* **2007**, *86*, 59.
- [357] D. S. Jones, C. J. Lorimer, G. P. Andrews, C. P. McCoy, S. P. Gorman, *Chem. Eng. Sci.* **2007**, *62*, 990.
- [358] G. B. Kharkwal, S. K. Sharma, Y. Huang, T. Dai, *Lasers Surg. Med.* **2012**, *43*, 755.
- [359] F. F. Sperandio, C. P. Sabino, D. Vecchio, M. Garcia-Diaz, L. Huang, Y.-Y. Huang, M. R. Hamblin, *Lasers Dent. Guid. Clin. Pract.* **2015**, *40*.
- [360] F. Giuliani, M. Martinelli, A. Cocchi, D. Arbia, L. Fantetti, G. Roncucci, *Antimicrob. Agents Chemother.* **2010**, *54*, 637.
- [361] M. Merchat, G. Bertolini, P. Giacomini, A. Villanueva, G. Jori, *J. Photochem. Photobiol. B Biol.* **1996**, *32*, 153.

- [362] S. Perni, P. Prokopovich, J. Pratten, I. P. Parkin, M. Wilson, *Photochem. Photobiol. Sci.* **2011**, *10*, 712.
- [363] V. Zand, A. S. Milani, M. Amini, M. H. S. Barhaghi, M. Lotfi, S. Rikhtegaran, A. Sohrabi, *Photomed. Laser Surg.* **2014**, *32*, 245.
- [364] I. C. J. Zanin, R. B. Gonçalves, A. B. Junior, C. K. Hope, J. Pratten, *J. Antimicrob. Chemother.* **2005**, *56*, 324.
- [365] L. P. Rosa, F. C. Da Silva, S. A. Nader, G. A. Meira, M. S. Viana, *Arch. Oral Biol.* **2015**, *60*, 675.
- [366] A. Azizi, Z. Amirzadeh, M. Rezai, S. Lawaf, A. Rahimi, *J. Photochem. Photobiol. B Biol.* **2016**, *158*, 267.
- [367] J. Donso, M. Wilson, *Archs oral Biol.* **1992**, *37*, 883.
- [368] F. Freire, C. Ferraresi, A. O. C. Jorge, M. R. Hamblin, *J. Photochem. Photobiol. B Biol.* **2016**, *159*, 161.
- [369] A. Simões, B. M. Benites, C. Benassi, G. Torres-Schroter, J. R. de Castro, L. Campos, *Photodiagnosis Photodyn. Ther.* **2017**, *20*, 18.
- [370] F. M. Lauro, P. Pretto, L. Covolo, G. Jori, G. Bertoloni, *Photochem. Photobiol. Sci.* **2002**, *1*, 468.
- [371] P. A. Haag, V. Steiger-Ronay, P. R. Schmidlin, *Int. J. Mol. Sci.* **2015**, *16*, 27327.
- [372] M. Petelin, K. Perkič, K. Seme, B. Gašpirc, *Lasers Med. Sci.* **2014**, *30*, 1647.
- [373] A. Sculean, A. Aoki, G. Romanos, F. Schwarz, R. J. Miron, R. Cosgarea, *Dent. Clin. North Am.* **2015**, *59*, 831.
- [374] L. H. Theodoro, A. B. Lopes, M. A. A. Nuernberg, M. M. Cláudio, D. M. J. Miessi, M. L. F. Alves, C. Duque, A. Mombelli, V. G. Garcia, *J. Photochem. Photobiol. B Biol.* **2017**, *174*, 364.
- [375] Y. Wang, Y. Wang, Y. Wang, C. K. Murray, M. R. Hamblin, D. C. Hooper, T. Dai, *Drug Resist. Updat.* **2017**, *33*, 1.
- [376] Z. S. Silva, S. K. Bussadori, K. P. S. Fernandes, Y.-Y. Huang, R. M. Hamblin, *Biosci. Rep.* **2015**, *35*, 1.
- [377] L. Ge, R. Shu, Y. Li, C. Li, L. Luo, Z. Song, Y. Xie, D. Liu, *Photomed. Laser Surg.* **2011**, *29*, 33.
- [378] N. Loebel, V. Benhamou, *Photodiagnosis Photodyn. Ther.* **2011**, *8*,

182.

- [379] S. Noimark, C. W. Dunnill, I. P. Parkin, *Adv. Drug Deliv. Rev.* **2013**, *65*, 570.
- [380] S. J. Bonsor, R. Nichol, T. M. S. Reid, G. J. Pearson, *Br. Dent. J.* **2006**, *200*, 337.
- [381] I. B. Juric, V. Plecko, D. G. Panduric, I. Anic, *Photodiagnosis Photodyn. Ther.* **2014**, *11*, 549.
- [382] D. Vecchio, A. Gupta, L. Huang, G. Landi, P. Avci, A. Rodas, M. R. Hamblin, *Antimicrob. Agents Chemother.* **2015**, *59*, 5203.
- [383] J. Qiao, S. Wang, Y. Wen, H. Jia, *Photodiagnosis Photodyn. Ther.* **2014**, *11*, 290.
- [384] U. D. Ramos, F. A. Suaid, U. M. E. Wikesjö, C. Susin, M. Taba, A. B. Novaes, *Clin. Oral Implants Res.* **2017**, *28*, 1388.
- [385] B. W. Sigusch, S. Dietsch, A. Berg, A. Voelpel, A. Guellmar, U. Rabe, M. Schnabelrauch, D. Steen, B. Gitter, V. Albrecht, D. C. Watts, S. Kranz, *Dent. Mater.* **2018**, *34*, 1542.
- [386] M. Raxworthy, *Perio-STRATeGi Horizon 2020 Application*, York, England, **2014**.
- [387] P. Iddon, S. Wood, L. P. Serino, R. Telford, X. Yang, M. Raxworthy, *Poster Present. Univ. Leeds* **2014**.
- [388] J. Chen, R. Ahmad, W. Li, M. Swain, Q. Li, *J. R. Soc. Interface* **2015**, *12*, 20150325.
- [389] E. Darabpour, N. Kashef, S. Mashayekhan, *Photodiagnosis Photodyn. Ther.* **2016**, *14*, 211.
- [390] Porometer Filter and Membrane Testing Technology, "Assesment of Non-Woven Materials By Capillary Flow Porometry," can be found under <http://www.porometer.com/porometers/application-notes/>, **2016**.
- [391] C. Martins, F. Sousa, F. Araújo, B. Sarmento, *Adv. Healthc. Mater.* **2018**, *7*, 1.
- [392] Y. Xu, C. S. Kim, D. M. Saylor, D. Koo, *J. Biomed. Mater. Res. - Part B Appl. Biomater.* **2017**, *105*, 1692.
- [393] K. Makino, T. Nakajima, M. Shikamura, F. Ito, S. Ando, C. Kochi, H. Inagawa, G. I. Soma, H. Terada, *Colloids Surfaces B Biointerfaces*

- 2004**, 36, 35.
- [394] N. Alnuman, R. Al-Jafary, F. Manna, R. Almuhtaseb, *2018 IEEE EMBS Conf. Biomed. Eng. Sci. IECBES 2018 - Proc.* **2019**, 560.
- [395] D. J. Hines, D. L. Kaplan, *Crit. Rev. Ther. Drug Carrier Syst.* **2013**, 30, 257.
- [396] B. J. Sobieski, I. Noda, J. F. Rabolt, D. B. Chase, *Appl. Spectrosc.* **2017**, 71, 2339.
- [397] X. Zong, S. Ran, D. Fang, B. S. Hsiao, B. Chu, *Polymer (Guildf).* **2003**, 44, 4959.
- [398] R. A. Thakur, C. A. Florek, J. Kohn, B. B. Michniak, *Int. J. Pharm.* **2008**, 364, 87.
- [399] R. Stepanyan, A. V. Subbotin, L. Cuperus, P. Boonen, M. Dorschu, F. Oosterlinck, M. J. H. Bulters, *Polymer (Guildf).* **2016**, 97, 428.
- [400] O. Hartman, C. Zhang, E. L. Adams, M. C. Farach-carson, J. Petrelli, B. D. Chase, J. F. Rabolt, *Biomaterials* **2010**, 31, 5700.
- [401] A. Sadeghi, S. Nokhasteh, A. M. Molavi, M. Khorsand-Ghayeni, H. Naderi-Meshkin, A. Mahdizadeh, *Mater. Sci. Eng. C* **2016**, 66, 130.
- [402] S. Fakirov, *Biodegradable Polyesters*, John Wiley & Sons, **2015**.
- [403] R. Jean-Gilles, D. Soscia, S. Sequeira, M. Melfi, A. Gadre, J. Castracane, M. Larsen, *J. Nanotechnol. Eng. Med.* **2010**, 1, 1.
- [404] Y. You, S. J. Lee, B. M. Min, W. H. Park, *J. Appl. Polym. Sci.* **2006**, 99, 1214.
- [405] H. Xi, H. Zhao, *J. Mater. Sci.* **2019**, 54, 4246.
- [406] A. da S. Nectoux, L. F. Medeiros, R. da S. Bussamara Rodrigues, R. M. Duarte Soares, A. N. Fernandes, *J. Appl. Polym. Sci.* **2018**, 47189, 1.
- [407] L. W. Chow, A. Armgarth, J. P. St-Pierre, S. Bertazzo, C. Gentilini, C. Aurisicchio, S. D. McCullen, J. A. M. Steele, M. M. Stevens, *Adv. Healthc. Mater.* **2014**, 3, 1381.
- [408] C. Garapati, B. Clarke, S. Zadora, C. Burney, B. D. Cameron, R. Fournier, R. F. Baugh, S. H. S. Boddu, *Photodiagnosis Photodyn. Ther.* **2015**, 12, 9.
- [409] X. Meng, J. D. Schiffman, S. L. Perry, *Macromolecules* **2018**, 51, acs.

macromol.8b01709.

- [410] S. Chuangchote, T. Sagawa, S. Yoshikawa, *J. Appl. Polym. Sci.* **2009**, *114*, 2777.
- [411] M. Zheng, J. Tian, Á. Mulero, *Fluid Phase Equilib.* **2013**, *360*, 298.
- [412] X. Li, J. Tian, A. Mulero, *Fluid Phase Equilib.* **2013**, *352*, 54.
- [413] A. J. Queimada, I. M. Marrucho, E. H. Stenby, J. A. P. Coutinho, *Fluid Phase Equilib.* **2004**, *222–223*, 161.
- [414] D. H. Reneker, A. L. Yarin, *Polymer (Guildf)*. **2008**, *49*, 2387.
- [415] R. Gharaei, G. Tronci, R. P. W. Davies, C. Gough, R. Alazragi, P. Goswami, S. J. Russell, *J. Mater. Chem. B* **2016**, *4*, 5475.
- [416] R. Nirmala, B. Woo-il, R. Navamathavan, D. Kalpana, Y. S. Lee, H. Y. Kim, *Colloids Surfaces B Biointerfaces* **2013**, *104*, 262.
- [417] H. Fong, I. Chun, D. H. Reneker, *Polymer (Guildf)*. **1999**, *40*, 4585.
- [418] J. L. Lowery, N. Datta, G. C. Rutledge, *Biomaterials* **2010**, *31*, 491.
- [419] S. J. Eichhorn, W. W. Sampson, *J. R. Soc. Interface* **2010**, *7*, 641.
- [420] A. Mills, D. Hawthorne, L. Burns, D. Hazafy, *Sensors Actuators, B Chem.* **2017**, *240*, 1009.
- [421] V. Nagarajan, K. Zhang, M. Misra, A. K. Mohanty, *ACS Appl. Mater. Interfaces* **2015**, *7*, 11203.
- [422] G. Perego, G. Cella, C. Bastioli, *J. Appl. Polym. Sci.* **1996**, *59*, 37.
- [423] A. Sonseca, L. Peponi, O. Sahuquillo, J. M. Kenny, E. Gimenez, *Polym. Degrad. Stab.* **2012**, *97*, 2052.
- [424] F. De Santis, R. Pantani, V. Speranza, G. Titomanlio, *Ind. Eng. Chem. Res.* **2010**, *49*, 2469.
- [425] S. Meruva, M. D. Donovan, *AAPS PharmSciTech* **2019**, *20*, 93.
- [426] M. . Pop, C. Croitoru, T. Bedo, V. Geaman, I. Radomir, M. Cosnita, S. . Zaharia, L. . Chicos, I. Milosan, *J. Appl. Polym. Sci.* **2018**, *136*, 1.
- [427] R. H. Ansary, M. B. Awang, M. M. Rahman, *Trop. J. Pharm. Res.* **2014**, *13*, 1179.
- [428] R. P. F. Lanao, A. M. Jonker, J. G. C. Wolke, J. A. Jansen, J. C. M. van Hest, S. C. G. Leeuwenburgh, *Tissue Eng. Part B Rev.* **2013**, *19*, 380.
- [429] P. Gentile, V. Chiono, I. Carmagnola, P. V. Hatton, *Int. J. Mol. Sci.*

2014, 15, 3640.

- [430] M. Cadek, J. N. Coleman, V. Barron, K. Hedicke, W. J. Blau, *Appl. Phys. Lett.* **2002**, 81, 5123.
- [431] F. Calvo, in *Front. Nanosci.*, Elsevier Ltd., **2019**, pp. 295–331.
- [432] Z. Song, X. Hou, L. Zhang, S. Wu, *Materials (Basel)*. **2010**, 4, 621.
- [433] A. Nicolas, S. A. Safran, *Biophys. J.* **2006**, 91, 61.
- [434] S. F. Chou, K. A. Woodrow, *J. Mech. Behav. Biomed. Mater.* **2017**, 65, 724.
- [435] A. M. Jordan, L. S. T. J. Korley, *Macromolecules* **2015**, 48, 2614.
- [436] L. Tammaro, C. Saturnino, S. D’Aniello, G. Vigliotta, V. Vittoria, *Int. J. Pharm.* **2015**, 490, 32.
- [437] M. H. Lacoste-Ferré, P. Demont, J. Dandurand, E. Dantras, D. Duran, C. Lacabanne, *J. Mech. Behav. Biomed. Mater.* **2011**, 4, 269.
- [438] R. O. Ritchie, *Nat. Mater.* **2011**, 10, 817.
- [439] A. R. Studart, *Chem. Soc. Rev.* **2016**, 45, 359.
- [440] K. Livanov, L. Yang, A. Nissenbaum, H. D. Wagner, *Sci. Rep.* **2016**, 6, 1.
- [441] M. B. Linder, P. Mohammadi, W. Wagermaier, M. S. Toivonen, O. Ikkala, *Sci. Rep.* **2017**, 7, 1.
- [442] D. P. Dowling, I. S. Miller, M. Ardhaoui, W. M. Gallagher, *J. Biomater. Appl.* **2011**, 26, 327.
- [443] H.-J. Sung, C. Meredith, C. Johnson, Z. S. Galis, *Biomaterials* **2004**, 25, 5735.
- [444] A. Lis-Bartos, A. Smieszek, K. Frańczyk, K. Marycz, *Polymers (Basel)*. **2018**, 10, 1073.
- [445] G. Bracco, B. Holst, in *Springer Ser. Surf. Sci.*, **2013**.
- [446] F. Huang, Q. Wei, Y. Cai, N. Wu, *Int. J. Polym. Anal. Charact.* **2008**, 13, 292.
- [447] M. Krok-Borkowicz, E. Filova, J. Chlupac, J. Klepetar, L. Bacakova, E. Pamuła, *Mater. Lett.* **2019**, 241, 1.
- [448] C. Gentilini, Y. Dong, J. R. May, S. Goldoni, D. E. Clarke, B. H. Lee, E. T. Pashuck, M. M. Stevens, *Adv. Healthc. Mater.* **2012**, 1, 308.
- [449] H. Sun, S. Onneby, *Polym. Int.* **2006**, 55, 1336.

- [450] S. Agarwal, J. H. Wendorff, A. Greiner, *Polymer (Guildf)*. **2008**, *49*, 5603.
- [451] G. G. Pitt, M. M. Gratzl, G. L. Kimmel, J. Surles, A. Sohindler, *Biomaterials* **1981**, *2*, 215.
- [452] R. J. Vance, D. C. Miller, A. Thapa, K. M. Haberstroh, T. J. Webster, *Biomaterials* **2004**, *25*, 2095.
- [453] C. F. Liu, S. J. Li, W. T. Hou, Y. L. Hao, H. H. Huang, *Appl. Surf. Sci.* **2019**, *476*, 325.
- [454] P. I. P. Park, S. Jonnalagadda, *J. Appl. Polym. Sci.* **2006**, *100*, 1983.
- [455] J. A. González-Delgado, P. J. Kennedy, M. Ferreira, J. P. C. Tomé, B. Sarmiento, *J. Med. Chem.* **2016**, *59*, 4428.
- [456] G. K. Srivastava, M. L. Alonso-Alonso, I. Fernandez-Bueno, M. T. Garcia-Gutierrez, F. Rull, J. Medina, R. M. Coco, J. C. Pastor, *Sci. Rep.* **2018**, *8*, 1.
- [457] K. A. Rieger, R. Thyagarajan, M. E. Hoen, H. F. Yeung, D. M. Ford, J. D. Schiffman, *RSC Adv.* **2016**, *6*, 24438.
- [458] O. B. Inc., *Periowave™ HHL-1000*, **2010**.
- [459] E. Alberdi, C. Gómez, *Photodermatol. Photoimmunol. Photomed.* **2018**, 69.
- [460] M. Berakdar, A. Callaway, M. Fakhr Eddin, A. Roß, B. Willershausen, *Head Face Med.* **2012**, *8*, 2.
- [461] D. C. S. Costa, M. C. Gomes, M. A. F. Faustino, M. G. P. M. S. Neves, Â. Cunha, J. A. S. Cavaleiro, A. Almeida, J. P. C. Tomé, *Photochem. Photobiol. Sci.* **2012**, *11*, 1905.
- [462] D. Metcalf, C. Robinson, D. Devine, S. R. Wood, *J. Antimicrob. Chemother.* **2006**, *58*, 190.
- [463] H. C. De Vijlder, H. J. C. M. Sterenborg, H. A. Martino Neumann, D. J. Robinson, E. R. M. De Haas, *Acta Derm. Venereol.* **2012**, *92*, 641.
- [464] H. S. De Bruijn, S. Brooks, A. Van Der Ploeg-Van Den Heuvel, T. L. M. Ten Hagen, E. R. M. De Haas, D. J. Robinson, *PLoS One* **2016**, *11*, 1.
- [465] P. Babilas, V. Schacht, G. Liebsch, O. S. Wolfbeis, M. Landthaler, R. M. Szeimies, C. Abels, *Br. J. Cancer* **2003**, *88*, 1462.

- [466] A. Syed, S. Busi, P. Parasuraman, K. Kaviyarasu, M. Arshad, V. T. Anju, S. B. Sruthil Lal, A. Sharan, T. M. S. Dawoud, *Photochem. Photobiol. Sci.* **2019**, *18*, 563.
- [467] A. Kishen, M. Upadya, G. P. Tegos, M. R. Hamblin, R. M. Hamblin, *Photochem. Photobiol.* **2010**, *86*, 1343.
- [468] L. Conti, G. Boccacini, C. Montis, D. Bani, A. Bencini, D. Berti, C. Giorgi, A. Mengoni, B. Valtancoli, *J. Mater. Chem. B* **2017**, *5*, 2788.
- [469] M. Neves, M. Faustino, M. Mesquita, C. Dias, A. Almeida, *Molecules* **2018**, *23*, 2424.
- [470] M. Wainwright, T. Maisch, S. Nonell, K. Plaetzer, A. Almeida, G. P. Tegos, M. R. Hamblin, *Lancet Infect. Dis.* **2017**, *17*, e49.
- [471] M. Wainwright, D. A. Phoenix, S. L. Laycock, D. R. A. Wareing, P. A. Wright, *FEMS Microbiol. Lett.* **1998**, *160*, 177.
- [472] M. Wainwright, D. A. Phoenix, M. Gaskell, B. Marshall, *J. Antimicrob. Chemother.* **1999**, *44*, 823.
- [473] L. P. Rosa, F. C. da Silva, S. A. Nader, G. A. Meira, M. S. Viana, *Photodiagnosis Photodyn. Ther.* **2015**, *12*, 276.
- [474] R. Kent, C. R. Fontana, M. J. Young, N. S. Soukos, L. R. Morse, R. A. Battaglini, Y. Xu, T. C. Pagonis, *J. Endod.* **2009**, *35*, 1567.
- [475] S. R. da Costa, M. da C. Monteiro, F. M. R. da Silva Júnior, J. Z. Sandrini, *Cell Biol. Int.* **2016**, *40*, 895.
- [476] N. S. Soukos, M. Wilson, T. Burns, P. M. Speight, *Lasers Surg. Med.* **1996**, *18*, 253.
- [477] S. Finger, C. Wiegand, H. J. Buschmann, U. C. Hipler, *Int. J. Pharm.* **2013**, *452*, 188.
- [478] F. Cieplik, L. Tabenski, W. Buchalla, T. Maisch, *Front. Microbiol.* **2014**, *5*, 1.
- [479] N. S. Soukos, J. M. Goodson, *Periodontol. 2000* **2011**, *55*, 143.
- [480] V. S. Muller Campanile, C. Giannopoulou, G. Campanile, J. A. Cancela, A. Mombelli, *Lasers Med. Sci.* **2013**, *1*.
- [481] T. N. Demidova, M. R. Hamblin, *Int. J. Immunopathol. Pharmacol.* **2004**, *17*, 245.
- [482] J. Angerer, U. Bernauer, C. Chambers, Q. Chaudhry, G. Degen, G.

Eisenbrand, T. Platzek, S. Chandra Rastogi, V. Rogiers, C. Rousselle, T. Sanner, K. Savolainen, J. Van Engelen, M. Pilar Vinardell, R. Waring, I. R. White, *Scientific Committee on Consumer Safety OPINION ON CI 45430 (Erythrosine)*, **2010**.

- [483] C. Y. Wang, J. J. Liu, C. Y. Fan, X. M. Mo, H. J. Ruan, F. F. Li, *J. Biomater. Sci. Polym. Ed.* **2012**, *23*, 167.
- [484] Y. Hong, K. Fujimoto, R. Hashizume, J. Guan, J. J. Stankus, K. Tobita, W. R. Wagner, *Biomacromolecules* **2008**, *9*, 1200.
- [485] K. A. Rieger, M. Porter, J. D. Schiffman, *Materials (Basel)*. **2016**, *9*, 297.
- [486] K. Avgoustakis, in *Encycl. Biomater. Biomed. Eng.*, **2005**, pp. 1–11.
- [487] L. T. Lim, R. Auras, M. Rubino, *Prog. Polym. Sci.* **2008**, *33*, 820.
- [488] H. Montes de Oca, I. M. Ward, *Polymer (Guildf)*. **2006**, *47*, 7070.
- [489] M. J. Jenkins, K. L. Harrison, *Polym. Adv. Technol.* **2008**, *19*, 1901.
- [490] H. Peng, S. Zhou, T. Guo, Y. Li, X. Li, J. Wang, J. Weng, *Colloids Surfaces B Biointerfaces* **2008**, *66*, 206.
- [491] X. Xu, X. Chen, X. Xu, T. Lu, X. Wang, L. Yang, X. Jing, *J. Control. Release* **2006**, *114*, 307.
- [492] B. Pukanszky, I. Mudra, P. Staniek, *J. Eng. Appl. Sci.* **1996**, *2*, 2317.
- [493] A. El-Hadi, R. Schnabel, E. Straube, G. Müller, S. Henning, *Polym. Test.* **2002**, *21*, 665.
- [494] T. Yu, C. M. Wu, C. Y. Chang, C. Y. Wang, S. P. Rwei, *Express Polym. Lett.* **2012**, *6*, 318.
- [495] S. Li, *Inc. J Biomed Mater Res (Appl Biomater)* **1999**, *48*, 342.
- [496] T. G. Park, *Biomaterials* **1995**, *16*, 1123.
- [497] M. Partini, R. Pantani, *Polym. Degrad. Stab.* **2007**, *92*, 1491.
- [498] J. Jagur-Grodzinski, *Polym. Adv. Technol.* **2006**, *17*, 395.
- [499] W. Zhao, J. Li, K. Jin, W. Liu, X. Qiu, C. Li, *Mater. Sci. Eng. C* **2016**, *59*, 1181.
- [500] A. López-Córdoba, G. R. Castro, S. Goyanes, *Handb. Compos. from Renew. Mater.* **2017**, *1–8*, 361.
- [501] L. Deng, X. Zhang, Y. Li, F. Que, X. Kang, Y. Liu, F. Feng, H. Zhang, *Food Hydrocoll.* **2018**, *75*, 72.

- [502] C. C. Chen, J. Y. Chueh, H. Tseng, H. M. Huang, S. Y. Lee, *Biomaterials* **2003**, *24*, 1167.
- [503] T. Patrício, P. Bártolo, *Procedia Eng.* **2013**, *59*, 292.
- [504] A. K. Matta, R. U. Rao, K. N. Suman, V. Rambabu, *Procedia Mater. Sci.* **2014**, *6*, 1266.
- [505] S. W. Kuo, C. F. Huang, F. C. Chang, *J. Polym. Sci. Part B Polym. Phys.* **2001**, *39*, 1348.
- [506] A. Bianco, M. Calderone, I. Cacciotti, *Mater. Sci. Eng. C* **2013**, *33*, 1067.
- [507] U. Riaz, S. M. Ashraf, *Charact. Polym. Blends Miscibility, Morphol. Interfaces* **2015**, *9783527331*, 625.
- [508] J. Z. Liang, D. R. Duan, C. Y. Tang, C. P. Tsui, D. Z. Chen, *Polym. Test.* **2013**, *32*, 617.
- [509] M. L. Focarete, C. Gualandi, A. Fiorani, A. Bigi, S. Panzavolta, M. Gioffrè, P. Torricelli, M. Fini, *Mater. Sci. Eng. C* **2013**, *36*, 130.
- [510] J. Deliversky, M. Yaneva-deliverska, M. Lyapina, *J. IMAB* **2015**, *21*, 713.
- [511] N. A. Romanova, L. Y. Brovko, L. Moore, E. Pometun, A. P. Savitsky, N. N. Ugarova, *Appl. Environ. Microbiol.* **2003**, *69*, 6393.
- [512] Y. Nagai, A. Suzuki, H. Katsuragi, K. Shinkai, *Odontology* **2018**, *106*, 154.
- [513] T. Rödig, S. Endres, F. Konietschke, O. Zimmermann, H. G. Sydow, A. Wiegand, *Clin. Oral Investig.* **2017**, *21*, 1753.
- [514] P. Soria-Lozano, Y. Gilaberte, M. Paz-Cristobal, L. Pérez-Artiaga, V. Lampaya-Pérez, J. Aporta, V. Pérez-Laguna, I. García-Luque, M. Revillo, A. Rezusta, *BMC Microbiol.* **2015**, *15*, 187.
- [515] I. M. A. Diniz, I. D. Horta, C. S. Azevedo, T. R. Elmadjian, A. B. Matos, M. R. L. Simionato, M. M. Marques, *Photodiagnosis Photodyn. Ther.* **2015**, *12*, 511.
- [516] A. Ichinose-Tsuno, A. Aoki, Y. Takeuchi, T. Kirikae, T. Shimbo, M.-C. Lee, F. Yoshino, Y. Maruoka, T. Itoh, I. Ishikawa, Y. Izumi, *BMC Oral Health* **2014**, *14*, 152.
- [517] A. M. Mebert, G. S. Alvarez, R. Peroni, C. Illoul, C. Hélyary, T. Coradin,

- M. F. Desimone, *Mater. Sci. Eng. C* **2018**, 93, 170.
- [518] I. M. A. Diniz, K. I. R. Teixeira, P. V. Araújo, M. S. S. Araújo, M. M. Marques, L. T. de A. Poletto, M. E. Cortés, *Photodiagnosis Photodyn. Ther.* **2014**, 11, 300.
- [519] Y. Xu, M. J. Young, R. A. Battaglino, L. R. Morse, C. R. Fontana, T. C. Pagonis, R. Kent, N. S. Soukos, *J. Endod.* **2009**, 35, 1567.
- [520] J. T. Y. Lee, K. L. Chow, *Scanning* **2012**, 34, 12.
- [521] S. M. Ayuk, N. N. Houreld, H. Abrahamse, *Lasers Med. Sci.* **2018**, 33, 1085.
- [522] G. Jin, M. P. Prabhakaran, D. Kai, M. Kotaki, S. Ramakrishna, *Photochem. Photobiol. Sci.* **2013**, 12, 124.
- [523] C. H. Collins, P. M. Lyne, J. M. Grange, J. O. Falkinham, *Microbiological Methods*, Arnold, London, **2004**.
- [524] J.-H. Park, M.-Y. Ahn, Y.-C. Kim, S.-A. Kim, Y.-H. Moon, S.-G. Ahn, J.-H. Yoon, *Biol. Pharm. Bull.* **2012**, 35, 509.
- [525] A. Pfitzner, B. W. Sigusch, V. Albrecht, E. Glockmann, *J. Periodontol.* **2005**, 75, 1343.
- [526] N. R. Naylor, R. Atun, N. Zhu, K. Kulasabanathan, S. Silva, A. Chatterjee, G. M. Knight, J. V. Robotham, *Antimicrob. Resist. Infect. Control* **2018**, 7, 1.
- [527] A. Chatterjee, M. Modarai, N. R. Naylor, S. E. Boyd, R. Atun, J. Barlow, A. H. Holmes, A. Johnson, J. V. Robotham, *Lancet Infect. Dis.* **2018**, 18, e368.
- [528] J. Chen, C. Chen, G. Liang, X. Xu, Q. Hao, D. Sun, *Carbohydr. Polym.* **2019**, 220, 170.
- [529] A. De Mori, M. Hafidh, N. Mele, R. Yusuf, G. Cerri, E. Gavini, G. Tozzi, E. Barbu, M. Conconi, R. R. Draheim, M. Roldo, *Pharmaceutics* **2019**, 11, DOI 10.3390/pharmaceutics11030116.
- [530] K. Dzobo, N. E. Thomford, D. A. Senthebane, H. Shipanga, A. Rowe, C. Dandara, M. Pillay, K. S. C. M. Motaung, *Stem Cells Int.* **2018**, 2018.
- [531] L. Lin, Y. Fang, Y. Liao, G. Chen, C. Gao, P. Zhu, *Adv. Eng. Mater.* **2019**, 21, 1.

- [532] Y. Ma, L. Xie, B. Yang, W. Tian, *Biotechnol. Bioeng.* **2019**, 116, 452.
- [533] I. Ishikawa, T. Iwata, K. Washio, T. Okano, T. Nagasawa, K. Iwasaki, T. Ando, *Periodontol. 2000* **2009**, 51, 220.
- [534] K. Nishiyama, T. Akagi, S. Iwai, M. Akashi, *Tissue Eng. - Part C Methods* **2019**, 25, 262.
- [535] A. J. T. Naik, S. Ismail, C. Kay, M. Wilson, I. P. Parkin, *Mater. Chem. Phys.* **2011**, 129, 446.
- [536] L. Beytollahi, M. Pourhajibagher, N. Chiniforush, R. Ghorbanzadeh, R. Raoofian, B. Pourakbari, A. Bahador, *Photodiagnosis Photodyn. Ther.* **2017**, 17, 56.
- [537] J. Mankins, *Off. Sp. Access Technol. NASA* **1995**, 4.
- [538] J. C. Mankins, *Acta Astronaut.* **2009**, 65, 1208.
- [539] S. Barr, T. Baker, S. Markham, A. Kingon, *Acad. Manag. Learn. Educ.* **2009**, 8, 370.
- [540] D. 31993L0042, *Official Journal of the European Communities - COUNCIL DIRECTIVE 93/42/EEC*, **1993**.
- [541] H. Achakri, P. Fennema, I. Udofia, *BSI Stand. Ltd.* **2014**, 1.
- [542] I. C. T. Santos, G. S. Gazelle, L. A. Rocha, J. M. R. S. Tavares, in *5th Eur. Conf. Int. Fed. Med. Biol. Eng.*, **2012**, pp. 1–4.
- [543] European Parliament and the Council of the European Union, *Off. J. Eur. Union* **2017**, L117, 1.
- [544] Medicines & Healthcare Products Regulatory Agency, *An Introductory Guide to the Medical Device Regulation (MDR) and the in Vitro Diagnostic Medical Device Regulation (IVDR)*, **2017**.
- [545] A. S. Jati, L. Z. Furquim, A. Consolaro, *Dental Press J. Orthod.* **2016**, 21, 18.
- [546] J. L. Wennström, *Ann Periodontol* **1996**, 1, 671.
- [547] K. M. Kimble, R. M. Eber, S. Soehren, Y. Shyr, H.-L. Wang, *J. Periodontol.* **2004**, 75, 210.
- [548] J. S. Jundt, K. W. Odom, J. W. Wilson, *J. Oral Maxillofac. Surg.* **2011**, 69, 1255.
- [549] I. Elgali, O. Omar, C. Dahlin, P. Thomsen, *Eur. J. Oral Sci.* **2017**, 125, 315.

- [550] A. Sculean, R. Gruber, D. D. Bosshardt, *J. Clin. Periodontol.* **2014**, *41*, S6.
- [551] K. Markowitz, M. Moynihan, M. Liu, S. Kim, *Oral Surgery, Oral Med. Oral Pathol.* **1992**, *73*, 729.
- [552] Z. Baghani, M. Kadkhodazadeh, *J. Dent. Res. Dent. Clin. Dent. Prospects* **2013**, *7*, 183.
- [553] P. Avci, A. Gupta, M. Sadasivam, D. Vecchio, Z. Pam, N. Pam, M. R. Hamblin, *Semin. Cutan. Med. Surg.* **2013**, *32*, 41.
- [554] S. Strassburg, M. Caduc, G. B. Stark, N. Jedrusik, P. Tomakidi, T. Steinberg, F. Simunovic, G. Finkenzeller, *J. Biomed. Mater. Res. - Part A* **2019**, *107*, 1605.
- [555] A. C. Vea-Barragan, E. Bucio, D. Quintanar-Guerrero, M. L. Zambrano-Zaragoza, S. G. Meléndez-López, A. Serrano-Medina, J. M. Cornejo-Bravo, *Radiat. Phys. Chem.* **2019**, *164*, 108372.
- [556] D. Pauluk, A. K. Padilha, N. M. Khalil, R. M. Mainardes, *Food Hydrocoll.* **2019**, *94*, 411.
- [557] R. P. Brannigan, V. V. Khutoryanskiy, *Macromol. Biosci.* **2019**, *1900194*, 1.
- [558] D. L. Mayfield, *Mo. Med.* **2016**, *113*, 456.
- [559] G. de Rassenfosse, *Small Bus. Econ.* **2012**, *39*, 437.
- [560] V. V. Chagovets, M. V. Kosevich, S. G. Stepanian, O. A. Boryak, V. S. Shelkovsky, V. V. Orlov, V. S. Leontiev, V. A. Pokrovskiy, L. Adamowicz, V. A. Karachevtsev, *J. Phys. Chem. C* **2012**, *116*, 20579.
- [561] J. P. Tardivo, A. Del Giglio, C. S. De Oliveira, D. S. Gabrielli, H. C. Junqueira, D. B. Tada, D. Severino, R. De Fátima Turchiello, M. S. Baptista, *Photodiagnosis Photodyn. Ther.* **2005**, *2*, 175.
- [562] M. N. Usacheva, M. C. Teichert, M. A. Biel, *J. Photochem. Photobiol. B Biol.* **2003**, *71*, 87.
- [563] R. Pokrowiecki, *Drug Deliv.* **2018**, *25*, 1504.
- [564] K. Müller, C. Figueroa, C. Martínez, M. Medel, E. Obreque, A. Peña-Neira, I. Morales-Bozo, H. Toledo, R. O. López-Solis, *Food Qual. Prefer.* **2010**, *21*, 569.
- [565] M. Kilian, I. L. C. Chapple, M. Hannig, P. D. Marsh, V. Meuric, A. M. L.

- Pedersen, M. S. Tonetti, W. G. Wade, E. Zaura, *Br. Dent. J.* **2016**, 221, 657.
- [566] C. Tang, Y. X. Guan, S. J. Yao, Z. Q. Zhu, *Int. J. Pharm.* **2014**, 473, 434.
- [567] H. E. Colley, P. C. Eves, A. Pinnock, M. H. Thornhill, C. Murdoch, *Int. J. Radiat. Biol.* **2013**, 89, 907.
- [568] N. Fenwick, G. Griffin, C. Gauthier, *Can. Vet. J.* **2009**, 50, 523.
- [569] D. A. C. Méndez, E. Gutierrez, E. J. Dionísio, T. M. Oliveira, M. A. R. Buzalaf, D. Rios, M. A. A. M. Machado, T. Cruvinel, *Lasers Med. Sci.* **2018**, 33, 479.
- [570] R. D. Rossoni, J. O. Barbosa, F. E. de Oliveira, L. D. de Oliveira, A. O. C. Jorge, J. C. Junqueira, *Lasers Med. Sci.* **2014**, 29, 1679.
- [571] G. Katara, N. Hemvani, S. Chitnis, V. Chitnis, D. Chitnis, *Indian J. Med. Microbiol.* **2008**, 26, 241.
- [572] Z. Dai, J. Ronholm, Y. Tian, B. Sethi, X. Cao, *J. Tissue Eng.* **2016**, 7, 1.
- [573] T. J. A. G. Münker, S. E. C. M. van de Vijfeijken, C. S. Mulder, V. Vespasiano, A. G. Becking, C. J. Kleverlaan, A. G. Becking, L. Dubois, L. H. E. Karssemakers, D. M. J. Milstein, S. E. C. M. van de Vijfeijken, P. R. A. M. Depauw, F. W. A. Hoefnagels, W. P. Vandertop, C. J. Kleverlaan, T. J. A. G. Münker, T. J. J. Maal, ... S. A. J. Zaat, *J. Mech. Behav. Biomed. Mater.* **2018**, 81, 168.
- [574] D. Leonard, F. J. Buchanan, *Trans. - 7th World Biomater. Congr.* **2004**, 23, 456.
- [575] A. R. Siddiqui, J. M. Bernstein, *Clin. Dermatol.* **2010**, 28, 519.
- [576] J. F. Guest, N. Ayoub, T. McIlwraith, I. Uchegbu, A. Gerrish, D. Weidlich, K. Vowden, P. Vowden, *BMJ Open* **2015**, 5, e009283.

Appendix A

General Description of University of Sheffield External Placement

The process of generating the models used during the placement is described in detail in the relevant publications^[39,567]. Briefly, freeze-dried rat tail collagen was dissolved and combined with primary normal oral fibroblast cells, added to well inserts and incubated in media for 24 hours. The cell-embedded collagen gels were then brought to an air-liquid interface and FNB6 cells (oral epithelial cells) were added. The oral mucosal models were incubated for 10 days with media changes every other day. Following this time, the models were either used as controls or infected with *S. mutans Ingbritt* bacteria. After 24 hours, the models were fixed in formalin, dehydrated, wax embedded, sectioned, stained with Gram's stain and visualised on a light microscope (**Figure A1**).

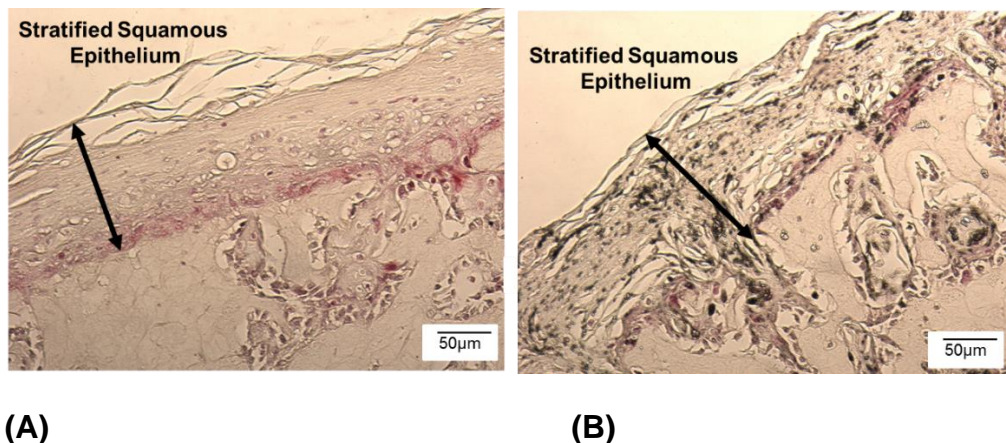


Figure A1 – Histology slides of Gram-Stained Oral Mucosal Models generated during an external placement to Dr Helen Colley’s laboratory at the University of Sheffield. (A): Control non-infected model; (B): Model infected with *S. mutans Ingbritt* bacteria. Images taken at 20x magnification on a light microscope